UNIVERSIDADE ESTADUAL PAULISTA
"JÚLIO DE MESQUITA FILHO"
Câmpus de São José do Rio Preto

Leticia Ribeiro de Assis

Síntese e Atividade Antibacteriana e Antimicobacteriana de Isobavachalcona e seus Análogos

São José do Rio Preto
2022

Leticia Ribeiro de Assis

Síntese e Atividade Antibacteriana e Antimicobacteriana de Isobavachalcona e seus Análogos

Tese apresentada como requisito para a obtenção do título de Doutor em Química, junto ao Programa de Pós-Graduação em Química, do Instituto de Biociências, Letras e Ciências Exatas da Universidade Estadual Paulista "Júlio de Mesquita Filho", Campus de São José do Rio Preto.

Financiadora: Capes

Orientador: Prof. Dr. Luis Octavio Regasini
Coorientador: Prof. Dr. Fernando Rogério Pavan

São José do Rio Preto
2022

A848s

Assis, Leticia Ribeiro de

Síntese e Atividade Antibacteriana e Antimicobacteriana de Isobavachalcona e seus Análogos / Leticia Ribeiro de Assis. -- São José do Rio Preto, 2022

220 p. : il., tabs.

Tese (doutorado) - Universidade Estadual Paulista (Unesp), Instituto de Biociências Letras e Ciências Exatas, São José do Rio Preto

Orientador: Luis Octavio Regasini

Coorientador: Fernando Rogério Pavan

1. Bactérias. 2. Biofilme. 3. Chalcona. 4. Isoprenila. 5. Tuberculose. I. Título.

Sistema de geração automática de fichas catalográficas da Unesp. Biblioteca do Instituto de Biociências Letras e Ciências Exatas, São José do Rio Preto. Dados fornecidos pelo autor(a).

Essa ficha não pode ser modificada.

Leticia Ribeiro de Assis

Síntese e Atividade Antibacteriana e Antimicobacteriana de Isobavachalcona e seus Análogos

Tese apresentada como requisito para a obtenção do título de Doutor em Química, junto ao Programa de Pós-Graduação em Química, do Instituto de Biociências, Letras e Ciências Exatas da Universidade Estadual Paulista "Júlio de Mesquita Filho", Campus de São José do Rio Preto.

Financiadora: Capes

COMISSÃO EXAMINADORA

Prof. Dr. Luis Octávio Regasini (Orientador)
Universidade Estadual Paulista "Júlio de Mesquita Filho" – UNESP

Prof. Dr. Antônio Eduardo Miller Crotti
Universidade de São Paulo – USP

Prof. Dr. Joao Henrique Ghilardi Lago
Universidade Federal do ABC - UFABC

Profa. Dra. Amanda Danuello Pivatto
Universidade Federal de Uberlândia – UFU

Prof. Dr. Daniel Fábio Kawano
Universidade Estadual de Campinas – UNICAMP

São José do Rio Preto
10 de agosto de 2022

Dedico este trabalho à minha família, especialmente, aos meus pais, ***Ivonete*** *e* ***Samuel****, e aos meus irmãos* ***Samila****,* ***Patrícia*** *e* ***Samuel Junior***

AGRADECIMENTOS

À **Deus**, por me proporcionar momentos de felicidade e realizações, me auxiliando e me dando forças em todos os momentos dessa caminhada.

Aos meus pais **Ivonete L R Assis** e **Samuel P de Assis**, que passaram por tanta dificuldade para ver os 4 filhos formados. Vocês são meus pilares e minhas maiores inspirações de vida. O apoio e amor de vocês foram fundamentais nessa longa jornada. Agradeço também aos meus irmãos, **Samila R. de Assis**, **Patricia R de Assis**, e **Samuel P. de Assis Júnior**, pelo amor e apoio.

Ao meu orientador **Dr. Luis Octavio Regasini**, o qual eu admiro e sou muito grata pela orientação, carinho e amizade desde o meu mestrado. Obrigada pela oportunidade de poder crescer profissionalmente e pessoalmente junto ao seu laboratório. Foi um prazer poder fazer parte dessa história.

À **Capes**, pela bolsa concedida (Código de Financiamento 001), a **Fapesp** e **CNPq** pelos auxílios financeiros que foram essenciais na realização da pesquisa.

Ao meu namorado e amigo Me. **Reinaldo dos Santos Theodoro**, por todo amor, parceria, e discussões científicas. Te admiro pela sua trajetória de vida, humildade e dedicação em tudo o que faz.

À minha amiga Me. **Julyanna Andrade**, por todo auxílio profissional e emocional, pelas inúmeras ajudas, conversas, e momentos de descontrações.

Ao **Dr. Miguel Divino da Rocha**, que foi essencial na parte experimental do início meu doutorado. Obrigada pela paciência, amizade, e discussões científicas.

Aos alunos de iniciação cientifica que coorientei durante o curso de doutorado **Pedro Jacob**, **Eduarda Cardoso**, **Ana Luiza**, **Larissa Diniz**, e **Gabriela Payão**. Foi um prazer fazer parte da formação de vocês. Aprendi demais.

Ao Prof. Dr. **Fernando Rogério Pavan**, pela coorientação. Agradeço também a você e seus alunos pela realização dos experimentos antimicobacterianos.

Ao Prof. Dr. **Carlos Henrique Gomes Martins** e as suas alunas **Meliza Arantes de Souza Bessa** e **Ralciane de Paula Menezes**, Universidade Federal de Uberlândia, Laboratório de Ensaios Antimicrobianos – LEA, pela realização dos ensaios antibacterianos e antimicobacterianos.

Ao Me. **Guilherme Dilarri** e Prof. Dr. **Henrique Ferreira**, membros do Laboratório de Genética de Bactérias, Instituto de Biociências, UNESP/Rio Claro, pela realização dos ensaios de permeação em membrana.

Ao Laboratório de Antibióticos e Quimioterápicos – LAQ, onde desenvolvi toda a parte experimental química. Agradeço a todos que de alguma forma contribuíram com esse trabalho, especialmente aos meus amigos **Julyanna Andrade**, **Reinaldo Theodoro**, **Maria Beatriz**, **Miguel Rocha**, **Pedro Jacob**, **Larissa Dinis**, **Dinis Caina**, e **Veridianna Pattini**.

Ao Centro Multiusuário de Inovação Biomolecular, Instituto de Biociências, Letras e Ciências Exatas, UNESP/São José do Rio Preto (FAPESP – Processo nº 2009/53989-4), especialmente, ao Dr. **Fábio Moraes**, pela realização dos experimentos de Ressonância Magnética Nuclear. À Me. **Dani C Oliveira Lisboa**, Laboratório de Bioenergia (UNESP/São José do Rio Preto), pelas análises de HPLC. Ao pesquisador **Alan Roberto Costa**, Centro de Contaminantes Orgânicos, Instituto Adolfo Lutz, pelos experimentos de espectrometria de massas.

DADOS CURRICULARES

FORMAÇÃO ACADÊMICA

Doutorado em Química (2018)

Universidade Estadual Paulista "Júlio de Mesquita Filho", UNESP, São Paulo, Brasil.

Título: Síntese e Atividade Antibacteriana e Antimicobacteriana de Isobavachalcona e seus Análogos

Orientador: Prof. Dr. Luis Octávio Regasini. Coorientador: Prof Dr. Fernando Rogério Pavan

Mestrado em Química (2015–2017)

Universidade Estadual Paulista "Júlio de Mesquita Filho", UNESP, São Paulo, Brasil.

Título: Síntese e avaliação biológica de novos híbridos tuberculostático-chalcona como potenciais agentes contra a tuberculose

Orientador: Prof. Dr. Luis Octávio Regasini. Coorientador: Prof Dr. Fernando Rogério Pavan

Graduação em Farmácia-Bioquímica (2010–2014)

Universidade Paulista – UNIP

PRODUÇÕES BIBLIOGRÁFICAS

Artigos completos publicados em periódicos

Assis, L.R.; Theodoro, R. S; Silva, M. B. C. Nascentes, J. A. A.; Rocha, M. D.; Bessa, M. A. S.; Menezes, R. P.; Dilarri, G.; Hypolito, G. B.; Santos, V. R. ; Duque, C.; Ferreira, H.; Martins, C. H. G.; Regasini, L. O. Antibacterial Activity of Isobavachalcone (IBC) is Associated with Membrane Disruption. **Membranes**, v. 12, p. 269, 2022.

Satokata, A.A.C.; Souza, J.H.; Silva, L.L.O; Santiago, M.B.; Ramos, S. B.; **Assis, L.R.**; Theodoro, R.S.; Oliveira, L.R.; Regasini, L.O.; Martins, C.H.G. Chalcones with potential antibacterial and antibiofilm activities against periodontopathogenic bacteria. **Anaerobe**, v. 76, p. 102588, 2022.

Anselmo, D.B.; Polaquini, C.R.; Marques, B.C.; Ayusso, G.M.; **Assis, L.R.**; Torrezan, G.S; Rahal, P.; Fachin, A.L.; Calmon, M.F.; Marins, M.A.; Regasini, L.O. Curcumin-

cinnamaldehyde hybrids as antiproliferative agents against women's cancer cells. Medicinal **Chemistry Research**, v. 30, p. 2007–2015, 2021.

Lima, C.S.; Mottin, M.; **Assis, L.R.**; Mesquita, N.C.M.R; Sousa, B. K. P; Coimbra, L.D; Santos, K.B; Zorn, K. M.; Guido, R.V.C.; Ekins, S.; Marques, R.E; proença-Modena, J.L; Oliva, G.; Andrade, C.H; Regasini, L.O. Flavonoids from *Pterogyne nitens* as Zika virus NS2B-NS3 protease inhibitors. **Bioorganic Chemistry**, v. 109, p. 104719, 2021.

Bila, N.M; Orlandi, C.B.O; Vaso, C.O; Bonatti, J.L.C; **Assis, L.R.**; Regasini, L.O.; Fontana, C.R; Almeida, A.M.F.; Giannini, M.J.S.M. 2-Hydroxychalcone as a Potent Compound and Photosensitizer Against Dermatophyte Biofilms. **Frontiers in Cellular and Infection Microbiology**, v. 11, p. 679460, 2021.

Fernandes, N.A.R; Camilli, A.C; Maldonado, L.A.G.; Pacheco, C.G.P.; Silva, A.F.; Molon, R.S; Spolidorio, L.C; **Assis, L.R.**; Regasini, L.O.; Rossa-Junior, C.; Guimarães'stabili, M.R. Chalcone T4, a novel chalconic compound, inhibits inflammatory bone resorption in vivo and suppresses osteoclastogenesis in vitro. **Journal of Periodontal Research**, v. 56, p. 569–578, 2021.

Silva, S.; Shimizu, J.F.; Oliveira, D.M.; **Assis, L.R.**; Bittar, C.; Mottin, M.; Sousa, B.K.P.; Mesquita, N.C.M.R; Regasini, L.O; Rahal, P.; Oliva, G.; Perryman, A.L.; Ekins, S.; Andrade, C.H.; Goulart, L.R.; Sabino-silva, R.; Merits, A.; Harris, M.; Jardim, A.C.G. A Diarylamine Derived from Anthranilic Acid Inhibits ZIKV replication. **Scientific Reports**, v. 9, p. 17703, 2019.

Campos, G.R.F.; Bittar, C; Jardim, A.C.G; Shimizu, J.F.; Batista, M.N; Paganini, E.R.; **Assis, L.R.**; Bartlett, C.; Harris, M.; Bolzani, V.S.; Regasini, L.O.; Rahal, P. Hepatitis C Virus in vitro Replication is Efficiently Inhibited by Acridone Fac4. **Journal of General Virology**, v. 98, p. 1693-1701, 2017.

ORIENTAÇÕES

Trabalho de conclusão de curso

Pedro Henrique de Deus Jacob. Síntese e Avaliação de Análogos de Isobavachalcona (IBC) contra Micobactérias e Bactérias. 2022. Trabalho de Conclusão de Curso. (Graduação em Química) - Universidade Estadual Paulista Júlio de Mesquita Filho - SJRP, Conselho Nacional de Desenvolvimento Científico e Tecnológico. Coorientadora

Eduarda Silva Cardoso. Síntese de chalconas *O*-preniladas como potenciais agentes contra Carcinoma de Cólon. 2022. Trabalho de Conclusão de Curso. (Graduação em Química) - Universidade Estadual Paulista Júlio de Mesquita Filho - SJRP, Conselho Nacional de Desenvolvimento Científico e Tecnológico. Coorientadora

Ana Luiza Moreira Silva. Síntese e avaliação antibacteriana de análogos simplificados da 4-hidroxiderricina. 2022. Trabalho de Conclusão de Curso. (Graduação em Química) - Universidade Estadual Paulista Júlio de Mesquita Filho - SJRP, Conselho Nacional de Desenvolvimento Científico e Tecnológico. Coorientadora.

Larissa Alves Faria Diniz. Síntese e avaliação de análogos simplificados da Isobavachalcona contra *M. tuberculosis* sensível e fármaco resistente. 2022. Trabalho de Conclusão de Curso. (Graduação em Biologia) - Universidade Estadual Paulista Júlio de Mesquita Filho - SJRP, Conselho Nacional de Desenvolvimento Científico e Tecnológico. Coorientadora.

Gabriela Migliati Payão. Caracterização de extrato dos frutos de *Pterogyne nitens*. 2021. Trabalho de Conclusão de Curso. (Graduação em Química) - Universidade Estadual Paulista Júlio de Mesquita Filho - SJRP, Conselho Nacional de Desenvolvimento Científico e Tecnológico. Coorientadora

RESUMO

A isobavachalcona (**IBC**) é uma chalcona prenilada de ocorrência natural com atividade antibacteriana bem conhecida contra bactérias patogênicas, incluindo espécies resistente a múltiplos fármacos. Considerando as evidências das propriedades farmacológicas de **IBC**, 25 análogos de **IBC** com modificações nos anéis aromáticos A e B, assim como na ponte *trans*-enônica foram planejados e sintetizados. Dentre esses, seis análogos são chalconas de ocorrência natural (isoliquiritigenina, xantoangelol, isocordoína, hayeanachalcona, morachalcona A e corilifol B) e quinze são substâncias inéditas. As substâncias foram sintetizadas em cinco a sete etapas, incluindo iodação regiosseletiva, condensação aldólica de Claisen-Schmidt, acoplamento de Suzuki-Miyuara, reduções, e rearranjo [1,3]-sigmatrópico, obtendo rendimentos globais de 1 a 37%. Inicialmente, a atividade antibacteriana da **IBC** e análogos foi avaliada *in vitro* contra *Staphylococcus aureus* sensível (MSSA) e resistente à meticilina (MRSA). Nove substâncias (**IBC**, **IBC 1–IBC 4**, **IBC 8**, **IBC 22**, **IBC 23**, e **DHIBC**) mostraram valores de concentração inibitória mínima (CIM) entre 1,56 e 12,5 µg/mL contra MSSA e MRSA. **IBC** e seu regioisômero, 2-hidroxi-isocordoína (**IBC 2**), foram os mais promissores contra MSSA (CIM = 1,56 µg/mL) e MRSA (CIM = 3,12 µg/mL), com baixa toxicidade contra queratinócitos humanos. **IBC** e **IBC 2** inibiram mais de 50% da formação de biofilme de MSSA e MRSA em concentrações subinibitórias. **IBC** e **IBC 2** provocaram danos à membrana de *Bacillus subtilis*. Bioensaios adicionais demonstraram que **IBC** e **IBC 2** possuem um espectro de ação antibacteriana contra *Streptococcus pneumoniae* (CIM = 50 µg/mL), *Streptococcus sanguinis* (CIM = 3,12 µg/mL), *Streptococcus sobrinus* (CIM = 6,25–12,5 µg/mL), *Streptococcus mutans* (CIM = 6,25 µg/mL). Adicionalmente a **IBC 2** também demonstrou atividade contra espécies Gram-negativa de *Helicobacter pylori* (CIM = 3,90 µg/mL) e *Klebsiella pneumoniae* (MIC = 100 µg/mL). A atividade antimicobacteriana da **IBC** e análogos foi avaliada contra *Mycobacterium tuberculosis* H37Rv. Doze chalconas preniladas (**IBC**, **IBC 1–IBC 3**, **IBC 6**, **IBC 7**, **IBC 10**, **IBC 13**–**IBC 16**, **IBC 22** e **IBC 23**) demonstraram atividade antimicobacteriana contra *M. tuberculosis* com CIM_{90} (concentração inibitória mínima de 90%) de 2,7 a 25 µg/mL. A nitrochalcona (**IBC 14**, CIM_{90} = 2,7 µg/mL) e a trifluormetilchalcona (**IBC 13**, CIM_{90} = 3,8 µg/mL) foram as chalconas antimicobacterianas mais potentes. Esses resultados corroboram **IBC** como uma estrutura privilegiada na descoberta e desenvolvimento de novos derivados biologicamente ativos para combater bactérias patogênicas humanas.

Palavras-chave: Bactérias. Biofilme. Chalcona. Isoprenila. Tuberculose

ABSTRACT

Isobavachalcone (**IBC**) is a naturally occurrence prenylated compound with well-known antibacterial activity against pathogenic bacteria, including multidrug resistant species. Considering the pharmacological evidences of **IBC**, 25 analogs of **IBC** with modifications on aromatic rings A and B and at the *trans*-enonic bridge. Among them, six analogs are naturally occurrence (isoliquiritigenin, xanthoangelol, isocordoin, hayeanachalcone, morachalcone A and corylifol B) and fifteen are new chemical entities. The compounds were synthesized in five to seven steps, including regioselective iodination, Claisen-Schmidt aldol condensation, Suzuki-Miyuara coupling, reductions, and [1,3]-sigmatropic rearrangement, obtaining overall yields from 1 to 37 %. First, **IBC** and analogs were evaluated *in vitro* against standard strains of Methicillin-Susceptible *Staphylococcus aureus* (MSSA) and Methicillin-Resistant *Staphylococcus aureus* (MRSA). Nine compounds (**IBC**, **IBC 1– IBC 4**, **IBC 8**, **IBC 22**, **IBC 23**, and **DHIBC**) showed Minimal Inhibitory Concentration (MIC) values between 1.56 and 12.5 µg/mL against MSSA and MRSA. **IBC** and its regioisomer, 2-hydroxycordoin (**IBC 2**), were the most promising compounds against MSSA (MIC = 1.56 µg/mL) and MRSA (MIC = 3.12 µg/mL) with low toxicity against human keratinocytes. **IBC** and **IBC 2** inhibited more than 50% of MSSA and MRSA biofilm formation in subinhibitory concentrations. **IBC** and **IBC 2** caused damage to membrane of *Bacillus subtilis*. Additional bioassays demonstrated that **IBC** and **IBC 2** have a spectral of antibacterial action against *Streptococcus pneumoniae* (MIC = 50 µg/mL), *Streptococcus sanguinis* (MIC = 3.12 µg/mL), *Streptococcus sobrinus* (MIC = 6.25–12.5 µg/mL), and *Streptococcus mutans* (MIC = 6.25 µg/mL). Additionally, **IBC 2** demonstrated also demonstrated antibacterial activity against Gram-negative species of *Helicobacter pylori* (MIC = 3.90 µg/mL) and *Klebsiella pneumoniae* (MIC = 100 µg/mL). Antimycobacterial activity of **IBC** and analogs was evaluated against *Mycobacterium tuberculosis* H37Rv. Twelve compounds (**IBC**, **IBC 1–IBC 3**, **IBC 6**, **IBC 7**, **IBC 10**, **IBC 13**–**IBC 16**, **IBC 22** and **IBC 23**) showed antimycobacterial activity against *M. tuberculosis* with MIC_{90} (minimal inhibitory concentration of 90%) ranging from 2.7 to 25 µg/mL. Nitrochalcone (**IBC 14**, MIC = 2.7 µg/mL) and trifluoromethylchalcone (**IBC 13**, MIC = 3.8 µg/mL) were the most potent antimycobacterial chalcones. These results corroborate **IBC** as a privileged structure for discovery and development of new biologically active derivatives against human pathogenic bacteria.

Keywords: Bacteria. Biofilm. Chalcones. Isoprenyl. Tuberculosis

FIGURES

CHAPTER I

CHAPTER II

CHAPTER IV

CHAPTER V

Supplementary material of Chapter II

Supplementary material of Chapter III

Supplementary material of Chapter IV

TABLES

CHAPTER I

CHAPTER II

CHAPTER III

CHAPTER IV

SCHEMES

CHAPTER I

CHAPTER II

CHAPTER III

ABBREVIATIONS AND SYMBOLS

δ: chemical shift

ADME: absorption, distribution, metabolism and excretion

ATCC: American Type Culture Collection

BBB: blood-brain barrier

CFU: colony-forming unit

CHX: chlorhexidine

d: doublet

dd: double doublet

ddd: double double doublet

DHIBC: Di-hydroxyisobavachalcone

DNA: Deoxyribonucleic Acid

FDA: Food and Drug Administration

FIC: fractional inhibitory concentration

FICI: fractional inhibitory concentration index

GI: gastrointestinal

IBC: Isobavachalcone

INH: isoniazid

HBA hydrogen bond acceptor

HBD: hydrogen bond donor

HIA: human intestinal absorption

HIV: human immunodeficiency virus

HPLC: high-performance liquid chromatography

J: coupling constant

log *P*: log of partition coefficient

log *S*: log of solubility constant

m: multiplet

MBC: minimal bactericidal concentration

MBIC: minimal biofilm inhibitory concentration

MDR: multidrug-resistant

MDR-TB: multidrug-resistant tuberculosis

MIC = minimal inhibitory concentration

MOM: methoxymethyl

MSSA: methicillin-susceptible *Staphylococcus aureus*

MRSA: methicillin-resistant *Staphylococcus aureus*

MR: molar refractivity

MS: mass spectrometry

MTB: *Mycobacterium tuberculosis*

MW: molecular weight

NA: number of atoms

NMR: Nuclear Magnetic Resonance

NP: natural products

NROT: number of rotatable bonds

NTM: nontuberculous mycobacteria

PAD: photodiode array detector

PI: propidium iodide

REMA: Resazurin microtiter assay

R&D: research & development

RMP: rifampicin

RNA: Ribonucleic acid

RR-TB: rifampicin resistance

SARS-CoV2: respiratory syndrome coronavirus-2

SAR: structure-activity relationship

TB: tuberculosis

TC: tetracycline

TLC: Thin Layer Chromatography

TPSA: topological polar surface area

VISA: vancomycin intermediate-resistant *Staphylococcus aureus*

VRE_{fm}: Vancomycin-resistant *Enterococcus faecium*

VRSA: vancomycin-resistant *Staphylococcus aureus*

XDR-TB: extensively drug-resistant tuberculosis

WHO: World Health Organization

SUMMARY

CHAPTER I

General introduction, Literature Review and Aims

Chapter I

1. General introduction

The discovery of antibacterial drugs in 1940s was able to revolutionize the treatment of infectious diseases, decreasing morbidity and mortality worldwide. However, the emergence and fast global spread of multidrug-resistance (MDR) among human pathogenic bacteria reduced the efficacy of conventional drugs. Currently, about 700 mil people die annually due to antibiotic-resistant infections worldwide, and there is a projection that this number may increase by 10 million deaths/year until 2050 (O'NEILL, 2016; VIKESLAND et al., 2019). This scenario represents a significant challenge to be overcome in the 21st Century, requiring several efforts to develop new antibiotics and improve the existing ones (O'NEILL, 2016). Many antibacterial drugs are natural products or their derivatives, highlighting their relevance for the combat of infectious diseases (NEWMAN; CRAGG, 2020).

Isobavachalcone (**IBC**) is a natural *C*-prenylated chalcone isolated from medicinal plants. **IBC** has a broad spectrum of pharmacological activities, including its antimicrobial effects against bacteria and fungi (KUETE; SANDJO, 2012). In this context, **IBC** has been considered a versatile compound, which can be used as a prototype for chemical modification and optimizations in drug discovery (WANG et al., 2021).

We selected **IBC** as prototype to design 25 analogs (**IBC 1–23**, **DHIBC**, **DHIBC 2**) with modifications on aromatic rings A and B and on α,β-unsaturated ketone bridge. Compounds were synthesized and evaluated *in vitro* against human pathogenic bacteria, including mycobacteria (*Mycobacterium tuberculosis, Mycobacterium avium, Mycobacterium kansasii*), Gram-negative bacteria (*Pseudomonas aeruginosa*, *Klebsiella pneumoniae*, and *Helicobacter pilory*), and Gram-positive bacteria (*Staphylococcus aureus*, *Streptococcus pneumoniae, Streptococcus sanguinis, Streptococcus sobrinus, Streptococcus mutans*, *Streptococcus pneumoniae*, and *Streptococcus aureus*).

This thesis was organized in five chapters (I–V). **Chapter I** presented a literature review about the problem of MDR bacterial pathogens and the relevance of natural prenylated chalcones as a source of new antibiotics. Among natural products, we highlighted **IBC** and its antibacterial and antimycobacterial activity against several pathogenic bacteria. Moreover, we review all total synthesis approaches described for **IBC**. At the end of chapter I, we present the general and specific aims of chapters II–IV.

In **chapter II,** we presented our total synthesis of **IBC** and its antibacterial activity against six Gram-positive (*S. aureus*, *S. pneumoniae*, *S. sanguinis*, *S. sobrinus*, *S. mutans*, *S. pneumoniae* and *S. aureus*) and two Gram-negative (*Pseudomonas aeruginosa* and *Klebsiella pneumoniae*) bacterial species, as well as against three mycobacteria (*M. tuberculosis*, *M. avium*, *M. kansasii*). Moreover, its synergistic effect, antibiofilm activity, cytotoxicity and mechanism of antibacterial action were elucidated. This chapter was fully published in Membranes journal (ASSIS et al., 2022)

In **chapter III**, we proposed the design, synthesis and antimycobacterial activity against *M. tuberculosis* of **IBC** and its analogs **IBC 1–23** and **DHIBC** discussing structure-antimycobacterial activity-relationship and *in silico* physicochemical, pharmacokinetic and drug-likeness properties.

In **chapter IV**, the antibacterial activity of **IBC** derivatives (**IBC 1–IBC 23**, **DHIBC** and **DHIBC 2**) was evaluated against methicillin-susceptible *Staphylococcus aureus* (MSSA) and methicillin-resistant *Staphylococcus aureus* (MRSA). The most promising compound, 2-hydroxyisocordoin (**IBC 2**) was selected for additional bioassays such as synergistic test, antibiofilm activity, cytotoxicity and mechanism of antibacterial action. Moreover, its spectrum of antibacterial action was investigated against S. *pneumoniae*, *S. sanguinis*, *S. sobrinus*, *S. mutans*, *S. pneumoniae*, *S. aureus*, *P. aeruginosa*, *K. pneumoniae* and *H. pylori*.

Finally, in **chapter V**, we presented a general conclusion, highlighting the main chemical and biological concluding remarks of **IBC** and its analogs, as well as references and supplementary material, containing spectra and chromatograms.

2. Literature Review

2.1. Drug resistance & Antibacterial Drugs

Antibacterial drugs are compounds from natural sources or synthesis procedures, which are used to combat human, animal and plant infections caused by prokaryotic species (WALLER; SAMPSON, 2018). Antibacterial drugs can be classified as bacteriostatic, which inhibit bacterial growth and metabolism without lethal effect, and as bactericidal, which kills bacteria. Moreover, antibacterial drugs can be grouped according to their mechanisms of action: (*i*) inhibition of cell wall biosynthesis (e.g., *β*-lactams and glycopeptides), (*ii*) inhibition of protein biosynthesis (e.g., aminoglycosides, macrolides, tetracyclines, oxazolidinones, lincosamides, streptogramins and amphenicols), (*iii*) increased permeability of bacterial cell

membrane, leading to leakage of intracellular contents (e.g., polymyxins), and (*iv*) interference with replication of bacterial DNA or RNA (e.g., quinolones, rifamycin, sulfonamides and trimethoprim) (WALLER; SAMPSON, 2018).

The drug therapy against urinary tract infections, pulmonary infections, wounds, sepsis, sexually transmitted infections, and some forms of diarrhea, is becoming ineffective due to the high rates of resistance against multiple conventional agents. Drug resistance can be acquired through several mechanisms, mainly involving drug uptake limitation, drug target modification, drug inactivation, biofilm formation and active drug efflux, making infections hard or impossible to treat (BEYER; PAULIN, 2020; REYGAERT, 2018).

The major concern is the infections associated with multidrug-resistant (MDR) strains of *Pseudomonas aeruginosa*, *Acinetobacter baumannii*, *Staphylococcus aureus*, Enterococci and Enterobacteriaceae. In general, these MDR bacteria are involved in nosocomial infections; however, they are becoming prevalent causes of community-acquired infections. These pathogens have become resistant to most available antibiotics, including carbapenems and third-generation cephalosporins, one of the fewer drug classes against MDR infections. (VAN DUIN; PATERSON, 2016).

Annually, approximately 700 mil people die worldwide due to antibiotic-resistant infections, and there is concern that this number may increase by 10 million deaths per year by 2050 (O'NEILL, 2016; VIKESLAND et al., 2019). Several multidisciplinary efforts are required to avoid or reduce impacts, including the discovery and development of innovative antibacterial drugs or improving existing ones.

World Health Organization (WHO) suggested a list of priority of pathogenic bacteria to encourage global efforts in research & development (R&D) of new antibiotics (WHO, 2017). This list (Table 1) included 12 groups of bacterial species grouped according to priority category, critical, high and medium, considering their risks to human health. The criteria applied to establish this ranking are related to fatality rate of infection, including prolonged hospitalizations; resistance of microorganisms to antibiotics in clinical use; transmissibility between people and people as well as people and animals; success of prevention programs and conventional and novel treatments.

Table 1. Priority Pathogens List for Research and Development (R&D) of New Antibiotics

Priority	Bacteria	Drug-resistance
1-CRITICAL	*Acinetobacter baumannii* *Pseudomonas aeruginosa*	carbapenem-resistant
	*Enterobacteriaceae**	carbapenem-resistant, 3rd generation cephalosporin-resistant
2 - HIGH	*Enterococcus faecium*	vancomycin-resistant
	Staphylococcus aureus	methicillin-resistant vancomycin-intermediate and resistant
	Helicobacter pylori	clarithromycin-resistant
	Campylobacter spp. *Salmonellae*	fluoroquinolone-resistant
	Neisseria gonorrhoeae	cephalosporin-resistant fluoroquinolone-resistant
3- MEDIUM	*Streptococcus pneumoniae*	penicillin-non-susceptible
	Haemophilus influenzae	ampicillin-resistant
	Shigella spp	fluoroquinolone-resistant

*Enterobacteriaceae includes *Klebsiella pneumoniae*, *Escherichia coli*, *Enterobacter* spp., *Serratia* spp., *Proteus* spp., and *Providencia* spp, *Morganella* spp.

On the other hand, the number of novel approved drugs is low in comparison to the rate that bacterial resistance spreads. In the last ten years, 15 novel antibacterial agents have been approved by Food and Drug Administration (FDA) for clinical use (BROWN; WOBST, 2021). Among them, avibactam (**1**, *β*-lactamase inhibitor) in combination with ceftazidime, vaborbactam (**2**, *β*-lactamase inhibitor) in combination with meropenem, and lefamulin (**3**, inhibit bacterial protein synthesis) (Figure 1). The other approved drugs are me-too of known antibiotic classes such as tetracyclines, aminoglycosides, fluoroquinolones and others (BROWN; WOBST, 2021).

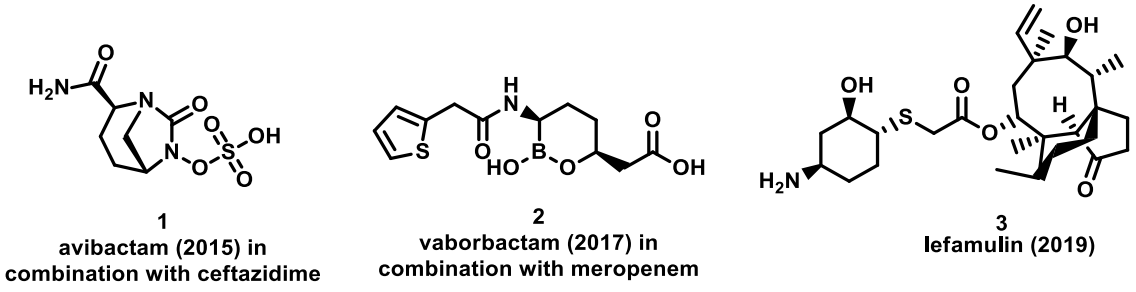

Figure 1. Recently approved antibacterial drugs

Another global infectious disease challenge is tuberculosis (TB), which remained as leading cause of death for several years worldwide from a single infectious agent

(*Mycobacterium tuberculosis*). In 2020, about 1.5 died from TB, the second leading cause of death worldwide, after severe acute respiratory syndrome coronavirus-2 (SARS-CoV2), responsible for the COVID-19 pandemic (WHO, 2021). It was reported 9.9 million TB cases, a slight decline (2%) in comparison to the previous year. However, this reduction may be a consequence of disruption of health services for several months, which difficulted the diagnosis of new TB cases. As an aggravating consequence, the number of TB death rise for the first time in more than a decade last year (WHO, 2021). Moreover, people with pre-existing tuberculosis have a higher chance of developing severe complications due to SARS-CoV2 co-infection (GAO et al., 2021).

Standardized TB treatment has at least six months in length, comprising a combination of rifampicin (**4**; RMP), isoniazid (**5**; INH), pyrazinamide (**6**) and ethambutol (**7**) (Figure 2). In 2020, 71% (2.1/3.0 million) of people diagnosed with pulmonary TB were bacteriologically tested for rifampicin resistance (RR-TB), an increase of 61% compared with 2019. Among these, approximately 132 mil new cases of multidrug-resistant TB (MRD-TB; resistant to INH and RMP) were detected (WHO, 2021).

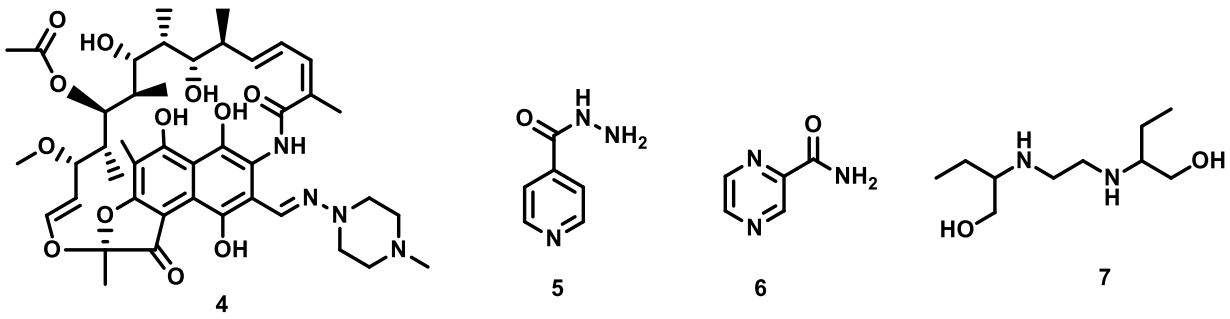

Figure 2. Drugs used for TB treatment

The pharmacotherapy of MDR-TB is relatively more complex, leading to high abandonment rates and treatment failure (SEUNG; KESHAVJEE; RICH, 2015). MDR-TB treatment requires a combination of a least one fluoroquinolone (ofloxacin, levofloxacin or moxifloxacin) and one injectable drug (capreomycin, kanamycin or amikacin) for 18 months. Moreover, the emergence of extensively drug-resistant TB (XDR-TB), resistant to first- and second-line drugs, represents a massive global health challenge (SEUNG; KESHAVJEE; RICH, 2015; WHO, 2021). In the last ten years, delamanid (**8**), pretomanid (**9**), and bedaquiline (**10**) (Figure 3) were approved against MDR-TB and XDR-TB, shortening and improving the anti-MDR TB and anti-XDR TB therapies to 9–11 months (WHO, 2021). However, drug

resistance against these drugs has been reported (BLOEMBERG et al., 2015; GÓMEZ-GONZÁLEZ et al., 2021).

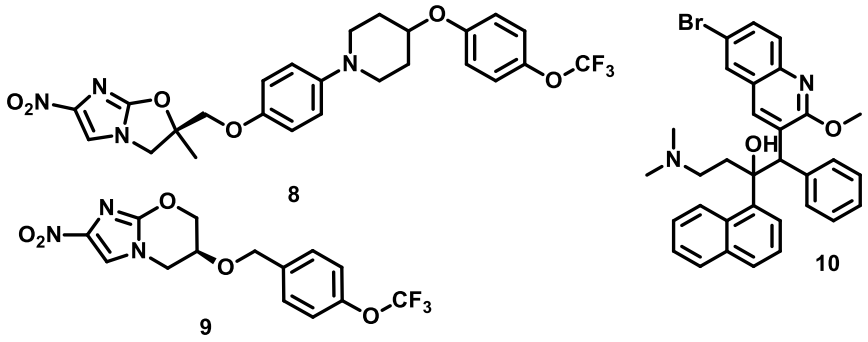

Figure 3. Drugs for MDR-TB and XDR-TB treatment

Other *Mycobacterium* species are involved in pulmonary disease without causing TB, defined as nontuberculous mycobacteria (NTM). Although about 150 species of NTM have been described, just a few species are involved in human pulmonary infections, such as *Mycobacterium avium* complex, *Mycobacterium kansasii*, and *Mycobacterium abscessus.* NTM is becoming a global concern due to the increasing number of cases reported in the last years, including those caused by MDR strains (WASSILEW et al., 2016). The infection caused by NTM is challenging the diagnosis and treatment, requiring a combination of several drugs for a long time, leading to a high dropout rate and treatment failure (RATNATUNGA et al., 2020).

2.2. Natural products & Prenylated Chalcones

FDA and other regulatory agencies for health registration approved 162 antibacterial agents from 1981 to 2019 (NEWMAN; CRAGG, 2020). About 55% were unaltered natural products and their derivatives, highlighting the relevance of natural products as valuable sources for developing new antimicrobial agents (NEWMAN; CRAGG, 2020; ROSSITER; FLETCHER; WUEST, 2017)

One of the promising natural product classes includes chalcones. Structurally, chalcones have a 1,3-diaryl-2-propen-1-one skeleton which can exist as *trans* or *cis* isomers, with the *trans*-isomer being thermodynamically more stable and more abundantly isolated (Figure 4) (ZHUANG et al., 2017). In nature, chalcones are central precursors of further flavonoids with ring C, which is produced after modifications in α,β-unsaturated ketone bridge between rings A and B (ROZMER; PERJÉSI, 2016).

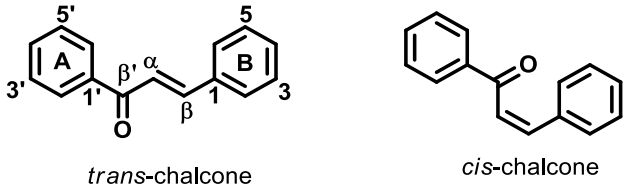

Figure 4. Isomers of chalcone skeleton

There are three chalcone-based compounds marketed as drugs: metochalcone (**11**), with choleretic action; sofalcone (**12**), with antiulcer and gastroprotective properties; and hesperidin methylchalcone associate with *Ruscus aculeatus* extract (Cyclo 3 Fort®, **14**) as vasoprotective agent (Figure 5) (ALLAERT et al., 2011; KONTUREK et al., 1986; SAHU et al., 2012). In the initial screening of antiulcer assays, sofalcone (**12**) was selected among a series of synthetic derivatives of sophoradine (**13**), which is isolated from roots of *Sophora subprostrata*, a Chinese medicinal herb (Figure 5) (KYOGOKU et al., 1979). These findings reinforce the relevance of natural chalcones as a prototype compound in develop of new biologically active entities.

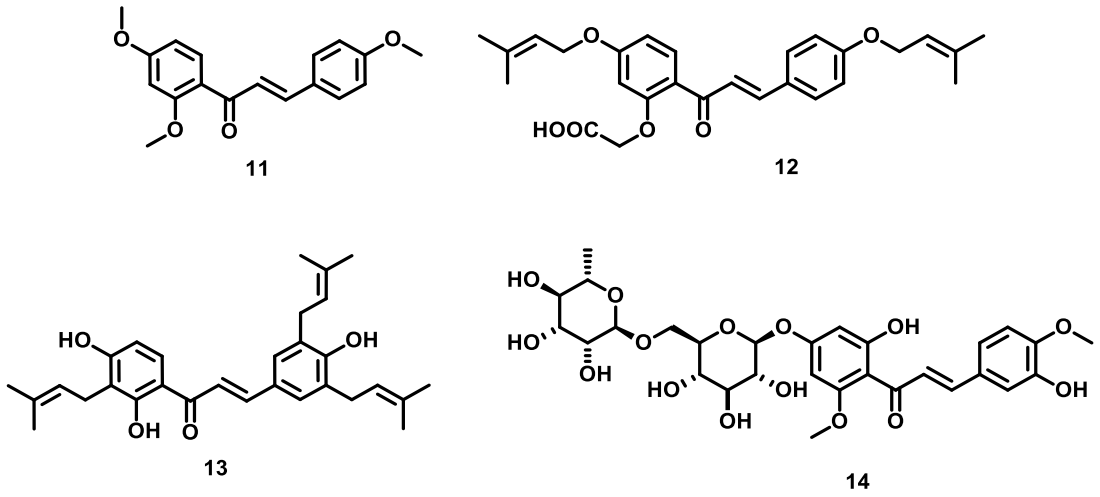

Figure 5. Metochalcone (**11**), sofalcone (**12**), sophoradin (**13**) and hesperidin methylchalcone (**14**)

There is a great diversity of natural chalcone reported in literature due to the variety of substituents on aromatic rings (ZHUANG et al., 2017). Most of natural chalcones demonstrates hydroxyl and methoxyl groups on aromatic rings. Prenyl is another common substituent group that composes the structure of several natural chalcones (CAESAR; CECH, 2016; CHEN et al., 2014).

The prenyl side chain is linked at rings A and B by carbon and oxygen atoms., generating *O*-prenylchalcones and *C*-prenylchalcones, respectively (CHEN et al., 2014; ROZMER; PERJÉSI, 2016). Prenyl side chain is a terpenoyl group containing at least five carbon atoms, which can be found with different organization and lengths, such as 3,3-dimethylallyl in xanthohumol (**15**) and 4-hydroxycordoin (**16**) (EPIFANO et al., 2007; SRINIVASAN; GOLDBERG; HAAS, 2004); as 1,1-dimethylallyl in licochalcone A (**17**) (NIELSEN et al., 1998); as geranyl ((*E*)-3,7-dimethyl-2,6-octadienyl) in xanthoangelol (**18**) (INAMORI et al., 1991), and as lavandullyl (5-methyl-2-isoprophenyl-hex-4-enyl) in kuraridin (**19**) (SASAKI et al., 2014) (Figure 6). Moreover, these substituents can be found in their oxidated or cyclized forms (**20**–**23**) (CHIANG et al., 2010; ELSOHLY et al., 2001; FRÖLICH et al., 2005; YE et al., 2016).

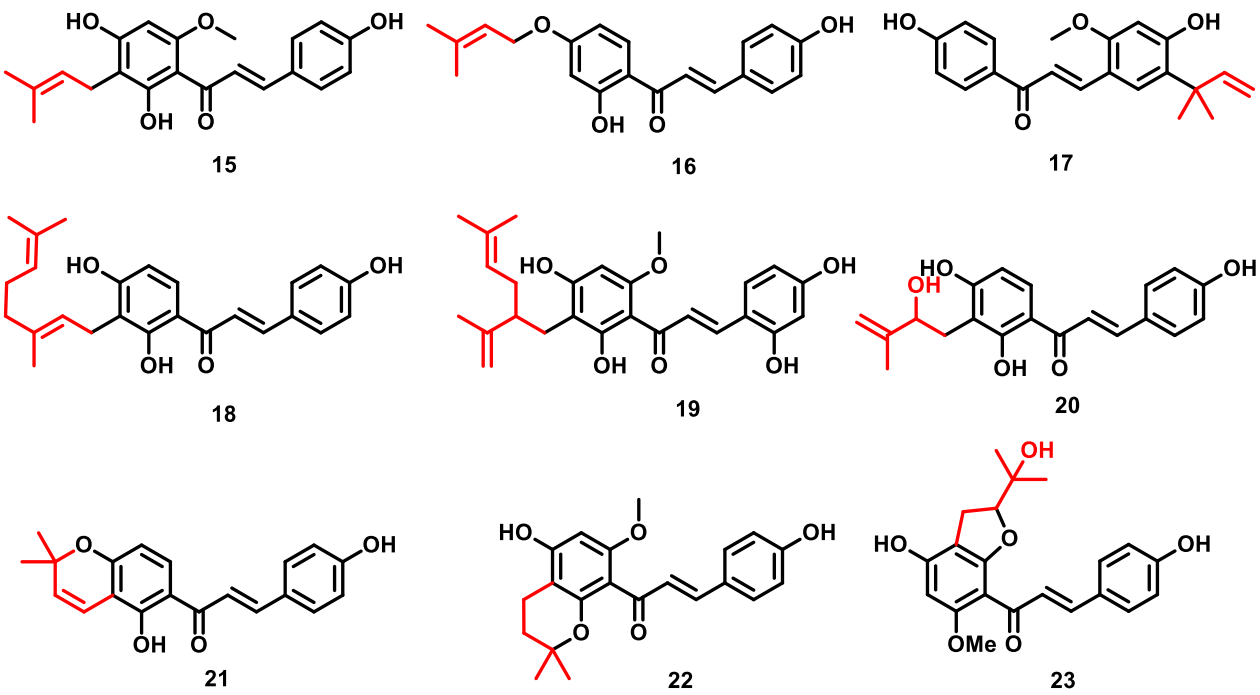

Figure 6. Natural prenylated chalcones

C-prenylated chalcones are abundant in specie of Fabaceae, Moraceae, Cannabaceae, Guttiferae, Umbelliferae, and Rutaceae families (ROZMER; PERJÉSI, 2016). Several bioactivities are described for extracts of these plants, including anticancer, antioxidant, anti-inflammatory, antiviral, antibacterial and antifungal. Most of them were related to their *C*-prenyl phenolic compounds (BOLTON et al., 2019; CAESAR; CECH, 2016; CHEN et al., 2014; KIL et al., 2017; KOUL et al., 2019; LIU et al., 2015; PENICHE-PAVÍA; VERA-KU;

PERAZA-SÁNCHEZ, 2018). Moreover, prenyl group generally increases the lipophilicity of phenolic compounds facilitating their penetration through biological membranes, which can increase their biological activity due to higher interaction between chalcone and intracellular receptors (BOTTA et al., 2010).

2.2.1 Isobavachalcone

Isobavachalcone (**IBC**) (Figure 7) is a *C*-prenylated chalcone, which was isolated in 1968 from *Psoralea corylifolia*, a traditional Chinese medicinal plant (BHALLA; NAYAK; DEV, 1968). **IBC** has been found in 18 plant species from Fabaceae, Clusiaceae, Moraceae, Schisandraceae and Apiaceae families (KUETE; SANDJO, 2012).

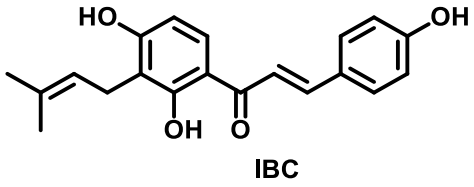

Figure 7. Isobavachalcone (**IBC**)

Several bioactivities has been described for **IBC**, such as anticancer, antiviral, antibacterial, antifungal and others (KUETE; SANDJO, 2012; WANG et al., 2021). Due to the great variety of bioactivities found for **IBC**, it was recently reported as a versatile compound which can be used for modification and optimization in drug discovery processes (WANG et al., 2021). Herein, we highlighted the antibacterial and antimycobacterial activities of **IBC**.

2.2.1.1 Antibacterial Activity of IBC

The antibacterial activity of **IBC** is well-known, including the effects against human pathogenic bacteria (WANG et al., 2021). Yin and co-workers (2004) reported for the first time the antibacterial activity of **IBC** from *Psoralea corylifolia* seeds, against Gram-positive bacteria (*Staphylococcus aureus* and *Staphylococcus epidermidis*), using bakuchiol and magnolol, two natural antibacterial agents as positive controls. **IBC** showed Minimal Inhibitory Concentration (MIC) of 5.8 µg/mL and 2.9 µg/mL against *S. aureus* and *S. epidermidis*, respectively, which was twice lower than bakuchiol and magnolol (YIN et al., 2004).

Chacha and co-workers (2005) isolated **IBC** from *Erythrina latissimi* stems, which was assayed against *S. aureus*, *Bacillus cereus*, and *Escherichia coli* using a thin layer chromatography (TLC) bioautographic technique. **IBC** was more active against Gram-positive

species, showing Minimal Inhibitory Amount (MIA) of 0.01 µg/spot against *S. aureus* and *B. cereus*. Whereas against Gram-negative *Escherichia coli*, the MIA was 0.50 µg/spot (CHACHA; BOJASE-MOLETA; MAJINDA, 2005).

Gram-positive bacteria were more susceptible to **IBC** than Gram-negative bacteria according to studies of Ávila (2008) and Sugamoto (2011). Ávila et al. demonstrated that **IBC** showed MIC and Minimal Bactericidal Concentration (MBC) values of 31.2 µg/mL against *S. aureus* and *B. cereus* (ÁVILA et al., 2008). While in studies of Sugamoto, **IBC** showed potent activity against *B. subtilis*, *S. epidermidis*, and *Micrococcus luteus*, with MIC of 4 µg/mL (SUGAMOTO et al., 2011). In both studies, **IBC** was inactive against Gram-negative species (*P. aeruginosa*, *E. coli*, *Proteus mirabilis* and *Pseudomonas fluorescens*) (ÁVILA et al., 2008; SUGAMOTO et al., 2011).

The comparison between antibacterial activity of **IBC** and related analogs, such as isoliquiritigenin (**24**) and isocordoin (**25**) (Figure 8), suggested that a *p*-hydroxyl an C-3' isoprenyl on rings B and ring A, respectively, were essential, considering that their removal led to the loss of **IBC** bioactivity (ÁVILA et al., 2008; SUGAMOTO et al., 2011). Furthermore, the prenyl group attached to the aromatic ring A in its cyclized or *O*-prenylated form, as found in 4-hydroxylonchocarpin (**21**, Figure 6) and 4-hydroxycordoin (**16**, Figure 6), respectively, led to a significant bioactivity decreasing (SUGAMOTO et al., 2011). The variation of prenyl from C-3' to C-5' in bavachalcone (**26**, Figure 8) and its permutation to geranyl group in xanthoangelol (**18**, Figure 6) did not affect antibacterial activity.

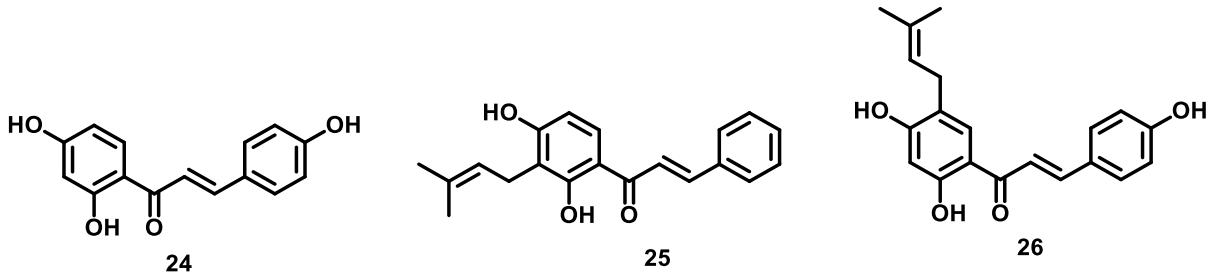

Figure 8. Structure of isoliquiritigenin (**24**), isocordoin (**25**) and bavachalcone (**26**)

Mbaveng and co-workers investigated the antibacterial of **IBC** against several clinical isolates of Gram-positive and Gram-negative species (MBAVENG et al., 2008). **IBC** demonstrated remarkable activity against all Gram-positive species (*Streptococcus faecalis*, *S. aureus*, *Bacillus cereus*, *Bacillus megaterium*, *Bacillus stearothermophilus*, and *B. subtilis*) with MIC and MBC values ranging from 0.3 to 1.2 µg/mL. Additionally, **IBC** was active against most Gram-negative bacteria (*Citrobacter freundii*, *Enterobacter aerogens*,

Enterobacter cloacae, E. coli, Klebsiella pneumoniae, Morganella morganii, Proteus mirabilis, Proteus vulgaris, P. aeruginosa, Shigella dysenteriae, Shigella flexneri, and *Salmonella typhi*), demonstrating MIC and MBC values ranging from 0.6 to 39.1 µg/mL. The lowest MIC value (0.3 µg/mL) observed against Gram-positive and Gram-negative bacteria strains was about 4-fold lower than gentamycin, which was used as the reference antibiotic drug.

The activity of **IBC** against American Type Culture Collection (ATCC) strains and MDR clinical isolates of *E. coli, E. aerogenes, K. pneumoniae, P. aeruginosa*, and *Enterobacter cloacae* was increased with phenylalanine arginine ß-naphthylamide (PAßN), an efflux pump inhibitor (KUETE et al., 2010a). Efflux pump is one of the major mechanisms of Gram-negative bacteria that pump out the antibiotics from intracellular medium to the external environment. **IBC** alone exhibited antibacterial activity against most of bacteria, with the lowest MIC value (8 µg/mL) against *E. aerogenes* EA298. MDR isolated of *E. aerogens* and *K. pneumoniae* were more susceptible to **IBC** than chloramphenicol. In the presence of PAßN, the antibacterial activities of **IBC** against *E. coli*, *K. pneumoniae*, *P. aeruginosa, E. aerogens* and *E. cloacae* were significantly increased, by 4 to 64-fold. The antibacterial activity of **IBC** + PAßN was higher than chloramphenicol against six out of eight *E. aerogenes* strains.

Antibacterial activity of **IBC** against Gram-negative bacteria was evaluated by Kuete et al. (2010a) against *Neisseria gonorrhoeae* strains, including one drug-susceptible (MIC = 0.6 µg/mL) and nine resistant clinical isolates (0.6 µg/mL ≤ MIC ≤ 9.8 µg/mL). These MIC values were lower than or equal to gentamycin, indicating **IBC** could be a promising compound to treat gonorrheal infections (KUETE et al., 2010b).

Osório et al. (2012) demonstrated that **IBC** was active against Methicillin-Susceptible *Staphylococcus aureus* (MSSA) and fourteen clinical isolates of Methicillin-Resistant *Staphylococcus aureus* (MRSA), displaying MIC values of 31.1 µg/mL against MSSA and MIC ranging from 15.6 to 62.5 µg/mL against MRSA (OSÓRIO et al., 2012). The anti-MRSA activity of **IBC** from *P. corylifolia* was tested in the studies of Cui and co-workers against two clinical isolates (OM481 and OM584) with MIC value of 7.8 µg/mL (CUI et al., 2015).

Song et al (2021) demonstrated **IBC** antibacterial activity against MSSA, MRSA (T144) and Vancomycin-Resistant *Enterococcus faecium* (VRE_{fm}) in concentrations lower than 4 µg/mL. Otherwise, **IBC** was inactive against colistin-sensitive and resistant strains of *P. aeruginosa, A. baumannii*, *K. pneumoniae*, and *E. coli*. However, in combination with colistin, **IBC** fully restored the sensitivity of colistin-resistant *E. coli* strains to colistin, decreasing the MIC values to lower than 0.5 µg/mL. Song and co-workers demonstrated the efficacy of **IBC** *in vivo* in two mouse model associated with bacterial infections. **IBC** at 8 mg/Kg decreased the

MSSA skin wound infection and VRE gut colonization about 7 to 15 days after infection (SONG et al., 2021).

The antibacterial mode of action of **IBC** is related to the disrupting action on bacterial membranes (DZOYEM et al., 2013; HE et al., 2018; SONG et al., 2021). **IBC** damaged the MSSA membrane, evidenced by diS-C3-(5) dye experiments, leading to macromolecular biosynthesis inhibition (DZOYEM et al., 2013). Song and collaborators described the **IBC** binding to the MSSA phospholipids, resulting in the dissipation of proton motive force and metabolic perturbations (SONG et al., 2021). Additionally, the antibacterial effect of **IBC** has been correlated with the leakage of alkaline phosphatase due to the impairment of the cell wall and cell membrane damage, the inhibition of protein and nucleic acids biosynthesis, and the inhibition of energy metabolism (HE et al., 2018).

2.2.1.2 Antimycobacterial activity of **IBC**

Two studies reported the antimycobacterial activity of **IBC** (CHIANG et al., 2010; KUETE et al., 2010b). Kuete et al. (2010b) isolated **IBC** from *D. barteri* twigs and assayed it against *Mycobacterium smegmatis*, *M. tuberculosis* H37Rv (ATCC 27294), and two clinical isolates of *M. tuberculosis*, including drug-sensitive strain (MTCS2) and INH-resistant strain (MTCS1) (KUETE et al., 2010b). **IBC** demonstrated activity against *M. smegmatis* with MIC value equal to ciprofloxacin (MIC = 2.44 µg/mL). This MIC value was also detected against *M. tuberculosis* H37Rv, with INH as reference tuberculostatic drug (MIC = 0.31 µg/mL). **IBC** was active against MTCS1 (MIC = 19.5 µg/mL), whereas INH was inactive (MIC_{INH} > 39.1 µg/mL), indicating that the drug-resistance mechanism of MTCS1 to INH was not involved or was less effective against **IBC**. **IBC** was also active against MTCS2 (MIC = 4.88 µg/mL), being twice less active than INH. Moreover, **IBC** demonstrated mycobactericidal action at MIC × 4 after nine days of exposure, whereas for **INH** this effect was observed after 15 days at MIC × 4 (KUETE et al., 2010b).

IBC from *Fatoua pilosa* displayed antimycobacterial activity against *M. tuberculosis* H37Rv, with MIC value of 17.5 µg/mL, 2.8-fold higher than ethambutol used as reference tuberculostatic drug (CHIANG et al., 2010). In addition, **IBC** was an inhibitor of extracellular nuclease (Rv0888) from *Mtb* H37Rv, which may act as a virulence factor related to the persistence of *M. tuberculosis* in the host (DANG et al., 2016).

2.2.1.3 Total Syntheses of Isobavachalcone (IBC)

Dong et al. have firstly described the total synthesis of **IBC** in 2009 (Scheme 1) (DONG et al., 2009). From the first total synthesis, other three synthetic routes were well-established (GREALIS et al., 2013; SUGAMOTO et al., 2011; WANG et al., 2014, 2015). All synthetic routes used 2',4'-dihydroxyacetophenone (**27**) as starting material. In the first step described by Dong (2009), **27** was prenylated at C-3' position using isoprenyl bromide under alkali conditions, obtaining **27a** and its 5' prenylated regioisomer **27b** (DONG et al., 2009) (Scheme 1). Then, further steps proceeded as follows: *p*-methomethoxylation of **27a** to obtain **28**; Claisen-Schmidt aldol condensation between **28** with 4-methoxymethoxybenzaldehyde, furnishing chalconic intermediary **29**, which was submitted to deprotection reaction, yielding **IBC** (Scheme 1).

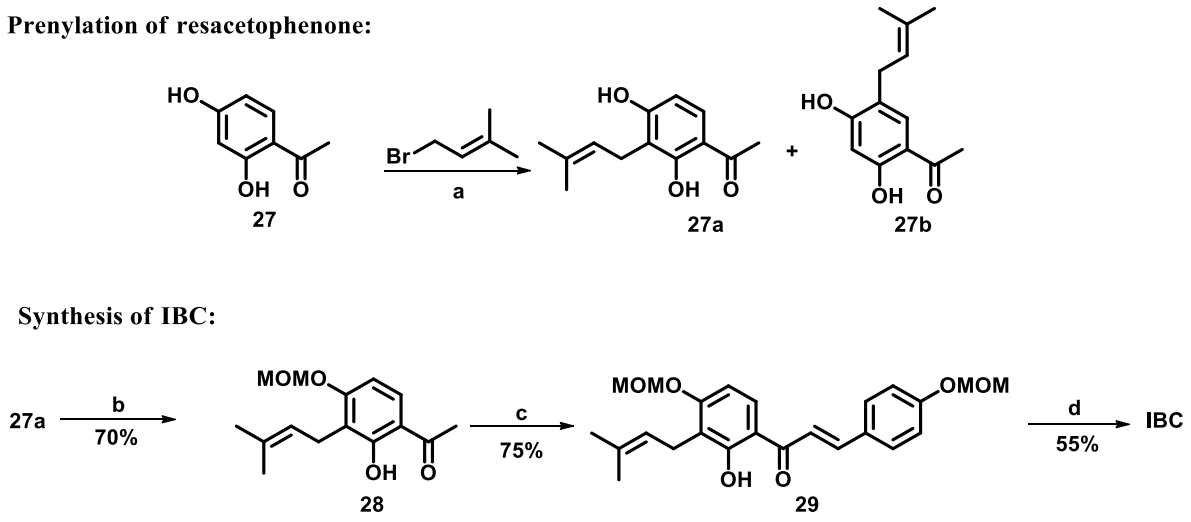

Scheme 1. First Total Synthesis of **IBC** by Dong et al. (2009): (a) 1.3M NaOH, acetone, 3,3-dimethylallyl bromide, reflux (b) methoxymethyl chloride (MOMCl), K_2CO_3, acetone, 0 ºC → rt; (c) 4-methoxymethoxybenzaldehyde, KOH, EtOH, rt; (d) 3M HCl, MeOH, reflux

Grealis and collaborators reported the *C*-prenylation of **27** using similar conditions used by Dong et al., yielded four prenylated resacetophenones **27a** (12%), **27b** (12%), 3,5-diprenyl derivative **27c** (5 %), and a prenyloxy-resacetophenone **27d** (2%) (Scheme 2). Moreover, **27** was recovered more than 50% amount. Due to the difficult in stressful chromatographic purifications and low regioselectivity, Grealis proposed *C*-3'-prenylation using regioselective iodination and Stille coupling reaction as key steps (Scheme 3) (GREALIS et al., 2013). First, **27** was regioselectivity iodized at C3-position, obtaining **30** with 74% yield, which was *bis*-methoxymethylated. Then, 2,4-*Bis*(methoxymethoxy)-3-iodo-resacetophenone (**30a**) was *C*-

prenylated using prenyltributylstannane and $Pd(PPh_3)_4$, furnishing prenylated acetophenone **31** (45%). However, there was a release of iodine in 51%, furnishing 2',4'-*bis*(methoxymethoxy)resacetophenone **31a**. Using this route, **IBC** was obtained with an overall yield of 15% (GREALIS et al., 2013).

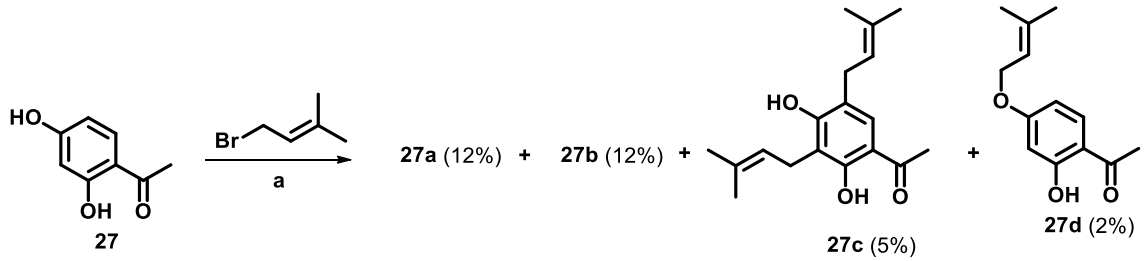

Scheme 2. Prenylation of resacetophenone (GREALIS et al., 2013): (a) KOH, acetone,3,3-dimethylallyl bromide, water, N_2, overnight.

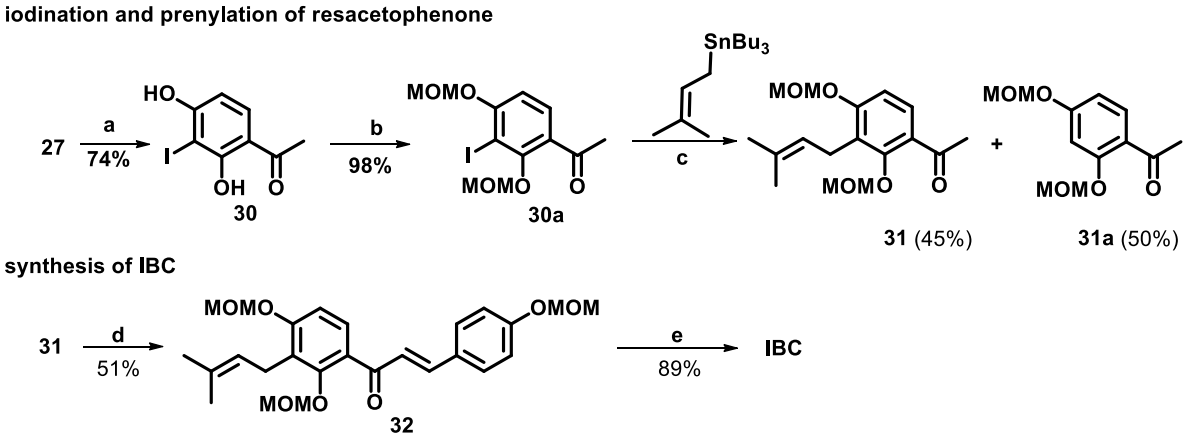

Scheme 3. Total Synthesis of **IBC** by Grealis et al (2013) (a) KIO_3, NaI, AcOH, rt, 4 h; (b) NaH, MOMCl, THF, rt, overnight; (c) $Pd(PPh_3)_4$, DMF, 100 ºC, 40 h; (d) 4-methoxymethoxybenzaldehyde, K_2CO_3, MeOH, reflux., overnight (e) 2M HCl, MeOH, reflux, 3h.

Sugamoto and co-workers described the total synthesis of **IBC** using [1,3]-sigmatropic rearrangement of 2'-prenyloxychalcone **33** and montmorillonite K10 clay (SUGAMOTO et al., 2011). The rearrangement of **23** led to formation of two *C*-prenylated chalcones at C-3', C-5' or both, with yields of 33, 28, and 1 %, respectively (Scheme 4). In this reaction occurred the release of prenyl group, furnishing 2'-hydroxy-4',4-*bis*(methoxymethoxy)chalcone with 28% yield. Excepting digenarylated analogue, these chalcones were deprotected under acid conditions, giving **IBC**, bavachalcone (**26**), and isoliquiritigenin (**24**), respectively. **IBC** was obtained with an overall yield of 17% (SUGAMOTO et al., 2011).

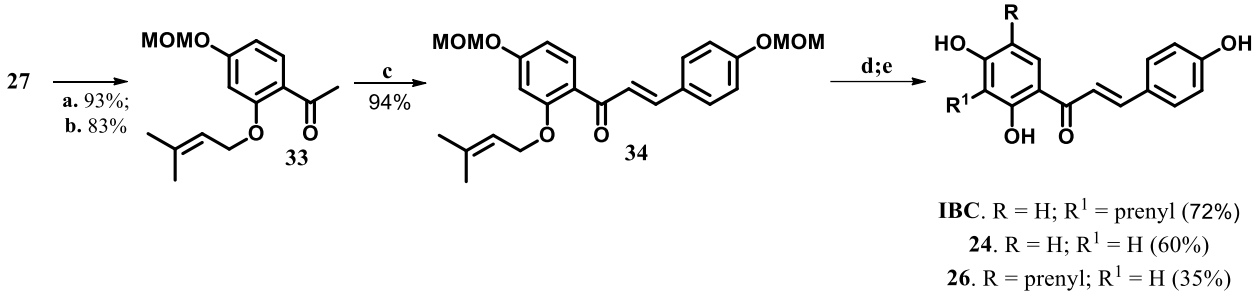

Scheme 4. Total synthesis of **IBC**, xanthoangelol, and isoliquiritigenin by Sugamoto et al (2011): (a) MOMCl, K_2CO_3, acetone, 0ºC, 3h; (b) 3,3-dimethylallyl chloride, acetone, reflux, 24h; (c) 4-methoxymethoxybenzaldehyde, 3M NaOH, EtOH, rt, 24h; (d) Montmorillonite K10, CH_2Cl_2, 0ºC, 0.5h; (e) 3M HCl, MeOH, reflux, 0.5h.

Wang et al. reported the total synthesis of **IBC** with a relatively high overall yield (55%), using regioselective iodination and Suzuki-Miyaura cross-coupling reactions as key steps (Scheme 5) (WANG et al., 2014, 2015). 3-iodo-resacetophenone (**30**) was obtained with high yield (98%), which was *Bis*-MOM protected and used to prepare iodized chalconic intermediary **35** by Claisen-Schmidt condensation with 4-methoxymethoxybenzaldehyde. This intermediary was submitted to Suzuki-Miyaura cross-coupling reaction, using prenyl boronic acid pinacol ester (**37**) and $PdCl_2$(ddpf) as catalyst. Prenylated chalcone **32** was MOM-deprotected, furnishing **IBC** with 75% yield.

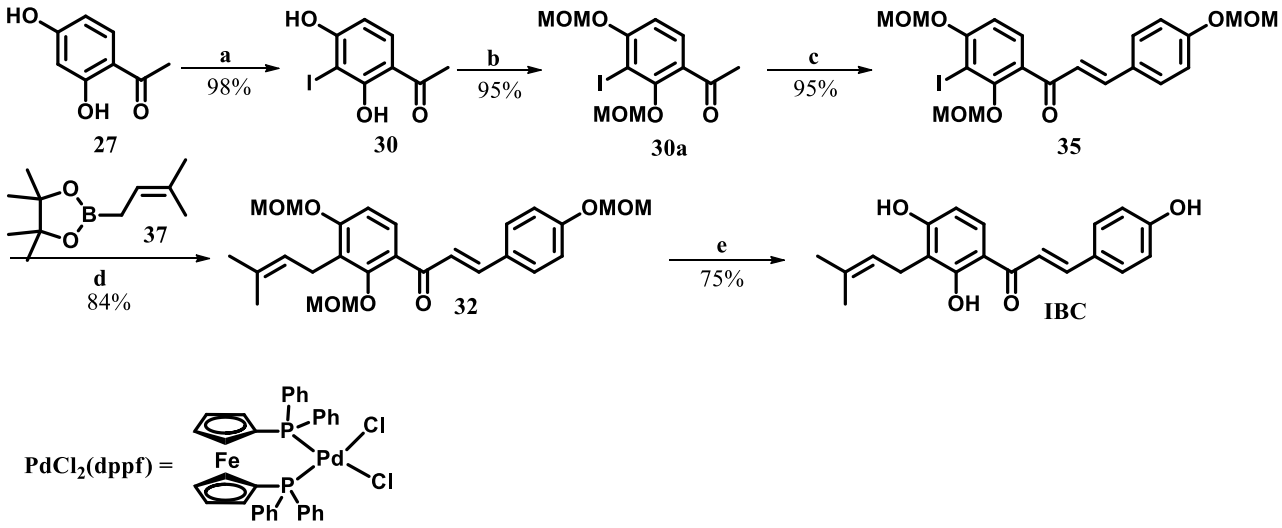

Scheme 5. Total Synthesis of **IBC** by Wang et al (WANG et al., 2015): (a) iodine, KIO_3, EtOH:H_2O (2:3), rt, overnight. (b) MOMCl, NaH, 0 ºC, 2h; (c) 4-methoxymethoxybenzaldehyde, 60% KOH, EtOH, rt, 12h; (d), $PdCl_2$ (ddpf), Cs_2CO_3, DMF, 70 ºC, microwave, 2 h; (e) 1M HCl, 50 ºC, 5h.

3. AIMS

3.1. General aim

In order to design, synthesize and biological evaluate **IBC** and its analogs (**IBC 1–IBC 23**) (Figure 9) against mycobacteria, Gram-positive and Gram-negative species.

3.2. Detailed aims of Chapter II

a) Synthesis and antibacterial activity of **IBC** against *Staphylococcus aureus*, *Streptococcus pneumoniae*, *Streptococcus sanguinis*, *Streptococcus sobrinus*, *Streptococcus mutans*, *Klebsiella pneumoniae*, *Pseudomonas aeruginosa*, *Mycobacterium tuberculosis*, *Mycobacterium avium*, and *Mycobacterium kansasii*;

b) Investigation of the synergetic effects of **IBC** with vancomycin against MSSA and MRSA;

c) Evaluation of **IBC** against MSSA and MRSA biofilm formation;

f) Investigation of **IBC** against membrane of *Bacillus subtilis* membrane;

g) Toxicity evaluation of **IBC** against human keratinocytes.

3.3 Detailed aims of Chapter III

a) Design and synthesis of **IBC** and analogs with modifications on rings A and B and α,β-unsaturated ketone bridge;

b) Antimycobacterial activity of **IBC** and its analogs against *M. tuberculosis* H37Rv;

c) *In silico* investigation of physical-chemistry, pharmacokinetic and drug-likeness properties of antimycobacterial compounds.

3.4. Detailed aims of Chapter IV

a) Antibacterial activity of **IBC** analogs against MSSA and MRSA;

b) Investigation of synergetic effect of selected analog **IBC 2**, a bioactive regioisomer of **IBC**, with vancomycin against MSSA and MRSA;

c) Evaluation of **IBC 2** against MSSA and MRSA biofilm formation;

d) Investigation of **IBC 2** against *Bacillus subtilis* membrane;

e) Toxicity evaluation of **IBC 2** against human keratinocytes.

f) Investigation of antibacterial activity of **IBC 2** against *Streptococcus pneumoniae*, *Streptococcus sanguinis*, *Streptococcus sobrinus*, *Streptococcus mutans*, *Klebsiella pneumoniae*, *Pseudomonas aeruginosa*, and *Helicobacter pylori*.

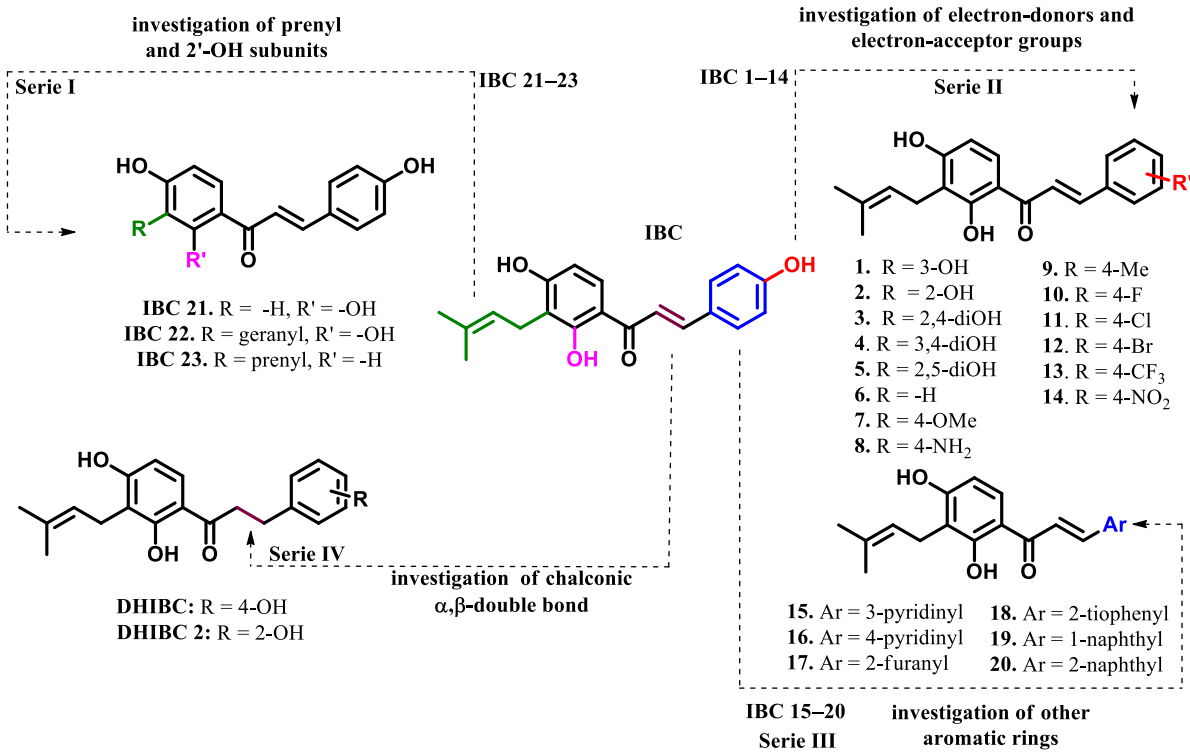

Figure 9. Isobavachalcone (**IBC**) analogs designed in this thesis

CHAPTER II

Antibacterial Activity of Isobavachalcone (IBC) is Associated with Membrane Disruption

Chapter II

Published article

Membranes 2022, v. 12 (3), p. 269

Antibacterial Activity of Isobavachalcone (IBC) is Associated with Membrane Disruption

Leticia Ribeiro de Assis[1], Reinaldo dos Santos Theodoro[1], Maria Beatriz Silva Costa[1], Julyanna Andrade Silva Nascentes[1], Miguel Divino da Rocha[1], Meliza Arantes de Souza Bessa[2], Ralciane de Paula Menezes[2], Guilherme Dilarri[3], Giovane Böerner Hypolito[3], Vanessa Rodrigues dos Santos[4], Cristiane Duque[4], Henrique Ferreira[3], Carlos Henrique Gomes Martins[2], Luis Octavio Regasini[1,*]

[1]Department of Chemistry and Environmental Sciences, Institute of Biosciences, Humanities and Exact Sciences, São Paulo State University (Unesp), São José do Rio Preto 15054-000, SP, Brazil; leticia.assis@unesp.br (L.R.A), reinaldo.theodoro@unesp.br (R.S.T), mb.costa@unesp.br (M.B.S.C.), jullyana.as.nascentes@unesp.br (J.A.S.N), miguelquimic@gmail.com (M.D.R)

[2]Department of Microbiology, Institute of Biomedical Sciences, Federal University of Uberlândia (UFU), Umuarama 38405-320, MG, Brazil; melizaarantes@gmail.com (M.A.S.B), ralciane@ufu.br (R.P.M), carlos.martins2@ufu.br (C.H.G.M)

[3]Department of Biochemistry and Microbiology, Institute of Biosciences, São Paulo State University (Unesp), Rio Claro 130506-900, SP, Brazil; gui_dila@hotmail.com (G.D), giovane.boerner@unesp.br (G.B.H), henfer72@gmail.com (H.F.)

[4]Department of Preventive and Restorative Dentistry, School of Dentistry, São Paulo State University (Unesp), Araçatuba 16015-050, SP, Brazil, vanessarodrigues_22@hotmail.com (V.R.S), cristianeduque@yahoo.com.br (C.D.)

*****Correspondence: luis.regasini@unesp.br (LO Regasini). Tel. +55 17 32212362

ABSTRACT

Isobavachalcone (**IBC**) is a natural prenylated chalcone with a broad spectrum of pharmacological properties. In this work, we synthesized and investigated the antibacterial activity of **IBC** against Gram-positive, Gram-negative and mycobacterial species. **IBC** was active against Gram-positive bacteria, mainly against Methicillin-Susceptible *Staphylococcus aureus* (MSSA) and Methicillin-Resistant *Staphylococcus aureus* (MRSA), with minimum inhibitory concentration (MIC) values of 1.56 and 3.12 µg/mL, respectively. On the other hand, **IBC** was not able to act against Gram-negative species (MIC > 400 µg/mL). **IBC** displayed activity against mycobacterial species (MIC = 64 µg/mL), including *Mycobacterium tuberculosis*, *Mycobacterium avium* and *Mycobacterium kansasii*. **IBC** was able to inhibit more than 50% of the MSSA and MRSA biofilm formation at 0.78 µg/mL. Its antibiofilm activity was similar to vancomycin, which was active at 0.74 µg/mL. In order to study the mechanism of action by fluorescence microscopy, the propidium iodide (PI) and SYTO9 fluorophores indicated **IBC** disrupted the membrane of *Bacillus subtilis*. Toxicity assays using huma keratinocytes (HaCaT cell line) showed **IBC** had not capacity to reduce the cell viability. These results suggested **IBC** is a promising antibacterial agent with elucidated mode of action and potential applications as antibacterial drug and medical devices coating.

Keywords: chalcone, membrane, natural product, antibacterial, biofilm

1. Introduction

Approximately 1 million people died due to antibiotic-resistant infections between 2014 and 2016 around the world, and there is a projection that multidrug resistance will lead 300 million people to premature deaths until 2050 (O'NEILL, 2016; VIKESLAND et al., 2019). The fast and global spread of multidrug-resistant bacteria has been recognized as a great challenge to be overcome in the 21st Century. Thus, stronger efforts are necessary to investigate new antibacterial drugs, which must be active against resistant pathogens to current anti-infective therapy (O'NEILL, 2016).

Natural products (NP) from plants and microorganisms are sources of new antibacterial compounds (NEWMAN; CRAGG, 2020). Among 162 antibacterial agents approved by FDA between 1981 and 2019, about 55% are NP and their derivatives, highlighting their relevance to modern drug discovery (NEWMAN; CRAGG, 2020; ROSSITER; FLETCHER; WUEST, 2017). Among the promising NP, isobavachalcone (**IBC**) is a prenylated chalcone isolated from plants of Fabaceae, Clusiaceae, Moraceae, Schisandraceae and Apiaceae families (Figure 1) (KUETE; SANDJO, 2012; WANG et al., 2021). Moreover, the concise synthesis of **IBC** has

been described by several groups (DONG et al., 2009; GREALIS et al., 2013; SUGAMOTO et al., 2011; WANG et al., 2014, 2015). **IBC** is a privileged compound due to its extensive pharmacological properties, including antibacterial (WANG et al., 2021), anti-cancer (YANG et al., 2019), antifungal (ELSOHLY et al., 2001), antioxidant (ABDULLAH et al., 2017), neuroprotective (XU et al., 2018) and anti-inflammatory (SHIN; SHON; YOUN, 2013) properties.

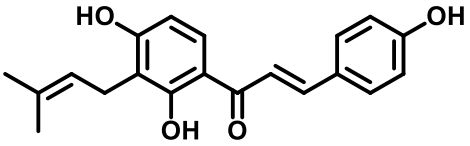

Figure 1. Structure of Isobavachalcone (**IBC**)

As part of our continuing search for novel antibacterial drugs that acts on bacterial membranes, we newly synthesized **IBC** and evaluated its antibacterial activity against Gram-positive, Gram-negative and *Mycobacteria* planktonic cells. Additionally, we investigated the antibacterial activity of **IBC** against biofilms of Methicillin-Susceptible *Staphylococcus aureus* (MSSA) and Methicillin-Resistant *Staphylococcus aureus* (MRSA). **IBC** was tested regarding its effects on the membrane of *Bacillus subtilis*, as well as its toxicity toward human keratinocytes.

2. Materials and Methods

2.1. Isobavachalcone (IBC)

Synthesis **of IBC** was performed according to Sugamoto and collaborators, using six steps (SUGAMOTO et al., 2011). Structure of **IBC** was confirmed by ^{1}H and ^{13}C Nuclear Magnetic Resonance (NMR) and mass spectrometry (MS) data analyses. The purity of **IBC** was determined by high-performance liquid chromatography with a photodiode array detector (HPLC-PAD). Detailed synthetic experimental procedures, NMR spectra, mass spectrum and the HPLC-PAD chromatogram are presented in the Supplementary Material.

2.2. Antibacterial and Antimycobacterial Assays

The strains were purchased directly from the American Type Culture Collection (ATCC) and were maintained in the culture collection of the Laboratory of Antimicrobial Testing (LEA) of the Federal University of Uberlândia state of Minas Gerais, Brazil.

The antibacterial activity was determined against Methicillin-susceptible *Staphylococcus aureus* (ATCC 6538), Methicilin-Resistant *Staphylococcus aureus* (ATCC BAA44), *Streptococcus pneumoniae* (ATCC 6305), *Streptococcus sanguinis* (ATCC 10556), *Streptococcus sobrinus* (ATCC 33478), *Streptococcus mutans* (ATCC 25175), *Klebsiella pneumoniae* (ATCC 10031) and *Pseudomonas aeruginosa* (ATCC 15442). The antimycobacterial activity was determined against *Mycobacterium tuberculosis* H37Rv (ATCC 27294), *Mycobacterium avium* (ATCC 25291) and *Mycobacterium kansasii* (ATCC 12478).

The minimal inhibitory concentration (MIC) against Gram-positive and Gram-negative bacterial species was determined in triplicate using broth microdilution method in 96-well microplates as previously reported, using resazurin as colorimetric indicator of cell viability (LEANDRO et al., 2014). **IBC** was dissolved in DMSO at 1 mg/mL, followed by dilution in brain heart infusion to achieve final concentrations ranging from 400.0 to 0.195 μg/mL. The final DMSO content was 5% (v/v) and this solution was used as negative control. The inoculum was adjusted for each microorganism to reach cell suspension of 5.0×10^5 colony forming units per mL (CFU/mL), as preconized by the Clinical and Laboratory Standards Institute, with modifications in culture medium (CLSI, 2012). Growth control (inoculated well) and sterility control (non-inoculated well free of antimicrobial agent) were also included. Tetracycline and chlorhexidine were used as positive controls and were tested in concentration ranging from 0.0115 μg/mL to 5.9 μg/mL and 0.115 to 59 μg/mL, respectively. The 96-wells microplates were sealed with plastic film and incubated at 37 °C for 24 h. After this period, 30 μL of aqueous solution of resazurin (0.02%) was added to the microplates and was incubated for 15 min at 37 °C. MIC value was defined as the lowest concentration able to inhibit the microorganism growth indicated by the color change of resazurin from blue to pink.

MIC values of **IBC** against mycobacteria species were determined according to Palomino and collaborators protocol, with slight modifications (ALVES et al., 2020; PALOMINO et al., 2002). A stock solution of **IBC** was prepared in DMSO and diluted in Middlebrook 7H9 broth to achieve final concentrations ranging from 7.8 to 1000 μg/mL. Isoniazid was dissolved in DMSO and used as positive control in concentrations ranging from 0.015 to 1.0 μg/mL. The inoculum was prepared by introducing a range of colonies grown in Ogawa-Kudoh in a tube containing glass beads with 500 μL of sterile water. An aliquot of 200 μL was transferred to a tube containing 2 mL of 7H9 broth, incubated at 37 ºC for 7 days and compared with McFarland scale 1 (3.0×10^8 cells/mL). Inoculum was suspended in 96-well plates at a 1:25 ratio with 7H9 broth. The growth controls (without antibiotic) and sterility controls (without inoculation) were also included. The 96-wells plates were incubated at 37 ºC

for 7 days. After this period, 30 µL resazurin 0.02% aqueous solution was added to each plate well. The MIC value was defined as the lowest drug concentration able to inhibit the mycobacterial growth, which was expressed in µg/mL. The assay was conducted in triplicate.

2.3. Checkerboard Assay

The combination effect of **IBC** with vancomycin was evaluated against MSSA and MRSA using microdilution broth checkerboard assay according to White and collaborators, adapted from the standard procedure established by CLSI (CLSI, 2012; WHITE et al., 1996). The fractional inhibitory concentration (FIC) of combination between **IBC** and vancomycin was determined using Mueller-Hinton broth culture medium into 96-well plates, with a final inoculum suspension of 5.0×10^5 CFU/mL. The plates were incubated at 37 ºC for 24 h. After incubation, 0.02% aqueous resazurin solution it was added to wells. Fractional inhibitory concentration index (FICI) was calculated using the Equation 1:

$$\Sigma FIC = FICA + FICB \quad (1)$$

where the FIC is the ratio between the MIC of the drug in combination with the MIC alone. The combination was classified as synergistic (FICI ≤ 0.5), additive (1> FICI > 0.5), indifferent (4> FICI > 1) and antagonistic (FICI ≥ 4) (WHITE et al., 1996). The assays were performed in triplicate on independent experiments.

2.4. Antibiofilm Assay

The inhibition of **IBC** against MSSA and MRSA biofilm formation was evaluated using broth microdilution methodology proposed by CLSI (2012) (CLSI, 2012). The minimum biofilm inhibitory concentration (MBIC) was established as the concentration of **IBC** able to inhibit 50% or more of biofilm formation (WEI; CAMPAGNA; BOBEK, 2006). The MBIC values were determined using two protocols, including biomass assessment by optical density (OD) reading and determination of viable biofilm cells by counting colony-forming units per milliliter (CFU/mL). Two microplates were used for each protocol. Assays were performed in triplicate in three independent experiments. The inoculum concentration and optimal incubation time for this assay were determined by standardizing biofilm formation (data not shown).

Briefly, in 96-well flat-bottom microplates containing Brain Heart Infusion (BHI) broth supplemented with 2% glucose, serial dilutions of the samples were made from the stock solution (1600 µg/mL), obtaining a final concentration between 0.195 to 400 µg/mL. From a 24-h culture on BHI agar plates, the inoculum of *S. aureus* was prepared in BHI broth

supplemented with 2% glucose, with equivalent turbidity on a spectrophotometer operating at 625 nm, to match 0.5 in the McFarland scale (1.5×10^8 CFU/mL). The bacterial suspensions were diluted to the final concentration of 1.0×10^6 CFU/mL. The microplates were incubated at 37 ºC for 24 h. Subsequently, the contents of the wells were aspirated and non-adhered cells were removed by washing with Phosphate Buffered Saline (PBS) buffer (pH = 7.2). The biofilm formed was fixed with methanol for 15 min, dried at room temperature and stained with a crystal violet solution (0.2%) for 20 min. After removing the crystal and washing the wells with PBS buffer, 33% acetic acid was added for 30 min to solubilize the crystal retained in the biofilm. The absorbance of the wells was determined in a spectrophotometer at 595 nm. The determination of CIMB was performed using the Equation 2 (VIEIRA et al., 2018; WEI; CAMPAGNA; BOBEK, 2006).

$$MBIC = (A595\ of\ the\ test \div A595\ of\ the\ untreated\ control) \times 100 \qquad (2)$$

For the determination of viable cells, plates were prepared following the same methodology described above. After the incubation period, the contents of each well were aspirated and washed with PBS buffer to remove non-adhered cells. Then, 200 µL of BHI broth with 2% glucose was added to the wells and the microplate was subjected to an ultrasound bath for 15 min. The content of the wells was homogenized and decimal dilutions was performed (100 to 10^{-7}). After that, 50 µL aliquots of each dilution were plated on BHI agar plates and incubated at 37 ºC for 24 h. Finally, the colonies were counted and the results expressed in $\log_{10}$ scale (CFU/mL).

Vancomycin was used as positive control and was tested in concentrations ranging from 0.0115 to 5.9 µg/mL. Bacterial cells were evaluated in the absence of the antibacterial compounds and was used as negative control. Antibiofilm assays data were analyzed by nonparametric Kruskal–Wallis one-way analysis of variance (ANOVA) with Steel-Dwass-Critchlow-Fligner pairwise comparison test. Results were considered statistically significant with $p<0.05$.

2.5. Membrane Disruption Assay

For the membrane permeabilization assay *Bacillus subtilis* strain 168 was kindly donated by Dr. Frederico Gueiros-Filho, Department of Biochemistry, Institute of Chemistry, São Paulo University.

B. subtilis was cultivated in LB/LB-agar at 30 ºC, with stirring at 200 rpm for liquid medium. A stock solution of **IBC** at 10 mg/mL was diluted into the wells of a 96-multiwell plate to furnish the final concentrations ranging from 100 to 0.781 µg/mL, in total volumes of 100 µL/well (NYG medium) (SAMBROOK; FRITSCH; MANIATIS, 2012; SILVA et al., 2013). The bacteria were inoculated at 1.0×10^5 cells per 100 µL of LB medium per well. Plates were incubated for 12 h at 30 ºC. 15 µL of 0.1 mg/mL resazurin Sigma-Aldrich (Taufkirchen, Germany) was added into each well, followed by a 2h incubation at 30 ºC. The post-reaction plates were evaluated through excitation and emission wavelengths at 530 and 590 nm, respectively, using the Fluorescence Synergy H1N1. The data obtained were used to plot the concentration of the compound versus cell growth inhibition, and through a polynomial curve regression, it was possible to determine the percentages able to inhibit cellular metabolism (MORÃO et al., 2019).

The minimum bactericidal concentration (MBC) was established by inoculating the contents of each REMA well into a 15 cm Petri dish with solid LB medium before the resazurin addition. The microbial transfer was aided by a stamping replicator fit for a 96-well microtiter plate. The cells were incubated in triplicates at 30 °C for 24 h to quantify their growth.

Cells of *B. subtilis* were exposed to the **IBC** at its MBC. In 1 microcentrifuge tubes, 100 µL of 1.0×10^5 cells were used per treatment. After 15 min, 900 µL of saline solution (0.85%) were added to each tube to dilute the compound and stop the contact reaction. For the membrane integrity analyses, cells were stained using the Live/Dead BacLight kit following the instructions of the manufacturer. Cells treated with 1% DMSO and nisin (5 µg/mL) were used as negative control and positive control, respectively (MORÃO et al., 2019). Cells were immobilized on agarose-covered slides before the microscope observations with Olympus BX-61 microscope, equipped with a monochromatic OrcaFlash-2.8 camera. Image acquisition and processing were performed with the software CellSens version 11 (Olympus). Data analyses were conducted with a minimum of 100 cells per treatment (MARTINS et al., 2010).

2.6. Cytotoxicity Assay

Human keratinocytes cells (HaCat) were cultivated in Dulbecco's Modified Eagle's Medium (DMEM; Gibco, Grand Island, NY, USA) supplemented with 10% fetal bovine serum (FBS), penicillin (100 IU/mL), streptomycin (100 µg/mL), and glutamine (2 mmol/L) (ThermoFisher, Waltham, MA, USA) in an incubator with 5% CO_2 at 37 ºC (Isotemp Fisher Scientific, Pittsburgh, PA, USA), being subcultured every 2 days. The cells were seeded (5×

10^5 cells/well) and pre-incubated for 24 h. After that, the cells were treated with **IBC** and standard drug (chlorhexidine) at concentrations ranging from 25 to 0.39 μg/mL in 96 wells microplates for 24h. Then, the culture medium was aspirated, and the cells were incubated with resazurin (70 μM, Sigma Aldrich) in the culture medium and re-incubated for another 4h. Cell viability was read in a spectrophotometer (Biotek, Winooski, VT) at wavelengths of 570 and 600 nm. The values were converted into a percentage of cell viability in comparison to the negative control (DMEM), which was defined as having 100% cell metabolism. The means were determined for each compound.

3. Results and Discussion

3.1. Isobavachalcone (IBC)

Scheme 1 shows our synthetic route for synthesis of **IBC**. As illustrated, resacetophenone (**1**) was used as accessible starting material. A set of six steps, including MOM protection/desprotection, [1,3]-sigmatropic rearrangement and Claisen–Schmidt reactions furnished **IBC** with an overall yield of 12% (Scheme 1). NMR parameters, including chemical shifts, coupling constants and multiplicities as well as molecular weight corresponded to **IBC** structure and were compared with former literature reports(SUGAMOTO et al., 2011; WANG et al., 2015). HPLC-PAD analysis indicated 99% purity according to area peak at 372 nm.

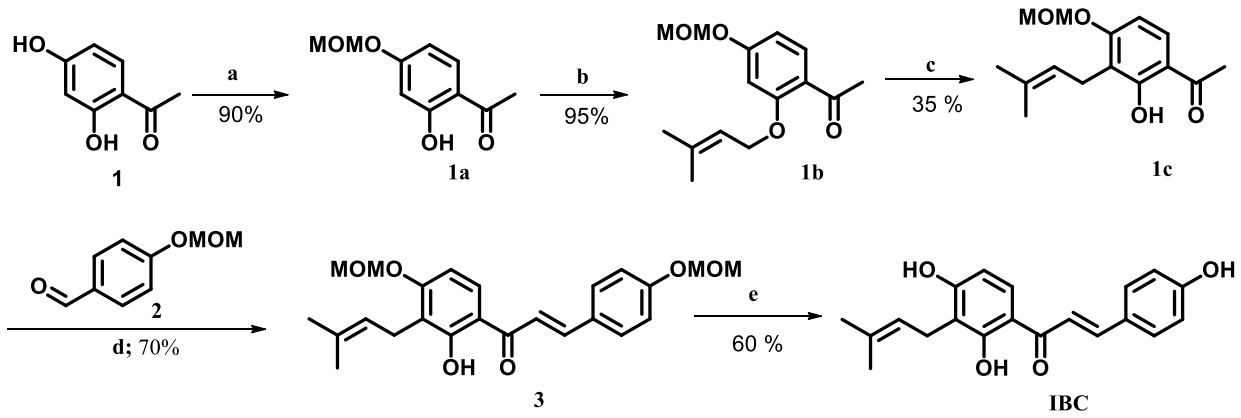

Scheme 1. Synthesis of **IBC**. Reagents and conditions: a) MOMCl, K_2CO_3, acetone, rt, 2h; b) isoprenyl bromide, K_2CO_3, acetone, rt, 24h; c) montmorillonite K10, DCM, rt, 0.5 hours, d) KOH 60%, EtOH, rt, 2h; e) HCl 1 mol L^{-1}, MeOH:THF (1:1), 55 ºC, 6h**.** MOM = methoxymethyl.

3.2. Antibacterial and Antimycobacterial Activities of IBC

In order to assess the antibacterial and antimycobacterial activities, **IBC** was evaluated against five Gram-positive, two Gram-negative and three *Mycobacterium* species (Table 1). Among these species, five microorganisms are in the World Health Organization (WHO) priority list, justifying the discovery for innovative antibacterial agents (WHO, 2017). **IBC** was active against *S. aureus, S. pneumoniae, S. sanguinis, S. sobrinus and S. mutans* planktonic cells, exhibiting MIC values ranging from 1.56 to 50.0 μg/mL. Among these, **IBC** displayed potent activity against MSSA and MRSA, demonstrating MIC values of 1.56 and 3.12 μg/mL. These data are according to studies on anti-*Staphylococcus aureus* effect of **IBC** against standard strains and clinical isolates (DZOYEM et al., 2013; HE et al., 2018). **IBC** was inactive against *P. aeruginosa* and *K. pneumoniae* planktonic cells (MIC > 400 μg/mL).

Table 1. Antibacterial and antimycobacterial activities of **IBC**

	Species	**MIC (μg/mL)**			
		IBC	**Tetracycline**	**Chlorhexidine**	**Isoniazid**
Gram-positive	MSSA	1.56	0.20	-	-
	MRSA	3.12	>5.90	-	-
	Streptococcus pneumoniae	50.0	0.40	-	-
	Streptococcus sanguinis	3.12	-	1.82	-
	Streptococcus sobrinus	6.25	-	3.64	-
	Streptococcus mutans	6.25	-	0.91	-
Mycobacteria	*Mycobacterium avium*	62.5	-	-	0.50
	Mycobacterium kansasii	62.5	-	-	1.00
	Mycobacterium tuberculosis	62.5	-	-	>1.00
Gram-negative	*Pseudomonas aeruginosa*	>400	5.90	-	-
	Klebsiella pneumoniae	>400	2.95	-	-

MSSA = Methicillin-susceptible *Staphylococcus aureus*; MRSA = Methicillin-resistant *Staphylococcus aureus*.

Antimycobacterial assays indicated MIC values of 62.5 μg/mL against *M. avium*, *M. kansasii* and *M. tuberculosis* (Table 1). Two studies described the antitubercular activity of **IBC** against *M. tuberculosis* (CHIANG et al., 2010; KUETE et al., 2010b). In addition, **IBC** was described as an inhibitor of extracellular nuclease Rv0888 from *M. tuberculosis* H37Rv, which acts as a virulence factor and could be related to the persistence of *M. tuberculosis* in the host (DANG et al., 2016).

3.3. Checkerboard assay

In anti-infective drug therapy, the association of drugs is a useful strategy to treat bacterial infections, enhancing the antibacterial potency and decreasing side effects (COTTAREL; WIERZBOWSKI, 2007; VUUREN; VILJOEN, 2011). In this context, hydroxychalcones and aminochalcones showed synergistic association with vancomycin (GARCIA et al., 2021; TRAN et al., 2012). Considering the potent activity of **IBC** against *S. aureus*, we used this species for the checkerboard assay. We evaluated the effect of the combination of **IBC** with vancomycin against MSSA and MRSA planktonic cells (Table 2). The association between **IBC** and vancomycin displayed FICI values of 2.5 and 2.0 against MSSA and MRSA, respectively, indicating an indifferent association.

Table 2. Antibacterial activities of **IBC** in combination with vancomycin

***S. aureus* strain**	**Combination**	**MIC (µg/mL)**				**FICI**	**Type of Combination**
		Alone		**Combined**		**$FIC^{IBC}+FIC^{VAN}$**	
		IBC	**VAN**	**IBC**	**VAN**		
MRSA	**IBC+VAN**	3.12	0.73	1.56	1.47	2.5	indifferent
MSSA	**IBC+VAN**	1.56	0.73	1.56	0.73	2.0	indifferent

VAN = vancomycin

3.4. Antibiofilm Assay

Biofilm can be described as a highly organized sessile community of cells, which are attached to a substratum, interface and complex polymeric matrix (YIN et al., 2019). *S. aureus* has been known to infect and form a chronic biofilm infection in medical devices, being the most common pathogen associated with nosocomial infections (ARCHER et al., 2011; OTTO, 2018). Several chronic infections are associated with *S. aureus* biofilms, including osteomyelitis, periodontitis, chronic wound infections, chronic rhinosinusitis, endocarditis and ocular infections. After the attachment stage, *S. aureus* biofilms are difficult to eradicate with con-ventional antibacterial agents and the host response (ARCHER et al., 2011).

Current antibacterial drugs have not been effective against *S. aureus* biofilms, requir-ing its surgical removal (BHATTACHARYA et al., 2015). Some therapeutic alternatives have been investigated, including antibacterial peptides, vaccines, matrix-degrading enzymes, modulation of quorum-sense system and small molecules inhibitors. Most of them are in preclinical development stage (BHATTACHARYA et al., 2015; OTTO, 2018). Xanthohumol, a prenylated chalcone from hop extracts, showed a potent anti-adherent and antibiofilm activities against *S. aureus* (BOGDANOVA et al., 2018; ROZALSKI et al., 2013). As part of

our efforts in the discovery of novel antibiofilm agents, we described the effect of chalcones against bacterial and fungal biofilms (EMERI et al., 2019; GARCIA et al., 2021; SARDI et al., 2017).

IBC and vancomycin were evaluated in concentrations ranging from 0.195 to 400 µg/mL and 0.0115 to 5.9 µg/mL, respectively. **IBC** displayed antibiofilm activity with MBIC values of 0.78 µg/mL against MSSA and MRSA (Figure 2). At this concentration, **IBC** was able to inhibit 75% biofilm formation. Vancomycin displayed MBIC value of 0.74 µg/mL against MSSA and MRSA, demonstrating 90% biofilm formation inhibition. Moreover, in the presence of IBC at MBIC value, the number of viable cells of MSSA and MRSA decreased about 9 CFU/mL when compared with the untreated control.

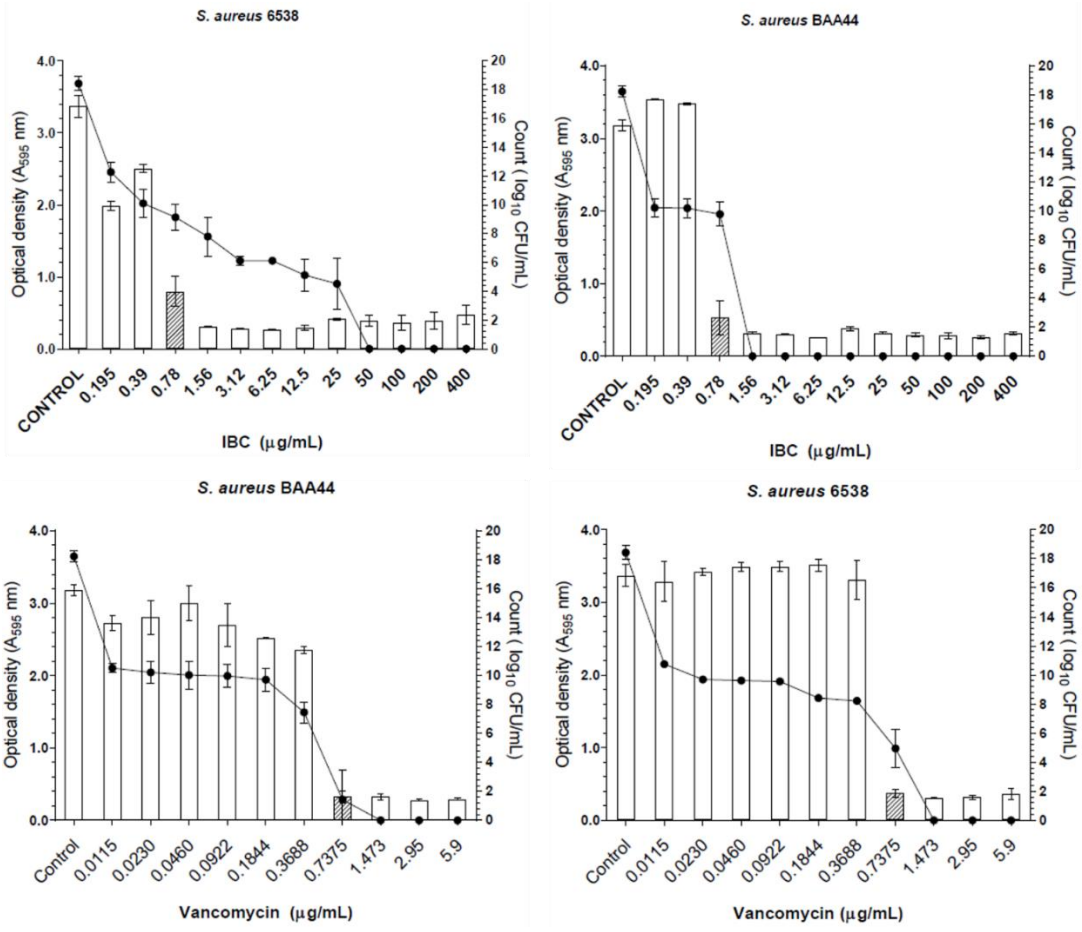

Figure 2. Effect of **IBC** and vancomycin on MSSA (*S. aureus* 6538) and MRSA (*S. aureus* BAA44) biofilm formation. The hatched bars represent the MBIC values. The lines represent the $\log_{10}$ CFU/mL.

3.5. Membrane Disruption Assay

In order to investigate the action of **IBC** on the bacterial membrane, we used *B. subtilis*, which is a non-pathogenic Gram-positive bacteria used for studies of antibacterial mode of action (MORÃO et al., 2019). Bacterial cells were treated with **IBC** at its MBC value (3.13 µg/mL) for 15 min, as well as with nisin (positive control), an antibiotic that targets the bacterial membrane producing pores (WIEDEMANN; BENZ; SAHL, 2004). Two fluorescent dyes propidium iodide (PI) and SYTO9 were added, which stain cells with disrupted membranes (in red) and intact membranes (in blue) (NAVARRO et al., 2020). Representative fluorescence microscopy images of the negative control (cells treated with 1% DMSO), the positive control (nisin at 5.0 µg/mL) and **IBC** were presented in Figure 3. The percentages of cells with damaged membranes were quantified from the microscope images (Figure 4). Cultures treated with 1% DMSO had approximately 10% of the cells with membranes permeabilized. Treatment with nisin demonstrated 95% of the cells stained with PI/SYTO9 due to its ability to makes pores in the bacterial membrane. Treatment of **IBC** displayed damage percentages of 75%.

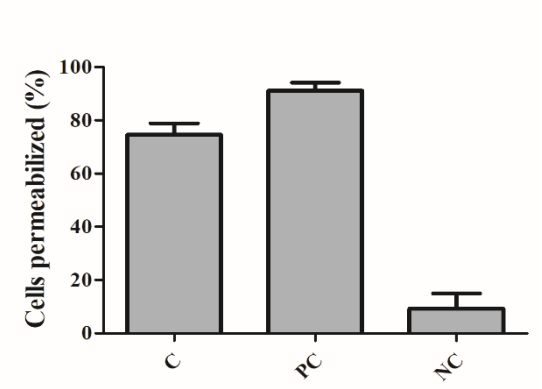

Figure 3. Percentage of disrupted *Bacillus subtilis* cells. C: cells treated with **IBC**; PC: cells treated with nisin (positive control) and NC: cells treated with 1% DMSO (negative control).

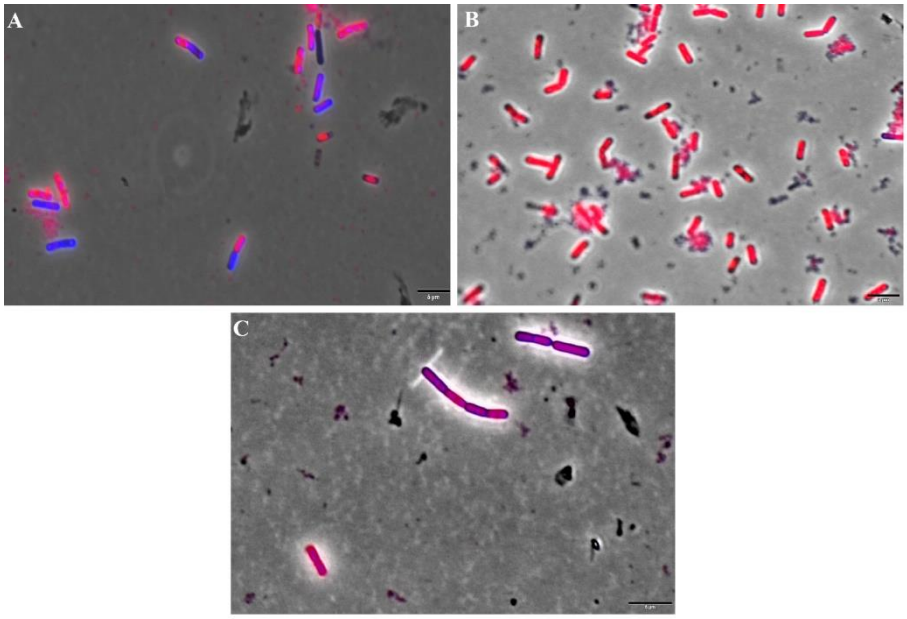

Figure 4. Fluorescence Microscopy of *Bacillus subtilis* stained with propidium iodide and SYTO9. (**A**) negative control (cells treated with 1% DMSO); (**B**) positive control (cells treated with nisin at 5.0 µg/mL). (**C**) cells treated with **IBC**. Magnification 100 ×; Scale bar 5 µm.

Our finds are corroborated by other studies, which reported that the antibacterial mode of action of **IBC** is related to the disrupting action on bacterial membranes. **IBC** was able to cause damage to the MSSA membrane, evidenced by diS-C3-(5) dye experiments, leading to macromolecular biosynthesis inhibition (DZOYEM et al., 2013). Song and collaborators described how **IBC** binds to the phospholipids of MSSA membrane, resulting in the dissipation of proton motive force and metabolic perturbations (SONG et al., 2021). Palko-Labuz and coauthors identified **IBC** as membrane-perturbing agent of human colorectal adenocarcinoma cells. **IBC** was able to be intercalated into model membranes, affecting phospholipid phase transition (PALKO-ŁABUZ et al., 2021). Additionally, the antibacterial effect of **IBC** has been correlated with the leakage of alkaline phosphatase (AKP) due to the impairment of the cell wall and cell membrane damage, the inhibition of protein and nucleic acids biosynthesis as well as the inhibition of energy metabolism (CUSHNIE; LAMB, 2011; HE et al., 2018).

3.6. Cytotoxicity Assay

The evaluation of new antibacterial compounds against human cells is an important step for investigations of their selectivity and safety. The toxicity of **IBC** was tested against epidermal human keratinocytes (HaCaT cell line), which was chosen because skin is a typical site of *S. aureus* colonization (GONG et al., 2006). **IBC** was not able to reduce the cell viability

of HaCaT cells at the highest concentrations (25 µg/mL) after 24 h (Figure 5). This concentration is approximatively 20 times higher than the MIC values obtained from assays MSSA and MRSA, indicating **IBC** has selectivity at its antibacterial concentration. Moreover, **IBC** demonstrated to be less cytotoxic than chlorhexidine at concentrations equal to or higher than 12.5 µg/mL.

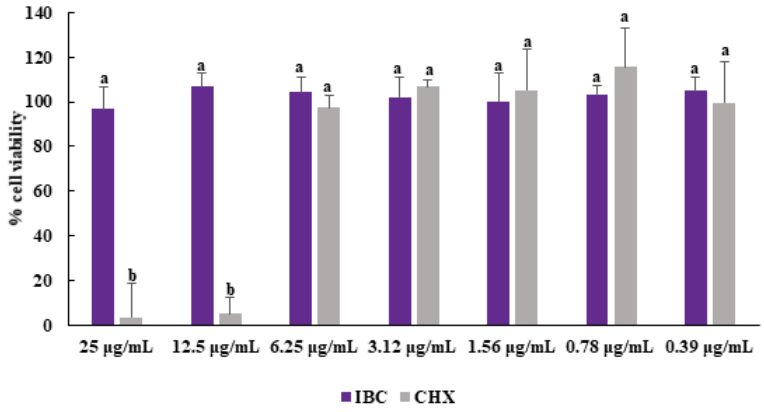

Figure 5. Effect of **IBC** and chlorhexidine on the viability of HaCaT cells. The results are expressed as means ± SDs. Different lowercase letters (a,b) show statistical difference between **IBC** and **CHX** according to ANOVA and Tukey's test ($p < 0.05$).

In spite of the non-toxic effect of **IBC** against skin cells, several studies have reported its toxicity against leukemic cells (YANG et al., 2019) and solid tumor cells (KUETE et al., 2015), including colorectal (HCT116) (LI et al., 2019b), tongue (Tca 8113) (SHI et al., 2015), liver (HepG2) (LI et al., 2019a), breast (MCF-7) (SHI et al., 2018), prostate (PC-3) (LI et al., 2018), gastric (MGC803) (JIN; SHI, 2016), cervical (HeLa) (SZLISZKA et al., 2012), ovarian (OVCAR-08) (JING et al., 2010) and neuroblastoma (IMR-32) (NISHIMURA et al., 2007). The mechanism of **IBC** cytotoxicity is related to apoptosis induction via the mitochondrial pathway, decreasing its transmembrane potential (JIN; SHI, 2016; LI et al., 2019a, 2019b; NISHIMURA et al., 2007; SZLISZKA et al., 2012).

4. Conclusions

In summary, we newly synthesized and evaluated **IBC** as part of our ongoing search for antibacterial agents. **IBC** has potent activity against Gram-positive (MIC = 1.56–50.0 µg/mL) and *Mycobacterium* species (MIC = 62.5 µg/mL). The combination of IBC and vancomycin exhibited indifferent effects against MSSA and MRSA planktonic cells. Antibiofilm activity of

IBC was equipotent to vancomycin, displaying similar MBIC values. The mode of action of **IBC** involved membrane disruption, which is a crucial target for the bacterial survival. Furthermore, investigations of toxicity against human keratinocytes indicated that **IBC** is a selective compound. Altogether, our findings open new avenues for **IBC** as an antibacterial agent, with potential applications as a drug candidate and medical device coating.

CHAPTER III

Design, Synthesis and Activity against Mycobacterium tuberculosis of isobavachalcone and analogs

Chapter III

Design, Synthesis and Activity against *Mycobacterium tuberculosis* of isobavachalcone and analogs

Leticia Ribeiro de Assis[a], Reinaldo dos Santos Theodoro[a], Pedro Henrique de Deus Jacob[a], Larissa Faria Diniz[a], Maria Beatriz Silva Costa[a], Julyanna Andrade Silva Nascentes[a], Fernando Rogério Pavan[b], Luis Octavio Regasini[a+]

[a]Laboratory of Antibiotics and Chemotherapeutics, Department of Chemistry and Environmental Sciences, Institute of Biosciences, Humanities and Exact Sciences, São Paulo State University (Unesp), São José do Rio Preto CEP 15054-000, SP, Brazil.
[b]São Paulo State University (Unesp), College of Pharmacy, Department of Biological Sciences, Araraquara, SP, Brazil.

ABSTRACT

Isobavachalcone (**IBC**) is a natural prenylated chalcone with well-known antibacterial and antimycobacterial activities. In this current study, we used **IBC** as prototype to the design and synthesis of twenty-four analogs, exploring its rings A and B as well as α,β-unsaturated ketone bridge. Compounds were synthesized with overall yields ranging from 1 to 37%, by using regioselective iodination and Suzuki-cross coupling reactions as key steps. All compounds were evaluated against *Mycobacterium tuberculosis* H37Rv. Thirteen bioactive chalcones demonstrated Minimal Inhibitory Concentration (MIC) ranging from 2.7 to 25.0 μg/mL. Structure-activity relationship (SAR) analyses showed *C*-prenyl group on ring A, *p*-hydroxyl on ring B, and carbon α-carbon-β double bond were essential for antimycobacterial activity. Nitrochalcone (**IBC 14**) and trifluoromethylchalcone (**IBC 13**) were the most active compounds, with MIC of 2.7 and 3.8 μg/mL, respectively. All antitubercular chalcones demonstrated satisfactory *in silico* pharmacokinetic and *drug-likeness* properties desired for oral drug administration. In summary, the exploitation of IBC as antitubercular prototype led to active analogs and conclusive SAR data.

1. Introduction

Tuberculosis (TB) is an infectious disease caused by *Mycobacterium tuberculosis*, which is recognized as a top lethal disease caused by infectious agent (WHO, 2021). According to annual global TB report, about 9,9 million people fell sick with TB in 2020, and approximately 1.5 million people have died. The actual treatment against drug-sensitive TB treatment consists of combinations using rifampicin (RMP), isoniazid (INH), pyrazinamide (PZA) and ethambutol (EMB) for at least six months. The increase of multidrug-resistant TB (MDR-TB), which includes the resistance against at least two first-line drugs, such as INH and RMP is a global health challenge (WHO, 2021). The treatment of MDR-TB is complex, requiring a combination of fluoroquinolones (ofloxacin, levofloxacin or moxifloxacin) and injectable aminoglycosides (capreomycin, kanamycin or amikacin) for 18 months. The long period, severe side effects, and socioeconomic factors led to failure of TB treatment (SEUNG; KESHAVJEE; RICH, 2015). Moreover, the emergence of extensively drug-resistant TB (XDR-TB), which involves the resistance against both first- and second-line drugs represent another massive global problem (SEUNG; KESHAVJEE; RICH, 2015; WHO, 2021). In this context, delamanid, pretomanid, and bedaquiline are new drugs an used in drug combinations against MDR-TB and XDR-TB, which allowed the shortening and improvement of TB therapy (IGNATIUS; DOOLEY, 2019). However, drug resistance against these drugs are emerging, demanding greater and continuous efforts in search of innovative antitubercular drugs (BLOEMBERG et al., 2015).

Natural products are recognized as the biggest source of bioactive compounds, exhibiting a high chemical diversity, which could be explored for drug discovery of antimycobacterial compounds (HAN et al., 2022). Among highlighted natural products, chalcones are at central position due to their concise synthesis and promising pharmacological properties (ZHUANG et al., 2017). The great chemical diversity of natural chalcones is related to versality of substituents on aromatic rings, including hydroxyl, methoxyl and prenyl groups (CAESAR; CECH, 2016; CHEN et al., 2014; RAMMOHAN et al., 2020; ROZMER; PERJÉSI, 2016). Prenyl groups are side unsaturated chains, which can be constituted by five (isoprenyl), ten (geranyl) and fifteen (farnesyl) carbon atoms, which can be linked at phenolic ring via a carbon or oxygen atoms (ROZMER; PERJÉSI, 2016). Some *C*-prenylated chalcones from Fabaceae, Moraceae, Cannabaceae, Euphorbiaceae and Asteraceae possess antimycobacterial activity (CHIANG et al., 2010; FRIIS-MØLLER et al., 2002; HONG et al., 2010; KUETE et al., 2010b; LALL; HUSSEIN; MEYER, 2006; LOU et al., 2020). Among them,

isobavachalcone (**IBC**) or corylifolinin from *Dorstenia barteri* demonstrated antimycobacterial activity against *Mycobacterium tuberculosis*, including its effects against INH-susceptible (MTCS2) and INH-resistant (MTCS1) clinical isolates (CHIANG et al., 2010; KUETE et al., 2010b). Moreover, **IBC** is an inhibitor of extracellular nuclease Rv0888 from *Mtb* H37Rv, a virulence factor associated with the persistence of *M. tuberculosis* in the host (DANG et al., 2016). In our previous study (ASSIS et al., 2022), **IBC** was active against three standard mycobacterial species, *M. tuberculosis*, *M. avium*, and *M. kansasii*. **IBC** also demonstrated activity against Gram-positive bacterial species (KUETE; SANDJO, 2012; WANG et al., 2021).

Considering the antimycobacterial activities of **IBC**, we selected it as prototype to access the structure-activity relationship (SAR) against *Mycobacterium tuberculosis*. We designed and synthesized 24 analogs, with structural modifications on prenyl subunit (**IBC 21–IBC 23**), ring B (**IBC 1–IBC 20**) and *trans*-enone chalconic bridge (**DH-IBC**). Among them, six are known bioactive natural compounds, such as isoliquiritigenin (**IBC 21**), xanthoangelol (**IBC 22**), morachalcone A (**IBC 3**), corylifol B (**IBC 4**), isocordoin (**IBC 6**) and hayneanachalcone (**IBC 7**) (BORGES-ARGÁEZ et al., 2009; CUI et al., 2015; DU et al., 2013; GANAPATY et al., 2006; INAMORI et al., 1991; PENG et al., 2015). Whereas two chalcones (**IBC 9** and **IBC 11**) were found as synthetic derivatives (ENOKI et al., 2004; NARENDER; REDDY, 2007), and 15 compounds are new chemical entities (**IBC 1**, **IBC 2**, **IBC 10**, **IBC 12–IBC 20**, and **DHIBC**). In addition, we determined *in silico* pharmacokinetic and drug-likeness properties of select analogs.

2. Results and Discussion

2.1. Chemistry

Synthesis of compounds (**IBC**, **IBC 1–IBC 23** and **DHIBC**) was achieved using five to eight steps (Schemes 1–7). 2’,4’-Dihydroxy-3’-iodo-acetophenone (**A.2**) was obtained as the majority product (90% yield) from regioselective iodination of starting material, 2’,4’-dihydroxyacetophenone (**A.1**) by using I_2/KIO_3 (Scheme 1) (WANG et al., 2015). 2’-hydroxy-3’-iodo-acetophenone (**A.4**) was obtained with 60% yield from iodination of 4’-hydroxyacetophenone (**A.3**), using iodine and hydrogen peroxide (Scheme 2) (GALLO et al., 2010).

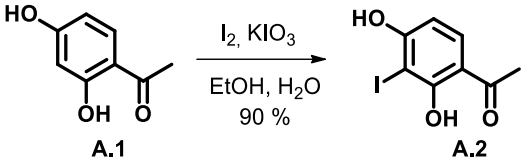

Scheme 1. Iodination of 2',4'-dihydroxyacetophenone

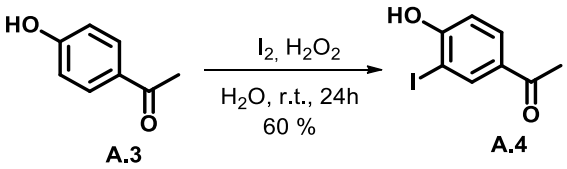

Scheme 2. Iodination of 4'-hydroxyacetophenone

Phenolic hydroxyl groups of **A.2** and **A.4**, as well as the hydroxybenzaldehyde derivatives were protected by MOM, with yields of 95%. Aldol condensation between **A.5** and **A.6** with several respective benzaldehyde derivatives, using KOH and ethanol, furnishing chalcone intermediaries **C.1–C.14** and **C.17–C.21**, with 60–95% yields. However, using these conditions, pyridinyl derivatives **C.15** and **C.16** was not obtained, with the formation of several products. Wachter and co-workers suggested that during aldol condensation involving pyridinylcarboxaldehyde can occurs an intramolecular metal complexation between carbonyl and nitrogen of the intermediate aldolate. This intramolecular complexation led to aldol adopt a gauche conformation, favoring the formation of thermodynamically less stable *cis*-chalcone, which can rapidly undergoes Michael addition with enolate resulting in a symmetric diketone (WACHTER-JURCSAK; RADU; REDIN, 1998). Bhambra and co-workers successful obtained halogenated pyridinylchalcone using LiOH and anhydrous 1,4-dioxane as the catalyst and solvent, respectively. Herein, similar conditions using a catalytic amount of NaOH led to the formation of the desired pyridinylchalcones **C.15** and **C.16**, with 30 and 40% yields, respectively (Scheme 3).

Reactant **R.1** is commercially available with high economical costs, encouraging us to prepare it (75% yield), using the protocol reported by Miralles et al., with slight modifications, using bis(pinacolato)diboron and 1,1-dimethylallyl alcohol (Scheme 4) (MIRALLES et al., 2016) (Scheme 4).

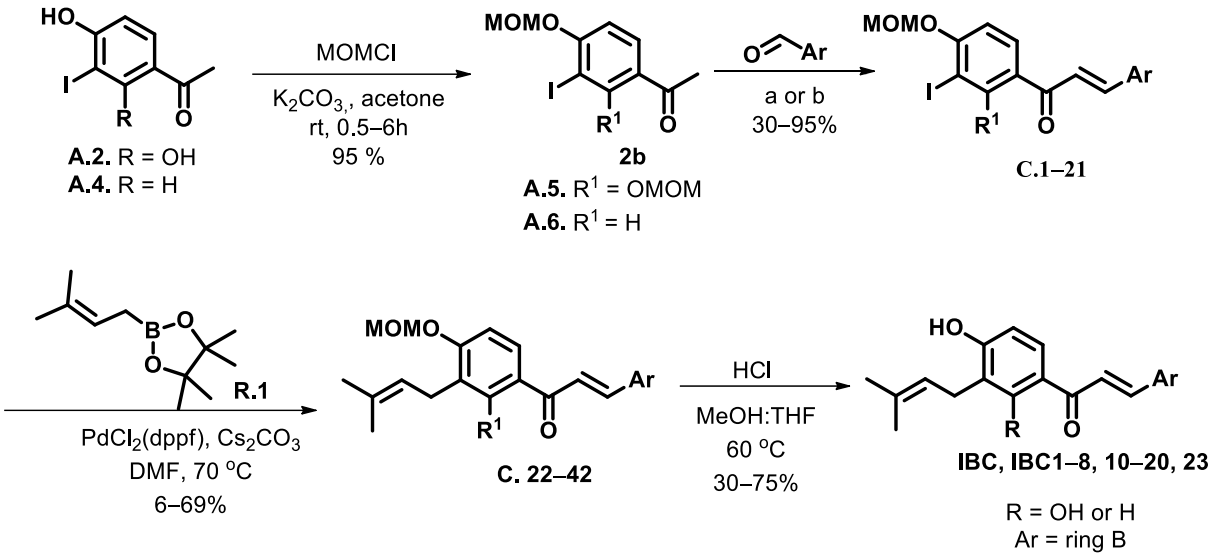

Scheme 3. Synthetic route for prenylated chalcones (**IBC**, **IBC 1–IBC 8**, **IBC 10–IBC 20** and **IBC 23**). a) reaction conditions for chalcones **C.1–C.14** and **C.17–C.21**: 60% KOH, EtOH, rt; b) reaction conditions for pyridinylchalcones **C.15** and **16**: NaOH, 1,4-dioxane, rt

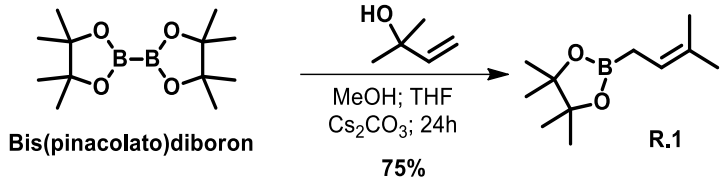

Scheme 4. Preparation of **R.1**

Suzuki-Myiuara cross-coupling reactions were performed between chalcones (**C.1–C.21**) and the prenyl boronic acid pinacol ester (**R.1**), using $PdCl_2$(dppf) as catalyst and Cs_2CO_3 as basis in DMF at 70 ºC (WANG et al., 2015), furnishing **C.22–C.42** with yields ranging from 6% to 69%. Most of the prenylated chalcones were obtained with ≥ 30% yields after chromatographic purifications. Four chalcones displayed ≤ 15% yields, including 4-pyridylchalcone (**C.36**, 15%), as well as chalcones substituted by Br (**C.33**, 6%), CF_3 (**C.34**, 10%), and NO_2 (**C.35**, 18%) (Scheme 3).

The last synthetic step involved the deprotection of **C.22–C.42** in acidic conditions, giving the respective phenolic prenylated chalcones **IBC 1–IBC 8**, **IBC 10–IBC 20**, and **IBC 23** with yields ranging from 30% to 75%. Eight chalcones were obtained with overall yields between 1 and 10% (**IBC 10–16**, **19**) and eleven > 10% (**IBC 1–7**, **IBC 9**, **IBC 17**, **IBC 18**,

IBC 20). Total synthesis of isobavachalcone (**IBC**), morachalcone A (**IBC 3**), corylifol B (**IBC 4**), hayeanachalcone (**IBC 7**) and isocordoin (**IBC 6**) were achieved with yields of 22%, 13%, 12%, 35%, and 1%, respectively (Scheme 3).

Reduction of **IBC 14** using tin(II) chloride in ethanol (SONMEZ et al., 2011) furnished aminochalcone **IBC 8** with 64%yield and an overall yield of 5% (Scheme 5).

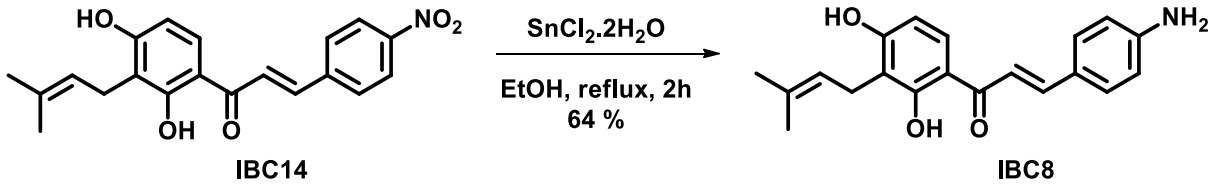

Scheme 5. Preparation of aminochalcone **IBC 8**

Wang and co-workers synthesized xanthoangelol, using geranylated boronic acid pinacol ester (WANG et al., 2015). However, this reactant is not commercially available, and its synthesis generally furnishes the *E*- and *Z*-isomers (MIRALLES et al., 2016). Thus, we used procedures described by Sugamoto and co-workers e (SUGAMOTO et al., 2011). Total synthesis of isoliquiritigenin (**IBC 21**, 75%) and xanthoangelol (**IBC 22**, 65%) were achieved with 22 and 17% overall yields, respectively, after six synthetic steps. First, compound **A.7** was 2'-*O*-geranylated with geranyl bromide furnishing **A.8**. Compound **A.8** was condensate with 4-(methoxymethoxy)benzaldehyde, furnishing 2'-geranyloxychalcone **C.43** (90 %). [1,3]-Sigmatropic rearrangement of geranyl group of **C.43** with montmorillonite K10 clay furnished *C*-geranylated chalcone (**C.45**, 38%) and unsubstituted C-3' chalcone (**C.44**, 35%). Finally, compounds **C.44** and **45** were submitted to deprotection reaction, furnishing isoliquiritigenin (**IBC 21**, 75%) and xanthoangelol (**IBC 22**, 65%) (Scheme 6).

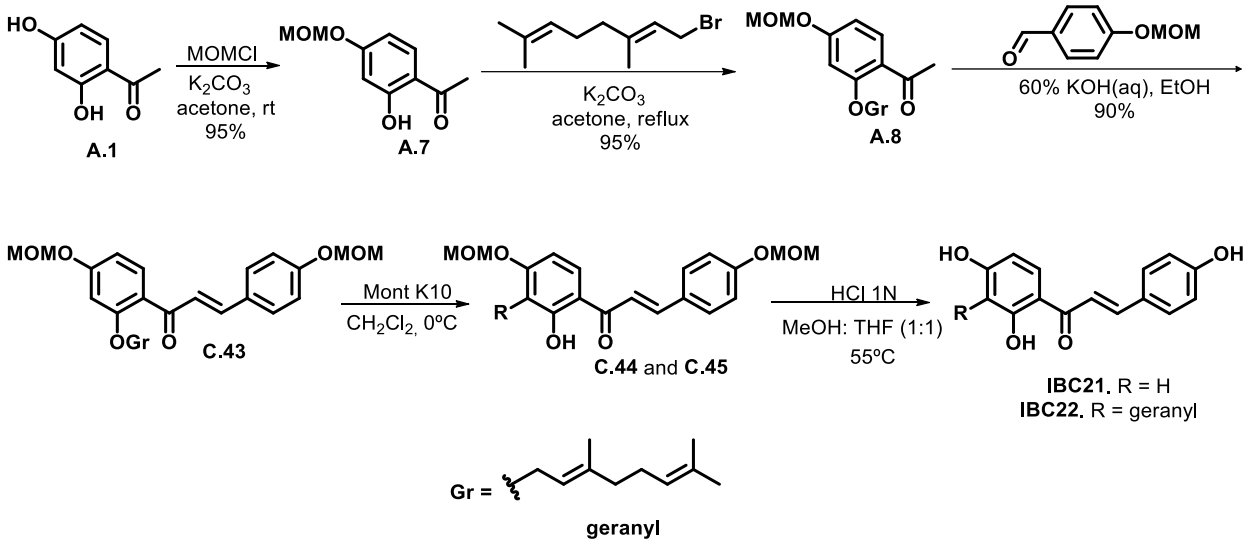

Scheme 6. Synthetic route of isoliquiritigenin (**IBC 21**) and xanthoangelol (**IBC 22**)

Ngmeni et al. (2007) reported the hydrogenation of **IBC** using H_2 and Pd-C as reducing agent and catalyst, respectively (NGAMENI et al., 2007). However, the hydrogenation co-occurred at α,β-double and prenyl double bonds. Herein, we used Et_3SiH and $Pd(OAc)_2$ as reducing agent and catalyst, respectively. We achieved a chemoselective reduction of α,β-double bond, furnishing the dihydroisobavachalcone (**DHIBC**) with 11% overall yield (Scheme 7).

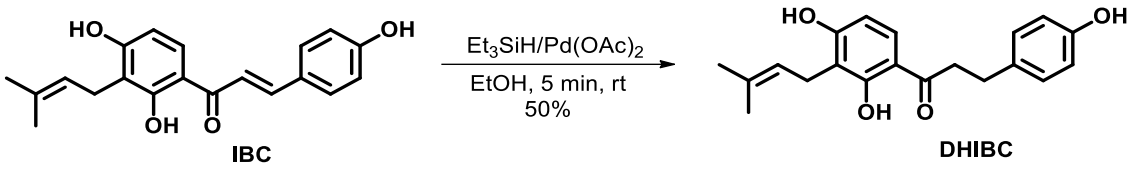

Scheme 7. Preparation of **DHIBC**

2.2. Activity against *Mycobacterium tuberculosis*

Antimycobacterial activities of compounds were evaluated against *M. tuberculosis* H37Rv (ATCC 27294) in concentrations ranging from 25 to 0.09 µg/mL. Minimal Inhibitory Concentration (MIC_{90}) was the lowest concentration that inhibited 90% or more the mycobacterial growth by using resazurin as viability indicator. Results are presented in Tables 1 and 2.

Among 22 chalcones, twelve inhibited *Mtb* growth with MIC values ranging from 2.7 to 25.0 µg/mL (Tables 1 and 2). Chalcones displayed the following decreasing antimycobacterial potency: **IBC 14** > **IBC 13** > **IBC 1**> **IBC 2** > **IBC 22** > **IBC 10** > **IBC 16**

> **IBC** > **IBC 3** = **IBC 7**, **IBC 15**, **IBC 23**. Chalcone substituted by *para*-nitro on ring B (**IBC 14**) was the most active compound, showing a MIC_{90} value of 2.7 µg/mL, followed by *para*-trifluoromethylchalcone (**IBC 13**) with MIC_{90} value of 3.8 µg/mL.

Table 1. Activity against *Mycobacterium tuberculosis* of **IBC** analogs of series I (**IBC 21–23**) and **DHIBC**

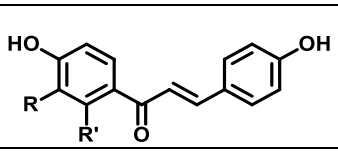

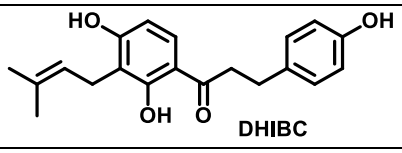

DHIBC

Cod.	R	R'	MIC_{90} (µg/mL)
IBC 21	H	OH	> 25.0
IBC 22	geranyl	OH	7.7
IBC 23	prenyl	H	25.0
DHIBC	-	-	> 25.0
RMP	-	-	0.01

RMP = rifampicin

Table 2. Activity against *Mycobacterium tuberculosis* of **IBC** and its analogs of series II and III

	Cod.	R or Ar	MIC_{90} (µg/mL)	π	σ
	IBC	4-OH	12.5	-0.61	-0.37
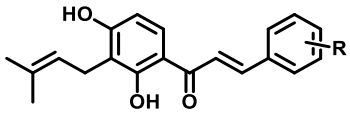	**IBC 1**	3-OH	5.9	-0.50	0.12
	IBC 2	2-OH	7.2	-0.41	-
	IBC 3	2,4-diOH	25.0	-	-
	IBC 4	3,4-diOH	> 25.0	-	-
	IBC 5	2,5-diOH	> 25.0	-	-
	IBC 6	H	25.0	0	0
	IBC 7	4-OMe	25.0	-0.02	-0.27
	IBC 8	4-NH_2	> 25.0	-1.30	-0.66
	IBC 9	4-Me	> 25.0	0.56	-0.17
	IBC 10	4-F	8.9	0.14	0.06
	IBC 11	4-Cl	> 25.0	0.71	0.23
	IBC 12	4-Br	> 25.0	0.86	0.23
	IBC 13	4-CF_3	3.8	0.88	0.54
	IBC 14	4-NO_2	2.7	0.22	0.78
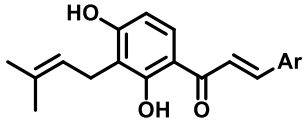	**IBC 15**	3-pyridinyl	25.0	-	-
	IBC 16	4-pyridinyl	11.7	-	-
	IBC 17	2-furanyl	> 25.0	-	-
	IBC 18	2-tiophenyl	> 25.0	-	-
	IBC 19	1-naphthyl	> 25.0	-	-
	IBC 20	2-naphtyl	> 25.0	-	-
-	**RMP**	-	0.01	-	-

series II

series III

π (hydrophobicity)(HANSCH et al., 1973) and **σ** (electronic effect)(HANSCH; LEO; TAFT, 1991) constants refer to substituents (-R) on phenyl (ring B). RMP = rifampicin

MIC_{90} values of prenylated chalcones against *Mtb* allowed a preliminary discussion about the structure-antimycobacterial activity relationship. Series I is constituted by three chalcones (**IBC 21–IBC 23**). Isoliquiritigenin (**IBC 21**) and xanthoangelol (**IBC 22**) were designed to evaluate hydrophobicity effect of isoprenyl on anti-*Mtb* activity, by removing or extending the isoprenyl group at position 3', respectively. Hydrophobic nature of the prenyl groups have been associated with the bioactivity of phenolic compounds, facilitating their penetration through biological membranes (ÁVILA et al., 2008; GO; WU; LIU, 2012; SHAMSUDIN et al., 2022). Indeed, we found that the isoprenyl groups was essential for anti-*Mtb* activity of **IBC** considering its non-isoprenylated congener isoliquiritigenin (**IBC 21)** was not active (MIC_{90} > 25 µg/mL). In addition, the elongation of prenyl side chain, from 5 to 10 carbon atoms, increased the antimycobacterial activity of **IBC 22** in about 1.6-fold (MIC_{90} = 7.7 µg/mL) in comparison with **IBC** (MIC_{90} = 12.5 µg/mL). We investigated the relevance of 2'-hydroxyl group to antimycobacterial activity. Unsubstituted C-2' **IBC** analog (**IBC 23**) was 2-fold less active than **IBC**. Hydroxyl at 2' is *ortho*-positioned to carbonyl group, allowing an intramolecular hydrogen bond and forming a pseudo-six-membered ring (Scheme 8). This pseudoring reduces potential intermolecular hydrogen bonds and increases lipophilicity, which may collaborate with the permeation into biological membranes, increasing the **IBC** activity. Moreover, this subunit can chelate different metallic ions, (JOHNSON; YARDILY, 2019; SYMONOWICZ; KOLANEK, 2012), which may deregulate the function of bacterial metalloproteins (BASIC et al., 2014; GÓRNIAK; BARTOSZEWSKI; KRÓLICZEWSKI, 2019).

Series II explored modifications on ring B with strategic substituents to investigate electronic (σ) and hydrophobic (π) parameter contributions to antimycobacterial activity. σ Constant characterizes the electron-donating or electron-acceptor effect of substituents on phenyl ring (HANSCH; LEO; TAFT, 1991). On the other hand, π constant describes hydrophobicity (HANSCH et al., 1973).

First, comparisons among compounds exhibiting phenyl (**IBC 6**), hydroxyphenyl (**IBC**, **IBC 1** and **IBC 2**), resorcinol (**IBC 3**), catechol (**IBC 4**), and hydroquinone (**IBC 5**) as ring B allowed to verify the effects of the presence, position and number of hydroxyl groups for antimycobacterial activity. The presence of *p*-phenolic ring B increased 2-fold the antimycobacterial activity of **IBC** (MIC_{90} = 12.5 µg/mL) when compared to **IBC 6** (MIC_{90} = 25.0 µg/mL). The increasing of MIC_{90} value was higher (4-fold) in analogs carrying *ortho*-hydroxyl (**IBC 2**) or *meta*-hydroxyl (**IBC 1**), which could be related to increasing of π parameter in comparison with **IBC**. Otherwise, an additional hydroxyl group has significantly

decreased the antimycobacterial activity of **IBC 3–IBC 5** when compared to hydroxyphenyl analogs (**IBC**, **IBC 1** and **IBC 2**).

Second, we investigated the substitution of phenyl ring by other electron-donor groups, such as *p*-CH_3 (**IBC 9**), *p*-OCH_3 (**IBC 7**) and *p*-NH_2 (**IBC 8**). These substitutions reduced the bioactivity in comparison to **IBC**, suggesting that electron-donation was not crucial, but the weak acidic property of phenol can be required for antimycobacterial activity.

Third, we compared the effects of electron-withdrawing groups on ring B for anti-*Mtb* activity, such as F (**IBC 10**), Cl (**IBC 11**), Br (**IBC 12**), CF_3 (**IBC 13**) and NO_2 (**IBC 14**). Analogs carrying NO_2, CF_3 and F displayed antimycobacterial activity with MIC_{90} of 2.7, 3.8 and 8.9 µg/mL, respectively. On the other hand, analogs carrying Cl and Br were inactive (MIC ≥ 25 µg/mL). Altogether, these groups promote an overall increase in π and σ parameters compared to unsubstituted ring B (**IBC 6**) and **IBC** (Table 1). Bromine (π = 0.86) and trifluoromethyl (π = 0.88) have similar hydrophobic effects; otherwise, the electronic influence is 2-fold higher in CF_3 (σ =0.23) than Br (σ =0.54), suggesting that it was preponderant for antimycobacterial activity of **IBC 13**. This σ+ effect on anti-*Mtb* activity was clearer when the substituent group was 4-NO_2, the most potent analog. Moreover, the potent antimycobacterial effect of nitrochalcone could result from enzymatic biotransformation of group nitro by mycobacterial nitroreductases (TENG; KIM, 2021). Interestingly, fluorine substituent (**IBC 10**) slightly increases the π and σ parameters when compared to hydrogen, whereas for chlorine (**IBC 11**) and bromine (**IBC 12**), these parameters are stronger. However, **IBC 10** showed antimycobacterial activity 3-fold higher than unsubstituted analog (**IBC 6**), whereas **IBC 11** and **IBC 12** were inactive. These data suggest that the stronger electronegative nature of fluorine in comparison to chlorine and bromine may be an additional property required for antimycobacterial activity.

For the series III of compounds (**IBC 15**–**IBC 20**), the replacement of phenol ring by homoaryl and heteroaryl rings was proposed. In order to investigate hypothetical ring bioisosterism, comparisons were carried out to determine the effect of replacement of phenyl ring B in **IBC 6** by heteroaryl rings with six π-electrons, including 2-furanyl (**IBC 17**), 2-thiophenyl (**IBC 18**), 3-pyridinyl (**IBC 15**) and 4-pyridinyl (**IBC 16**). Chalcones **IBC 17** and **18** were unable to inhibit mycobacteria growth (MIC_{90} > 25 µg/mL), whereas **IBC 15** did not affect antimycobacterial activity (MIC_{90} = 25 µg/mL). Otherwise, **IBC 16** was twice more potent than **IBC 6**, exhibiting MIC_{90} value of 11.7 µg/mL. These comparisons suggested π-electron density was not relevant to antimycobacterial activity. On the other hand, the high activity of **IBC 16** compared to **IBC 17** and **18** can be attributed to the basicity of pyridine ring.

In addition, we investigated the effect of expansion of π-electron number using homoaryl rings (1-naphthyl and 2-naphthyl), which demonstrate ten π-electrons. 1-Naphthylchalcone (**IBC 19**) and 2-naphthylchalcone (**IBC 20**) were inactive (MIC_{90} > 25 µg/mL).

Comparison between MIC_{90} values of **IBC** and **DHIBC** suggested α,β-unsaturated ketone bridge has pharmacophoric contribution, considering that **DHIBC** was completely inactive (MIC_{90} > 25 µg/mL). α,β-Unsaturated ketone bridge has potential as Michael acceptor, reacting with biological nucleophiles, such as cysteine residues (JOHANSSON, 2012; MAUCHER et al., 2017). Besides, this subunit is crucial for pharmacological effects of drugs (e.g., penicillins, cephalosporins, fosfomycin, acid acethylsalicylic), which can be classified as covalent inhibitors (BAUER, 2015).

In summary, we presented preliminary structure-antimycobacterial activity relationship data for **IBC** and its analogs. SAR investigation has not been explored in literature so far, and these finds will contribute to design new analogs with potent antimycobacterial activity (Scheme 8).

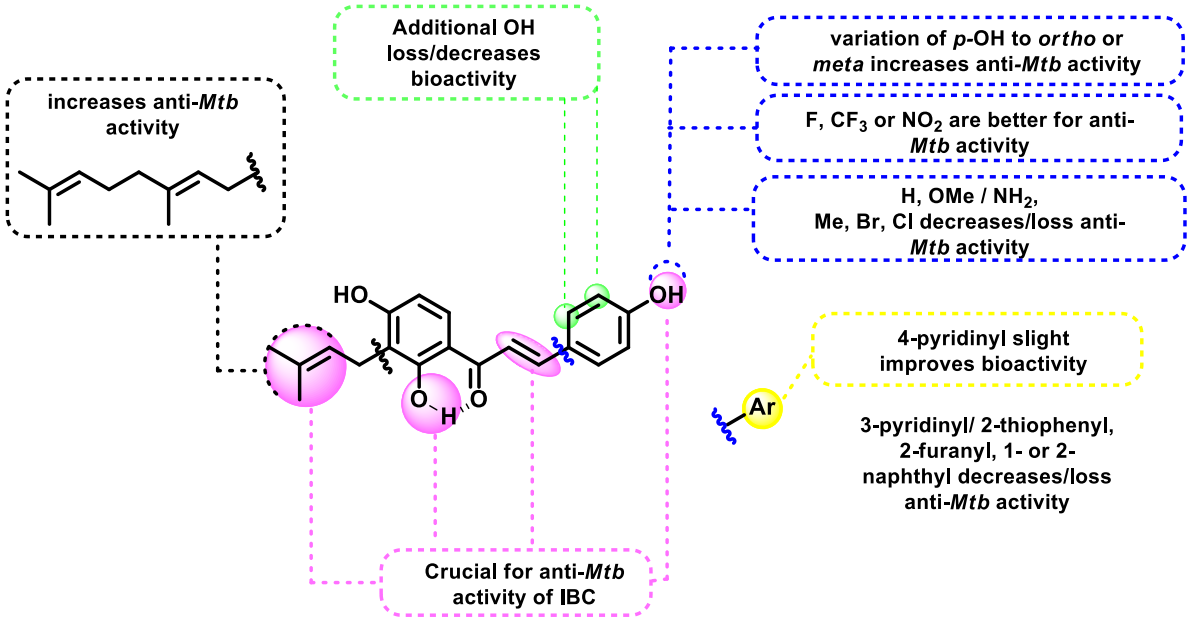

Scheme 8. Structure-Antimycobacterial Activity Relationship of **IBC** and its analogs

2.3. *In silico* drug-likeness and pharmacokinetic properties investigation

Among drug delivery routes, the oral pathway is frequently desirable for administration of tuberculostatic drugs due to the easy administration, feasibility for solid formulations,

controllable delivery and patient adhesion for periods (HOMAYUN; LIN; CHOI, 2019). Additionally, compounds must have physicochemical parameters to avoid further failure of absorption, distribution, metabolism and excretion (ADME) in advanced clinical phases. In this context, computational approaches can predict physicochemical and pharmacokinetics properties that classify the compound as drug like oral route. Using the SwissADME, a free web tool, (DAINA; MICHIELIN; ZOETE, 2017), we applied five *in silico* filters used by pharmaceutical companies to improve the quality of their proprietary chemical libraries: i) Lipinski (Pfizer) (LIPINSKI, 2004), Ghose (Amgen) (GHOSE; VISWANADHAN; WENDOLOSKI, 1999), Veber (GSK) (VEBER et al., 2002), Egan (Pharmacia) (EGAN; MERZ; BALDWIN, 2000), and Muegge (Bayer) (MUEGGE; HEALD; BRITTELLI, 2001). Results were summarized in table 3.

Physicochemical properties analyses include the molecular weight (MW), number of atoms (NA), number of rotatable bonds (NROT), number of hydrogens bond donor (HBD), number of hydrogen bond acceptor (HBA), molar refractivity (MR) and topological polar surface area (TPSA). Lipinski suggests that druglike compounds should have MW $\leq$ 500 g/mol, HBD $\leq$ 5, and HBA $\leq$ 10. Moreover, Ghose suggests MW = 160 to 480 g/mol, NA = 20 to 70 and MR = 40–130. Muegge stipulated that MW should be between 200 and 600, HBD $\leq$ 5, HBA $\leq$ 10 and, additionally, molecules should be 1 to 7 aromatics rings. All antimycobacterial chalcones did not violate these parameters.

TPSA and NROTB are two parameters used to predict drug absorption, including intestinal absorption, bioavailability, caco-2 permeability and blood-brain barrier penetration (DAINA; MICHIELIN; ZOETE, 2017). TPSA considers the sum surfaces of polar atoms like *O*- and *N*- in a molecule, while NROTB is a parameter that measures the degree of molecular flexibility. According to computational approach, Egan considers small molecules with good oral bioavailability with TPSA value $\leq$ 131.6 $Å^2$. Veber and collaborators, based on study in rats, established that TPSA $\leq$140 $Å^2$ and NROTB $\leq$ 10 are optimum values for satisfactory bioavailability of candidate drugs by oral route (VEBER et al., 2002). TPSA and NORTB values exhibited by selected chalcones suggest a good theoretical potential bioavailability by oral route (Table 3).

Table 3. Physicochemical, Pharmacokinetic & druglike properties of antimycobacterial chalcones

		IBC 1	IBC 2	IBC 10	IBC 13	IBC 14	IBC 16	IBC 22	IBC
Physicochemical parameter	MW(g/mol)	324.4	324.4	326.4	376.4	353.4	309.4	392.5	324.4
	NROT	5	5	5	6	6	5	8	5
	HBA	4	4	4	6	5	4	4	4
	HBD	3	3	2	2	2	2	3	3
	TPSA (Å²)	77.76	77.76	57.53	57.53	103.35	70.42	77.76	77.76
	MR	96.04	96.04	93.97	99.02	102.84	91.81	119.6	96.04
	log *S*[a]	-4.3	-4.0	-4.8	-5.6	-5.2	-4.3	-5.0	-4.3
	log *P*[b]	3.7	3.6	4.2	4.8	4.5	3.6	4.7	3.5
Pharmacokinetic parameter	GI absorption	high	high	high	high	high	high	high	High
	BBB	no	no	yes	no	no	yes	no	no
Druglike properties	Lipinski	0	0	0	0	0	0	0	0
	Ghose	0	0	0	0	0	0	0	0
	Veber	0	0	0	0	0	0	0	0
	Egan	0	0	0	0	0	0	0	0
	Muegge	0	0	0	0	0	0	0	0

MW = molecular weight; HBD = number of hydrogen bond donors; HBA = number of hydrogen acceptors donors; TPSA = topological polar surface area; NROTB = number of rotatable bonds; Log *P* = lipophilicity; GI = gastrointestinal; BBB = blood-brain barrier; Log *S* = solubility. [a]Log *S* = 0,5 -Log *P*-0,01×(MP-25)(YINGQING; JAIN; YALKIWSKU, 2003); [b]Determined by partition coefficient (*n*-octanol/water), HPLC method(OECD, 1989).

The coefficient partition between *n*-octanol and water (log *P*o/w) value is an important descriptor of lipophilicity, a common physicochemical parameter used to estimate the biological membranes permeability. A variety of methods can estimate the values of log *P* with satisfactory results. We have experimentally determined the log *P* values by HPLC method according to procedures described by OECD Guidelines for the Testing of Chemicals (OECD, 1989). Ghose suggest a log *P* ranging from -0.4 to 5.6; Lipinski log $P \leq 5$; Muegge log *P* = -2 to 5, and Egan log $P \leq 5.88$. We found that most potent antimycobacterial chalcones (**IBC**, **IBC 1**, **IBC 2**, **IBC 10**, **IBC13–IBC 16**, and **IBC 22**) displayed log *P* values ranging from 3.2 to 4.8 (Table 3).

Satisfactory oral bioavailability is achieved by an optimum balance between aqueous solubility and lipophilicity properties. Aqueous solubility affects the absorption and distribution profile (DELANEY, 2004). A log *S* value between -1 and -5 is desired for a bioactive compound, aiming to decrease the probability of failure in clinical phases (JORGENSEN; DUFFY, 2002). Thus, we predicted the aqueous solubility by General Solubility Equation (GSE), **log *S* = 0.5-log *P*-0.01 × (MP-25)** (YINGQING; JAIN; YALKIWSKU, 2003). According to log *S* range, compounds were classified as insoluble

(log *S* < -10), poorly soluble (log *S* = -10 to -6), moderately soluble (log *S* = -6 to -4), soluble (log *S* = -4 to -2), very soluble (log *S* -2 to 0), and highly soluble (Log *S* > 0) (JORGENSEN; DUFFY, 2002). The results were summarized in table 3. For GSE application, we used the experimental log *P* (table 3) and experimental melting point (MP) (supplementary material). Antimycobacterial chalcones were classified as water-soluble or moderately soluble, displaying log *S* ranging values from -5.6 to -4.0, which are desired log *S* range for bioactive compounds (JORGENSEN; DUFFY, 2002).

Permeation through gastric tissue and intestinal epithelium (GI) and blood brain barrier (BBB) is a central data for bioactive compounds. We investigated the human intestinal absorption (HIA) and BBB permeation of antitubercular chalcones. This model is dependent on the lipophilicity and molecular polarity. All chalcones showed high predict HIA values. About BBB permeation, most compounds are not able to across this barrier, with exception of **IBC 10** and **16**.

3. Conclusions

In summary, we designed and synthesized isobavachalcone (**IBC**) and twenty-three related analogs with modifications on rings A and B (**IBC 1**–**IBC 23**), as well as on α,β-unsaturated ketone bridge (**DHIBC**). Among them, fifteen are novel chemical entities, and seven are naturally-occurring chalcones (isobavachalcone, isoliquiritigenin, xanthoangelol, hayneanachalcone, isocordoin, corilyfol B, and morachalcone A). We achieved the first total synthesis of the hayneanachalcone (**IBC 7**), with 37% overall yield. Twelve chalcones demonstrated activity against *M. tuberculosis* (MIC = 2.7–25 μg/mL). Preliminary structure-antimycobacterial activity relationship data suggested that prenyl side chain, hydroxyl on ring B, and double bound between carbons α,β are crucial subunits for antimycobacterial activity of **IBC**. Moreover, substitution on ring B by nitro (**IBC 14**) and trifluormethyl (**IBC 13**) led to most potent antimycobacterial agents. Also, the most promising antimycobacterial chalcones demonstrated satisfactory *in silico* oral drug-likeness profile.

4. Material and Methods

4.1. Chemistry

Reagents and solvents were purchased from Merck®. The reactions were checked by Thin Layer Chromatography (TLC) plates (Supelco ®), which were revealed under ultraviolet at 254 nm and 365 nm. Purification of compounds was performed over silica gel

chromatography column (230-400 mesh, Aldrich®), using mixtures of hexane and ethyl acetate as mobile phase. ^{1}H and ^{13}C Nuclear Magnetic Resonance (NMR) spectra, HPLC chromatograms, UV–Vis spectra and melting points (m.p.) were presented in Supplementary material (Chapter V).

4.1.1. Synthesis

1-(2,4-Dihydroxy-3-iodophenyl)ethanone (A.2)

To a mixture of 2',4'-dyhydroxyacetophenone (5.32 g, 35 mmol) and KIO_3 (1.5 g, 7.0 mmol) in ethanol (25 mL) and water (40 mL) was added iodine (4.0 g, 15.8 mmol) at 0°C (WANG et al., 2015). The crude product mixture was stirred for 12 h at room temperature. Then, 30 mL of 10% sodium bisulfite solution was added under ice bath, and the white precipitated was filtrated and recrystallized from hexane and ethyl acetate (9:1), affording **A.2** with 90% yield.

1-(4-hydroxy-3-iodophenyl)ethanone (A.4)

To a mixture of 4'-hydroxyacetophenone (0.27 g, 2 mmol) and iodine (0.76 g, 3 mmol) in distilled water (10 mL) was added 0.7 mL of hydrogen peroxide aqueous solution 30% (m/v) (GALLO et al., 2010). The mixture reaction was stirred at room temperature for 2 4h. After that, an aqueous solution of sodium thiosulfate was added to the mixture, which was extracted with ethyl acetate (3 × 25 mL). The combined organic layers were washed with brine, dried over $MgSO_4$, filtered and concentrated under reduced pressure. The crude product was purified by column chromatography over silica gel using a mixture of hexane:dichloromethane:acetone (0.5:0.4:0.1) furnishing **A.4** as a white solid with 60% yield.

1-(3-iodo-2,4-bis(methoymethoxy)phenyl)ethanone (A.5)

A mixture of **A.2** (10.8 mmol) and anhydrous K_2CO_3 (86.4 mmol) in acetone (20 mL) was stirred at room temperature for 30 min (WANG et al., 2015). Then, methoxymethyl chloride (5 mL) was added under an ice bath in aliquots for 1 h. The reaction was stirred at room temperature for 6 h. Crude product was extracted with ethyl acetate (3 × 25 mL). The combined organic layers were washed with K_2CO_3 solution (1 mol/L) and brine, dried over $MgSO_4$, filtered and concentrated under reduced pressure to give acetophenone **2b** as a yellowish oil with 95% yield.

1-(3-iodo-4-methoymethoxyphenyl)ethanone (A.6)

The procedure was the same used for **A.5**, using **A.4** as substrate furnishing **A.6** as a translucent colorless oil with 95% yield.

2-hydroxy-4-(methoxymethoxy)acetophenone (A.7)

The procedure was the same used for **A.5**, using **A.1** as substrate furnishing **A.7** as a translucent colorless oil with 90% yield.

(*E*)-1-(2-((3,7-dimethylocta-2,6-dien-1-yl)oxy)-4-(methoxymethoxy)phenyl)ethanone (A.8)

A mixture of **A.7** (2 mmol), anhydrous K_2CO_3 (4 mmol), and geranyl bromide (2 mmol) in dry acetone (10 mL) was stirred under reflux for 24 h (SUGAMOTO et al., 2011). The crude product was extracted with ethyl acetate (3 × 25 mL), dried over $MgSO_4$, and evaporated under reduced pressure, obtaining **A.8** as translucent oil with 90% yield.

Methoxymethoxybenzaldehydes (B.1–6)

The hydroxylated benzaldehydes derivatives were protected by MOM group using the same protocol reported to **A.5**, obtaining the following MOM-benzaldehydes: 2-*O*-MOM-benzaldehyde (**B.1**, 85% yield); 3-*O*-MOM-benzaldehyde (**B.2**, 95% yield); 4-*O*-MOM-benzaldehyde (**B.3**, 95% yield), 2,4-*Bis*-*O*-MOM-benzaldehyde (**B.4**, 90% yield), 3,4-*Bis*-*O*-MOM-benzaldehyde (**B.5**, 85% yield), and 2,5-*Bis*-*O*-MOM-benzaldehyde (**B.6**, 82% yield).

General procedure for synthesis of chalcones C.1–21 and C.43

Procedure for compounds C.1–14, **C.17–21 and C.43**: To a stirred ethanolic solution (5 mL) of acetophenone (2 mmol) and respective benzaldehydes (2.2 mmol) was added dropwise an aqueous solution of KOH (60% w/v, 2 mL) at 0 °C (WANG et al., 2015). The reaction was stirred for 2–6 hours at room temperature. Upon total conversion, the crude product was extracted with ethyl acetate (3 × 25 mL). The organic layers were combined and washed with saturated $NaHSO_3$(aq) solution (2×10 mL) to remove benzaldehyde excess (BOUCHER et al., 2017), dried over $MgSO_4$, filtered, and concentrated under reduced pressure, furnishing respective chalcones **C.1–14** and **C.17–21**.

Procedure for C.15 and C.16: Chalcones were prepared according to Bhambra et al., with slight modifications (BHAMBRA et al., 2017). To a stirred mixture of 3- or 4-

pyridinecarboxaldehyde (2 mmol) and NaOH (2 mmol) in anhydrous 1,4-dioxane (5 mL) in ice bath was added slowly 2 mL of the solution of **A.5** (1.5 mmol) for 1 h. The mixture reaction was stirred at room temperature for 30 minutes. Upon conversion, the crude product was extracted with ethyl acetate (3 × 25 mL), dried over $MgSO_4$, filtered, and concentrated under reduced pressure. The crude product was purified over silica gel chromatography column using a mixture of ethyl acetate:hexane (3:7) as mobile phase, furnishing the respective chalcones **C.15** and **C.16**.

Synthesis of 3-methyl-2-butenylboronic acid pinacol ester (R.1)

In a three-neck round-bottom flask containing a solution of Bis(pinacolato)diboron in THF (10 mL) was added Cs_2CO_3 (20 mmol), methanol (8 mL) and 2-methyl-3-buten-2-ol (8.6 mL; 80 mmol) (MIRALLES et al., 2016) The mixture reaction was stirred under N_2 atmosphere at 40 ºC for 24 h. After this period, crude product was extracted with ethyl acetate (3×25 mL), washed with brine, dried over $MgSO_4$ and concentrated under reduced pressure to give **R.1** as a translucent oil (75% yield).

General procedure for synthesis of prenylated chalcones C.22–42

In a three-neck round-bottom flask were added the respective chalcones (**C.1–21**) (2 mmol) in DMF (3 mL), $CsCO_3$ (4 mmol), $PdCl_2$(ddpf) (0.2 mmol), and 3-methyl-2-butenylboronic acid pinacol ester (**R.1**) (3 mmol) (WANG et al., 2015). The reaction mixture was stirred at 80 ºC for 1–2 h under nitrogen atmosphere. Then, the mixture reaction was cooled to room temperature, diluted with ethyl acetate (30 mL) and filtrated over celite column. The filtered was washed with distilled water (4×50 mL) and brine (1×50 mL), dried over magnesium sulfate, filtrated and evaporated under reduced pressure to give a dark-colored oil, which was purified over silica gel column chromatography, furnishing the respective prenylated chalcones.

Rearrangement of chalcone C.43

To a stirred solution of **C.43** (1.8g, 3.7 mmol) in dry CH_2Cl_2 (50 mL) was added montmorillonite K10 (2 g) at 0 ºC and the reaction was stirred for 1 h at room temperature (SUGAMOTO et al., 2011). The crude product was filtrated, washed several times with ethyl acetate and concentrated under reduced pressure, obtaining a brown oil. The oil was purified over silica gel column chromatography with hexane/ethyl acetate/acetone (9.5:0.25:0.25) to afford compounds **C.44** and **C.45** as a yellow solids with yields of 35 and 38%, respectively.

General procedure for deprotection

To a stirred solution of MOM-protected chalcones **C.22–42** and **C.44–45** (1 mmol eq) in approximately 3–5 mL of MeOH:THF (1:1) it was added HCl 1 mol/L aqueous solution (3–5 mmol eq) at 0 ºC. The mixture reaction was stirred under reflux for 6 h. The mixture reaction was poured into crushed ice, and additionally, for pyridinyl derivatives **C.36** and **C.37**, it was neutralized with 10% $NaHCO_3$. The crude product was extracted using ethyl acetate (3 × 20 mL). The organic layers were combined, washed with brine, dried over $MgSO_4$, filtrated, and evaporated under reduced pressure. The crude product obtained was purified over silica gel column chromatography with hexane/ethyl acetate to afford respective chalcones **IBC**, **IBC 1–7** and **IBC 9–23**.

Synthesis of IBC 8

In a ethanolic solution (2 mL) of **IBC 14** (0.08 mmol) was added $SnCl_2.2H_2O$ (0.4 mmol) (SONMEZ et al., 2011). The mixture reaction was refluxed under stirring for 2h. The reaction was poured onto crushed ice and neutralized with a solution of 5% $NaHCO_3$. The orange precipitate was filtrated, and purified over silica gel column chromatography using a mixture of hexane, ethyl acetate and ethanol (4:0.9:0.1) as mobile phase furnishing **IBC 8** as an orange oil with 64% yield.

Synthesis of DHIBC

In an ethanolic solution (1 mL) containing **IBC** (30 mg, 0.12 mmol) under stirring, was added Et_3SiH (40 µL, 0.24 mmol) and a catalytic amount of $Pd(Ac)_2$ (3 mg, 0.01 mmol) at room temperature. After five min, the color of reaction changed from yellow to colorless, indicating the end of reaction, which was confirmed TLC inspection. The mixture was filtrated under celite column, and the solvent was evaporated under reduced pressure, obtaining a white powder, which was purified over silica gel chromatographic column using mobile phase with hexane, ethyl acetate and acetone (8:1:1) furnishing **DHIBC** as a white powder with 50% yield.

4.1.2. Partition coefficient (n-octanol/water) measured by HPLC

Log $P_{o/w}$ values were determined using a constructed log *k* versus log *P*o/w plot with good linear relationships by using procedures preconized by OECD Guidelines for the Testing of Chemicals (OECD, 1989). The theoretical log *P* used for reference compounds was extracted from SwissADME (DAINA; MICHIELIN; ZOETE, 2017). Capacity factor (*k*) values of reference compounds were calculated according to their respective retention time (rt) in HPLC

chromatogram analysis by the formula k = (rt–rt0)/rt0, where rt0 is the retention time of thiourea. As reference compounds it was used acetophenone, cinnamic acid, benzophenone, thymol, toluene, biphenyl, fluoranthene, and triphenylamine. A standard curve was plotted for respective isocratic flow of MeOH:H_2O (70:30, 75:25 and 80:20).

4.2. Antimycobacterial assay

The antimycobacterial activity of compounds was determined against *Mycobacterium tuberculosis* H37Rv (ATCC 27294) using Resazurin Microtiter Assay (REMA) method from Palomino et al (PALOMINO et al., 2002). The inoculum was prepared in Middlebrook 7H9 media and an aliquot was incubated at 37 ºC for 7 days at 120 rpm, which was compared with McFarland scale. The mycobacterial suspension was diluted to achieve 3.0×10^5 CFU/mL, which was distributed into 96-well plates. Stock solutions of compounds were prepared in DMSO (Synth, Diadema, Brazil) and diluted in Middlebrook 7H9 broth (DifcoTM, Detroit, MI, USA) to achieve final concentrations ranging from 25 to 0.09 µg/mL. Rifampicin was used as reference antitubercular drug. Plates were incubated at 37 ºC with 5% CO_2 for seven days. Then, 30 µL of resazurin was added to the wells, and after 24 h the plates were examined by fluorescence spectrometer at 530 and 590 nm. The MIC_{90} value was defined as the lowest drug concentration able to inhibit 90% of mycobacterial growth, which was expressed in µg/mL. The assays were conducted in triplicate.

CHAPTER IV

2-hydroxyisocordoin inhibits MSSA and MRSA biofilm formation and targets the cell membrane of Gram-positive bacteria

Chapter IV

2-hydroxyisocordoin inhibits MSSA and MRSA biofilm formation and targets the cell membrane of Gram-positive bacteria

Leticia Ribeiro de Assis[a], Reinaldo dos Santos Theodoro[a], Julyanna Andrade Silva Nascentes[a], Maria Beatriz Silva Costa[a], Meliza Arantes de Souza Bessa[b], Ralciane de Paula Menezes[b], Guilherme Dilarri[c], Vanessa R. dos Santos[d], Cristiane Duque[d], Henrique Ferreira[c], Carlos Henrique Gomes Martins[b], Luis Octavio Regasini[a]

[a]Institute of Biosciences, Humanities and Exact Sciences, São Paulo State University (UNESP), Department of Chemistry and Environmental Sciences, São José do Rio Preto CEP 15054-000, SP, Brazil.

[b]Institute of Biomedical Sciences, Federal University of Uberlândia (UFU), Department of Microbiology, Institute of Biomedical Sciences, Uberlândia, CEP 38405-320, MG, Brazil

[c]Institute of Biosciences, São Paulo State University (UNESP), Department of Biochemistry and Microbiology, Rio Claro, CEP 130506-900, SP, Brazil.

[d]São Paulo State University (UNESP), School of Dentistry, Department of Preventive and Restorative Dentistry, Araçatuba, CEP 16015-050, SP, Brazil

ABSTRACT

Staphylococcus aureus is one of the most common pathogens in nosocomial and community-acquired infections. Resistance of *S. aureus* against current antibiotics represents a great challenge to be overcome, requiring efforts in drug discovery of anti-*S. aureus* agents. Herein, we evaluated 24 *C*-prenylated analogs against Methicillin-Susceptible *Staphylococcus aureus* (MSSA) and Methicillin-Resistant *Staphylococcus aureus* (MRSA) *S. aureus*. 2-hydroxyisocordoin (**IBC 2**), 3-hydroxyisocordoin (**IBC 1**), corylifol B (**IBC 4**), and dihydroisobavachalcone (**DHIBC**) were the most potent compounds, showing MIC of 1.56–12.5 µg/mL against MSSA and MRSA. Among them, we selected **IBC 2** for additional bioassays. **IBC 2** inhibited more than 50% of MSSA and MRSA biofilm formation at 0.78 and 1.56 µg/mL concentrations, respectively. The Live/Dead test with *Bacillus subtilis* suggested that the mode of antibacterial action of **IBC 2** is related to the damage it causes to cytoplasmic membrane. Non-cytotoxic effect was observed against keratinocytes (HaCaT cells) after their exposure for 24 h to **IBC 2** in concentrations ranging from 0.39 to 12.5 µg/mL. In addition, its antibacterial activity spectrum indicated action against *Streptococcus sanguinis* (MIC = 3.12 µg/mL), *S. mutans* (MIC = 6.25 µg/mL), *S. pneumoniae* (MIC = 50 µg/mL), *Klebsiella pneumoniae* (MIC = 100 µg/mL), and *Helicobacter pylori* (MIC = 3.90 µg/mL). Altogether, **IBC 2** has promising antibacterial potential, which can be explored in the research & development of novel antibacterial drugs.

1. Introduction

The pharmacological treatment of bacterial infections, such as urinary tract infections, pulmonary infections, wounds, sepsis, sexually transmitted infections, and some forms of diarrhea, is becoming ineffective due to the high rates of resistance against multiple antimicrobial agents. Antibiotic-resistant bacterial infections caused about 1.2 million deaths in 2019 worldwide (MURRAY et al., 2022), and there is a projection that this number will significantly raise to 10 million per year till 2050 (O'NEILL, 2016; VIKESLAND et al., 2019). Multisectoral approach is urgently required to mitigate this problem, which includes discovery and development of new antimicrobial drugs, especially against WHO list priority pathogens such as *Acinobacter baumannii*, *Pseudomonas aeruginosa*, *Klebsiella pneumoniae*, *Helicobacter pylori*, *Enterobacter* species, *Enterococcus faecium*, *Streptococcus pneumoniae*, *Staphylococcus aureus*, *Haemophilus influenzae*, *Mycobacterium tuberculosis* and others (WHO, 2017).

According to WHO list priority pathogens, *S. aureus* ranks as the highest priority among Gram-positive species. *S. aureus* is well-adapted to human hosts and the healthcare environment. Moreover, it is responsible for endocarditis, bacteremia, osteomyelitis, and skin and soft tissue infections. *β*-Lactam antibiotics are frequently used to treat cutaneous and systemic *S. aureus* infections. However, these infections are becoming difficult to combat due to the rise of Methicillin-Resistant *Staphylococcus aureus* (MRSA) (TURNER et al., 2019). Vancomycin, daptomycin, orally active linezolid or ceftaroline and ceftobiprole has been used to treat MRSA infections (TURNER et al., 2019). The biggest challenge is the fast spread of Vancomycin Intermediate-Resistant *Sthaphylococcus aureus* (VISA) and Vancomycin-Resistant *Staphylococcus aureus* (VRSA) infections. Thus, there is an urgent need to develop novel antibiotics to overcome the several resistance mechanisms involved in MDR staphylococci infections (GARDETE; TOMASZ, 2014). *S. aureus* can infect and form a chronic biofilm on abiotic or biotic surfaces. Once established, biofilms are difficult to combat due to their resistance against sanitizing compounds, antibacterial drugs and host immune response (YIN et al., 2019). Currently, antibacterial therapy with one drug is not enough to eradicate *S. aureus* biofilm infections, requiring combined therapy, the prevention of its formation or surgical removal (BHATTACHARYA et al., 2015). Several efforts are necessary to combat *S. aureus* infections, including investment in new drugs and improvement of the existing ones (O'NEILL, 2016).

Chalcones or 1,3-diphenyl-2-propen-1-one are precursor compounds of biosynthesis of flavonoids, abundantly present in plants (ROZMER; PERJÉSI, 2016). Several chalcones have antibacterial activity against MSSA and MRSA planktonic cells and their biofilms, turning this class of compounds as valuable inspiration for discovery and development of new antibiotics (BOCQUET et al., 2019; DAN; DAI, 2020; MEIER et al., 2019; WU et al., 2019). Among them, isobavachalcone (**IBC**) or 4-hydroxyisocordoin has been reported to possess several biological activities such as antimicrobial, antiviral, anti-inflammatory, antitumoral and others (WANG et al., 2021). **IBC** has *in vitro* and *in vivo* antibacterial activity against MSSA and MRSA strains (ÁVILA et al., 2008; DZOYEM et al., 2013; HE et al., 2018; OSÓRIO et al., 2012; SONG et al., 2021; SUGAMOTO et al., 2011). In this context, we described that **IBC** prevents MSSA and MRSA biofilm formation at subinhibitory concentrations (ASSIS et al., 2022).

Herein, we evaluated a series of analogs of **IBC** (Figure 9, Chapter I), and evaluated their anti-MSSA and MRSA activity. Aiming to access antibacterial spectrum of all analogs, antibacterial activities was determined against Gram-positive (*Streptococcus pneumoniae*, *S.*

sanguinis, *S. sobrinus*, and *S. mutans*), and Gram-negative bacteria (*Pseudomonas aeruginosa*, *Klebsiella pneumoniae* and *Helicobacter pylori*). We investigated the structure-activity relationship using modifications on rings A and B, isoprenyl subunit, and *trans*-enonic bridge. Among promising chalcones, we selected 2-hydroxycordoin (**IBC 2**) to further assays against MSSA and MRSA, including checkerboard assay with vancomycin and its antibiofilm activity. We tested the effect of **IBC 2** on the cell membrane of *B. subtilis* and its cytotoxicity of **IBC 2** against human keratinocytes (HaCaT cells).

2. Materials and Methods

2.1. Chemical procedures

General procedure, synthesis and structural characterizations of chalcones **IBC 1–IBC 23** and **DH-IBC** were previously reported in Chapter III, item 4.1. The structures of compounds are presented in figure 9, chapter I.

2.1.1. Synthesis

The Dihydrochalcone **DH-IBC 2** was synthesized using previously reported protocol (chapter III). To an ethanolic solution (1 mL) containing 2-hydroxyisocordoin (**IBC 2**, 30 mg, 0.12 mmol) was added Et_3SiH (40 µL, 0.24 mmol) at room temperature. A catalytic amount of $Pd(Ac)_2$ (3 mg, 0.01 mmol) was added to the mixture, and after five minutes, the color of the reaction changed from yellow to colorless. The mixture was filtrated under celite column, and the solvent was evaporated under reduced pressure, obtaining a white crude product, which was purified over silica gel chromatographic column using hexane, ethyl acetate and acetone (8:1:1) as mobile phase, obtaining **DH-IBC 2** with 60% yield. White crystalline powder; overall yield: 8%. HPLC purity: 99%; m.p.: 125–130 ºC. ^{1}H NMR (600 MHz, acetone-d_6): δ 1.63 (s, H-4”), 1.76 (s, H-5”), 3.0 (t, *J* = 7.5 Hz, 2H, H-β), 3.25 (t, *J* = 7.5 Hz, H-α), 3.34 (d, *J* = 7.2 Hz, H-1”), 5.24 (d, *J* = 7.2 Hz, H-2”), 6.48 (d, *J* = 8.8 Hz, H-5’), 6.76 (dd, *J* = 0.9, 7.4 and 8.0 Hz), 7.03 (ddd, *J* = 1.4, 7.4 and 8.0 Hz), 7.17 (dd, *J* = 1.4 and 7.4 Hz, H-6), 7.72 (d, *J* = 8.8 Hz, H-6’), 8.70 (brs, 4’-OH), 13.8 (s, 2’-OH).

2.2. Antibacterial Assays

Antibacterial activity against MSSA, MRSA, S. pneumoniae, S. sanguinis, S. mutans, S. sobrinus, K. pneumoniae, and P. aeruginosa

Chapter II, item 2.2

Anti-Helicobacter pylori activity

H. pylori (ATCC 43526) was obtained from the American Type Culture Collection (ATCC) and maintained under cryopreservation (-80 °C) in Mueller Hinton broth (Difco Labs, Detroit, MI, USA) supplemented with 5 % fetal bovine serum, containing 20 % glycerol and 0.5 mL of defibrinated sheep blood (Bio Boa Vista, Valinhos, SP, Brazil). Antibacterial activity of selected analogs against *H. pylori* was determined using protocols reported by Moraes et al. (MORAES et al., 2021). Mueller Hinton broth (Difco) supplemented with 10% fetal bovine serum was used for microdilution assay. The compounds were dissolved in 5% DMSO in 96-well plates to reach concentrations ranging from 1000 to 0.48 µg/mL. The inoculum concentration was adjusted to 5×10^5 Colony Forming Units per milliliter (CFU/mL). Plates were prepared in triplicate and incubated at 37 °C for three days in 10% CO_2 atmosphere. Tetracycline (Merck) was used as antibacterial drug reference in concentrations ranging from 5.9 to 0.015 µg/mL, and DMSO was used as negative control. An aqueous solution of resazurin (Merck) (30 µL, 0.01%) was added to each well for visual inspection (SARKER; NAHAR; KUMARASAMY, 2007). The Minimal Inhibitory Cconcentration (MIC) was defined as the lowest concentration able to inhibit visible growth, indicated by coloring change from pink (metabolically active cells) to blue (nonviable cells). Three independent assays were performed.

2.3 Checkerboard Assay

Chapter II, item 2.3

2.4. Antibiofilm Assay

Chapter II, item 2.4

2.5. Membrane Disruption Assay

Chapter II, item 2.5

2.6. Cytotoxicity Assay

Chapter II, item 2.6

3. Results and Discussion

3.1. Anti-MSSA and anti-MRSA activity

First, we determined the minimal inhibitory concentration (MIC) of all compounds against MSSA (Tables 1 and 2), and the most active compounds, with MIC values ranging from 1.56 µg/mL to 12.5 µg/mL, were tested against MRSA. 2-Hydroxyisocordoin (**IBC 2**) was the most potent compounds against MSSA, showing MIC of 1.56 µg/mL, followed by chalcones

3-hydroxyisocordoin (**IBC 1**), corylifol B (**IBC 4**), and dihydroisobavachalcone (**DHIBC**) (MIC = 3.12 μg/mL). These chalcones also inhibited the MRSA growth in MIC concentrations ranging from 1.56 to 12.5 μg/mL^{-1}. Among them, corylifol was the most active compound against MRSA (MIC = 1.56 μg/mL), followed by IBC 1–IBC 3 (MIC = 3.12 μg/mL). All other compounds **(IBC 5**– **IBC 7**, **IBC 9**, **IBC 14**, and **IBC 13–IBC 20**) were weakly active (MIC = 50–200 μg/mL) or inactive (MIC > 400 μg/mL) against MSSA.

Table 1. Anti-MSSA and anti-MRSA activities of **IBC 1–IBC 20**

	Chalcone	R or Ar	MIC(μg/mL)	
			MSSA	MRSA
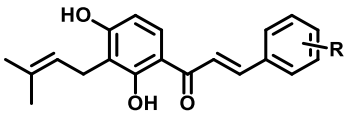	**IBC 1**	3-OH	3.12	3.12
	IBC 2	2-OH	1.56	3.12
	IBC 3	2,4-diOH	12.5	3.12
	IBC 4	3,4-diOH	3.12	1.56
	IBC 5	2,5-diOH	200	N.T
	IBC 6	-H	100	N.T
	IBC 7	4-OMe	> 400	N.T
	IBC 8	4-NH_2	6.25	12.5
	IBC 9	4-Me	> 400	N.T
	IBC 10	4-F	> 400	N.T
	IBC 11	4-Cl	> 400	N.T
	IBC 12	4-Br	> 400	N.T
	IBC 13	4-CF_3	> 400	N.T
	IBC 14	4-NO_2	50.0	N.T
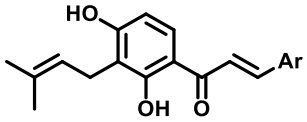	**IBC 15**	3-pyridinyl	> 400	N.T
	IBC 16	4-pyridinyl	> 400	N.T
	IBC 17	2-furanyl	> 400	N.T
	IBC 18	2-tiophenyl	> 400	N.T
	IBC 19	1-naphthyl	> 400	N.T
	IBC 20	2-naphtyl	> 400	N.T
-	**TC**	-	0.20	> 5.90

TC = tetracycline; NT = not tested

Table 2. Anti-MSSA and anti-MRSA activities of chalcones **IBC 21**– **IBC 23** and di-hydrochalcones (**DHIBC** and **DHIBC 2**)

	Compound	R	R'	MIC (µg/mL)	
				MSSA	MRSA
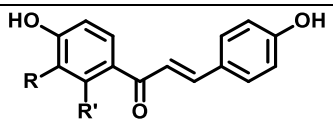	**IBC 21**	H	OH	50.0	N.T
	IBC 22	geranyl	OH	12.5	N.T
	IBC 23	isoprenyl	H	6.25	6.25
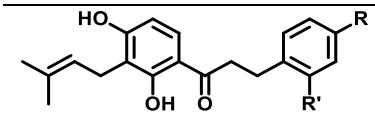	**DHIBC**	OH	H	3.12	3.12
	DHIBC 2	H	OH	100	N.T
	IBC	isoprenyl	OH	1.56	3.12
	TC	-	-	0.20	5.90

TC = tetracycline; NT = not tested

The anti-MSSA and anti-MRSA activities of **IBC** was well-explored in Chapter II. Herein, we used antibacterial activity of **IBC** for set a structure relationship activity (SAR). SAR investigation using MIC values from anti-MSSA experiments suggested that isoprenyl at C-3' and hydroxyls at 2' and 4 were crucial groups for the potent anti-MSSA activity of **IBC** since their removal led to 4- to 64-fold fewer active compounds. Moreover, the increasing of prenyl side chain from isoprenyl to geranyl group decreased bioactivity, considering that **IBC 22** (MIC = 12.5 µg/mL) was less active than **IBC** about 8-fold.

Ávila and co-workers demonstrated the replacement of hydroxyl from *para* to *ortho*- or *meta*-positions on ring B of C-3' prenylated chalcones led to inactive compounds against MSSA (ÁVILA et al., 2008). We found that the regioisomers of **IBC**, carrying hydroxyl at 2 (**IBC-2**) and 3 (**IBC 1**) on ring B, demonstrated strong anti-MSSA properties, with MIC values of 1.56 µg/mL and 3.12 µg/mL, respectively, similar to those reported for **IBC** (MIC = 1.56 µg/mL**)**. Chalcones with resorcinol (**IBC 3**, MIC = 12.5 µg/mL), catechol (**IBC 4**, MIC = 3.12 µg/mL) and aminobenzene (**IBC 8**, MIC = 6.2 µg/mL) as ring B displayed similar antibacterial activity in comparison to chalcones carrying a monohydroxylated phenolic ring B. Otherwise, a hydroquinone as ring B (**IBC 5**) demonstrated weak antibacterial activity (MIC = 200 µg/mL), evidencing the relevance of *para* hydroxyl on ring B for anti-MSSA activity.

For chalcones, the α,β-unsaturated ketone moiety has been recognized by its pharmacophoric contribution for several bioactivities (DAN; DAI, 2020; ZHUANG et al., 2017). This subunit has potential as a Michael's acceptor, reacting with bionucleophiles such as cysteine residues present in cellular peptides or proteins, forming a Michael adduct, which

may play an important role as covalent modifier (JOHANSSON, 2012; MAUCHER et al., 2017). Many approved and clinically investigated drugs have Michael's acceptor subunit, acting as pharmacophoric electrophile site (BAUER, 2015). We found that *trans*-olefin bridge of **IBC 2** is essential for antibacterial activity (Table 1), since its reduced analog **DH-IBC 2** was significantly less active against most bacterial species. In contrast, the hydrogenation of *trans*-olefin bridge of **IBC** was not relevant or slightly contributes to antibacterial activity since **DHIBC** demonstrated anti-MSSA activity.

Compounds **IBC 15**–**IBC 20** exhibits non-phenyl ring B, including pyridinyl, furanyl, tiophenyl and naphthyl and did not present anti-MSSA activity. The promising antibacterial activity of **IBC 2** encourages us to select it for additional bioassays investigations.

3.2. Checkerboard assay

Former literature has demonstrated that association of chalcones and antibacterial drugs is a useful strategy to improve antibacterial activity of both (GARCIA et al., 2021; SONG et al., 2021). Thus, we investigated the effect of combination of **IBC 2** and vancomycin by checkerboard assay against MSSA and MRSA planktonic cells, aiming the improvement of their potency in association when compared to their individual activities. This combination was classified as indifferent, with FICI values of 2 and 3 for MSSA and MRSA, respectively, since it did not affect or slightly affect the antibacterial activity compared to individual MIC values of **IBC 2** and vancomycin (Table 3).

Table 3. Antibacterial effect of combination between **IBC 2** and vancomycin against MSSA and MRSA

strain	combination	MIC (µg/mL)				FICI	type of combination
		Alone		Combined			
		C	V	C	V	FIC^c+FIC^v	
MSSA	**C + V**	1.56	0.73	1.56	0.73	2	indifferent
MRSA	**C + V**	3.12	0.73	3.12	1.47	3	indifferent

C = **IBC 2**, V = vancomycin

3.3. Antibiofilm Assay

Naturally-occurrence *C*-prenylated chalcones such as xanthohumol (BOCQUET et al., 2019; BOGDANOVA et al., 2018) and licochalcone A (SHEN et al., 2015), as well as synthetic chalconic derivatives (BOZIC et al., 2014; EMERI et al., 2019; GARCIA et al., 2021; ZHANG et al., 2017), are found to prevent the formation and eradicate the *S. aureus* biofilm. In previous studies from our group (ASSIS et al., 2022), we found that **IBC** inhibited the formation of

MSSA and MRSA biofilms. Herein, we investigated the antibiofilm activity of **IBC 2** against MSSA and MRSA. Vancomycin was used as reference drug.

IBC 2 prevented the MSSA and MRSA biofilm formation by more than 50% at subinhibitory concentrations (MIC/2) of 0.78 µg/mL and 1.56 µg/mL in comparison to untreated control, respectively. The BMIC values demonstrated by **IBC 2** was similar to those recorded for vancomycin against MSSA and MRSA biofilm formation (BMIC = 0.74 µg/mL). In four cases, the MSSA and MRSA biofilms reductions were accompanied by a decrease in CFU/mL (Figure 1).

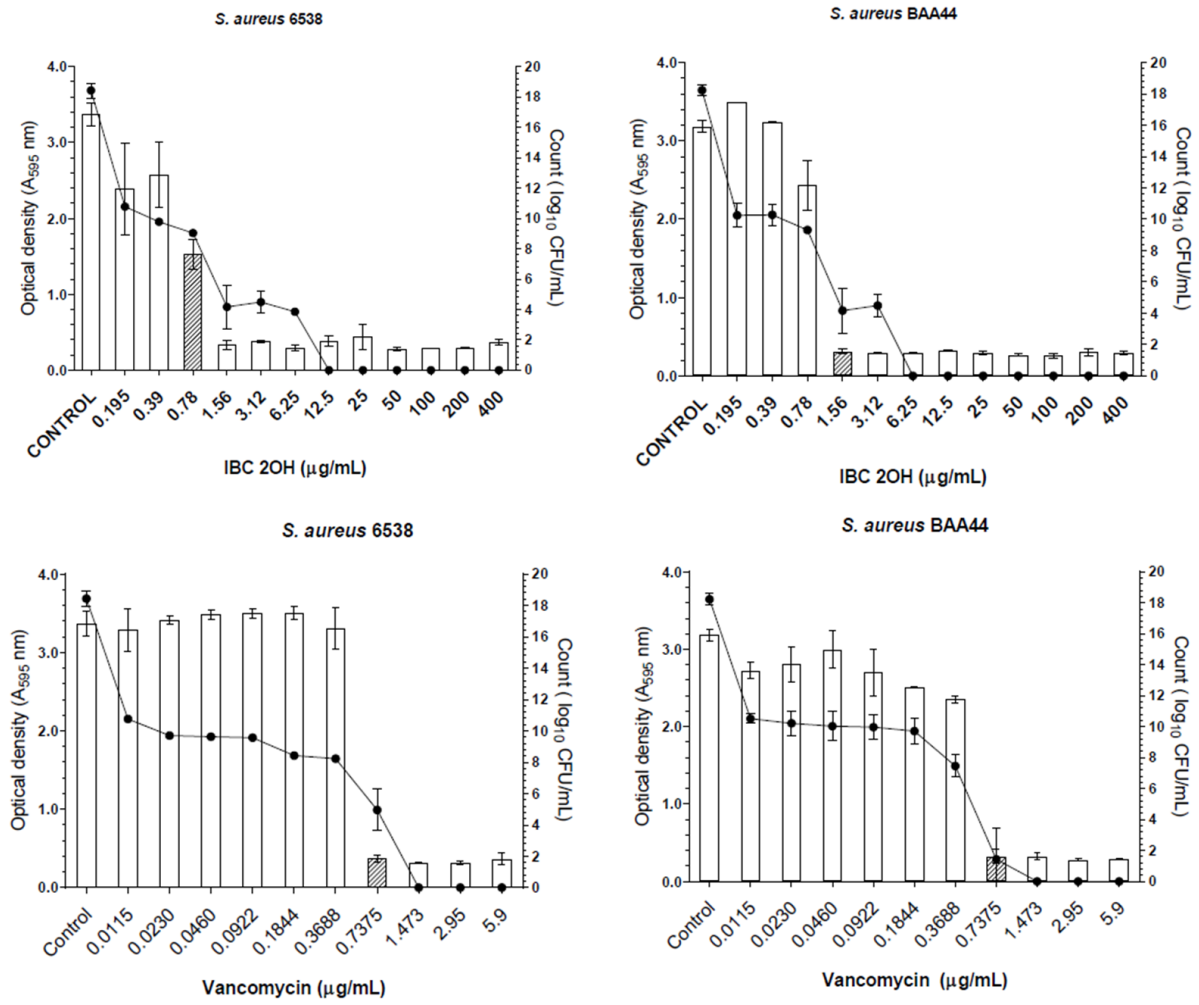

Figure 1. Effect of **IBC 2** and vancomycin on MSSA (*S. aureus* 6538) and MRSA (*S. aureus* BAA44) biofilm formation. The hatched bars represent the MBIC values. The lines represent the $\log_{10}$ CFU/mL.

3.4. Membrane Disruption Assay

Bacterial membranes have been recognized as primary target of phenolic compounds. Eugenol is a volatile phenylpropanoid and causes damage to *S. aureus* membrane via Reactive Oxygen Species (ROS) (DAS et al., 2016). The bacteriostatic effect of quercetin, a widespread flavonoid in plants, is provoked by disrupting bacterial membranes (WANG et al., 2018). In our previous studies, we found that **IBC** (ASSIS et al., 2022), 4-hydroxyderricin (THEODORO, 2022), and synthetic antibacterial analogs of curcumin were able to disrupt bacterial membrane of Gram-positive bacteria (MORÃO et al., 2019; POLAQUINI et al., 2019).

Aiming to assess the potential membrane disruption of **IBC 2**, similarly to its prototype (**IBC**), the cells of *B. subtilis* were submitted to with propidium iodide (PI)/ SYTO9 stains and analyzed by fluorescence under microscopy inspection. *B. subtilis* is a Gram-positive non-pathogenic bacteria commonly used in studies of antibacterial mode of action (MORÃO et al., 2019). SYTO9 is a blue fluorescent dye that stains the bacterial nucleoid, whereas IP is a cell red fluorescent dye that just can cross disrupted cell membranes (NAVARRO et al., 2020).

B. subtilis was treated with **IBC 2** at its MBC value (6.25 µg/mL), as well as with nisin (positive control, 5.0 µg/mL), an drug that targets the bacterial membrane producing pores (WIEDEMANN; BENZ; SAHL, 2004). The microscopy analysis displayed that cells treated with **IBC 2** were predominantly stained in red, indicating membrane damage (Figure 2). This damage occurs in about 60% of the cells compared to negative control (1% DMSO) (Figure 3). Treatment with nisin indicated about 95% of membrane damage.

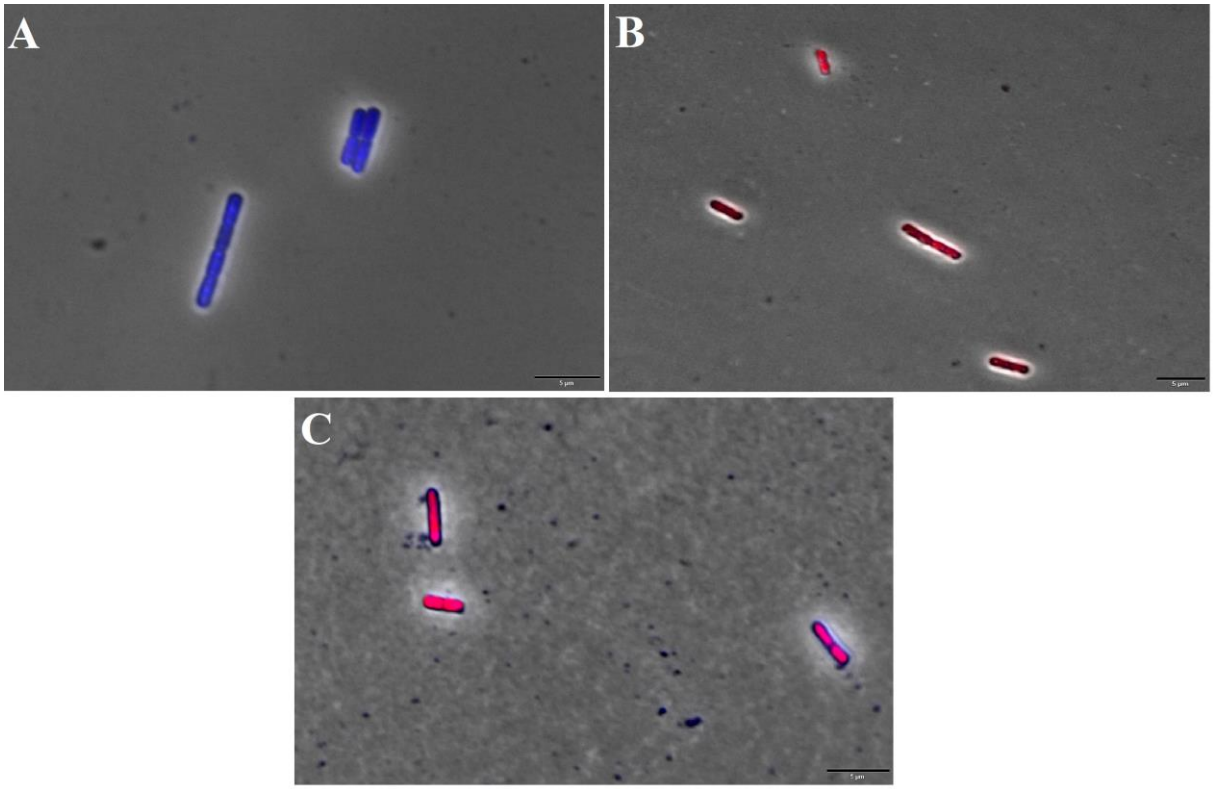

Figure 2. Fluorescence microscopy of *Bacillus subtilis* stained with propidium iodide and SYTO9. A) negative control (*B. subtilis* treated with 1% DMSO); B) positive control (cells treated with nisin at 5.0 µg/mL); C) cells treated with **IBC 2** at 6.25 µg/mL. Scale bar 5 µm; Magnification of 100×

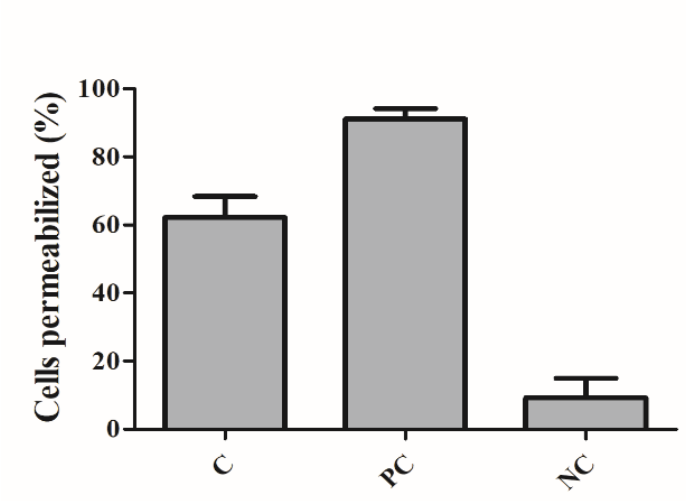

Figure 3. Percentage of disrupted *B. subtilis* cells. C, cells treated with **IBC 2**, PC, cells treated with positive control (nisin); NC, negative control (DMSO 1 %).

3.5. Effect of IBC 2 on keratinocytes

Toxicity assay was performed against human epidermal keratinocytes (HaCaT). HaCaT cell viability was not affected at concentrations of **IBC 2** ranging from 0.39 to 12.5 µg/mL after 24h, whereas at 25 µg/mL, the viability decreased by about 15 to 20% (Figure 4). The highest non-cytotoxic concentration of **IBC 2** was about 4 to 8-time higher than its MIC values recorded against MRSA and MSSA, respectively, indicating that **IBC 2** has selectivity at its antibacterial concentration. Moreover, **IBC 2** was less cytotoxic than chlorhexidine (CHX) at 12.5 µg/mL.

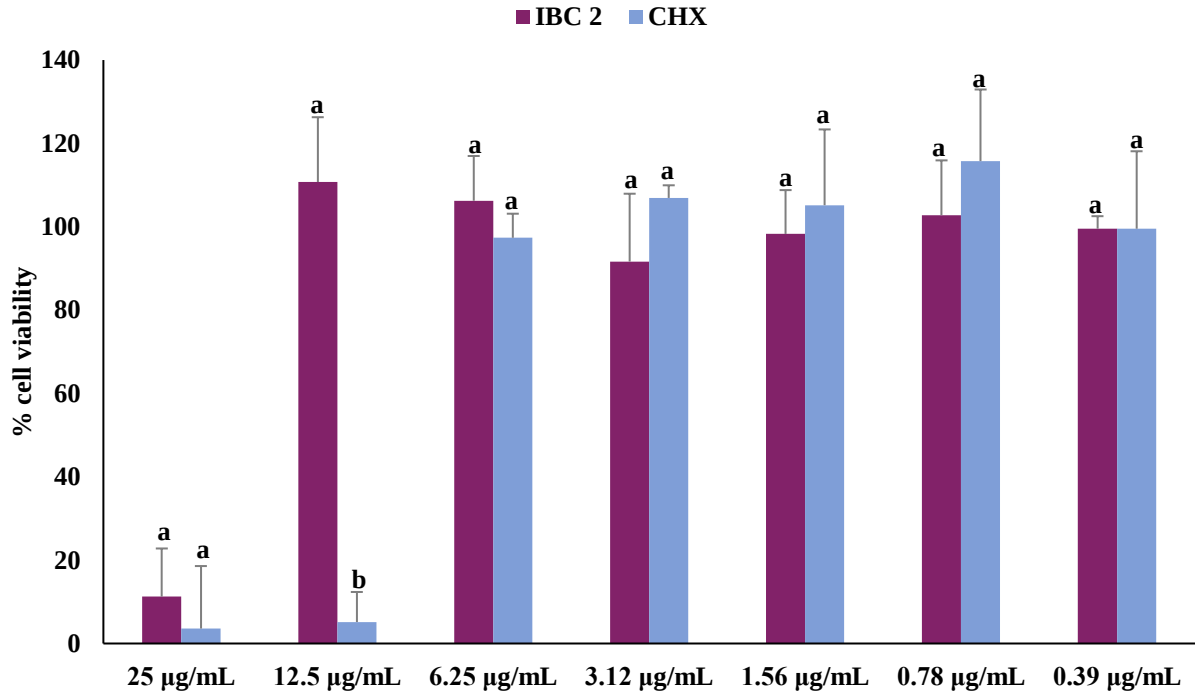

Figure 4. Effect of different concentrations of **IBC 2** and chlorhexidine (CHX) on the viability of HaCaT cells. The results are expressed as means ± SDs. Different lowercase letters (a,b) show statistical differences between IBC 2 and CHX, according to ANOVA and Tukey's test (p <0.05).

3.6. Spectrum of antibacterial activity of IBC 2

Aiming to access the antibacterial spectrum of **IBC 2**, it was evaluated against other four Gram-positive (*Streptococcus pneumoniae*, *S. sanguinis*, *S. sobrinus*, and *S. mutans*) and three Gram-negative (*Pseudomonas aeruginosa*, *Klebsiella pneumoniae* and *Helicobacter pylori*) (Table 4). Among them, four (*S. pneumoniae*, *P. aeruginosa*, *K. pneumoniae* and *H. pylori*) are on the WHO priority pathogens list that are urgently needed for drug development (WHO, 2017). **IBC 2** was able to inhibit the growth of all Gram-positive bacteria (MIC = 3.12

to 50 µg/mL), *H. pylori* (MIC = 3.90 µg/mL) and *K. pneumoniae* (MIC = 100 µg/mL). Whereas against *P. aeruginosa*, **IBC 2** was inactive (MIC > 400 µg/mL).

Table 4. Antibacterial spectrum of **IBC 2** against Gram-positive and Gram-negative species

		MIC (µg/mL)		
	Species	**IBC 2**	**Tetracycline**	**Chlorhexidine**
Gram-positive	*S. pneumoniae*	50.0	0.40	-
	S. sanguinis	3.12	-	1.82
	S. sobrinus	12.5	-	3.64
	S. mutans	6.25	-	0.91
Gram-negative	*P. aeruginosa*	> 400	5.90	-
	K. pneumoniae	100	2.95	-
	H. pylori	3.90	1.47	-

4. Conclusions

Twenty-four analogs of **IBC** were evaluated against MSSA and MRSA. Among them, 2-hydroxyisocordoin (**IBC 2**), 3-hydroxyisocordoin (**IBC 1**), corylifol B (**IBC 4**), and dihydroisobavachalcone (**DHIBC**) were the most promising compounds, showing MIC values of 1.56–12.5 µg/mL against MSSA and MRSA. Structure-activity relationship data suggested that isoprenyl, 2'-hydroxyl group on ring A and phenyl ring B carrying hydrophilic groups such as amino and hydroxyl demonstrated a key role in anti-MSSA activity. Among promising chalcones, we selected 2-hydroxyisocordoin (**IBC 2**) for detailed bioassays. The combination of **IBC 2** with vancomycin demonstrates an indifferent effect against MSSA and MRSA. Moreover, **IBC 2** inhibited MSSA and MRSA biofilm formation at its subinhibitory concentrations. The investigation of antibacterial mode of action of **IBC 2** is related to disruption of the cytoplasmatic membrane, similarly to **IBC**. **IBC 2** exhibited a low toxic effect against human keratinocytes. Moreover, the antibacterial properties of **IBC 2** were confirmed against *S. pneumoniae*, *S. mutans*, *S. sanguinis*, *S. sobrinus*, *H. pylori*, and *K. pneumoniae.* Altogether, this research provides **IBC 2** as a new antibacterial agent, with potential application as a drug candidate in the fight against MDR pathogens.

CHAPTER V

General conclusions, References and Appendix

Chapter V

1. General conclusions and Perspectives

Due to evidences of pharmacological activities of isobavachalcone (**IBC**), a natural C-prenylated chalcone, it was used as prototype compound to design 25 analogs, with modifications on ring A and ring B and on *trans*-enone bridge. Among these analogs, 15 are novel chemical entities and 6 are chalcone of naturally-occurrence in plants (xanthoangelol, corylifol B, morachalcone A, hayeanachalcone, isocordoin, and isoliquiritigenin). The synthetic route used to achieve the synthesis of **IBC** and its analogs furnished a total of 85 compounds, including 59 intermediaries and 26 target compounds. The final compounds were synthesized in five to seven synthetic steps, with variable overall yields ranging from 1 to 37%. Among them, we achieved the total synthesis of hayeanachalcone (**IBC 7**) for the first time, with overall yield of 37%.

Using **IBC** as framework, we found seven promising antibacterial chalcones against MSSA and MRSA, with MIC values ranging from 1.56 to 12.5 µg/mL. Among them, **IBC** and its novel regioisomer 2-hydroxyisocordoin (**IBC 2**) showed the lowest MIC values against MSSA and MRSA, and low toxicity against human keratinocytes cells, indicating a good selectivity. **IBC** and **IBC 2** inhibited more than 50% of MSSA and MRSA biofilm formation at their respective subinhibitory concentrations. Moreover, the antibacterial mode of action of **IBC** and **IBC** involved damages in membrane of *B. subtilis*. Additional bioassays demonstrated that **IBC** and **IBC 2** have a spectral of antibacterial action against *S. pneumoniae* (MIC = 50 µg/mL), *S. sanguinis* (MIC = 3.12 µg/mL), *S. sobrinus* (MIC = 6.25–12.5 µg/mL), *S. mutans* (MIC = 6.25 µg/mL), *H. pylori* (MIC = 3.90 µg/mL), and *K. pneumoniae* (MIC = 100 µg/mL).

Highlights of promising antibacterial compounds

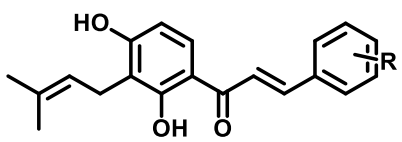

IBC. R = 4-OH
IBC 2. R = 2-OH

- ✓ MIC against MSSA = 1.56 µg/mL
- ✓ MIC against MRSA = 3.12 µg/mL
- ✓ **IBC** and **IBC 2** inhibited MSSA and MRSA biofilm formation
- ✓ **IBC** and **IBC 2** disrupted *B. subtilis* cell membrane
- ✓ **IBC** and **IBC 2** displayed non-toxic against

Twelve chalcones demonstrated activity against *M. tuberculosis* H37Rv, including seven analogs were more active than prototype **IBC**, demonstrating MIC lower than 12.5 μg/mL. SAR data suggested that isoprenyl side chain, hydroxyl on ring B, and the *trans*-enone bridge are crucial subunits for **IBC** antimycobacterial activity. Moreover, nitro substituent (**IBC 14**) and trifluormethyl substituent (**IBC 13**) led to most potent anti-*Mtb* agents. The *in silico* pharmacokinetic investigation demonstrated that antimycobacterial chalcones had a satisfactory theorical oral drug-likeness profile.

Highlights of promising anti-*M. tuberculosis* chalcones

IBC 13

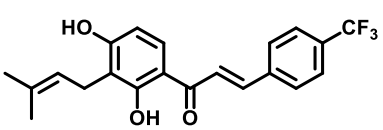

MIC = 3.8 μg/mL

IBC 14

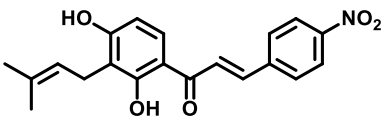

MIC = 2.7 μg/mL

In conclusion, this work corroborates the relevance of isobavachalcone as a privileged scaffold for development of novel biologically active compounds since their derivatives showed potent antibacterial and antimycobacterial activity. Moreover, these results provide SAR data that could aid further bioassays and development of new bioactive analogs.

REFERENCES

ABDULLAH, S. A. et al. Flavonoids from the leaves and heartwoods of *Artocarpus lowii* King and their bioactivities. **Natural Product Research**, v. 31, n. 10, p. 1113–1120, 2017.

ALLAERT, F. A. et al. Correlation between improvement in functional signs and plethysmographic parameters during venoactive treatment (Cyclo 3 Fort). **International Angiology**, v. 30, n. 3, p. 272–277, 2011.

ALVES, J. A. et al. Investigation of Copaifera genus as a new source of antimycobaterial agents. **Future Science OA**, v. 6, n. 7, p. FSO587, 2020.

ARCHER, N. K. et al. *Staphylococcus aureus* biofilms: Properties, regulation and roles in human disease. **Virulence**, v. 2, n. 5, p. 445–459, 2011.

ASSIS, L. R. DE et al. Antibacterial Activity of Isobavachalcone (IBC) Is Associated with Membrane Disruption. **Membranes**, v. 12, n. 3, p. 269, 25 fev. 2022.

ÁVILA, H. P. et al. Structure–activity relationship of antibacterial chalcones. **Bioorganic & Medicinal Chemistry**, v. 16, n. 22, p. 9790–9794, 2008.

BASIC, J. et al. Synthesis, QSAR analysis and mechanism of antibacterial activity of simple 2′-hydroxychalcones. **Digest Journal of Nanomaterials and Biostructures**, v. 9, n. 4, p. 1537–1546, 2014.

BAUER, R. A. Covalent inhibitors in drug discovery: from accidental discoveries to avoided liabilities and designed therapies. **Drug Discovery Today**, v. 20, n. 9, p. 1061–1073, 2015.

BEYER, P.; PAULIN, S. The Antibacterial Research and Development Pipeline Needs Urgent Solutions. **ACS Infectious Diseases**, v. 6, n. 6, p. 1289–1291, 2020.

BHALLA, V. K.; NAYAK, U. R.; DEV, S. Some New Flavonoids from *Psoralea Corylifolia*. **Tetrahedron**, v. 20, p. 2401–2406, 1968.

BHAMBRA, A. S. et al. Synthesis and antitrypanosomal activities of novel pyridylchalcones. **European Journal of Medicinal Chemistry**, v. 128, p. 213–218, 2017.

BHATTACHARYA, M. et al. Prevention and treatment of *Staphylococcus aureus* biofilms. **Expert Review of Anti-Infective Therapy**, v. 13, n. 12, p. 1499–1516, 2015.

BLOEMBERG, G. V. et al. Acquired Resistance to Bedaquiline and Delamanid in Therapy for Tuberculosis. **New England Journal of Medicine**, v. 373, n. 20, p. 1986–1988, 2015.

BOCQUET, L. et al. Phenolic compounds from *Humulus lupulus* as natural antimicrobial products: New weapons in the fight against methicillin resistant *Staphylococcus aureus*, *Leishmania mexicana* and *Trypanosoma brucei strains*. **Molecules**, v. 24, n. 6, 2019.

BOGDANOVA, K. et al. Antibiofilm activity of bioactive hop compounds humulone, lupulone and xanthohumol toward susceptible and resistant staphylococci. **Research in Microbiology**, v. 169, n. 3, p. 127–134, 2018.

BOLTON, J. L. et al. The Multiple Biological Targets of Hops and Bioactive Compounds. **Chemical Research in Toxicology**, v. 32, n. 2, p. 222–233, 2019.

BORGES-ARGÁEZ, R. et al. Antiprotozoal and cytotoxic studies on some isocordoin derivatives. **Planta Medica**, v. 75, n. 12, p. 1336–1338, 2009.

BORGES-ARGÁEZ, R.; PEA-RODRÍGUEZ, L. M.; WATERMAN, P. G. Flavonoids from two Lonchocarpus species of the Yucatan Peninsula. **Phytochemistry**, v. 60, n. 5, p. 533–540, 2002.

BOTTA, B. et al. Prenylated Flavonoids: Pharmacology and Biotechnology. **Current Medicinal Chemistry**, v. 12, n. 6, p. 713–739, 2010.

BOUCHER, M. M. et al. Liquid-Liquid Extraction Protocol for the Removal of Aldehydes and Highly Reactive Ketones from Mixtures. **Organic Process Research and Development**, v. 21, n. 9, p. 1394–1403, 2017.

BOZIC, D. D. et al. Newly-synthesized chalcones-inhibition of adherence and biofilm formation of methicillin-resistant *Staphylococcus aureus*. **Brazilian Journal of Microbiology**, v. 45, n. 1, p. 263–270, 2014.

BROWN, D. G.; WOBST, H. J. A decade of FDA-approved drugs (2010-2019): Trends and future directions. **Journal of Medicinal Chemistry**, v. 64, p. 2312–2338, 2021.

CAESAR, L. K.; CECH, N. B. A review of the medicinal uses and pharmacology of Ashitaba. **Planta Medica**, v. 82, n. 14, p. 1236–1245, 2016.

CHACHA, M.; BOJASE-MOLETA, G.; MAJINDA, R. R. T. Antimicrobial and radical scavenging flavonoids from the stem wood of *Erythrina latissima*. **Phytochemistry**, v. 66, n. 1, p. 99–104, 2005.

CHEN, X. et al. A systematic review on biological activities of prenylated flavonoids. **Pharmaceutical Biology**, v. 52, n. 5, p. 655–660, 2014.

CHIANG, C. C. et al. A novel dimeric coumarin analog and antimycobacterial constituents from *Fatoua pilosa*. **Chemistry and Biodiversity,** v. 7, n. 7, p. 1728–1736, 2010.

CLSI. **Methods for Dilution Antimicrobial Susceptibility Tests for Bacteria That Grow Aerobically**; Approved Standard−Ninth Edition. v. 32

COTTAREL, G.; WIERZBOWSKI, J. Combination drugs, an emerging option for antibacterial therapy. **Trends in Biotechnology**, v. 25, n. 12, p. 547–555, 2007.

CUI, Y. et al. Constituents of *Psoralea corylifolia* fruits and their effects on methicillin-resistant *Staphylococcus aureus*. **Molecules**, v. 20, n. 7, p. 12500–12511, 2015.

CUSHNIE, T. P. T.; LAMB, A. J. Recent advances in understanding the antibacterial properties of flavonoids. **International Journal of Antimicrobial Agents**, v. 38, n. 2, p. 99–107, 2011.

DAINA, A.; MICHIELIN, O.; ZOETE, V. SwissADME: A free web tool to evaluate pharmacokinetics, drug-likeness and medicinal chemistry friendliness of small molecules. **Scientific Reports**, v. 7, p. 1–13, 2017.

DAN, W.; DAI, J. Recent developments of chalcones as potential antibacterial agents in medicinal chemistry. **European Journal of Medicinal Chemistry**, v. 187, p. 111980, 2020.

DANG, G. et al. Characterization of Rv0888, a Novel Extracellular Nuclease from *Mycobacterium tuberculosis*. **Scientific Reports**, v. 6, p. 1–11, 2016.

DAS, B. et al. Eugenol Provokes ROS-Mediated Membrane Damage-Associated Antibacterial Activity against Clinically Isolated Multidrug-Resistant *Staphylococcus aureus Strains*. **Infectious Diseases**: **Research and Treatment**, v. 9, n. 1, p. 11–19, 2016.

DELANEY, J. S. ESOL: Estimating Aqueous Solubility Directly from Molecular Structure. **Journal of Chemical Information and Computer Sciences**, v. 44, n. 3, p. 1000–1005, 2004.

DONG, X. et al. Design, synthesis, and biological evaluation of prenylated chalcones as vasorelaxant agents. **Archiv der Pharmazie**, v. 342, n. 7, p. 428–432, 2009.

DU, G. et al. Chalcones from the flowers of *Rosa rugosa* and their anti-tobacco mosaic virus activities. **Bulletin of the Korean Chemical Society**, v. 34, n. 4, p. 1263–1265, 2013.

DZOYEM, J. P. et al. Antimicrobial Action Mechanism of Flavonoids from *Dorstenia* Species. **Drug Discoveries & Therapeutics,** v. 7, n. 2, p. 66–72, 2013.

EGAN, W. J.; MERZ, K. M.; BALDWIN, J. J. Prediction of drug absorption using multivariate statistics. **Journal of Medicinal Chemistry,** v. 43, n. 21, p. 3867–3877, 2000.

ELSOHLY, H. N. et al. Antifungal Chalcones from *Maclura tinctoria*. **Planta Medica**, v. 67, n. 1, p. 87–89, 2001.

EMERI, F. T. DE A. S. DE et al. Antimicrobial activity of nitrochalcone and pentyl caffeate against hospital pathogens results in decreased microbial adhesion and biofilm formation. **Biofouling**, v. 35, n. 2, p. 129–142, 2019.

ENOKI, T. et al. **European Patent Aplication - WO 2004/096198**, France, 2004.

EPIFANO, F. et al. Chemistry and pharmacology of oxyprenylated secondary plant metabolites. **Phytochemistry**, v. 68, n. 7, p. 939–953, 2007.

FRIIS-MØLLER, A. et al. In Vitro Antimycobacterial and Antilegionella Activity of Licochalcone A from Chinese Licorice Roots. **Planta Medica**, v. 68, n. 5, p. 416–419, 2002.

FRÖLICH, S. et al. In vitro antiplasmodial activity of prenylated chalcone derivatives of hops (Humulus lupulus) and their interaction with haemin. **Journal of Antimicrobial Chemotherapy**, v. 55, n. 6, p. 883–887, 2005.

GALLO, R. D. C. et al. Efficient and selective iodination of phenols promoted by iodine and hydrogen peroxide in water. **Journal of the Brazilian Chemical Society**, v. 21, n. 4, p. 770–774, 2010.

GANAPATY, S. et al. *C*-Prenylflavonoids from *Derris heyneana* Seru. **Natural Product Communications**, v. 1, n. 2, p. 81–85, 1 set. 2006.

GAO, Y. et al. Association between tuberculosis and COVID-19 severity and mortality: A rapid systematic review and meta-analysis. **Journal of Medical Virology**, v. 93, n. 1, p. 194–196, 2021.

GARCIA, M. A. R. et al. Design, synthesis and antibacterial activity of chalcones against MSSA and MRSA planktonic cells and biofilms. **Bioorganic Chemistry**, v. 116, p. 105279, 2021.

GARDETE, S.; TOMASZ, A. Mechanisms of vancomycin resistance in *Staphylococcus aureus*. **Journal of Clinical Investigation**, v. 124, n. 7, p. 2836–2840, 2014.

GHOSE, A. K.; VISWANADHAN, V. N.; WENDOLOSKI, J. J. A knowledge-based approach in designing combinatorial or medicinal chemistry libraries for drug discovery. 1. A qualitative and quantitative characterization of known drug databases. **Journal of Combinatorial Chemistry**, v. 1, n. 1, p. 55–68, 1999.

GO, M.; WU, X.; LIU, X. Chalcones: An Update on Cytotoxic and Chemoprotective Properties. **Current Medicinal Chemistry**, v. 12, n. 4, p. 483–499, 2012.

GÓMEZ-GONZÁLEZ, P. J. et al. Genetic diversity of candidate loci linked to *Mycobacterium tuberculosis* resistance to bedaquiline, delamanid and pretomanid. **Scientific Reports**, v. 11, n. 1, p. 1–13, 2021.

GONG, J. Q. et al. Skin colonization by *Staphylococcus aureus* in patients with eczema and atopic dermatitis and relevant combined topical therapy: a double-blind multicentre randomized controlled trial. **British Journal of Dermatology**, v. 155, n. 4, p. 680–687, 2006.

GÓRNIAK, I.; BARTOSZEWSKI, R.; KRÓLICZEWSKI, J. Comprehensive review of antimicrobial activities of plant flavonoids. **Phytochemistry Reviews**. v. 18, n. 1, p. 241–272

GREALIS, J. P. et al. Synthesis of isobavachalcone and some organometallic derivatives. **European Journal of Organic Chemistry**, v. 2013, n. 2, p. 332–347, 2013.

HAN, J. et al. Anti-mycobacterial natural products and mechanisms of action. **Natural Product Reports**, v.39, n.1, p. 77–89, 2021.

HANSCH, C. et al. “Aromatic” Substituent Constants for Structure-Activity Correlations. **Journal of Medicinal Chemistry**, v. 16, n. 11, p. 1207–1216, 1973.

HANSCH, C.; LEO, A.; TAFT, R. W. A Survey of Hammett Substituent Constants and Resonance and Field Parameters. **Chemical Reviews**, v. 91, n. 2, p. 165–195, 1991.

HE, N. et al. The mechanism of antibacterial activity of corylifolinin against three clinical bacteria from *Psoralen corylifolia* L. **Open Chemistry**, v. 16, n. 1, p. 882–889, 2018.

HOMAYUN, B.; LIN, X.; CHOI, H. J. Challenges and recent progress in oral drug delivery systems for biopharmaceuticals. **Pharmaceutics**, p. 1–29, v. 11, n. 3, 2019.

HONG, Q. et al. Anti-tuberculosis Compounds from *Mallotus philippinensis*. **Natural Product Communications**, v. 5, n. 2, p. 211–217, 1 fev. 2010.

IGNATIUS, E. H.; DOOLEY, K. E. New Drugs for the Treatment of Tuberculosis. **Clinics in Chest Medicine,** v. 40, n. 4, p. 811–827, 2019.

INAMORI, Y. et al. Antibacterial Activity of Two Chalcones, Xanthoangelol and 4-Hydroxyderricin, Isolated from the Root of *Angelica keiskei* Koidzumi. **Chemical and Pharmaceutical Bulletin**, v. 39, n. 6, p. 1604–1605, 1991.

JIN, X.; SHI, Y. Isobavachalcone induces the apoptosis of gastric cancer cells via inhibition of the Akt and Erk pathways. **Experimental and Therapeutic Medicine**, v. 11, n. 2, p. 403–408, 2016.

JING, H. et al. Abrogation of Akt signaling by Isobavachalcone contributes to its anti-proliferative effects towards human cancer cells**. Cancer Letters**, v. 294, n. 2, p. 167–177, 2010.

JOHANSSON, M. H. Reversible Michael Additions: Covalent Inhibitors and Prodrugs. **Mini-Reviews in Medicinal Chemistry**, v. 12, p. 1330–1344, 2012.

JOHNSON, J.; YARDILY, A. Chalconoid metal chelates: spectral, biological and catalytic applications. **Journal of Coordination Chemistry**, v. 72, n. 15, p. 2437–2488, 2019.

JORGENSEN, W. L.; DUFFY, E. M. Prediction of drug solubility from structure. **Advanced Drug Delivery Reviews**, v. 54, n. 3, p. 355–366, 2002.

KIL, Y. S. et al. *Angelica keiskei*, an emerging medicinal herb with various bioactive constituents and biological activities. **Archives of Pharmacal Research**, v. 40, n. 6, p. 655–675, 2017.

KONTUREK, S. J. et al. Antiulcer and gastroprotective effects of solon, a synthetic flavonoid derivative of sophoradin. Role of endogenous prostaglandins. **European Journal of Pharmacology**, v. 125, n. 2, p. 185–192, 1986.

KOUL, B. et al. Genus Psoralea: A review of the traditional and modern uses, phytochemistry and pharmacology. **Journal of Ethnopharmacology**, v. 232, p. 201–226, 2019.

KUETE, V. et al. Efflux pumps are involved in the defense of gram-negative bacteria against the natural products isobavachalcone and diospyrone. **Antimicrobial Agents and Chemotherapy**, v. 54, n. 5, p. 1749–1752, 2010a.

KUETE, V. et al. Evaluation of flavonoids from *Dorstenia barteri* for their antimycobacterial, antigonorrheal and anti-reverse transcriptase activities. **Acta Tropica**, v. 116, n. 1, p. 100–104, 2010b.

KUETE, V. et al. Cytotoxicity of three naturally occurring flavonoid derived compounds (artocarpesin, cycloartocarpesin and isobavachalcone) towards multi-factorial drug-resistant cancer cells. **Phytomedicine**, v. 22, n. 12, p. 1096–1102, 2015.

KUETE, V.; SANDJO, L. P. Isobavachalcone: An overview. **Chinese Journal of Integrative Medicine**, v. 18, n. 7, p. 543–547, 2012.

KYOGOKU, K. et al. Anti-ulcer Effect of Isoprenyl Flavonoids. II. Synthesis and Anti-ulcer Activity of New Chalcones related to Sophoradin. **Chemical and Pharmaceutical Bulletin**, v. 27, n. 12, p. 2943–2953, 1979.

LALL, N.; HUSSEIN, A. A.; MEYER, J. J. M. Antiviral and antituberculous activity of *Helichrysum melanacme* constituents. **Fitoterapia**, v. 77, n. 3, p. 230–232, 2006.

LEANDRO, L. F. et al. Antibacterial activity of *Pinus elliottii* and its major compound, dehydroabietic acid, against multidrug-resistant strains. **Journal of Medical Microbiology**, v. 63, p. 1649–1653, 2014.

LI, B. et al. Isobavachalcone exerts anti-proliferative and pro-apoptotic effects on human liver cancer cells by targeting the ERKs/RSK2 signaling pathway. **Oncology Reports**, v. 41, n. 6, p. 3355–3366, 2019a.

LI, K. et al. Isobavachalcone induces ROS-mediated apoptosis via targeting thioredoxin reductase 1 in human prostate cancer PC-3 cells. **Oxidative Medicine and Cellular Longevity**, v. 2018, 2018.

LI, Y. et al. Isobavachalcone isolated from *Psoralea corylifolia* inhibits cell proliferation and induces apoptosis via inhibiting the AKT/GSK-3β/β-catenin pathway in colorectal cancer cells. **Drug Design, Development and Therapy**, v. 13, p. 1449–1460, 2019b.

LIPINSKI, C. A. Lead- and drug-like compounds: The rule-of-five revolution. **Drug Discovery Today: Technologies**, v. 1, n. 4, p. 337–341, 2004.

LIU, M. et al. Pharmacological profile of xanthohumol, a prenylated flavonoid from hops (*Humulus lupulus*). **Molecules**, v. 20, n. 1, p. 754–779, 2015.

LOU, H. et al. Xanthohumol from: *Humulus lupulus* L. potentiates the killing of *Mycobacterium tuberculosis* and mitigates liver toxicity by the combination of isoniazid in mouse tuberculosis models. **RSC Advances**, v. 10, n. 22, p. 13223–13231, 2020.

MARTINS, P. M. M. et al. Subcellular localization of proteins labeled with GFP in *Xanthomonas citri* ssp. citri: Targeting the division septum. **FEMS Microbiology Letters**, v. 310, n. 1, p. 76–83, 2010.

MAUCHER, I. V. et al. Michael acceptor containing drugs are a novel class of 5-lipoxygenase inhibitor targeting the surface cysteines C416 and C418. **Biochemical Pharmacology**, v. 125, p. 55–74, 2017.

MBAVENG, A. T. et al. Antimicrobial activity of the crude extracts and five flavonoids from the twigs of *Dorstenia barteri* (Moraceae). **Journal of Ethnopharmacology**, v. 116, n. 3, p. 483–489, 2008.

MEIER, D. et al. The plant-derived chalcone Xanthoangelol targets the membrane of Gram-positive bacteria. **Bioorganic and Medicinal Chemistry**, v. 27, n. 23, p. 115151, 2019.

MIRALLES, N. et al. Transition-metal-free borylation of allylic and propargylic alcohols. **Angewandte Chemie - International Edition**, v. 55, n. 13, p. 4303–4307, 2016.

MONACHE, G. D. et al. Comparison between metabolite productions in cell culture and in whole plant of *Maclura pomifera*. **Phytochemistry**, v. 39, n. 3, p. 575–580, 1995.

MORAES, T. DA S. et al. In vitro Antibacterial Potential of the Oleoresin, Leaf Crude Hydroalcoholic Extracts and Isolated Compounds of the Copaifera spp. Against *Helicobacter pylori*. **Journal of Biologically Active Products from Nature**, v. 11, n. 2, p. 183–189, 2021.

MORÃO, L. G. et al. A simplified curcumin targets the membrane of *Bacillus subtilis*. **MicrobiologyOpen**, v. 8, n. 4, p. 1–12, 2019.

MUEGGE, I.; HEALD, S. L.; BRITTELLI, D. Simple selection criteria for drug-like chemical matter. **Journal of Medicinal Chemistry**, v. 44, n. 12, p. 1841–1846, 2001.

MURRAY, C. J. et al. Global burden of bacterial antimicrobial resistance in 2019: a systematic analysis. **The Lancet**, v. 399, n. 10325, p. 629–655, 2022.

NARENDER, T.; REDDY, K. P. BF3-Et2O mediated biogenetic type synthesis of chromanochalcones from prenylated chalcones via a regioselective cyclization reaction. **Tetrahedron Letters**, v. 48, n. 43, p. 7628–7632, 2007.

NAVARRO, M. O. P. et al. Determining the Targets of Fluopsin C Action on Gram-Negative and Gram-Positive Bacteria. **Frontiers in Microbiology**, v. 11, p. 1–11, 2020.

NEWMAN, D. J.; CRAGG, G. M. Natural Products as Sources of New Drugs over the Nearly Four Decades from 01/1981 to 09/2019. **Journal of Natural Products**, v. 83, n. 3, p. 770–803, 2020.

NGAMENI, B. et al. Inhibition of matrix metalloproteinase-2 secretion by chalcones from the twigs of *Dorstenia barteri* Bureau. **Arkivoc**, v. 2007, n. 9, p. 91–103, 2007.

NIELSEN, S. F. et al. Antileishmaniai chalcones: Statistical design, synthesis, and three-dimensional quantitative structure-activity relationship analysis. **Journal of Medicinal Chemistry**, v. 41, n. 24, p. 4819–4832, 1998.

NISHIMURA, R. et al. Isobavachalcone, a chalcone constituent of *Angelica keiskei*, induces apoptosis in neuroblastoma. **Biological and Pharmaceutical Bulletin**, v. 30, n. 10, p. 1878–1883, 2007.

O'NEILL, J. Tackling Drug-Resistant Infections Globally: Final Report and Recommendations. **Review on Antimicrobial Resistance**, p. 1–80, 2016.

OECD. OECD117 guideline for testing of chemicals: Partitioning coefficient (n-octanol/water) HPLC method. p. 1–11, 1989.

OSÓRIO, T. M. et al. Antibacterial activity of chalcones, hydrazones and oxadiazoles against methicillin-resistant *Staphylococcus aureus*. **Bioorganic and Medicinal Chemistry Letters**, v. 22, n. 1, p. 225–230, 2012.

OTTO, M. Staphylococcal Biofilms. Microbiology Spectrum, v. 6, n. 4, p. 1–17, 2018.

PALKO-ŁABUZ, A. et al. Isobavachalcone as an active membrane perturbing agent and inhibitor of abcb1 multidrug transporter. **Molecules**, v. 26, n. 15, 2021.

PALOMINO, J. C. et al. Resazurin Microtiter Assay Plate: Simple and Inexpensive Method for Detection of Drug Resistance in *Mycobacterium tuberculosis*. **Antimicrobial Agents and Chemotherapy**, v. 46, n. 8, p. 2720–2722, 2002.

PENG, F. et al. A Review: The Pharmacology of Isoliquiritigenin. **Phytotherapy Research**, v. 29, n. 7, p. 969–977, 2015.

PENICHE-PAVÍA, H. A.; VERA-KU, M.; PERAZA-SÁNCHEZ, S. R. Phytochemical and Pharmacological Studies on Species of Dorstenia Genus (2000-2016). **Journal of the Mexican Chemical Society**, v. 62, n. 3, p. 9–23, 2018.

POLAQUINI, C. R. et al. Antibacterial activity of 3,3′-dihydroxycurcumin (DHC) is associated with membrane perturbation. **Bioorganic Chemistry**, v. 90, p. 103031, 2019.

RAMMOHAN, A. et al. Chalcone synthesis, properties and medicinal applications: a review. **Environmental Chemistry Letters**, v. 18, n. 2, p. 433–458, 2020.

RATNATUNGA, C. N. et al. The Rise of Non-Tuberculosis Mycobacterial Lung Disease. **Frontiers in Immunology**, v. 11, p. 1–12, 2020.

REYGAERT, W. C. An overview of the antimicrobial resistance mechanisms of bacteria. **AIMS Microbiology**, v. 4, n. 3, p. 482–501, 2018.

ROSSITER, S. E.; FLETCHER, M. H.; WUEST, W. M. Natural Products as Platforms to Overcome Antibiotic Resistance. **Chemical Reviews**, v. 117, n. 19, p. 12415–12474, 2017.

ROZALSKI, M. et al. Antiadherent and antibiofilm activity of *Humulus lupulus* L. derived products: New pharmacological properties. **BioMed Research International**, 2013.

ROZMER, Z.; PERJÉSI, P. Naturally occurring chalcones and their biological activities. **Phytochemistry Reviews**, v. 15, p. 87–120, 2016.

SAHU, N. K. et al. Exploring Pharmacological Significance of Chalcone Scaffold: A Review. **Current Medicinal Chemistry**, v. 19, n. 2, p. 209–225, 2012.

SAMBROOK, J.; FRITSCH, E. F.; MANIATIS, T. Molecular cloning: A laboratory manual. 4. ed. New York: Cold Spring Harbor Protocols, v. 1, 2012.

SARDI, J. C. O. et al. Antibacterial activity of diacetylcurcumin against *Staphylococcus aureus* results in decreased biofilm and cellular adhesion. **Journal of Medical Microbiology**, v. 66, n. 6, p. 816–824, 2017.

SARKER, S. D.; NAHAR, L.; KUMARASAMY, Y. Microtitre plate-based antibacterial assay incorporating resazurin as an indicator of cell growth, and its application in the in vitro antibacterial screening of phytochemicals. **Methods**, v. 42, n. 4, p. 321–324, 2007.

SASAKI, T. et al. Protein tyrosine phosphatase 1B inhibitory activity of lavandulyl flavonoids from roots of *Sophora flavescens*. **Planta Medica**, v. 80, n. 7, p. 557–560, 2014.

SEUNG, K. J.; KESHAVJEE, S.; RICH, M. L. Drug-Resistant Tuberculosis. **Cold Spring Harb Perspect Med**, v. 5, p. a017863, 2015.

SHAMSUDIN, N. F. et al. Antibacterial Effects of Flavonoids and Their Structure-Activity Relationship Study: A Comparative Interpretation. **Molecules**, v. 27, n. 4, p. 1149, 2022.

SHEN, F. et al. Phenotype and expression profile analysis of *Staphylococcus aureus* biofilms and planktonic cells in response to licochalcone A. **Applied Microbial Biotechnology**, v. 99, p. 359–373, 2015.

SHI, J. et al. Isobavachalcone sensitizes cells to E2-induced paclitaxel resistance by down-regulating CD44 expression in ER+ breast cancer cells. **Journal of Cellular and Molecular Medicine,** v. 22, n. 11, p. 5220–5230, 2018.

SHI, Y. et al. Inhibitory effect of isobavachalcone on migration and invasion of Tca8113 cells and its mechanism. **Chinese Pharmacological Bulletin**, v. 31, n. 12, p. 1741–1745, 2015.

SHIN, H. J.; SHON, D. H.; YOUN, H. S. Isobavachalcone suppresses expression of inducible nitric oxide synthase induced by Toll-like receptor agonists. **International Immunopharmacology**, v. 15, n. 1, p. 38–41, 2013.

SILVA, I. C. et al. Antibacterial activity of alkyl gallates against *Xanthomonas citri* subsp. citri. **Journal of Bacteriology**, v. 195, n. 1, p. 85–94, 2013.

SONG, M. et al. Plant Natural Flavonoids Against Multidrug Resistant Pathogens. **Advanced Science**, v. 8, n. 15, p. 2100749, 2021.

SONMEZ, F. et al. Evaluation of new chalcone derivatives as polyphenol oxidase inhibitors. **Bioorganic and Medicinal Chemistry Letters**, v. 21, n. 24, p. 7479–7482, 2011.

SRINIVASAN, V.; GOLDBERG, D.; HAAS, G. Contributions to the antimicrobial spectrum of Hop constituents. **Economic Botany**, v. 58, p. S230–S238, 2004.

SUGAMOTO, K. et al. Synthesis and antibacterial activity of chalcones bearing prenyl or geranyl groups from *Angelica keiskei*. **Tetrahedron**, v. 67, n. 29, p. 5346–5359, 2011.

SYMONOWICZ, M.; KOLANEK, M. Flavonoids and their properties to form chelate complexes. **Biotechnology and Food Sciences**, v. 76, n. 1, p. 35–41, 2012.

SZLISZKA, E. et al. Targeting death receptor TRAIL-R2 by chalcones for TRAIL-induced apoptosis in cancer cells. **International Journal of Molecular Sciences**, v. 13, n. 11, p. 15343–15359, 2012.

TENG, P. Y.; KIM, W. K. Roles of nitrocompounds in inhibition of foodborne bacteria, parasites, and methane production in economic animals. **Animals**, v. 11, n. 4, 2021.

THEODORO, R. S. **Síntese e Avaliação Antibacteriana e Antimicobacteriana de 4-hidroxiderricina e seus análogos**. 2022. 315 p. Dissertação (Mestrado em Química). Instituto de Biociências, Letras e Ciências Exatas, Universidade Estadual Paulista Júlio de Mesquita Filho, São José do Rio Preto, 2022.

TRAN, T. D. et al. Synthesis and Antibacterial Activity of Some Heterocyclic Chalcone Analogues Alone and in Combination with Antibiotics. **Molecules**, v. 17, n. 6, p. 6684–6696, 2012.

TURNER, N. A. et al. Methicillin-resistant *Staphylococcus aureus*: an overview of basic and clinical research. **Nature Reviews Microbiology**, v. 17, n. 4, p. 203–218, 2019.

VAN DUIN, D.; PATERSON, D. L. Multidrug-Resistant Bacteria in the Community: Trends and Lessons Learned. **Infectious Disease Clinics of North America**, v. 30, n. 2, p. 377–390, 2016.

VEBER, D. F. et al. Molecular properties that influence the oral bioavailability of drug candidates. **Journal of Medicinal Chemistry**, v. 45, n. 12, p. 2615–2623, 2002.

VIEIRA, R. G. L. et al. *In vitro* studies of the antibacterial activity of *Copaifera* spp. oleoresins, sodium hypochlorite, and peracetic acid against clinical and environmental isolates recovered from a hemodialysis unit. **Antimicrobial Resistance and Infection Control**, v. 7, n. 1, p. 1–13, 2018.

VIKESLAND, P. et al. Differential Drivers of Antimicrobial Resistance across the World. **Accounts of Chemical Research**, v. 52, n. 4, p. 916–924, 2019.

VUUREN, S. VAN; VILJOEN, A. Plant-based antimicrobial studies methods and approaches to study the interaction between natural products. **Planta Medica**, v. 77, n. 11, p. 1168–1182, 2011.

WACHTER-JURCSAK, N.; RADU, C.; REDIN, K. Addressing the unusual reactivity of 2-pyridinecarboxaldehyde and 2- quiuolinecarboxaldehyde in base-catalyzed aldol reactions with acetophenone. **Tetrahedron Letters**, v. 39, n. 23, p. 3903–3906, 1998.

WALLER, D. G.; SAMPSON, A. P. Chemotherapy of infections. 5. ed. Elsevier: Medical Pharmacology and Therapeutics, 2018.

WANG, H. et al. Concise synthesis of prenylated and geranylated chalcone natural products by regiospecific iodination and Suzuki coupling reactions. **Tetrahedron Letters**, v. 55, n. 4, p. 897–899, 2014.

WANG, H. et al. Synthesis and anti-cancer activity evaluation of novel prenylated and geranylated chalcone natural products and their analogs. **European Journal of Medicinal Chemistry**, v. 92, p. 439–448, 2015.

WANG, M. et al. Pharmacological review of isobavachalcone, a naturally occurring chalcone. **Pharmacological Research**, v. 165, p. 105483, 2021.

WANG, S. et al. Bacteriostatic effect of quercetin as an antibiotic alternative in vivo and its antibacterial mechanism in vitro. **Journal of Food Protection**, v. 81, n. 1, p. 68–78, 2018.

WASSILEW, N. et al. Pulmonary Disease Caused by Non-Tuberculous Mycobacteria. **Respiration**, v. 91, n. 5, p. 386–402, 2016.

WEI, G. X.; CAMPAGNA, A. N.; BOBEK, L. A. Effect of MUC7 peptides on the growth of bacteria and on *Streptococcus mutans* biofilm. **Journal of Antimicrobial Chemotherapy**, v. 57, n. 6, p. 1100–1109, 2006.

WHITE, R. L. et al. Comparison of three different in vitro methods of detecting synergy: Time-kill, checkerboard, and E test. **Antimicrobial Agents and Chemotherapy**, v. 40, n. 8, p. 1914–1918, 1996.

WHO, Word Health Organization. Global Priority List of Antibiotic-Resistant Bacteria to Guide Research, Discovery, and Development of New Antibiotics. Geneva, 2017.

WHO, World Health Organization. Global Tuberculosis Report 2020. World Health Organization, Geneva, 2021.

WIEDEMANN, I.; BENZ, R.; SAHL, H. G. Lipid II-Mediated Pore Formation by the Peptide Antibiotic Nisin: A Black Lipid Membrane Study. **Journal of Bacteriology**, v. 186, n. 10, p. 3259–3261, 2004.

WU, S. et al. Antibacterial Effect and Mode of Action of Flavonoids From Licorice Against Methicillin-Resistant Staphylococcus aureus. **Frontiers in Microbiology**, v. 10, p. 1–14, 2019.

XU, Q. X. et al. Multi-target anti-Alzheimer activities of four prenylated compounds from Psoralea Fructus. **Molecules**, v. 23, n. 3, p. 1–12, 2018.

YANG, L. et al. Isobavachalcone reveals novel characteristics of methuosis-like cell death in leukemia cells. **Chemico-Biological Interactions**, v. 304, p. 131–138, 2019.

YE, Y. et al. Chalcones from *Desmodium podocarpum* and Their Anti-Tobacco Mosaic Virus Activity. **Chemistry of Natural Compounds**, v. 52, n. 3, p. 409–412, 2016.

YEONG-HO LEE. Patent Application 2-2004-023332-0. Korean Intellectual Property Office, Patent application, 2020.

YIN, S. et al. Antibacterial prenylflavone derivatives from *Psoralea corylifolia*, and their structure-activity relationship study. **Bioorganic and Medicinal Chemistry**, v. 12, n. 16, p. 4387–4392, 2004.

YIN, W. et al. Biofilms: The Microbial "Protective Clothing" in Extreme Environments. **International Journal of Molecular Sciences**, v. 20, n. 14, p. 3423, 2019.

YINGQING, R.; JAIN, N.; YALKIWSKU, S. H. Prediction of Aqueous Solubility of Organic Compounds by Topological Descriptors. **QSAR & Combinatorial Science**, v. 22, n. 8, p. 821–829, 2003.

ZHANG, B. et al. Chalcone attenuates *Staphylococcus aureus* Virulence by Targeting Sortase A and Alpha-Hemolysin. **Frontiers in Microbiology**, v. 8, p. 1715, 2017.

ZHUANG, C. et al. Chalcone: A Privileged Structure in Medicinal Chemistry. **Chemical Reviews**, v. 117, n. 12, p. 7762–7810, 2017.

APPENDIX I

Supplementary material of chapter II

Antibacterial Activity of Isobavachalcone (IBC) is Associated with Membrane Disruption

Leticia Ribeiro de Assis[1], Reinaldo dos Santos Theodoro[1], Maria Beatriz Silva Costa[1], Julyanna Andrade Silva Nascentes[1], Miguel Divino da Rocha[1], Meliza Arantes de Souza Bessa[2], Ralciane de Paula Menezes[2], Guilherme Dilarri[3], Giovane Böerner Hypolito[3], Vanessa Rodrigues dos Santos[4], Cristiane Duque[4], Henrique Ferreira[3], Carlos Henrique Gomes Martins[2], Luis Octavio Regasini[1,*]

[1]Department of Chemistry and Environmental Sciences, Institute of Biosciences, Humanities and Exact Sciences, São Paulo State University (Unesp), São José do Rio Preto 15054-000, SP, Brazil; leticia.assis@unesp.br (L.R.A), reinaldo.theodoro@unesp.br (R.S.T), mb.costa@unesp.br (M.B.S.C.), jullyana.as.nascentes@unesp.br (J.A.S.N), miguelquimic@gmail.com (M.D.R)

[2]Department of Microbiology, Institute of Biomedical Sciences, Federal University of Uberlândia (UFU), Umuarama 38405-320, MG, Brazil; melizaarantes@gmail.com (M.A.S.B), ralciane@ufu.br (R.P.M), carlos.martins2@ufu.br (C.H.G.M)

[3]Department of Biochemistry and Microbiology, Institute of Biosciences, São Paulo State University (Unesp), Rio Claro 130506-900, SP, Brazil; gui_dila@hotmail.com (G.D), giovane.boerner@unesp.br (G.B.H), henfer72@gmail.com (H.F.)

[4]Department of Preventive and Restorative Dentistry, School of Dentistry, São Paulo State University (Unesp), Araçatuba 16015-050, SP, Brazil, vanessarodrigues_22@hotmail.com (V.R.S), cristianeduque@yahoo.com.br (C.D.)

*****Correspondence: luis.regasini@unesp.br (LO Regasini). Tel. +55 17 32212362

1. General Procedures

Melting point (mp) was measured using Melt Temperature apparatus MS Tecnopon PFM-II in open capillary tubes. NMR spectra were recorded on Bruker Avance III spectrometer, operating at 600 MHz for ^{1}H NMR and 150 MHz for ^{13}C NMR. Chemical shifts (δ) were referenced to residual non-deuterated solvent signals. Signal multiplicities were reported as singlet (s), and doublet (d). MS spectrum was recorded on Exactive Plus Thermo Scientific Electrospray Mass spectrometer, operating on positive mode. UV-Vis spectra and chromatograms were obtained by High Performance Liquid Chromatography (HPLC) with Photodiode Array Detector

(HPLC-PAD) Agilent Technologies® 1220 Infinity LC equipment, photodiode array system (Agilent Tecnologies® Model 1260 Infinity) and Agilent Zorbax Eclipse Plus C-18® column (250 mm × 4.6 mm, 5 μm) using methanol:water (3:1) with 0.5% of acetic acid as mobile phase (1.0 mL/min). Purity of **IBC** was established through area of peak at 372 nm.

1.1 Synthesis

2'-hydroxy-4'-(methoxymethoxy)acetophenone (1a)

To a mixture of resacetophenone (3 mmol) and anhydrous K_2CO_3 (6 mmol) in acetone (10 mL). The methoxymethyl chloride (MOMCl, 3.3 mmol) was added in portions for 30 min (SUGAMOTO et al., 2011). The mixture reaction was stirred for 2 h at room temperature. The reaction medium was extracted with ethyl acetate (3 × 25 mL) and combined organic phases were washed with brine, dried over $MgSO_4$, filtered and evaporated under reduced pressure to give **1a**, with 90% yield.

4-(methoxymethoxy)benzaldehyde (2)

To a mixture of 4-hydroxybenzaldehyde (3 mmol) and anhydrous K_2CO_3 (6 mmol) in acetone (10 mL). The methoxymethyl chloride (MOMCl) was added in portions for 30 min (SUGAMOTO et al., 2011). The mixture reaction was stirred for 5 h at room temperature. The reaction medium was extracted with ethyl acetate (3 × 25 mL), and the combined organic phases were washed with brine, dried over $MgSO_4$, filtered and evaporated under reduced pressure to furnish **2**, with 95% yield.

4'-(methoxymethoxy)-2'-prenyloxycetophenone (1b)

A mixture of **1a** (2.5 mmol) and K_2CO_3 (5 mmol) in acetone (5 mL) was stirred for 15 min at room temperature (SUGAMOTO et al., 2011). Isoprenyl bromide (3 mmol) was added in portions for 30 min and the reaction mixture was stirred for 24 h at room temperature. The reaction medium was extracted with ethyl acetate (3 × 25 mL) and the combined organic phases were washed with brine, dried over MgSO4, filtered and evaporated under reduced pressure, to give 4-methoxymethoxy-2-*O*-prenyloxyacetophenone (**1b**) as a yellowish oil with 95% yield.

2'-hydroxy-4'-methoxymethoxy-3'-prenylacetophenone (1c)

To a stirred solution of **1b** (0.610g, 2.3 mmol) in dry dichloromethane (5 mL) was added montmorillonite K10 (0.610 g) at ºC and the reaction medium was stirred for 30 min at room temperature (SUGAMOTO et al., 2011). The reaction mixture was filtered and washed several

times with ethyl acetate, which was reduced under vacuum, obtaining a brown oil. This residue was purified over silica gel column chromatography with hexane/ethyl acetate/acetone (9.5:0.25:0.25) to afford **1c** with 35% yield .

2'-hydroxy-4, 4'-Bis(methoxymethoxy)-3'-prenylchalcone (3)

To an ethanolic solution (3 mL) of **1b** (0.210 g, 0.8 mmol) was added dropwise under stirring an aqueous solution of KOH (60% w/v, 2 mL) at ºC [1]. 2-(methoxymethoxy)benzaldehyde (**2**, 0.166 g, 1 mmol) solubilized in EtOH (2 mL) was added to the mixture in portions for 1 h at room temperature. The reaction mixture was stirred for 2 h at room temperature and poured into crushed deionized ice and neutralized with HCl solution (1 mol/L). The mixture reaction was extracted with ethyl acetate (3 × 25 mL), and the organic phases were combined, washed with saturated aqueous $NaHSO_3$ solution (2 ×10 mL) and brine, dried over $MgSO_4$, filtered, and concentrated under reduced pressure, furnishing chalcone **3** as a yellow oil, with 70% yield.

(*E*)-1-(2,4-dihydroxy-3-(3-methylbut-2-en-1-yl)phenyl)-3-(4-hydroxyphenyl)prop-2-en-1-one (IBC)

To a stirred solution of MOM-protected chalcone **3** (0.6 mmol, 0.264g) in 3 mL of MeOH:THF (1:1) was added 2 mL of HCl aqueous solution (1 mol/L) at ºC (SUGAMOTO et al., 2011). The reaction mixture was stirred at 55 ºC for 6 h and poured into crushed deionized ice, filtered and the crude yellow powder was purified over silica gel column chromatography with hexane/ethyl acetate to afford **IBC**, with yield of 60%.

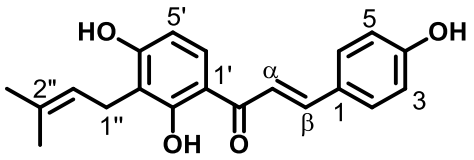

Yellow powder; HPLC purity: 99 %; m.p. literature: 156.8–157.8 ºC (SUGAMOTO et al., 2011), m.p. found: 134–137ºC. ^{1}H NMR (600 MHz, acetone-d_6) according to literature (WANG et al., 2015): δ 1.64 (s, H-5"), 1.78 (s, H-4"), 3.37 (d, *J* = 7.2 Hz, H-1"), 5.28 (t, *J* = 7.2 Hz, H-2"), 6.53 (d, *J* = 8.8 Hz, H-5'), 6.92 (d, *J* = 8.6 Hz, H-3 and H-5), 7.72 (d, *J* = 8.6 Hz, H-2 and H-6), 7.75 (d, *J* = 15.4 Hz, H-α), 7.83 (d, *J* = 15.3 Hz, H-β), 7.97 (d, *J* = 8.9 Hz, H-6'), 9.26 (brs, 4'-OH), 14.0 (s, 2'-OH). ^{13}C NMR (150 MHz, acetone-d_6): δ 17.84 (C-5"), 22.20 (C-1"), 25.80 (C-4"), 107.9 (C-5'), 114.3 (C-1'), 116.0 (C-3'), 116.7 (C-3 and C-5), 118.3

(C-α), 123.2 (C-2”), 127.5 (C-1), 130.2 (C-6’), 131.4 (C-3”), 131.6 (C-2 and C-6), 144.8 (C-β), 160.9 (C-4), 162.7 (C-2’), 165.1 (C-4’), 192.9 (C-β’). UV/Vis λmax (MeOH): 372 nm. MS (Mwt: 324.136): *m/z* 325.143 (M+1) (base peak).

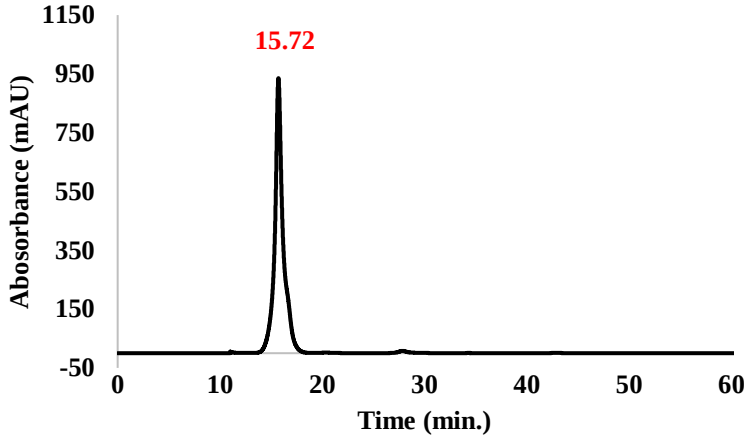

Figure S1. HPLC-PAD chromatogram of **IBC**. Methanol:Water (3:1), 372 nm

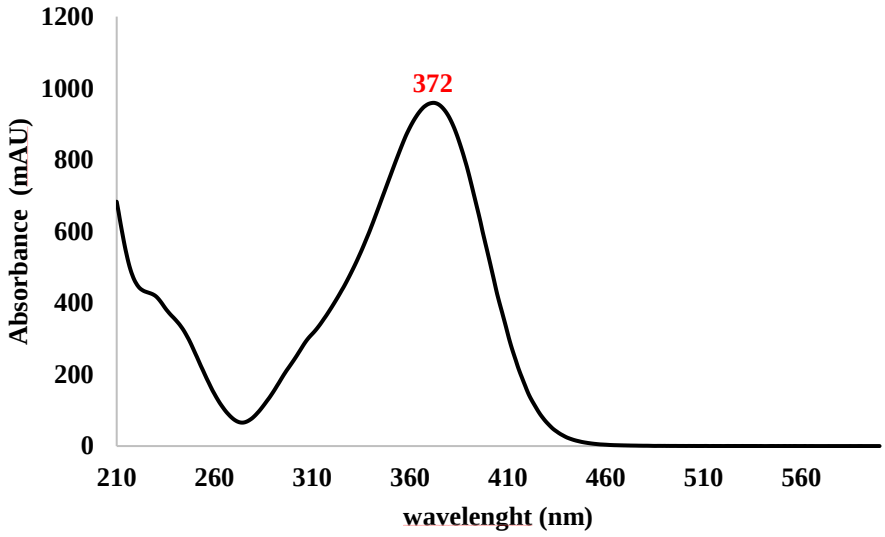

Figure S2. UV-Vis spectra of **IBC**

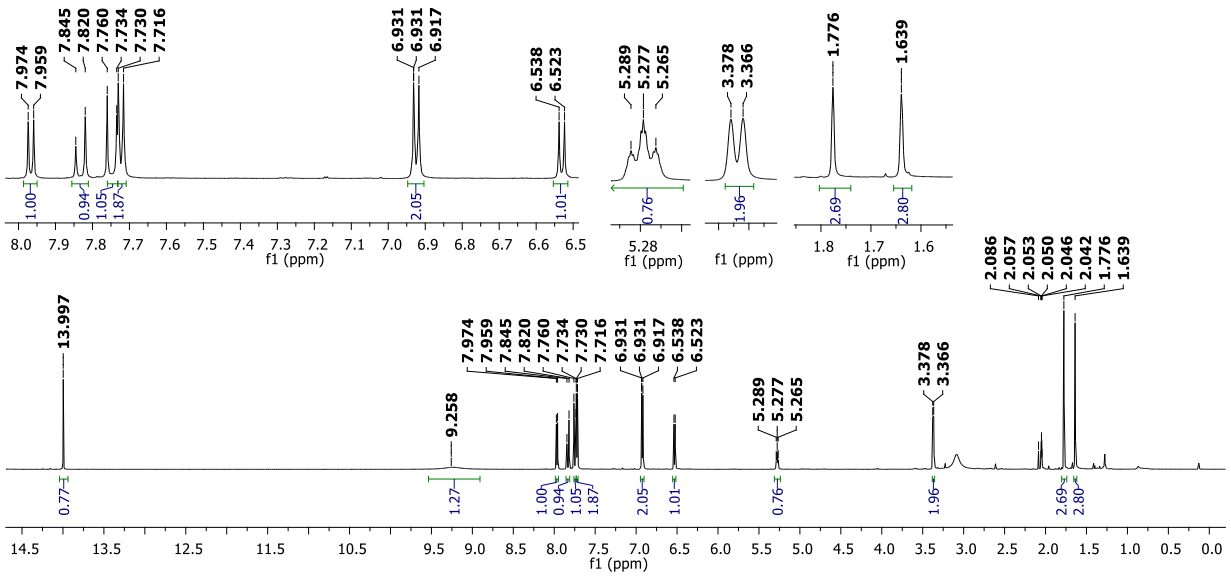

Figure S3. ^{1}H NMR spectrum of **IBC** (acetone-d_6; 600 MHz)

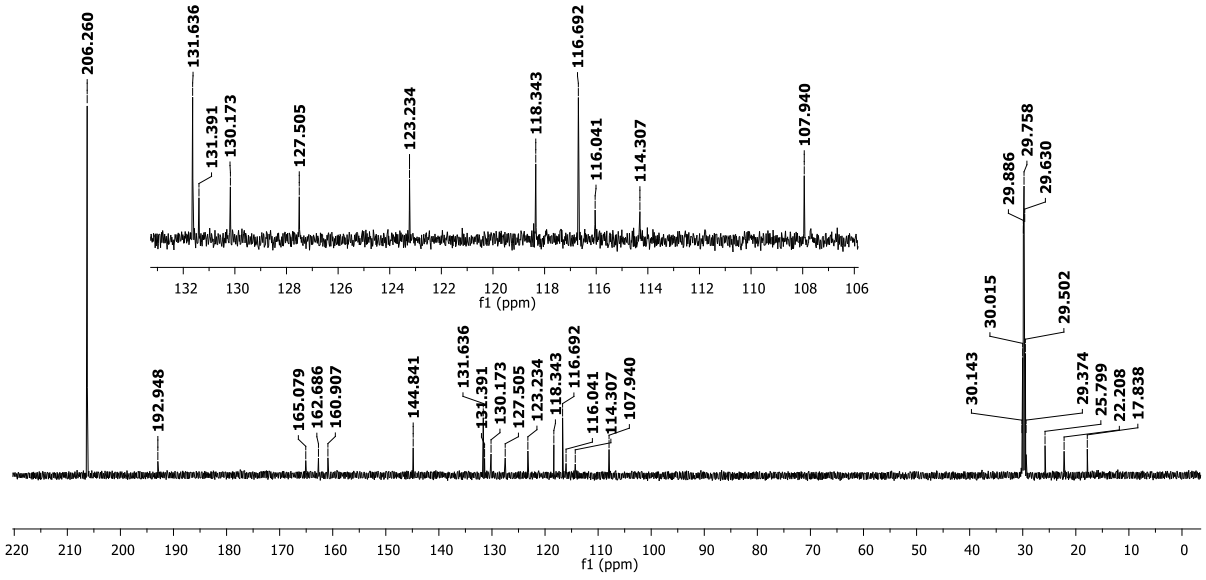

Figure S4. ^{13}C NMR spectrum of **IBC** (acetone-d_6; 150 MHz)

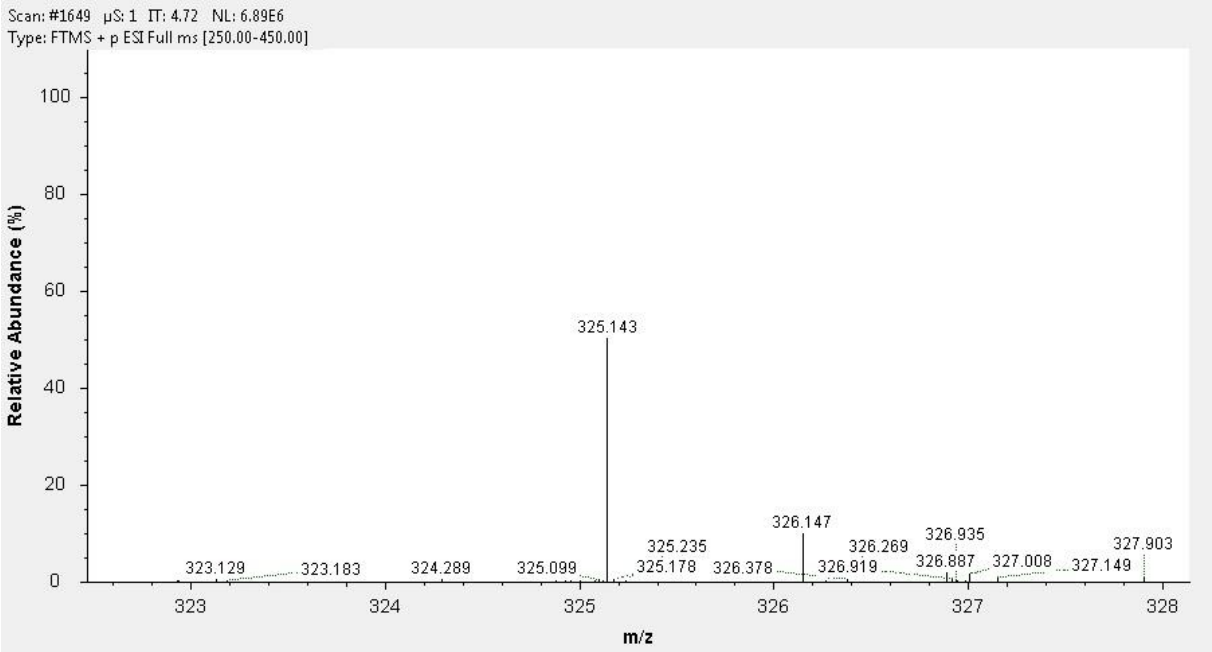

Figure S5. Mass spectrum (MS) of **IBC** (electrospray, positive mode)

APPENDIX II

Supplementary material of chapter III

Design, Synthesis and Activity against *Mycobacterium tuberculosis* of Isobavachalcone and Analogs

Leticia Ribeiro de Assis[a], Reinaldo dos Santos Theodoro[a], Pedro Henrique de Deus Jacob[a], Larissa Faria Diniz[a], Maria Beatriz Silva Costa[a], Julyanna Andrade Silva Nascentes[a], Fernando Rogério Pavan[b], Luis Octavio Regasini[a+]

[a]Laboratory of Antibiotics and Chemotherapeutics, Department of Chemistry and Environmental Sciences, Institute of Biosciences, Humanities and Exact Sciences, São Paulo State University (Unesp), São José do Rio Preto CEP 15054-000, SP, Brazil.
[b]São Paulo State University (Unesp), College of Pharmacy, Department of Biological Sciences, Araraquara, SP, Brazil.

1. General procedure

Appendix I, item 1

1.1 ^{1}H and C NMR, HPLC chromatogram, melting point and UV-Vis spectra

1-(2,4-Dihydroxy-3-iodophenyl)ethanone (A.2)

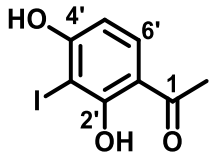

White crystalline powder (yield 90%). ^{1}H NMR (600 MHz, DMSO-d_6) identical to literature(WANG et al., 2015): δ 2.56 (s, 3H, H-2), 6.54 (d, *J* = 8.8 Hz, H-5'), 7.80 (d, *J* = 8.8 Hz, H-6'), 11.6 (brs, 4'-OH), 13.7 (s, 2'-OH).

1-(4-hydroxy-3-iodophenyl)ethanone (A.4)

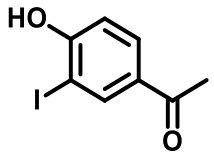

White powder (yield 60%). ^{1}H NMR (600 MHz, acetone-d_6) identical to literature (GALLO et al., 2010): δ 2.51 (s, 3H, H-2), 7.03 (d, *J* = 8.4 Hz, H-5'), 7.89 (dd, *J* = 2.1 and 8.4 Hz, H-6'), 8.35 (d, *J* = 2.1 Hz, H-2'), 10.1 (brs, 4'-OH).

1-(3-iodo-2,4-bis(methoymethoxy)phenyl)ethanone (A.5)

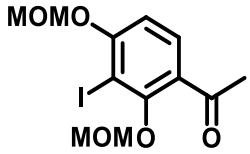

yield: 95 %; colorless oil. ^{1}H NMR (600 MHz, $CDCl_3$) according to literature (WANG et al., 2015): δ 2.60 (s, 3H), 3.51 (s, 3H), 3.56 (s, 3H), 5.06 (s, 2H), 5.29 (s, 2H), 6.90 (d, *J* = 8.7 Hz, 1H), 7.58 (s, d, *J* = 8.7 Hz, 1H).

1-(3-iodo-4-methoymethoxyphenyl)ethanone (A.6)

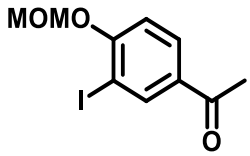

yield: 95 %; colorless oil. ^{1}H NMR (600 MHz, $CDCl_3$): 2.53 (s, 3H, H-2), 3.50 (s, 3H, 4'-OCH_2OCH_3), 5.30 (s, 2H, 4'-OCH_2OCH_3), 7.08 (d, *J* = 8.6 Hz, H-5'), 7.89 (dd, *J* = 2.2 and 8.6 Hz, H-6'), 8.38 (d, *J* = 2.2 Hz, H-2').

2-hydroxy-4-(methoxymethoxy)acetophenone (A.7)

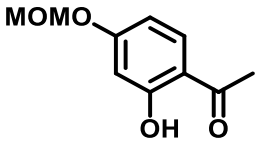

The procedure was displayed on supporting information of chapter II. Yield: 90%.

(*E*)-1-(2-geranyloxy)-4-(methoxymethoxy)phenyl)ethanone (A.8)

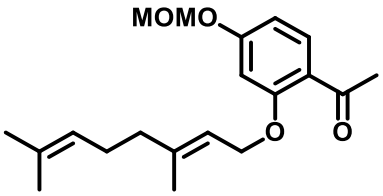

Translucid brown oil; yield: 98%.

Methoxymethoxybenzaldehydes (B.1–B.6)

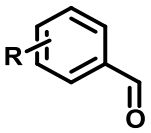

B.1. R = 2-OMOM; yield: 85%; Translucid yellowish oil

B.2. R = 3-OMOM; yield: 95%; Translucid yellowish oil

B.3. R = 4-OMOM; yield: 95%; Translucid colorless oil

B.4. R = 2,4-*Bis*(OMOM); yield: 90%; Translucid colorless oil

B.5. R = 3,4-*Bis*(OMOM); yield: 85%; brown powder

B.6. R = 2,5-*Bis*(MOM)benzaldehyde (yield: 82%); translucent colorless oil

(*E*)-1-(3-iodo-2,4-bis(methoxymethoxy)phenyl)-3-(4-(methoxymethoxy)phenyl)pro-2-en-1-one (C.1)

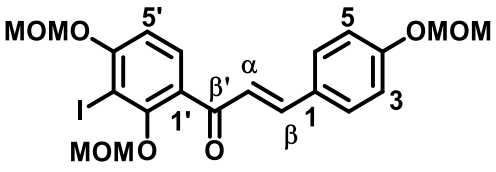

Yellow oil; yield 95 %. ^{1}H NMR ($CDCl_3$, 600 MHz) identical to literature (WANG et al., 2015): δ 3.48 (s, 3H), 3.50 (s, 3H), 3.53 (s, 3H), 5.03 (s, 2H), 5.21 (s, 2H), 5.31 (s, 2H), 6.94 (d, *J* = 8.6 Hz, H-5'), 7.05 (d, *J* = 8.7 Hz, H-3 and H-5), 7.23 (d, *J* = 15.8 Hz, H-α), 7.56 (d, *J* = 8.7 Hz, H-2 and H-6), 7.59 (d, *J* = 8.7 Hz, H-6'), 7.64 (d, *J* = 15.8 Hz, H-β).

(*E*)-1-(3-iodo-2,4-bis(methoxymethoxy)phenyl)-3-(3-(methoxymethoxy)phenyl)pro-2-en-1-one (C.2)

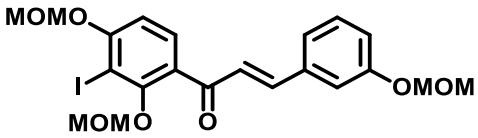

Yellow oil; yield 95 %. ^{1}H NMR ($CDCl_3$, 600 MHz): δ 3.48 (s, 3H), 3.49 (s, 3H), 3.51 (s, 3H), 5.02 (s, 2H), 5.18 (s, 2H), 5.30 (s, 2H), 6.94 (d, *J* = 8.6 Hz, H-5'), 7.07 (ddd, *J* = 1.0, 2.0 and 8.0 Hz, H-4), 7.24–7.32 (m, H-2 and H-6), 7.30 (dd, *J* = 7.9 and 8.2 Hz, H-5), 7.31 (d, *J* = 15.8 Hz, H-α), 7.59 (d, *J* = 8.6 Hz, H-6'), 7.62 (d, *J* = 15.8 Hz, H-β).

(*E*)-1-(3-iodo-2,4-bis(methoxymethoxy)phenyl)-3-(2-(methoxymethoxy)phenyl)pro-2-en-1-one (C.3)

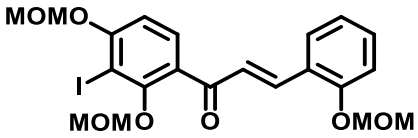

Yellow oil; yield 85 %. ^{1}H NMR ($CDCl_3$, 600 MHz): δ 3.49 (s, 3H), 3.51 (s, 3H), 3.52 (s, 3H), 5.03 (s, 2H), 5.25 (s, 2H), 5.31 (s, 2H), 6.94 (d, *J* = 8.6 Hz, H-5'), 7.02 (ddd, *J* = 0.8, 7.4 and 7.8 Hz, H-5), 7.15 (dd, *J* = 0.8 and 8.4 Hz, H-3), 7.34 (ddd, *J* = 1.6, 7.4 and 8.4 Hz, H-4), 7.38 (d, *J* = 16 Hz, H-α), 7.60 (d, *J* = 8.6 Hz, H-6'), 7.65 (dd, *J* = 1.6 and 7.8 Hz, H-6), 8.08 (d, *J* = 16 Hz, H-β).

(*E*)-3-(2,4-bis(methoxymethoxy)phenyl)-1-(3-iodo-2,4-bis(methoxymethoxy)phenyl)prop-2-en-1-one (C.4)

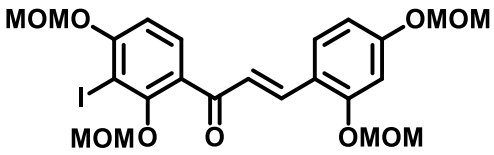

Yellow oil; yield 90%. ^{1}H NMR ($CDCl_3$, 600 MHz): δ 3.45 (s, 3H), 3.47 (s, 3H), 3.48 (s, 3H), 3.49 (s, 3H), 4.93 (s, 2H), 5.19 (s, 2H), 5.24 (s, 2H), 5.25 (s, 2H), 6.72 (dd, *J* = 1.0 and 8.5 Hz,

H-3), 6.84 (d, *J* = 1.0 Hz, H-3), 6.93 (d, *J* = 8.6 Hz, H-5'), 7.33 (d, *J* = 16 Hz, H-α), 7.48 (d, *J* = 8.5 Hz, H-6), 7.57 (d, *J* = 8.6 Hz, H-6'), 7.99 (d, *J* = 16 Hz, H-β).

(*E*)-3-(3,4-bis(methoxymethoxy)phenyl)-1-(3-iodo-2,4-bis(methoxymethoxy)phenyl)prop-2-en-1-one (C.5)

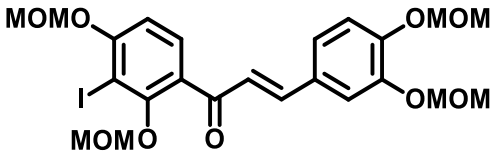

Yellow oil; yield 95%. ^{1}H NMR ($CDCl_3$, 600 MHz): δ 3.52 (s, 3H), 3.53 (s, 3H), 3.53 (s, 6H), 5.07 (s, 2H), 5.25 (s, 2H), 5.27 (s, 2H), 5.31 (s, 2H), 6.95 (d, *J* = 8.5 Hz, H-5'), 7.17 (d, *J* = 8.4 Hz, H-5), 7.20 (d, *J* = 16 Hz, H-α), 7.24 (dd, *J* = 1.2 and 8.4 Hz, H-6),7.40 (d, *J* = 1.2 Hz, H-2), 7.58 (d, *J* = 8.5 Hz, H-6'), 7.59 (d, *J* = 16 Hz, H-β).

(*E*)-3-(2,5-bis(methoxymethoxy)phenyl)-1-(3-iodo-2,4-bis(methoxymethoxy)phenyl)prop-2-en-1-one (C.6)

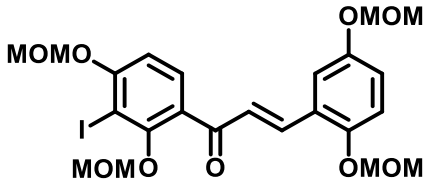

Yellow oil; yield 95%. ^{1}H NMR ($CDCl_3$, 600 MHz): 3.46 (s, 3H), 3.47 (s, 3H), 3.48 (s, 6H), 4.93 (s, 2H), 5.14 (s, 2H), 5.18 (s, 2H), 5.25 (s, 2H), 6.94 (d, *J* = 8.5 Hz, H-5'), 7.04 (dd, *J* = 2.9 and 9.0 Hz, H-6), 7.09 (dd, *J* = 9.0 Hz, H-3), 7.31 (d, *J* = 2.9 Hz, H-6), 7.37 (d, *J* = 16 Hz, H-α),7.49 (d, *J* = 8.5 Hz, H-6'), 8.0 (d, *J* = 16 Hz, H-β).

(*E*)-1-(3-iodo-2,4-bis(methoxymethoxy)phenyl)-3-phenylprop-2-en-1-one (C.7)

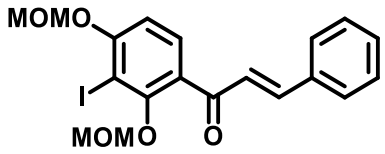

Yellow oil; yield 78 %. ^{1}H NMR ($CDCl_3$, 600 MHz): δ 3.50 (s, 3H), 3.53 (s, 3H), 5.03 (s, 2H), 5.31 (s, 2H), 6.98 (d, *J* = 8.6 Hz, H-5'), 7.38 (d, *J*= 16 Hz, H-α), 7.41–7.43 (m, 3H, H-3–5), 7.60 (d, *J* = 8.6 Hz, H-6'), 7.62–7.64 (m, 2H, H-2 and H-6), 7.61 (d, *J* = 16 Hz, H-β).

(*E*)-1-(3-iodo-2,4-bis(methoxymethoxy)phenyl)-3-(4-methoxyphenyl)prop-2-en-1-one (C.8)

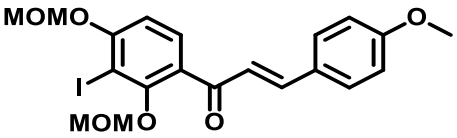

Yellow oil; yield 95 %. ^{1}H NMR (600 MHz, $CDCl_3$): δ 3.50 (s, 3H), 3.53 (s, 3H), 3.84 (s, 3H), 5.03 (s, 2H), 5.31 (s, 2H), 6.91 (d, *J* = 8.9 Hz, H-3 and H-5), 6.94 (d, *J* = 8.6 Hz, H-5'), 7.22 (d, *J* = 15.8 Hz, H-α), 7.56 (d, *J* = 8.1 Hz, H-2 and H-6), 7.59 (d, *J* = 8.6 Hz, H-6'), 7.64 (d, *J* = 15.8 Hz, H-β).

(*E*)-1-(3-iodo-2,4-bis(methoxymethoxy)phenyl)-3-(*p*-tolyl)prop-2-en-1-one (C.9)

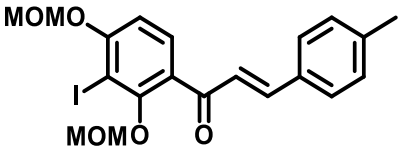

Yellow oil; yield 90 %. ^{1}H NMR (600 MHz, $CDCl_3$): δ 2.38 (s, 3H), 3.50 (s, 3H), 3.53 (s, 3H), 5.03 (s, 2H), 5.31 (s, 2H), 6.94 (d, *J* = 8.6 Hz, H-5'), 7.20 (d, *J* = 8.0 Hz, H-3 and H-5), 7.30 (d, *J* = 15.9 Hz, H-α), 7.51 (d, *J* = 8.1 Hz, H-2 and H-6), 7.59 (d, *J* = 8.6 Hz, H-6'), 7.66 (d, *J* = 15.9 Hz, H-β).

(*E*)-3-(4-fluorophenyl)-1-(3-iodo-2,4-bis(methoxymethoxy)phenyl)prop-2-en-1-one (C.10)

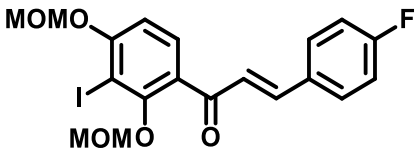

Yellow oil; yield 80 %. ^{1}H NMR (600 MHz, $CDCl_3$): δ 3.50 (s, 3H), 3.53 (s, 3H), 5.02 (s, 2H), 5.32 (s, 2H), 6.95 (d, *J* = 8.6 Hz, H-5'), 7.09 (dd, *J* = 8.6 and 8.6 Hz, H-3 and H-5), 7.29 (d, *J* = 15.9 Hz, H-α), 7.60 (d, *J* = 8.6 Hz, H-6'), 7.61 (d, *J* = 8.6 Hz, H-2 and H-6), 7.64 (d, *J* = 15.8 Hz, H-β).

(*E*)-3-(4-chlorophenyl)-1-(3-iodo-2,4-bis(methoxymethoxy)phenyl)prop-2-en-1-one (C.11)

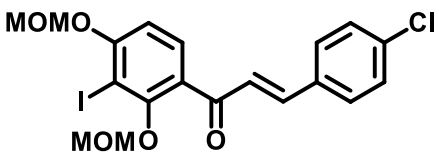

Yellow oil; yield 75 %. ^{1}H NMR (600 MHz, $CDCl_3$): δ 3.48 (s, 3H), 3.52 (s, 3H), 5.02 (s, 2H), 5.31 (s, 2H), 6.95 (d, *J* = 8.6 Hz, H-5'), 7.33 (d, *J* = 15.9 Hz, H-α), 7.36 (d, *J* = 8.5 Hz, H-3 and H-5), 7.53 (d, *J* = 8.5 Hz, H-2 and H-6), 7.60 (d, *J* = 8.6 Hz, H-6'), 7.62 (d, *J* = 15.9 Hz, H-β).

(*E*)-3-(4-bromophenyl)-1-(3-iodo-2,4-bis(methoxymethoxy)phenyl)prop-2-en-1-one (C.12)

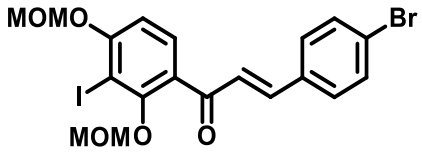

Yellow oil; yield 70 %. ^{1}H NMR (600 MHz, $CDCl_3$): δ 3.49 (s, 3H), 3.52 (s, 3H), 5.02 (s, 2H), 5.31 (s, 2H), 6.95 (d, *J* = 8.6 Hz, H-5'), 7.35 (d, *J* = 15.9 Hz, H-α), 7.47 (d, *J* = 8.5 Hz, H-2 and H-6), 7.52 (d, *J* = 8.5 Hz, H-3 and H-5), 7.60 (d, *J* = 8.6 Hz, H-6'), 7.61 (d, *J* = 15.9 Hz, H-β).

(*E*)-1-(3-iodo-2,4-bis(methoxymethoxy)phenyl)-3-(4-(trifluoromethyl)phenyl)prop-2-en-1-one (C.13)

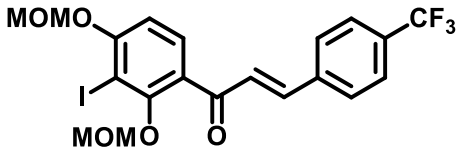

Yellow oil; yield 60 %. ^{1}H NMR (600 MHz, $CDCl_3$): δ 3.49 (s, 3H), 3.53 (s, 3H), 5.03 (s, 2H), 5.32 (s, 2H), 6.97 (d, *J* = 8.7 Hz, H-5'), 7.45 (d, *J* = 15.9 Hz, H-α), 7.63 (d, *J* = 8.7 Hz, H-6'), 7.65 (d, *J* = 9.0 Hz, H-2 and H-6), 7.67 (d, *J* = 15.9 Hz, H-β), 7.71 (d, *J* = 9.0 Hz, H-3 and H-6).

(*E*)-1-(3-iodo-2,4-bis(methoxymethoxy)phenyl)-3-(4-nitrophenyl)prop-2-en-1-one (C.14)

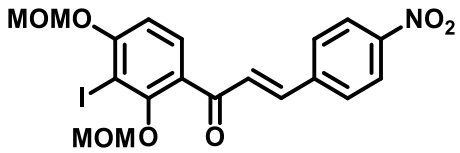

Yellow oil; yield 82 %. ^{1}H NMR (600 MHz, $CDCl_3$): δ 3.48 (s, 3H), 3.53 (s, 3H), 5.03 (s, 2H), 5.33 (s, 2H), 6.98 (d, *J* = 8.7 Hz, H-5'), 7.52 (d, *J* = 15.9 Hz, H-α), 7.65 (d, *J* = 8.7 Hz, H-6'), 7.71 (d, *J* = 15.9 Hz, H-β), 7.76 (d, *J* = 8.7 Hz, H-2 and H-6), 8.25 (d, *J* = 8.7 Hz, H-3 and H-5).

(*E*)-1-(3-iodo-2,4-bis(methoxymethoxy)phenyl)-3-(pyridin-3-yl)prop-2-en-1-one (C.15)

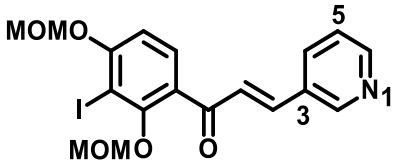

Brown oil; yield 30%. ^{1}H NMR (600 MHz, $CDCl_3$): δ 3.49 (s, 3H), 3.52 (s, 3H), 5.03 (s, 2H), 5.31 (s, 2H), 6.96 (d, *J* = 8.7 Hz, H-5'), 7.34 (dd, *J* = 4.8 and 7.9 Hz, H-5), 7.44 (d, *J* = 16.0 Hz, H-α), 7.62 (d, *J* = 8.7 Hz, H-6'), 7.67 (d, *J* = 16.0 Hz, H-β), 7.93 (ddd, *J* = 1.6, 0.9 and 7.9 Hz, H-4), 8.61 (d, *J* = 0.9 and 4.8 Hz, H-6), 8.81 (d, *J* = 1.6 Hz, H-2).

(*E*)-1-(3-iodo-2,4-bis(methoxymethoxy)phenyl)-3-(pyridin-4-yl)prop-2-en-1-one (C.16)

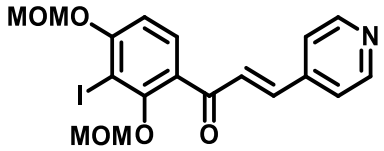

Brown oil; yield 40%. ^{1}H NMR (600 MHz, $CDCl_3$): δ 3.47 (s, 3H), 3.52 (s, 3H), 5.02 (s, 2H), 5.32 (s, 2H), 6.97 (d, *J* = 8.7 Hz, H-5'), 7.45 (d, *J* = 6.1 Hz, H-3 and H-5), 7.53 (d, *J* = 15.9 Hz, H-α), 7.58 (d, *J* = 15.9 Hz, H-β), 7.63 (d, *J* = 8.7 Hz, H-6'), 8.66 (d, *J* = 6.1 Hz, H-2 and H-6).

(*E*)-3-(furan-2-yl)-1-(3-iodo-2,4-bis(methoxymethoxy)phenyl)prop-2-en-1-one (C.17)

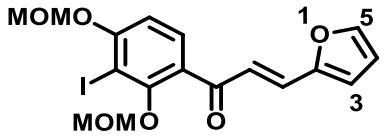

Brown oil; yield 92%. ^{1}H NMR (600 MHz, $CDCl_3$): δ 3.51 (s, 3H), 3.52 (s, 3H), 5.03 (s, 2H), 5.30 (s, 2H), 6.49 (dd, *J* = 1.75 and 3.30 Hz, H-4), 6.69 (d, *J* = 3.3 Hz, H-3), 6.93 (d, *J* = 8.6 Hz, H-5'), 7.23 (d, *J* = 15.6 Hz, H-α), 7.44 (d, *J* = 15.6 Hz, H-β), 7.50 (d, *J* = 1.39 Hz, H-5), 7.59 (d, *J* = 8.6 Hz, H-6').

(*E*)-1-(3-iodo-2,4-bis(methoxymethoxy)phenyl)-3-(thiophen-2-yl)prop-2-en-1-one (C.18)

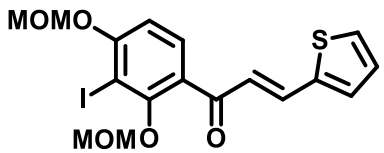

Brown oil; yield 92%. ^{1}H NMR (600 MHz, $CDCl_3$): δ 3.51 (s, 3H), 3.52 (s, 3H), 5.03 (s, 2H), 5.30 (s, 2H), 6.94 (d, *J* = 8.6 Hz, H-5'), 7.07 (dd, *J* = 3.7 and 5.0 Hz, H-4), 7.14 (d, *J* = 15.6 Hz, H-α), 7.41 (d, *J* = 5.0 Hz, H-3), 7.33 (d, *J* = 3.7 Hz, H-5), 7.59 (d, *J* = 8.6 Hz, H-6'), 7.80 (d, *J* = 15.6 Hz, H-β).

(*E*)-1-(3-iodo-2,4-bis(methoxymethoxy)phenyl)-3-(naphthalen-1-yl)prop-2-en-1-one (C. 19)

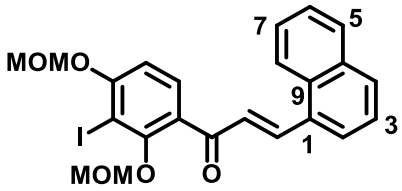

Yellow powder; yield 90%. ^{1}H NMR (600 MHz, $CDCl_3$): δ 3.51 (s, 3H), 3.54 (s, 3H), 5.07 (s, 2H), 5.33 (s, 2H), 6.98 (d, *J* = 8.6 Hz, H-5'), 7.45 (d, *J* = 15.6 Hz, H-α), 7.49–7.55 (m, H-6 e H-7), 7.57–7.60 (m, H-3), 7.88–7.92 (m, H-2, H-5 and H-8), 8.24 (d, *J* = 8.5 Hz, H-4), and 8.56 (d, *J* = 15.6 Hz, H-β)

(*E*)-1-(3-iodo-2,4-bis(methoxymethoxy)phenyl)-3-(naphthalen-2-yl)prop-2-en-1-one (C.20)

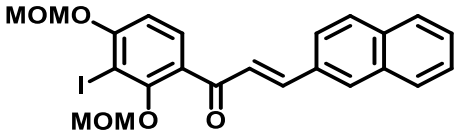

Yellow powder; yield 95%. ^{1}H NMR (600 MHz, $CDCl_3$): δ 3.51 (s, 3H), 3.54 (s, 3H), 5.05 (s, 2H), 5.32 (s, 2H), 6.97 (d, *J* = 8.7 Hz, H-5'), 7.47 (d, *J* = 15.8 Hz, H-α), 7.50–7.54 (m, H-6 and H-7), 7.64 (d, *J* = 8.7 Hz, H-6'), 7.76 (dd, *J* = 1.0 and 8.6 Hz, H-3), 7.82–7.88 (m, H-4, H-5 and H-8), 7.83 (d, *J* = 15.8 Hz, H-β), 8.00 (s, H-1).

(*E*)-1-(3-iodo-4-(methoxymethoxy)phenyl)-3-(4-(methoxymethoxy)phenyl)prop-2-en-1-one (C.21)

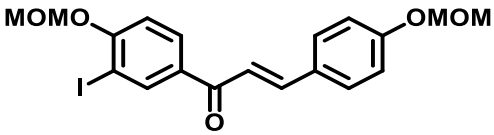

Yellow powder; yield 89%. ^{1}H NMR (600 MHz, $CDCl_3$): δ 3.49 (s, 3H), 3.52 (s, 3H), 5.22 (s, 2H), 5.32 (s, 3H), 7.07 (d, *J* = 8.7 Hz, H-3 and H-5), 7.13 (d, *J* = 8.6 Hz, H-5'), 7.36 (d, *J* = 15.5 Hz, H-α), 7.60 (d, *J* = 8.7 Hz, H-2 and H-6), 7.77 (d, *J* = 15.5 Hz, H-β), 7.98 (dd, *J* = 2.0 and 8.6 Hz, H-6'), 8.46 (d, *J* = 2.0 Hz, H-2').

(*E*)- 1- (2- (((*E*)- 3,7- dimethylocta- 2,6- dien- 1- yl)oxy)- 4- (methoxymethoxy)phenyl)- 3- (4- (methoxymethoxy)phenyl)prop-2-en-1-one (C.43)

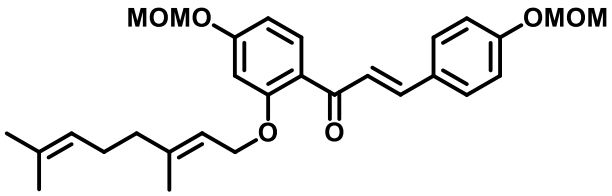

Yellow oil; yield 90%.

3-methyl-2-butenylboronic acid pinacol ester (22)

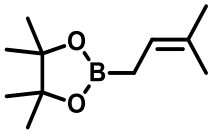

Translucent yellowish liquid; yield: 75%.

(*E*)- 1- (2,4- bis(methoxymethoxy)- 3- (3- methylbut- 2- en- 1- yl)phenyl)- 3- (4- (methoxy methoxy)phenyl)prop-2-en-1-one (C.22)

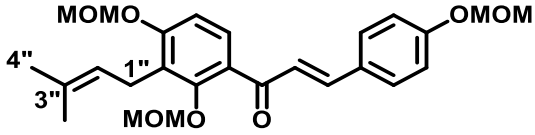

Yellow oil; yield 50 %. ^{1}H NMR ($CDCl_3$, 600 MHz) identical to literature (WANG et al., 2015): δ 1.80 (s, 3H), 1.69 (s, 3H), 3.44 (s, 3H), 3.46 (d, *J* = 7.3 Hz, 2H), 3.477 (s, 3H), 3.48 (s, 3H), 4.91 (s, 2H), 5.21 (s, 2H), 5.22 (t, *J* = 7.3 Hz, 1H), 5.25 (s, 2H), 6.94 (d, *J* = 8.6 Hz, H-5'), 7.05 (d, *J* = 8.7 Hz, H-3 and H-5), 7.23 (d, *J* = 15.9 Hz, H-α), 7.47 (d, *J* = 8.6 Hz, H-6'), 7.55 (d, *J* = 8.7 Hz, H-2 and H-6), 7.62 (d, *J* = 15.9 Hz, H-β).

(*E*)- 1- (2,4- bis(methoxymethoxy)- 3- (3- methylbut- 2- en- 1- yl)phenyl)- 3- (3- (methoxy methoxy)phenyl)prop-2-en-1-one (C.23)

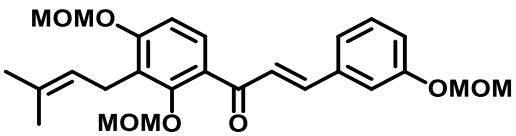

Yellow oil; yield 51 %. ^{1}H NMR (600 MHz, $CDCl_3$): δ 1.80 (s, 3H), 1.69 (s, 3H), 3.44 (s, 3H), 3.46 (d, *J* = 7.3 Hz, 2H), 3.47 (s, 3H), 3.48 (s, 3H), 4.91 (s, 2H), 5.19 (s, 2H), 5.22 (t, *J* = 7.3 Hz, 1H), 5.25 (s, 2H), 6.94 (d, *J* = 8.6 Hz, H-5'), 7.07 (ddd, *J* = 0.8, 2.4 and 8.0 Hz, H-3), 7.24 (dd, *J* = 0.8 and 2.4 Hz, H-2), 7.26 (ddd, *J* = 0.8, 2.4 and 7.7 Hz, H-6), 7.31 (dd, *J* = 7.7 and 8.0 Hz, H-4), 7.32 (d, *J* = 15.9 Hz, H-α), 7.48 (d, *J* = 8.6 Hz, H-6'), 7.60 (d, *J* = 15.9 Hz, H-β).

(*E*)- 1- (2,4- bis(methoxymethoxy)- 3- (3- methylbut- 2- en- 1- yl)phenyl)- 3- (2- (methoxy methoxy)phenyl)prop-2-en-1-one (C.24)

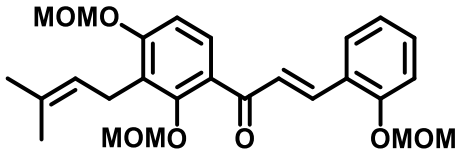

Yellow oil; yield 46 %. ^{1}H NMR ($CDCl_3$, 600 MHz): δ 1.69 (s, 3H), 1.80 (s, 3H), 3.45 (s, 3H), 3.46 (d, *J* = 7.0 Hz, 2H), 3.48 (s, 3H), 3.50 (s, 3H), 5.93 (s, 2H), 5.23 (t, *J* = 7.0 Hz, 1H), 5.25 (s, 2H), 5.26 (s, 2H), 6.94 (d, *J* = 8.7 Hz, H-5'), 7.02 (ddd, *J* = 1.0, 7.5 and 8.4 Hz, H-5), 7.16 (dd, *J* = 1.0 and 8.4 Hz, H-3), 7.33 (ddd, *J* = 1.7, 7.5 and 8.4 Hz, H-4), 7.42 (d, *J* = 16 Hz, H-α), 7.50 (d, *J* = 8.6 Hz, H-6'), 7.54 (dd, *J* = 1.7 and 7.5 Hz, H-6), 8.06 (d, *J* = 16 Hz, H-β).

(*E*)- 1- (2,4- bis(methoxymethoxy)- 3- (3- methylbut- 2- en- 1- yl)phenyl)- 3- (2,4- bis(met hoxymethoxy)phenyl)prop-2-en-1-one (C.25)

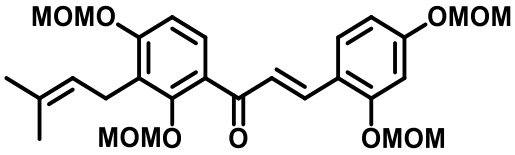

Yellow oil; yield 45%. ^{1}H NMR ($CDCl_3$, 600 MHz): δ 1.69 (s, 3H), 1.80 (s, 3H), 3.45 (s, 3H), 3.45–3.49 (m, H-1"), 3.47 (s, 3H), 3.48 (s, 3H), 3.49 (s, 3H), 4.92 (s, 2H), 5.19 (s, 2H), 5.19–5.25 (m, H-2), 5.24 (s, 2H), 5.25 (s, 2H), 6.72 (dd, *J* = 1.6 and 8.7 Hz, H-5), 6.84 (d, *J* = 1.6 Hz, H-3), 6.93 (d, *J* = 8.6 Hz, H-5'), 7.33 (d, *J* = 15.9 Hz, H-α), 7.48 (d, *J* = 8.7 Hz, H-6), 7.57 (d, *J* = 8.6 Hz, H-6'), 7.99 (d, *J* = 15.9 Hz, H-β).

(*E*)- 1- (2,4- bis(methoxymet(*E*)- 1- (2,4- bis(methoxymethoxy)- 3- (3- methylbut- 2- en- 1 - yl)phenyl)-3-(3,4-bis(methoxymethoxy)phenyl)prop-2-en-1-one (C.26)

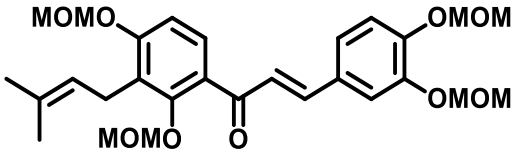

Yellow oil; yield 45 %. ^{1}H NMR (600 MHz, $CDCl_3$): δ 1.67 (s, H-5"), 1.80 (s, H-4"), 3.45 (s, 3H), 3.46 (d, *J* = 7.2 Hz, H-1"), 3.48 (s, 3H), 3.51 (s, 3H), 3.53 (s, 3H), 4.91 (s, 2H), 5.22 (t, *J* = 7.2 Hz, H-2"), 5.25 (s, 2H), 5.26 (s, 2H), 5.27 (s, 2H), 6.94 (d, *J* = 8.7 Hz, H-5'), 7.17 (d, *J* = 8.4 Hz, H-5), 7.20 (d, *J* = 15.8 Hz, H-α), 7.23 (dd, *J* = 2.0 and 8.4 Hz, H-6), 7.41 (d, *J* = 1.7 Hz, H-2), 7.45 (d, *J* = 8.7 Hz, H-6'), 7.56 (d, *J* = 15.3 Hz, H-β).

(*E*)- 1- (2,4- bis(methoxymet(*E*)- 1- (2,4- bis(methoxymethoxy)- 3- (3- methylbut- 2- en- 1 - yl)phenyl)-3-(3,4-bis(methoxymethoxy)phenyl)prop-2-en-1-one (C.27)

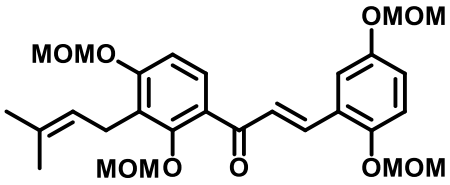

Yellow oil; yield 50%. ^{1}H NMR ($CDCl_3$, 600 MHz): δ 1.69 (s, H-5”), 1.80 (s, H-4”), 3.46 (s, 3H), 3.46–3.47 (m, H-1”), 3.48 (s, 3H), 3.48 (s, 3H), 4.92 (s, 2H), 5.14 (s, 2H), 5.18 (s, 2H), 5.20–5.25 (m, H-2”), 5.25 (s, 2H), 6.94 (d, *J* = 8.6 Hz, H-5’), 7.03 (dd, *J* = 2.9 and 9.0 Hz, H-4), 7.09 (dd, *J* = 9.0 Hz, H-3), 7.31 (d, *J* = 2.9 Hz, H-6), 7.37 (d, *J* = 16.1 Hz, H-α),7.49 (d, *J* = 8.6 Hz, H-6’), 8.0 (d, *J* = 16.0 Hz, H-β).

(*E*)-1-(2,4-bis(methoxymethoxy)-3-(3-methylbut-2-en-1-yl)phenyl)-3-phenylprop-2-en-1-one (C.28)

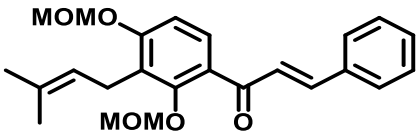

Yellow oil; yield 46%. ^{1}H NMR ($CDCl_3$, 600 MHz): δ 1.70 (s, 3H), 1.81 (s, 3H), 3.44 (s, 3H), 3.47 (d, *J* = 7.0 Hz, 2H), 3.48 (s, 3H), 4.92 (s, 2H), 5.23 (t, *J* = 7.0 Hz, 1H), 5.25 (s, 2H), 6.95 (d, *J* = 8.6 Hz, H-5’), 7.36 (d, *J* = 15.9 Hz, H-α), 7.38–7.42 (m, 3H, H-3–5), 7.49 (d, *J* = 8.6 Hz, H-6’), 7.60 (d, *J* = 2.3 and 7.1 Hz, H-2 and H-6), 7.66 (d, *J* = 15.9 Hz, H-β).

(*E*)- 1- (2,4- bis(methoxymethoxy)- 3- (3- methylbut- 2- en- 1- yl)phenyl)- 3- (4- methoxy phenyl)prop-2-en-1-one (C.29)

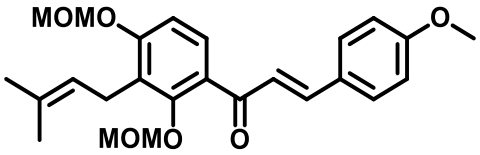

Yellow oil; yield 69 %. ^{1}H NMR ($CDCl_3$, 600 MHz): δ 1.69 (s, 3H), 1.80 (s, 3H), δ 3.45 (s, 3H), 3.47 (d, *J* = 7.5 Hz, 2H), 3.48 (s, 3H), 3.84 (s, 3H, 4-OMe), 4.91 (s, 2H), 5.22 (t, *J* = 7.5 Hz, 1H), 5.24 (s, 2H), 6.92 (d, *J* = 8.7 Hz, H-3 and H-5), 6.94 (d, *J* = 8.6 Hz, H-5’), 7.22 (d, *J* = 15.8 Hz, H-α), 7.47 (d, *J* = 8.6 Hz, H-6’), 7.55 (d, *J* = 8.7 Hz, H-2 and H-6), 7.62 (d, *J* = 15.9 Hz, H-β).

(*E*)- 1- (2,4- bis(methoxymethoxy)- 3- (3- methylbut- 2- en- 1- yl)phenyl)- 3- (4- methylph enyl)prop-2-en-1-one (C.30)

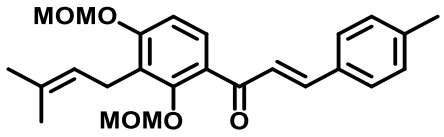

Yellow oil; yield 35%. ^{1}H NMR ($CDCl_3$, 600 MHz): δ 1.69 (s, 3H), 1.80 (s, 3H), 2.38 (s, 4-Me), 3.45 (s, 3H), 3.46 (d, *J* = 7.0 Hz, 2H), 3.48 (s, 3H), 4.92 (s, 2H), 5.23 (t, *J* = 7.0 Hz, 1H), 5.25 (s, 2H), 6.94 (d, *J* = 8.7 Hz, H-5'), 7.20 (d, *J*= 7.9 Hz, H-3 and H-5), 7.30 (d, *J* = 15.9 Hz, H-α), 7.48 (d, *J* = 8.6 Hz, H-6'), 7.50 (d, *J* = 8.0 Hz, H-2 and H-6), 7.64 (d, *J* = 15.9 Hz, H-β).

(*E*)- 1- (2,4- bis(methoxymethoxy)- 3- (3- methylbut- 2- en- 1- yl)phenyl)- 3- (4- fluorophe nyl)prop-2-en-1-one (C.31)

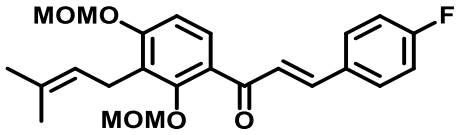

Yellow oil; yield 37 %. ^{1}H NMR ($CDCl_3$, 600 MHz): δ 1.69 (s, H-5"), 1.79 (s, H-4"), 3.44 (s, 3H), 3.47 (d, *J* = 7.2 Hz, H-1"), 4.92 (s, 2H), 5.22 (t, *J* = 7.2 Hz, H-2"), 5.25 (s, 2H), 6.95 (d, *J* = 8.7 Hz, H-5'), 7.08 (dd, *J* = 8.6 and 8.6 Hz, H-3 and H-5), 7.29 (d, *J* = 15.9 Hz, H-β), 7.49 (d, *J* = 8.7 Hz, H-6'), 7.59 (dd, *J* = 5.5 and 8.6 Hz, H-2 and H-6), 7.62 (d, *J* = 15.9 Hz, H-β).

(*E*)- 1- (2,4- bis(methoxymethoxy)- 3- (3- methylbut- 2- en- 1- yl)phenyl)- 3- (4- chloroph enyl)prop-2-en-1-one (C.32)

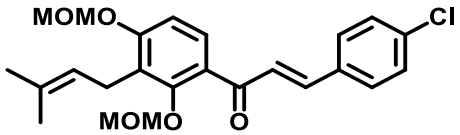

Yellow oil; yield 35%. ^{1}H NMR ($CDCl_3$, 600 MHz): δ 1.69 (s, H-5"), 1.80 (s, H-4"), 3.43 (s, 3H), 3.46 (d, *J* = 7.1 Hz, H-1"), 3.48 (s, 3H), 4.91 (s, 2H), 5.21 (t, *J* = 7.1 Hz, H-2"), 5.25 (s, 2H), 6.95 (d, *J* = 8.7 Hz, H-5'), 7.34 (d, *J* = 15.9 Hz, H-β), 7.36 (d, *J* = 8.5 Hz, H-3 and H-5), 7.49 (d, *J* = 8.7 Hz, H-6'), 7.53 (d, *J* = 8.5 Hz, H-2 and H-6), 7.61 (d, *J* = 15.9 Hz, H-β).

(*E*)- 1- (2,4- bis(methoxymethoxy)- 3- (3- methylbut- 2- en- 1- yl)phenyl)- 3- (4- bromoph enyl)prop-2-en-1-one (C.33)

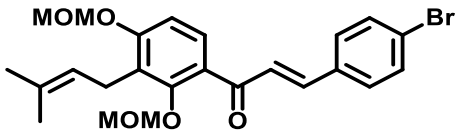

Yellow oil; yield 6%. ^{1}H NMR ($CDCl_3$, 600 MHz): δ 1.69 (s, H-5”), 1.80 (s, H-4”), 3.43 (s, 3H), 3.46 (d, *J* = 7.2 Hz, H-1”), 3.48 (s, 3H), 4.91 (s, 2H), 5.21 (t, *J* = 7.2 Hz, H-2”), 5.25 (s, 2H), 6.95 (d, *J* = 8.7 Hz, H-5’), 7.35 (d, *J* = 15.9 Hz, H-α), 7.46 (d, *J* = 8.4 Hz, H-2 and H-6), 7.49 (d, *J* = 8.7 Hz, H-6’), 7.53 (d, *J* = 8.4 Hz, H-3 and H-5), 7.59 (d, *J* = 15.9 Hz, H-β).

(*E*)- 1- (2,4- bis(methoxymethoxy)- 3- (3- methylbut- 2- en- 1- yl)phenyl)- 3- (4- (trifluoro methyl)phenyl)prop-2-en-1-one (C.34)

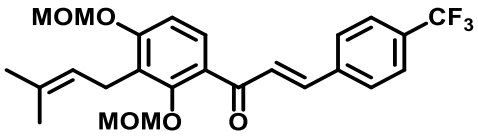

Yellow oil; yield 10%. ^{1}H NMR ($CDCl_3$, 600 MHz): δ 1.70 (s, H-5”), 1.80 (s, H-4”), 3.44 (s, 3H), 3.47 (d, *J* = 7.3 Hz, H-1”), 3.48 (s, H), 4.91 (s, 2H), 5.21 (t, *J* = 7.3 Hz, H-2”), 6.97 (d, *J* = 8.7 Hz, H-5’), 7.45 (d, *J* = 15.9 Hz, H-α), 7.52 (d, *J* = 8.7 Hz, H-6’), 7.65 (d, *J* = 8.2 Hz, H-2 and H-6), 7.67 (d, *J* = 15.9 Hz, H-β), 7.70 (d, *J* = 8.2 Hz, H-3 and H-5).

(*E*)- 1- (2,4- bis(methoxymethoxy)- 3- (3- methylbut- 2- en- 1- yl)phenyl)- 3- (4- nitrophe nyl)prop-2-en-1-one (C.35)

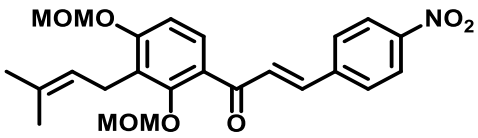

Yellow power; yield 18%. ^{1}H NMR ($CDCl_3$, 600 MHz): δ 1.68 (s, H-5”), 1.80 (s, H-4”), 3.43 (s, 3H), 3.46 (d, *J* = 7.3 Hz, H-1”), 4.91 (s, 2H), 5.20 (t, *J* = 7.3 Hz, H-2”), 5.26 (s, 2H), 6.97 (d, *J* = 8.7 Hz, H-5’), 7.51 (d, *J* = 15.9 Hz, H-α), 7.53 (d, *J* = 8.7 Hz, H-6’), 7.68 (d, *J* = 15.9 Hz, H-β), 7.74 (d, *J* = 8.8 Hz, H-2 and H-6), 8.25 (d, *J* = 8.8 Hz, H-3 and H-5).

(*E*)-1-(2,4-bis(methoxymethoxy)-3-(3-methylbut-2-en-1-yl)phenyl)-3-(pyridin-3-yl)prop-2-en-1-one (C.36)

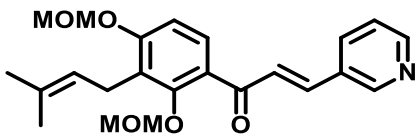

Brown oil; yield 30%. ^{1}H NMR (600 MHz, $CDCl_3$): δ 1.69 (s, H-5”), 1.80 (s, 4”), 3.43 (s, 3H), 3.46 (d, *J* = 7.0 Hz, H-1”), 4.91 (s, 2H), 5.21 (t, *J* = 7.0 Hz, H-2”), 5.26 (s, 2H), 6.96 (d, *J* = 8.7

Hz, H-5'), 7.34 (dd, *J* = 4.8 and 7.9 Hz, H-5), 7.45 (d, *J* = 16.0 Hz, H-α), 7.51 (d, *J* = 8.7 Hz, H-6'), 7.64 (d, *J* = 16.0 Hz, H-β), 7.91 (d, *J* = 7.9 Hz, H-4), 8.60 (d, *J* = 4.8 Hz, H-6), 8.81 (s, H-2).

(*E*)-1-(2,4-bis(methoxymethoxy)-3-(3-methylbut-2-en-1-yl)phenyl)-3-(pyridin-4-yl)prop-2-en-1-one (C.37)

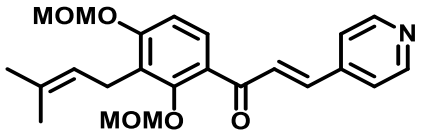

Brown oil; yield 15%. ^{1}H NMR (600 MHz, $CDCl_3$): δ 1.69 (s, H-5"), 1.80 (s, H-4"), 3.43 (s, 3H), 3.46 (d, *J* = 6.9 Hz, H-1"), 3.48 (s, 3H), 4.90 (s, 2H), 5.20 (t, *J* = 6.9 Hz, H-2"), 6.97 (d, *J* = 8.7 Hz, H-5'), 7.44 (d, *J* = 5.7 Hz, H-2 and H-6), 7.52 (d, *J* = 8.7 Hz, H-6'), 7.53 (d, *J* = 16.0 Hz, H-α), 7.56 (d, *J* = 16.0 Hz, H-β), 8.66 (d, *J* = 5.7 Hz, H-3 and H-5).

(*E*)-1-(2,4-bis(methoxymethoxy)-3-(3-methylbut-2-en-1-yl)phenyl)-3-(furan-2-yl)prop-2-en-1-one (C.38)

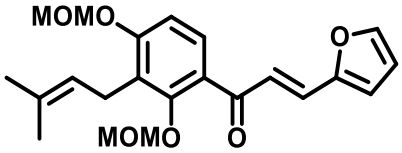

Brown oil; yield 43%. ^{1}H NMR ($CDCl_3$, 600 MHz): δ 1.68 (s, H-5"), 1.79 (s, H-4"), 3.46 (s, 3H), 3.46 (d, *J* = 7.0 Hz, H-1"), 3.47 (s, 3H), 4.92 (s, 2H), 5.21 (t, *J* = 7.0 Hz, H-2"), 5.25 (s, 2H), 6.49 (dd, *J* = 1.8 and 3.3 Hz, H-4), 6.67 (d, *J* = 3.3 Hz, H-3), 6.93 (d, *J* = 8.6 Hz, H-5'), 7.24 (d, *J* = 15.6 Hz, H-α), 7.43 (d, *J* = 15.6 Hz, H-β), 7.48 (d, *J* =8.6 Hz, H-6'), 7.50 (d, *J* = 1.8 Hz, H-5).

(*E*)- 1- (2,4- bis(methoxymethoxy)- 3- (3- methylbut- 2- en- 1- yl)phenyl)- 3- (thiophen- 2- yl)prop-2-en-1-one (C.39)

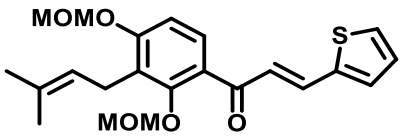

Brown oil; yield 32%. ^{1}H NMR ($CDCl_3$, 600 MHz): δ 1.69 (s, H-5"), 1.80 (s, H-4"), 3.46 (d, *J* = 7.0 Hz, H-1"), 3.466 (s, 3H), 3.473 (s, 3H), 4.92 (s, 2H), 5.21 (t, *J* = 7.0 Hz, H-2"), 5.25 (s, 2H), 6.94 (d, *J* = 8.7 Hz, H-5'), 7.07 (dd, *J* = 3.6 and 5.0 Hz, H-4), 7.16 (d, *J* = 15.6 Hz, H-α),

7.31 (d, *J* = 3.6 Hz, H-3), 7.39 (d, *J* = 5.0 Hz, H-5), 7.48 (d, *J* = 8.6 Hz, H-6'), 7.78 (d, *J* = 15.6 Hz, H-β).

(*E*)-1-(2,4-bis(methoxymethoxy)-3-(3-methylbut-2-en-1-yl)phenyl)-3-(naphthalen-1-yl)prop-2-en-1-one (C.40)

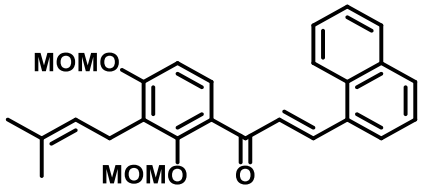

Yellow oil; yield 42%. ^{1}H NMR (600 MHz, $CDCl_3$): δ 1.70 (s, H-5"), 1.81 (s, H-4"), 3.45 (s, 3H), 3.49 (s, 3H), 3.49 (d, *J* = 7.0 Hz, H-1"), 4.97 (s, 2H), 5.25 (t, *J* = 7.0 Hz, H-2"), 5.27 (s, 2H), 6.99 (d, *J* = 8.7 Hz, H-5'), 7.44 (d, *J* = 15.6 Hz, H-α), 7.49–7.54 (m, H-6 e H-7),7.56–7.59 (m, H-3), 7.88–7.92 (m, H-2, H-5 and H-8), 8.24 (d, *J* = 8.3 Hz, H-4), 8.53 (d, *J* = 15.6 Hz, H-β).

(*E*)-1-(2,4-bis(methoxymethoxy)-3-(3-methylbut-2-en-1-yl)phenyl)-3-(naphthalen-2-yl)prop-2-en-1-one (C.41)

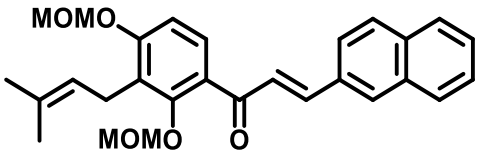

Yellow oil; yield 50%. ^{1}H NMR (600 MHz, $CDCl_3$): δ 1.71 (s, H-5"), 1.81 (s, H-4"), 3.45 (s, 3H), 3.48 (d, *J* = 7.3 Hz, H-1"), 3.49 (s, 3H), 4.94 (s, 2H), 5.24 (t, *J* = 7.3 Hz, H-2"), 5.27 (s, 2H), 6.97 (d, *J* = 8.7 Hz, H-5'), 7.47 (d, *J* = 15.9 Hz, H-α), 7.50–7.53 (m, H-6 and H-7), 7.53 (d, *J* = 8.7 Hz, H-6'), 7.77 (dd, *J* = 1.0 and 8.6 Hz, H-3), 7.82–7.53 (m, H-4, H-5 and H-8), 7.83 (d, *J* = 15.9 Hz, H-β), 7.89 (d, *J* = 1.0 Hz, H-1).

(*E*)- 1- (4- (methoxymethoxy)- 3- (3- methylbut- 2- en- 1- yl)phenyl)- 3- (4- (methoxymethoxy)phenyl)prop-2-en-1-one (C.42)

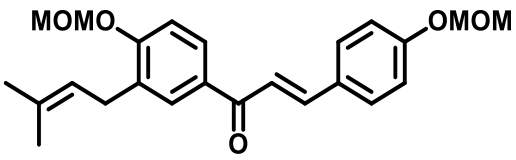

Yellow oil; yield 70%. ^{1}H NMR (600 MHz, $CDCl_3$): δ 1.74 (s, H-5"), 1.75 (s, H-4"), 3.39 (d, *J* = 7.3 Hz, H-1"), 3.49 (s, 3H), 3.49 (s, 3H), 5.21 (s, 2H), 5.28 (s, 2H), 5.32 (t, *J* = 7.3 Hz, H-2"),

7.07 (d, *J* = 8.7 Hz, H-3 and H-5), 7.12 (d, *J* = 8.8 Hz, H-5'), 7.41 (d, *J* = 15.6 Hz, H-α), 7.75 (d, *J* = 15.5 Hz, H-β), 7.85 (d, *J* = 2.2 Hz, H-2'), 7.86 (dd, *J* = 2.2 and 8.8 Hz, H-6').

(*E*)-1-(2-hydroxy-4-(methoxymethoxy)phenyl)-3-(4-(methoxymethoxy)phenyl)prop-2-en-1-one (C.44)

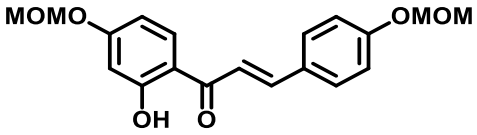

Yellow crystal powder; yield 35%. ^{1}H NMR (600 MHz, $CDCl_3$) in according to literature (SUGAMOTO et al., 2011): δ 3.489 (s, 3H), 3.493 (s, 3H), 5.22 (s, 2H), 5.23 (s, 2H), 6,59 (dd, *J* = 2.5 and 8.9 Hz, H-5'), 6.64 (d, *J* = 2.5 Hz, H-3'), 7.08 (d, *J* = 8.7 Hz, H-3 and H-5), 7.47 (d, *J* = 15.4 Hz, H-α), 7.61 (d, *J* = 8.7 Hz, H-2 and H-6), 7.84 (d, *J* = 8.9 Hz, H-6'), 13.3 (s, 2'-OH).

(*E*)-1-(3-((*E*)-3,7-dimethylocta-2,6-dien-1-yl)-2-hydroxy-4-(methoxymethoxy)phenyl)-3-(4-(methoxymethoxy)phenyl)prop-2-en-1-one (C.45)

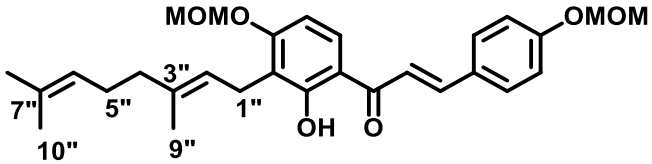

Yellow crystal powder; 38 %. ^{1}H NMR (Acetone-d_6, 600 MHz) in according to literature(SUGAMOTO et al., 2011): δ 1.56 (s, H-9"), 1.61 (s, H-10"), 1.83 (s, H-8"), 1.97 (t, *J* = 7.7 Hz, H-4"), 2.05–2.08 (m, H-5"), 3.43 (d, *J* = 7.0 Hz, H-1"), 3.47 (s, 3H), 3.48 (s, 3H), 5.08 (t, *J* = 7.0 Hz, H-6"), 5.27 (t, *J* = 7.0 Hz, H-2"), 5.29 (s, 2H), 5.38 (s, 2H), 6.77 (d, *J* = 9.0 Hz, H-5'), 7.14 (d, *J* = 8.7 Hz, H-3 and H-5), 7.85 (d, *J* = 8.7 Hz, H-2 and H-6), 7.88 (d, *J* = 15.9 Hz, H-β), 7.89 (d, *J* = 15.9 Hz, H-β), 8.14 (d, *J* = 9.0 Hz, H-6'), 13.8 (s, 2'-OH).

(*E*)-1-(2,4-dihydroxy-3-(3-methylbut-2-en-1-yl)phenyl)-3-(4-hydroxyphenyl)prop-2-en-1-one (IBC)

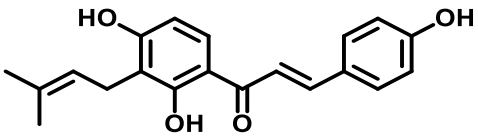

Deprotection Yield: 60%; Overall yield: 23%

Characterization data: Supporting information of Chapter II

(*E*)-1-(2,4-dihydroxy-3-(3-methylbut-2-en-1-yl)phenyl)-3-(3-hydroxyphenyl)prop-2-en-1-one (IBC 1)

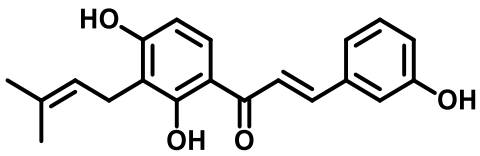

Yellow powder; yield 75%, overall yield: 30%. HPLC purity: 99 %; m.p.: 128–133ºC. ^{1}H NMR (600 MHz, acetone-d_6): δ 1.64 (s, H-5”), 1.77 (s, H-4”), 3.37 (d, *J* = 7.3 Hz, H-1”), 5.27 (t, *J* = 7.3 Hz, H-2”), 6.55 (d, *J* = 8.9 Hz, H-5’), 6.94 (ddd, *J* = 1.1, 2.4, and 7.8 Hz, H-4), 7.27 (dd, *J* = 1.1 and 2.4 Hz, H-2), 7.28 (dd, *J* = 7.8 and 7.8 Hz, H-5), 7.31 (ddd, *J* = 1.1, 2.4 and 7.8 Hz, H-6), 7.79 (d, *J* = 15.4 Hz, H-α), 7.86 (d, *J* = 15.4 Hz, H-β), 8.0 (d, *J* = 9.0 Hz, H-6’), 8.75 (brs, 4-OH), 9.57 (brs, 4’-OH), 13.8 (s, 2’-OH). ^{13}C NMR (150 MHz, acetone-d_6): δ 17.83 (C-5”), 22.18 (C-1”), 25.80 (C-4”), 108.1 (C-5’), 114.2 (C-1’), 116.0 (C-2), 116.1 (C-3’), 118.5 (C-4), 120.9 (C-6), 121.7 (C-α), 123.1 (C-2”), 130.5 (C-6’), 130.7 (C-5), 131.4 (C-3”), 137.2 (C-1), 144.6 (C-β), 158.7 (C-4), 163.0 (C-2’), 165.1 (C-4’), 192.9 (C-β’).

(*E*)-1-(2,4-dihydroxy-3-(3-methylbut-2-en-1-yl)phenyl)-3-(2-hydroxyphenyl)prop-2-en-1-one (IBC 2)

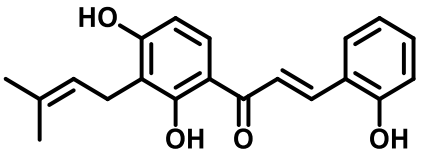

Yellow powder; deprotection yield: 70%; overall yield: 20%; HPLC purity: 99 %; m.p.: 115–120ºC. ^{1}H NMR (600 MHz, acetone-d_6): δ 1.64 (s, H-5”), 1.78 (s, H-4”), 3.38 (d, *J* = 7.2 Hz, H-1”), 5.28 (t, *J* = 7.2 Hz, H-2”), 6.54 (d, *J* = 8.9 Hz, H-5’), 6.92 (ddd, *J* = 1.1, 7.2 and 8.0 Hz, H-5), 7.0 (d, *J* = 7.28 (ddd, *J* = 1.7, 7.2 and 8.0 Hz, H-4), 7.93 (d, *J* = 8.8 Hz, H-6’), 7.81 (dd, *J* = 1.7 and 7.2 Hz, H-6), 7.96 (d, *J* = 15.6 Hz, H-α), 8.26 (d, *J* = 15.6 Hz, H-β), 9.34 (brs, 4’-OH), 14.0 (s, 2’-OH). ^{13}C NMR (150 MHz, acetone-d_6): δ 17.84 (C-5”), 22.21 (C-1”), 25.80 (C-4”), 108.0 (C-5’), 114.4 (C-1’), 116.1 (C-3’), 117.0 (C-3), 120.8 (C-5), 121.1 (C-α), 122.8 (C-1), 123.2 (C-2”), 129.9 (C-6), 130.2 (C-6’), 131.4 (C-3”), 132.6 (C-4), 140.1 (C-β), 157.9 (C-2), 162.7 (C-2’), 165.1 (C-4’), 193.3 (C-β’).

(*E*)-1-(2,4-dihydroxy-3-(3-methylbut-2-en-1-yl)phenyl)-3-(2,4-dihydroxyphenyl)prop-2-en-1-one (IBC 3)

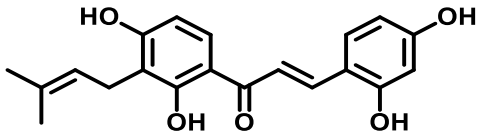

yellow powder; yield 45%, overall yield: 14 %. HPLC purity: 99%; m.p.: 127–132ºC. m.p. lit.: 204–205ºC (Et_2O) (MONACHE et al., 1995). ^{1}H NMR (600 MHz, acetone-d_6) according to literature(MONACHE et al., 1995): δ 1.64 (s, H-5”), 1.77 (s, H-4”), 3.37 (d, *J* = 7.2 Hz, H-1”), 5.28 (t, *J* = 7.2 Hz, H-2”), 6.46 (dd, *J* = 2.3 and 8.5 Hz, H-5), 6.51 (d, *J* = 8.9 Hz, H-5’), 6.52 (d, *J* = 2.3 Hz, H-3), 7.79 (d, *J* = 15.4 Hz, H-α), 7.88 (d, *J* = 8.9 Hz, H-6’), 8.22 (d, *J* = 15.4 Hz, H-β), 7.68 (d, *J* = 8.5 Hz, H-6), 14.1 (s, 2’-OH). ^{13}C NMR (150 MHz, acetone-d_6): δ 17.92 (C-5”), 22.30 (C-1”), 25.88 (C-4”), 103.5 (C-3), 107.8 (C-5’), 109.1 (C-5), 114.5 (C-1’), 115.2 (C-1), 116.0 (C-3’), 117.6 (C-α), 123.4 (C-2”), 130.0 (C-6’), 131.4 (C-3”), 131.7 (C-6), 140.8 (C-β), 159.9 (C-2), 162.2 (C-4), 162.4 (C-2’), 164.7 (C-4’), 192.9 (C-β’).

(*E*)-1-(2,4-dihydroxy-3-(3-methylbut-2-en-1-yl)phenyl)-3-(3,4-dihydroxyphenyl)prop-2-en-1-one (IBC 4)

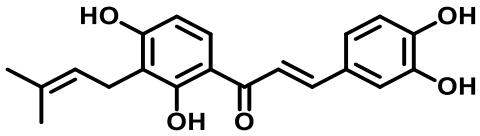

yellow powder; yield 40%; overall yield: 12%. HPLC purity: 99%; m.p: 97–100ºC. ^{1}H NMR (600 MHz, acetone-d_6) according to literature(YIN et al., 2004): δ 1.64 (s, H-5”), 1.77 (s, H-4”), 3.37 (d, *J* = 7.2 Hz, H-1”), 5.27 (t, *J* = 7.2 Hz, H-2”), 6.53 (d, *J* = 8.8 Hz, H-5’), 7.69 (d, *J* = 15.3 Hz, H-α), 7.77 (d, *J* = 15.3 Hz, H-β), 7.97 (d, *J* = 8.8 Hz, H-6’), 6.90 (d, *J* = 8.2 Hz, H-5), 7.27 (dd, *J* = 1.7 and 8.2 Hz, H-6), 7.34 (d, *J* = 1.7 Hz, H-2), 14.0 (2’-OH). ^{13}C NMR (150 MHz, acetone-d_6): δ 17.92 (C-5”), 22.30 (C-1”), 25.88 (C-4”), 107.9 (C-5’), 114.4 (C-1’), 115.9 (C-2), 116.0 (C-3’), 116.4 (C-5), 118.6 (C-α), 123.3 (C-2”), 123.4 (C-6), 128.3 (C-1), 130.3 (C-6’), 131.5 (C-3”), 143.8 (C-β), 148.3 (C-4), 146.1 (C-3), 162.6 (C-2’), 164.7 (C-4’), 192.9 (C-β’).

(*E*)-1-(2,5-dihydroxy-3-(3-methylbut-2-en-1-yl)phenyl)-3-(3,4-dihydroxyphenyl)prop-2-en-1-one (IBC 5)

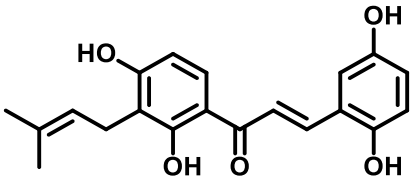

yellow powder; yield 40%; overall yield: 13%. HPLC purity: 99%; m.p: 175–180ºC. ^{1}H NMR (600 MHz, acetone-d_6): δ 1.64 (s, H-5”), 1.78 (s, H-4”), 3.37 (d, *J* = 7.2 Hz, H-2”), 5.27 (t, *J* = 7.2 Hz, H-1”), 6.54 (d, *J* = 8.8 Hz, H-5’), 6.81 (dd, *J* = 2.8 and 8.7 Hz, H-5), 6.85 (d, *J* = 8.7 Hz, H-3), 7.23 (d, *J* = 2.8 Hz, H-6), 7.87 (d, *J* = 15.5 Hz, H-α), 7.93 (d, *J* = 8.8 Hz, H-6’), 8.20 (d, *J* = 15.5 Hz, H-β), 8.06 (brs, 5-OH), 8.73 (brs, 2-OH), 9.49 (brs, 4’-OH), 14.0 (s, 2’-OH). ^{13}C NMR (150 MHz, acetone-d_6): δ 17.81 (C-5”), 25.79 (C-1”), 28.49 (C-4”), 103.4 (C-5’), 115.2 (C-4), 117.8 (C-5), 120.1 (C-1’), 121.2 (C-1), 121.1 (C-α), 114.2 (C-3’), 121.1 (C-α), 123.6 (C-2”), 132.0 (C-6’), 132.6 (C-3”), 123.1 (C-6), 140.4 (C-β), 151.3 (C-5), 151.4 (C-2), 163.6 (C-2’), 165.8 (C-4’), 193.0 (C-β’).

(*E*)-1-(2,4-dihydroxy-3-(3-methylbut-2-en-1-yl)phenyl)-3-phenylprop-2-en-1-one (IBC 6)

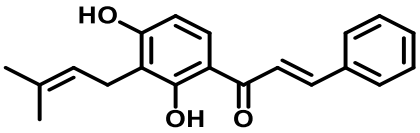

Yellow powder; yield 38%, overall yield: 14 %. HPLC purity: 99 %; m.p: 128–133ºC. ^{1}H NMR (600 MHz, acetone-d_6) according to literature(BORGES-ARGÁEZ; PEA-RODRÍGUEZ; WATERMAN, 2002): δ 1.64 (s, H-5”), 1.78 (s, H-4”), 3.38 (d, *J* = 7.3 Hz, H-1”), 5.27 (t, *J* = 7.3 Hz, H-2”), 6.55 (d, *J* = 8.9 Hz, H-5’), 7.45–7.49 (m, 3H, H-3–5), 7.86 (dd, *J* = 2.0 and 7.5 Hz, H-2 and H-6), 7.88 (d, *J* = 15.5 Hz, H-α), 7.96 (d, *J* = 15.5 Hz, H-β), 8.03 (d, *J* = 8.9 Hz, H-6’), 9.48 (brs, 4’-OH), 13.9 (s, 2’-OH). ^{13}C NMR (150 MHz, acetone-d_6): δ 17.98 (C-5”), 22.34 (C-1”), 25.95 (C-4”), 108.3 (C-5’), 114.4 (C-1’), 116.2 (C-3’), 121.9 (C-α), 123.3 (C-2”), 129.7 (C-2 and C-6), 129.9 (C-3 and C-5), 130.6 (C-6’), 131.4 (C-3”), 131.6 (C-4), 136.0 (C-1), 144.6 (C-β), 163.1 (C-2’), 165.3 (C-4’), 193.0 (C-β’).

(*E*)-1-(2,4-dihydroxy-3-(3-methylbut-2-en-1-yl)phenyl)-3-(4-methoxyphenyl)prop-2-en-1-one (IBC 7)

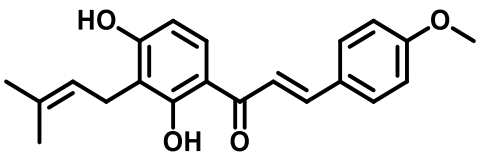

Yellow powder; yield 66%; overall yield: 37 %. HPLC purity: 99 %; m.p: 120–125ºC, m.p. lit.: 112–114ºC(GANAPATY et al., 2006). ^{1}H NMR (600 MHz, acetone-d_6) according to literature(GANAPATY et al., 2006): δ 1.64 (s, H-5”), 1.78 (s, H-4”), 3.37 (d, *J* = 7.2 Hz, H-1”), 3.86 (s, 4-OCH_3), 5.28 (t, *J* = 7.2 Hz, H-2”), 6.54 (d, *J* = 8.8 Hz, H-5’), 7.01 (d, *J* = 8.8 Hz, H-3 and H-5), 7.79 (d, *J* = 15.4 Hz, H-α), 7.80 (d, *J* = 8.8 Hz, H-2 and H-6), 7.85 (d, *J* = 15.4

Hz, H-β), 7.98 (d, *J* = 8.9 Hz, H-6'), 9.48 (brs, 4'-OH), 14.0 (s, 2'-OH). ^{13}C NMR (150 MHz, acetone-d_6): δ 17.86 (C-5"), 22.22 (C-1"), 25.83 (C-4"), 55.75 (4-OCH_3), 108.0 (C-5'), 114.3 (C-1'), 115.2 (C-3 and C-5), 116.1 (C-3'), 119.1 (C-α), 123.2 (C-2"), 130.27 (C-6'), 130.0 (C-3"), 131.4 (C-2 and C-6), 128.5 (C-1), 144.5 (C-β), 162.8 (C-4), 162.8 (C-2'), 165.1 (C-4'), 192.9 (C-β').

(*E*)-3-(4-aminophenyl)-1-(2,4-dihydroxy-3-(3-methylbut-2-en-1-yl)phenyl)prop-2-en-1-one (IBC 8)

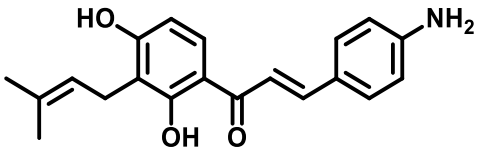

Orange oil, yield 64%; overall yield: 5 %. HPLC purity: 99 %. ^{1}H NMR (600 MHz, DMSO-d_6): δ 1.60 (s, H-5"), 1.71 (s, H-4"), 3.21 (d, *J* = 7.1 Hz, H-1"), 5.16 (t, *J* = 7.1 Hz, H-2"), 5.92 (brs, 4-NH_2), 6.44 (d, *J* = 8.9 Hz, H-5'), 6.60 (d, *J* = 8.6 Hz, H-3 and H-5), 7.56 (d, *J* = 8.6 Hz, H-2 and H-6), 7.56 (d, *J* = 15.1 Hz, H-α), 7.68 (d, *J* = 15.1 Hz, H-β), 7.96 (d, *J* = 8.9 Hz, H-6'), 14.2 (s, 2'-OH). ^{13}C NMR (150 MHz, DMSO-d_6): δ 17.81 (C-5"), 21.41 (C-1"), 25.59 (C-4"), 107.6 (C-5'), 112.5 (C-1'), 113.7 (C-3 and C-5), 114.2 (C-3'), 114.5 (C-α), 122.1 (C-2"), 122.7 (C-1), 129.5 (C-6'), 130.3 (C-3"), 131.4 (C-2 and C-6), 145.1 (C-β), 152.1 (C-4), 162.8 (C-2'), 163.6 (C-4'), 191.4 (C-β').

(*E*)-1-(2,4-dihydroxy-3-(3-methylbut-2-en-1-yl)phenyl)-3-(4-methylphenyl)prop-2-en-1-one (IBC 9)

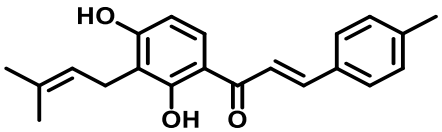

Yellow powder; yield 53%; overall yield: 14 %. HPLC purity: 99 %; m.p: 140–145ºC. ^{1}H NMR (600 MHz, acetone-d_6): δ 1.64 (s, H-5"), 1.79 (s, H-4"), 2.37 (s, 4-CH_3), 3.38 (d, *J* = 7.2 Hz, H-1"), 5.28 (t, *J* = 7.2 Hz, H-2"), 6.54 (d, *J* = 8.9 Hz, H-5'), 7.28 (d, *J* = 8.0 Hz, H-3 and H-5), 7.73 (d, *J* = 8.0 Hz, H-2 and H-6), 7.84 (d, *J* = 15.4 Hz, H-α), 7.89 (d, *J* = 15.4 Hz, H-β), 8.00 (d, *J* = 8.9 Hz, H-6'), 9.48 (brs, 4'-OH), 13.9 (s, 2'-OH). ^{13}C NMR (150 MHz, acetone-d_6): δ 17.91 (C-5"), 21.45 (4-CH_3), 22.26 (C-1"), 25.89 (C-4"), 108.1 (C-5'), 114.4 (C-1'), 116.1 (C-3'), 120.7 (C-α), 123.3 (C-2"), 129.7 (C-3 and C-5), 130.46 (C-6'), 130.48 (C-2 and C-6), 131.5 (C-3"), 133.5 (C-1), 141.9 (C-4), 144.6 (C-β), 163.0 (C-2'), 165.2 (C-4'), 193.0 (C-β').

(*E*)-1-(2,4-dihydroxy-3-(3-methylbut-2-en-1-yl)phenyl)-3-(4-fluorophenyl)prop-2-en-1-one (IBC 10)

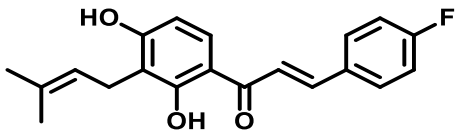

Yellow powder; yield 40%; overall yield: 10 %. HPLC purity: 97 %; m.p: 130–134ºC. ^{1}H NMR (600 MHz, acetone-d_6): δ 1.64 (s, H-5”), 1.78 (s, H-4”), 3.38 (d, *J* = 7.2 Hz, H-1”), 5.28 (t, *J* = 7.2 Hz, H-2”), 6.55 (d, *J* = 8.9 Hz, H-5’), 7.23 (dd, *J* = 8.7 and 8.7 Hz, H-3 and H-5), 7.85 (d, *J* = 15.5 Hz, H-β), 7.90 (d, *J* = 15.5 Hz, H-β), 7.92 (dd, *J* = 5.5 and 8.7 Hz, H-2 and H-6), e 8.0 (d, *J* = 8.9 Hz, H-6’), 9.40 (brs, 4’-OH), 13.8 (brs, 2’-OH). ^{13}C NMR (150 MHz, acetone-d_6): 17.97 (C-5”), 22.32 (C-1”), 25.93 (C-4”), 108.2 (C-5’), 114.4 (C-1’), 116.2 (C-3’), 116.8 (d, *J* = 22 Hz, C-3 and C-6), 121.8 (C-2”), 123,2 (C-α), 130.6 (C-6’), 131.6 (C-3”), 131.91 (d, *J* = 8.6 Hz, C-2 and C-6), 132.60 (d, *J* = 3.2 Hz, C-1), 143.3 (C-β), 163.1 (C-2’), 164.9 (d, *J* = 249,2 Hz, C-4), 165.3 (C-4’), 192.9 (C-β’).

(*E*)-3-(4-chlorophenyl)-1-(2,4-dihydroxy-3-(3-methylbut-2-en-1-yl)phenyl)prop-2-en-1-one (IBC 11)

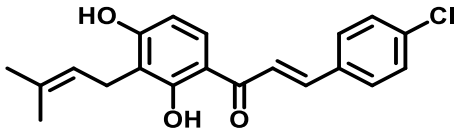

Yellow powder; yield 47%; overall yield: 11 %. HPLC purity: 99 %; m.p: 150–155ºC. ^{1}H NMR (600 MHz, acetone-d_6): δ 1.64 (s, H-5”), 1.78 (s, H-4”), 3.37 (d, *J* = 7.2 Hz, H-1”), 5.28 (t, *J* = 7.2 Hz, H-2”), 6.55 (d, *J* = 8.9 Hz, H-5’), 7.48 (d, *J* = 8.5 Hz, H-3 and H-5), 7.83 (d, *J* = 15.5 Hz, H-β), 7.87 (d, *J* = 8.5 Hz, H-2 and H-6), 7.96 (d, *J* = 15.5 Hz, H-β), 8.0 (d, *J* = 8.9 Hz, H-6’), 9.49 (brs, 4’-OH), 13.8 (brs, 4’-OH). ^{13}C NMR (150 MHz, acetone-d_6): 17.93 (C-5”), 22.28 (C-1”), 25.89 (C-4”), 108.3 (C-5’), 114.3 (C-1’), 116.2 (C-3’), 122.7 (C-2”), 123.2 (C-α), 129.9 (C-2 and C-6), 130.6 (C-6’), 131.1 (C-3 and C-5), 134.9 (C-1), 136.6 (C-4), 142.9 (C-β), 163.2 (C-2’), 165.3 (C-4’), 192.7 (C-β’).

(*E*)-3-(4-bromophenyl)-1-(2,4-dihydroxy-3-(3-methylbut-2-en-1-yl)phenyl)prop-2-en-1-one (IBC 12)

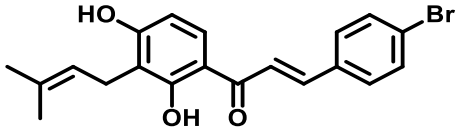

Yellow powder; yield 38%; overall yield: 1 %. HPLC purity: 97 %; m.p: 145–150ºC. ^{1}H NMR (600 MHz, acetone-d_6): δ 1.64 (s, H-5”), 1.78 (s, H-4”), 3.37 (d, *J* = 7.2 Hz, H-1”), 5.27 (t, *J* = 7.2 Hz, H-2”), 6.55 (d, *J* = 8.9 Hz, H-5’), 7.64 (d, *J* = 8.5 Hz, H-2 and H-6), 7.80 (d, *J* = 8.5 Hz, H-3 and H-5), 7.80 (d, *J* = 15.5 Hz, H-α), 7.98 (d, *J* = 15.5 Hz, H-β), 8.00 (d, *J* = 8.9 Hz, H-6’), 9.49 (brs, 4’-OH), 13.78 (s, 2’-OH). ^{13}C NMR (150 MHz, acetone-d_6): 17.95 (C-5”), 22.31 (C-1”), 25.92 (C-4”), 108.3 (C-5’), 114.4 (C-1’), 116.2 (C-4’), 122.8 (C-2”), 123.2 (C-α), 125.0 (C-1), 130.6 (C-6’), 131.4 (C-2 and C-6), 131.6 (C-3”), 135.3 (C-4), 143.7 (C-β), 163.2 (C-2’), 165.3 (C-4’), 192.8 (C-β).

(*E*)- 1- (2,4- dihydroxy- 3- (3- methylbut- 2- en- 1- yl)phenyl)- 3- (4- (trifluoromethyl)phenyl)prop-2-en-1-one (IBC 13)

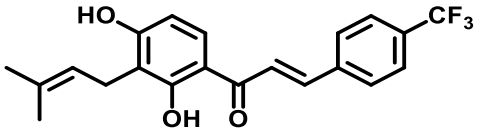

Yellow powder; yield 45%; overall yield: 2 %. HPLC purity: 99 %; m.p: 150–153ºC. ^{1}H NMR (600 MHz, acetone-d_6): δ 1.64 (s, H-5”), 1.78 (s, H-4”), 3.38 (d, *J* = 7.2 Hz, H-1”), 5.28 (t, *J* = 7.2 Hz, H-2”), 6.56 (d, *J* = 8.9 Hz, H-5’), 7.79 (d, *J* = 15.5 Hz, H-α), 8.02 (d, *J* = 8.9 Hz, H-6’), 8.06 (d, *J* = 8.1 Hz, H-2 and H-6), 8.07 (d, *J* = 8.1 Hz, H-3 and H-5), 7.67 (d, *J* = 15.9 Hz, H-β), 9.46 (brs, 4’-OH), 13.7 (s, 2’-OH). ^{13}C NMR (150 MHz, acetone-d_6): 17.97 (C-5”), 22.32 (C-1”), 25.93 (C-4”), 108.4 (C-5’), 114.4 (C-1’), 116.3 (C-4’), 123.2 (C-2”), 124.7 (C-α), 126.6 (q, *J* = 3.6 Hz, H-3 and H-5), 130.2 (C-2 and C-6), 130.8 (C-6’), 131.7 (C-3”), 139.9 (C-1), 142.5 (C-β), 163.4 (C-2’), 165.4 (C-4’), 192.7 (C-β’); $\delta_{4\text{-}CF3}$ not observed.

(*E*)-1-(2,4-dihydroxy-3-(3-methylbut-2-en-1-yl)phenyl)-3-(4-nitrophenyl)prop-2-en-1-one (IBC 14)

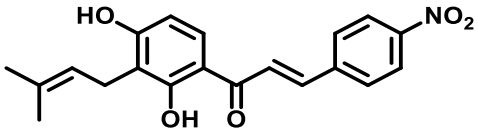

Yellow powder; yield 60%; overall yield: 8 %. HPLC purity: 99 %; m.p: 140–145ºC. ^{1}H NMR (600 MHz, acetone-d_6): δ 1.66 (s, H-5”), 1.80 (s, H-4”), 3.39 (d, *J* = 7.2 Hz, H-1”), 5.29 (t, *J* = 7.2 Hz, H-2”), 6.58 (d, *J* = 8.9 Hz, H-5’), 7.93 (d, *J* = 15.5 Hz, H-α), 8.05 (d, *J* = 8.9 Hz, H-6’), 8.14 (d, *J* = 8.7 Hz, H-2 and H-6), 8.15 (d, *J* = 15.5 Hz, H-β), 8.32 (d, *J* = 8.7 Hz, H-3 and H-5), 9.58 (brs, 4’-OH), 13.7 (s, 2’-OH). ^{13}C NMR (150 MHz, acetone-d_6,): 17.98 (C-5”), 22.31 (C-1”), 25.94 (C-4”), 108.5 (C-5’), 114.4 (C-1’), 116.3 (C-3’), 123.1 (C-2”), 124.8 (C-2 and C-

6), 126.1 (C-α), 130.5 (C-3 and C-5), 130.9 (C-6'), 131.8 (C-3"), 141.6 (C-β), 142.3 (C-1), 149.5 (C-4), 163.5 (C-2'), 165.4 (C-4'), 192.4 (C-β').

(*E*)-1-(2,4-dihydroxy-3-(3-methylbut-2-en-1-yl)phenyl)-3-(pyridin-3-yl)prop-2-en-1-one (IBC 15)

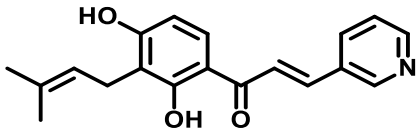

Yellow powder; yield 65%; overall yield: 5 %. HPLC purity: 99 %; m.p: 181–185ºC. ^{1}H NMR (600 MHz, DMSO-d_6): δ 1.62 (s, H-5"), 1.72 (s, 4"), 3.24 (d, *J* = 7.2 Hz, H-1"), 5.18 (t, *J* = 7.2 Hz, H-2"), 6.51 (d, *J* = 8.9 Hz, H-5'), 7.49 (dd, *J* = 4.8 and 7.9 Hz, H-5), 7.82 (d, *J* = 15.6 Hz, H-α), 8.09 (d, *J* = 8.9 Hz, H-6'), 8.10 (d, *J* = 15.6 Hz, H-β), 8.35 (d, *J* = 7.9 Hz, H-4), 8.61 (d, *J* = 4.8 Hz, H-6), 9.02 (s, H-2), 13.7 (s, 2'-OH); $\delta_{4'\text{-OH}}$; not observed. ^{13}C NMR (150 MHz, DMSO-d_6,): 17.73 (C-5"), 21.3 (C-1"), 25.51 (C-4"), 107.6 (C-5'), 112.7 (C-1'), 114.6 (C-3'), 122.3 (C-α),123.2 (C-2"), 123.9 (C-5), 130.3 (C-3), 130.5 (C-3"), 130.6 (C-6'), 135.2 (C-4), 140.1 (C-β), 150.4 (C-2), 151.0 (C-6), 162.9 (C-2'), 163.7 (C-4'), 191.4 (C-β').

(*E*)-1-(2,4-dihydroxy-3-(3-methylbut-2-en-1-yl)phenyl)-3-(pyridin-4-yl)prop-2-en-1-one (IBC 16)

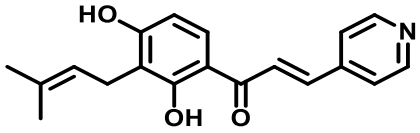

Yellow powder; yield 35%; overall yield: 2 %. HPLC purity: 99 %; m.p: 145–147ºC. ^{1}H NMR (600 MHz, DMSO-d_6): δ 1.62 (s, H-5"), 1.72 (s, 4"), 3.24 (d, *J* = 7.2 Hz, H-1"), 5.17 (t, *J* = 7.2 Hz, H-2"), 6.51 (d, *J* = 8.9 Hz, H-5'), 7.73 (d, *J* = 15.5 Hz, H-α), 7.84 (d, *J* = 5.6 Hz, H-3 and H-5), 8.09 (d, *J* = 9.0 Hz, H-6'), 8.42 (brs, 4'-OH), 8.18 (d, *J* = 15.5 Hz, H-β), 8.67 (d, *J* = 5.6 Hz, H-2 and H-6), 13.6 (s, 2'-OH). ^{13}C NMR (150 MHz, DMSO-d_6): 17.73 (C-5"), 21.3 (C-1"), 25.50 (C-4"), 107.8 (C-5'), 112.7 (C-1'), 114.6 (C-3'), 122.2 (C-3 and C-5), 122.6 (C-2"), 125.7 (C-α), 130.5 (C-3"), 130.7 (C-6"), 140.6 (C-β), 141.7 (C-1), 150.4 (C-2 and C-5), 163.2 (C-2'), 163.8 (C-4'), 191.3 (C-β').

(*E*)-1-(2,4-dihydroxy-3-(3-methylbut-2-en-1-yl)phenyl)-3-(furan-2-yl)prop-2-en-1-one (IBC 17)

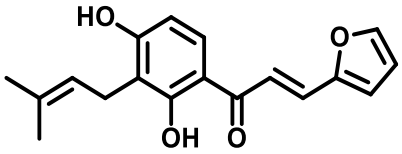

Yellow powder; yield 65%; overall yield: 22%. HPLC purity: 99 %; m.p: 165–160ºC. ^{1}H NMR (600 MHz, acetone-d_6,): δ 1.63 (s, H-5”), 1.77 (s, H-4”), 3.36 (d, *J* = 7.3 Hz, H-1”), 5.27 (t, *J* = 7.3 Hz, H-2”), 6.56 (d, *J* = 8.9 Hz, H-5’), 6.65 (dd, *J* = 1.8 and 3.4 Hz, H-4), 7.01 (d, *J* = 3.4 Hz, H-3), 7.60 (d, *J* = 15.6 Hz, H-α), 7.68 (d, *J* = 15.6 Hz, H-β), 7.78 (d, *J* = 1.8 Hz, H-5), 7.88 (d, *J* =8.9 Hz, H-6’), 9.53 (brs, 4’-OH), 13.8 (2’-OH). ^{13}C NMR (150 MHz, acetone-d_6,): 17.96 (C-5”), 22.31 (C-1”), 25.93 (C-4”), 108.3 (C-5’), 113.8 (C-3), 114.3 (C-1’), 116.3 (C-3’), 117.4 (C-4), 118.9 (C-α), 123.2 (C-2”), 130.2 (C-5), 130.8 (C-6’), 131.6 (C-3”), 146.6 (C-β), 152.7 (C-2), 163.0 (C-2’), 165.2 (C-4’), 192.4 (C-β’).

(*E*)-1-(2,4-dihydroxy-3-(3-methylbut-2-en-1-yl)phenyl)-3-(thiophen-2-yl)prop-2-en-1-one (IBC 18)

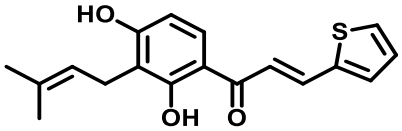

Yellow powder; yield 60%, overall yield: 15 %. HPLC purity: 99 %; m.p: 180–185ºC.^{1}H NMR (600 MHz, acetone-d_6): δ 1.64 (s, H-5”), 1.78 (s, H-4”), 3.37 (d, *J* = 7.2 Hz, H-1”), 5.27 (t, *J* = 7.0 Hz, H-2”), 6.55 (d, *J* = 8.9 Hz, H-5’), 7.19 (dd, *J* = 3.6 and 5.0 Hz, H-4), 7.62 (d, *J* = 15.1 Hz, H-α), 7.62 (d, *J* = 3.6 Hz, H-3), 7.70 (d, *J* = 5.0 Hz, H-5), 7.91 (d, *J* = 8.9 Hz, H-6’), 8.03 (d, *J* = 15.1 Hz, H-β), 9.49 (brs, 4’-OH), 13.8 (s, 2’-OH). ^{13}C NMR (150 MHz, acetone-d_6,): 17.83 (C-5”), 22.29 (C-1”), 25.89 (C-4”), 108.2 (C-5’), 114.2 (C-1’), 116.2 (C-3’), 120.3 (C-α), 123.2 (C-2”), 129.4 (C-3), 130.3 (C-4), 130.6 (C-6’), 131.6 (C-3”), 133.3 (C-5), 137.1 (C-β), 141.2 (C-2), 163.1 (C-2’), 165.2 (C-4’), 192.4 (C-β’).

(*E*)-1-(2,4-dihydroxy-3-(3-methylbut-2-en-1-yl)phenyl)-3-(naphthalen-1-yl)prop-2-en-1-one (IBC 19)

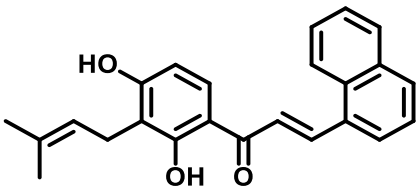

Yellow powder; yield 30%, overall yield: 10 %. HPLC purity: 98 %; m.p: 185–190ºC. ^{1}H NMR (600 MHz, acetone-d_6, 600 MHz): δ 1.65 (s, H-5”), 1.79 (s, H-4”), 3.40 (d, *J* = 7.3 Hz, H-1”),

5.30 (t, *J* = 7.3 Hz, H-2”), 6.58 (d, *J* = 8.8 Hz, H-5’), 7.60 (dd, *J* = 7.6 and 7.7 Hz, H-3), 7.61 (ddd, *J* = 1.8, 7.0 and 8.0 Hz, H-7), 7.68 (ddd, *J* = 1.3, 7.0 and 8.5 Hz, H-6), 8.00 (dd, *J* = 1.8 and 8.5 Hz, H-5), 8.01 (d, *J* = 15.2 Hz, H-α), 8.04 (dd, *J* = 7.7 and 1.9 Hz, H-2), 8.06 (d, *J* = 8.8 Hz, H-6’), 8.16 (dd, *J* = 1.9 and 7.6 Hz, H-4), 8.36 (dd, *J* = 1,3 and 8.5 Hz, H-8), 8.74 (d, *J* = 15.2 Hz, H-β), 9.54 (brs, 2’-OH), 13.89 (s, 2’-OH). ^{13}C NMR (150 MHz, acetone-d_6): 17.95 (C-5”), 22.31 (C-1”), 25.91 (C-4”), 108.3 (C-5’), 114.4 (C-1’), 116.3 (C-4’), 123.2 (C-2”), 124.1 (C-α), 124.4 (C-3), 126.4 (C-8), 126.5 (C-7), 127.2 (C-2), 128.0 (C-6), 129.7 (C-4), 130.7 (C-6’), 130.7 (C-5), 131.6 (C-3”), 131.7 (C-5), 132.7 (C-10), 132.9 (C-9), 134.8 (C-1), 140.8 (C-β), 163.2 (C-2’), 165.3 (C-4’), 192.8 (C-β’).

(*E*)-1-(2,4-dihydroxy-3-(3-methylbut-2-en-1-yl)phenyl)-3-(naphthalen-2-yl)prop-2-en-1-one (IBC 20)

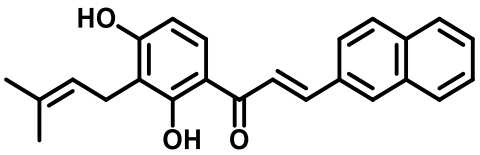

Yellow powder; yield 30%, overall yield: 12 %; HPLC purity: 99 %; m.p: 155–158ºC. ^{1}H NMR (600 MHz, acetone-d_6, 600 MHz): δ 1.65 (s, H-5”), 1.79 (s, H-4”), 3.39 (d, *J* = 7.3 Hz, H-1”), 5.29 (t, *J* = 7.3 Hz, H-2”), 6.57 (d, *J* = 8.7 Hz, H-5’), 7.56–7.59 (m, H-6 and H-7), 7.93–8.00 (m, H-3 and H-4), 7.97 (d, *J* = 8.8 Hz, H-6’), 8.05 (d, *J* = 15.5 Hz, H-α), 8.09 (d, *J* = 15.9 Hz, H-β), 8.05–8.10 (m, H-5 and 8), 8.29 (s, H-1), ^{13}C NMR (150 MHz, acetone-d_6): 17.99 (C-5”), 22.35 (C-1”), 25.94 (C-4”), 108.3 (C-5’), 114.5 (C-1’), 116.3 (C-3’), 122.1 (C-α), 123.3 (C-2”), 125.1 (C-3), 127.7 (C-7), 128.3 (C-6), 128.7 (C-4), 129.5 (C-1), 129.6 (C-5), 130.6 (C-6’), 131.6 (C-3”), 131.7 (C-8), 133.6 (C-2), 134.5 (C-10), 135.4 (C-9), 144.6 (C-β), 163.1 (C-2’), 165.3 (C-4’), 192.9 (C-β’).

(*E*)-1-(2,4-dihydroxyphenyl)-3-(4-hydroxyphenyl)prop-2-en-1-one (IBC 21)

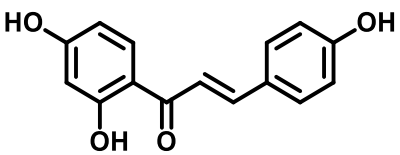

Orange powder; yield 75 %, overall yield: 20%. HPLC purity: 99 %; m.p. literature: 197–198 ºC (SUGAMOTO et al., 2011), m.p. found: 175–180 ºC.^{1}H NMR (600 MHz, DMSO-d_6) according to literature (SUGAMOTO et al., 2011): δ 6.28 (d, *J* = 2.3 Hz, H-3’), 6.40 (dd, *J* =

2.3 and 8.9 Hz, H-5'), 6.84 (d, *J* = 8.6 Hz, H-3 and H-5), 7.73 (d, *J* = 15.3 Hz, H-α), 7.75 (d, *J* = 8.6 Hz, H-2 and H-6), 7.76 (d, *J* = 15.3 Hz, H-β), 8.16 (d, *J* = 8.9 Hz, H-6'), 10.1 (brs, 4-OH), 10.7 (brs, 4'-OH), 13.6 (s, 2'-OH). ^{13}C NMR (DMSO-d_6): 102.6 (C-3'), 108.1 (C-5'), 113.0 (C-1'), 115.9 (C-3 and C-5), 117.4 (C-α), 125.8 (C-1), 132.9 (C-6'), 131.3 (C-2 and C-6), 160.3 (C-4), 165.0 (C-2'), 165.8 (C-4'), 191.6 (C-β').

(*E*)- 1- (3- ((*E*)- 3,7 - dimethylocta- 2,6- dien- 1- yl)- 2,4- dihydroxyphenyl)- 3- (4- hydroxyphenyl)prop-2-en-1-one (IBC 22)

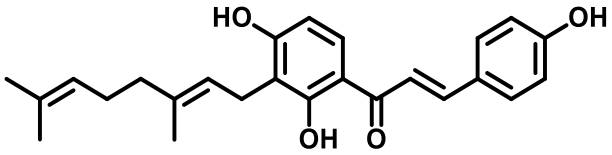

Yellow powder; yield 65%; overall yield: 19%. HPLC purity: 99 %; m.p.: 100–105 ºC, m.p. lit: 122.7–123.7 ºC (SUGAMOTO et al., 2011). ^{1}H NMR (600 MHz, acetone-d_6) according to literature (SUGAMOTO et al., 2011): δ 1.54 (s, H-9"), 1.60 (H-10"), 1.80 (s, H-8"), 1.96 (t, *J* = 7.6 Hz, H-4"), 2.03–2.07 (m, H-5"), 3.39 (d, *J* = 7.2 Hz, H-1"), 5.07 (t, *J* = 7.1 Hz, H-6"), 6.53 (d, *J* = 8.8 Hz, H-5'), 6.93 (d, *J* = 8.6 Hz, H-3 and H-5), 7.73 (d, *J* = 8.8 Hz, H-2 and H-6), 7.75 (d, *J* = 15.4 Hz, H-α), 7.84 (d, *J* = 15.4 Hz, H-β), 7.97 (d, *J* = 8.8 Hz, H-6'), 9.18 (brs, 4'-OH), 14.0 (s, 2'-OH). ^{13}C NMR (150 MHz, acetone-d_6): 16.30 (C-9"), 17.70 (C-10"), 22.24 (C-1"), 25.81 (C-8"), 27.41 (C-5"), 40.54 (C-4"), 108.0 (C-5'), 114.4 (C-1'), 116.2 (C-3'), 116.8 (C-3 and C-5), 118.5 (C-α), 123.3 (C-2"), 125.2 (C-6"), 127.6 (C-1), 130.3 (C-6'), 131.6 (C-7"), 131.7 (C-2 and C-6), 135.2 (C-3"), 144.9 (C-β), 161.0 (C-4), 162.8 (C-4'), 165.3 (C-2'), 193.0 (C-β').

(*E*)-1-(4-hydroxy-3-(3-methylbut-2-en-1-yl)phenyl)-3-(4-hydroxyphenyl)prop-2-en-1-one (IBC 23)

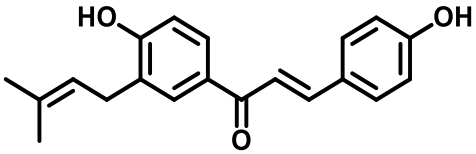

Yellow powder; yield 65%; overall yield: 23%. HPLC purity: 99 %; m.p.: 115–118 ºC, m.p. lit 75.1 ºC. ^{1}H NMR (600 MHz, acetone-d_6) according to literature (YEONG-HO LEE, 2020): δ 1.73 (s, H-5"), 1.74 (s, H-4"), 3.39 (d, *J* = 7.3 Hz, H-1"), 5.38 (t, *J* = 7.3 Hz, H-2"), 6.91 (d, *J* = 8.6 Hz, H-3 e H-5), 6.36 (d, *J* = 8.4 Hz, H-5'), 7.65 (d, *J* = 15.5 Hz, H-α), 7.66 (d, *J* = 8.6 Hz,

H-2 e H-6), 7.69 (d, *J* = 15.5 Hz, H-β), 7.90 (dd, *J* = 2.3 e 8.4 Hz, H-6'), 7.94 (d, *J* = 2.3 Hz, H-2'), 8.99 (sl, 4-OH), 9.21 (sl, 4'-OH). ^{13}C NMR (150 MHz, acetone-d_6): δ 17.90 (C-5"), 25.90 (C-1"), 29.10 (C-4"), 115.5 (C-5'), 116.7 (C-3 and C-5), 119.9 (C-α), 123.3 (C-2"), 127.9 (C-3'), 129.1 (C-1), 129.2 (C-2'), 131.2 (C-2 and C-6), 131.4 (C-6'), 131.6 (C-1'), 132.9 (C-3"), 143.8 (C-β), 160.2 (C-4), 160.5 (C-4'), 188.2 (C-β').

1-(2,4-dihydroxy-3-(3-methylbut-2-en-1-yl)phenyl)-3-(4-hydroxyphenyl)propan-1-one (DH-IBC)

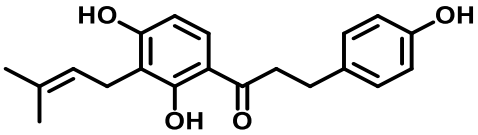

White powder; yield: 50 %; overall yield: 12 %; m.p.: 118–120ºC. ^{1}H NMR (600 MHz, acetone-d_6): δ 1.63 (s, H-5"), 1.76 (s, H-4"), 2.92 (d, *J* = 7.7 Hz, H-β), 3.23 (t, *J* = 7.7 Hz, H-α), 3.33 (d, *J* = 7.2 Hz, H-1"), 5.25 (t, *J* = 7.2 Hz, H-2"), 6.49 (d, *J* = 8.8 Hz, H-5'), 6.75 (d, *J* = 8.5 Hz, H-3 and H-5), 7.11 (d, *J* = 8.5 Hz, H-2 and H-6), 7.68 (d, *J* = 8.8 Hz, H-6'), 13.2 (s, 2'-OH). ^{13}C NMR (150 MHz, acetone-d_6): δ 17.86 (C-4"), 22.17 (C-1"), 25.87 (C-5"), 30.26 (C-β'), 40.50 (C-α), 103.3 (C-5'), 114.7 (C-1'), 116.1 (C-3 and C-5), 117.4 (C-3'), 123.1 (C-2"), 131.1 (C-6'), 130.2 (C-2 and C-6), 131.6 (C-1), 132.7 (C-3"), 156.6 (C-4), 162.5 (C-2'), 164.1 (C-4'), 205.8 (C-β').

Figure S1. ^{1}H NMR spectrum of **A.2** (DMSO-d_6; 600 MHz)

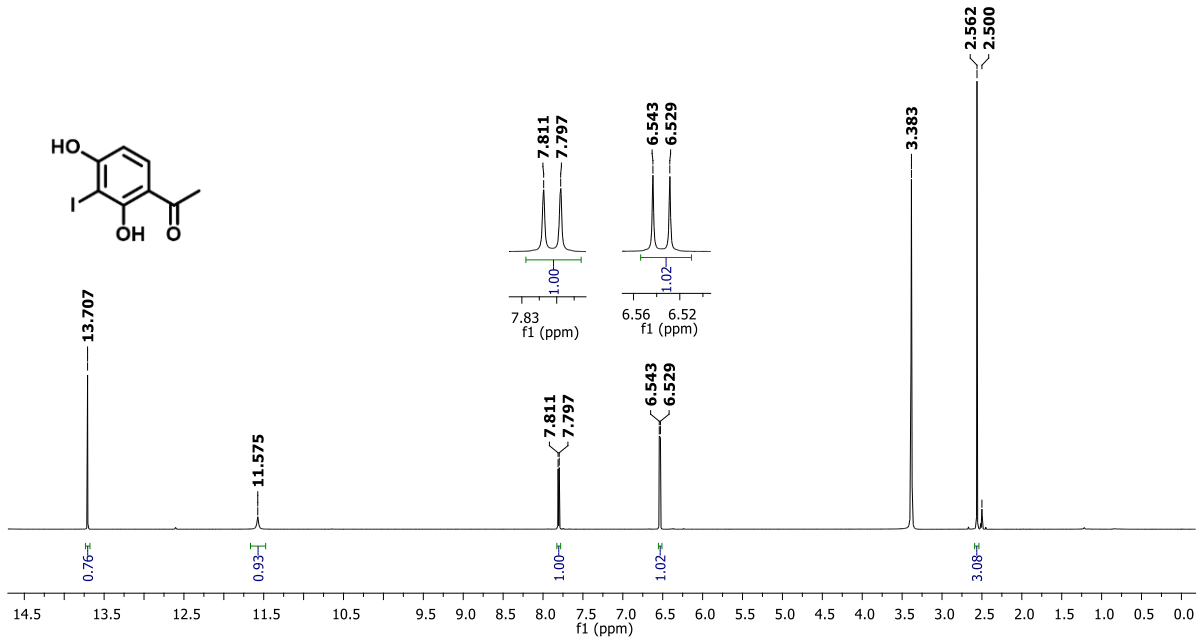

Figure S2. ^{1}H NMR spectrum of **A.4** (acetone-d_6; 600 MHz)

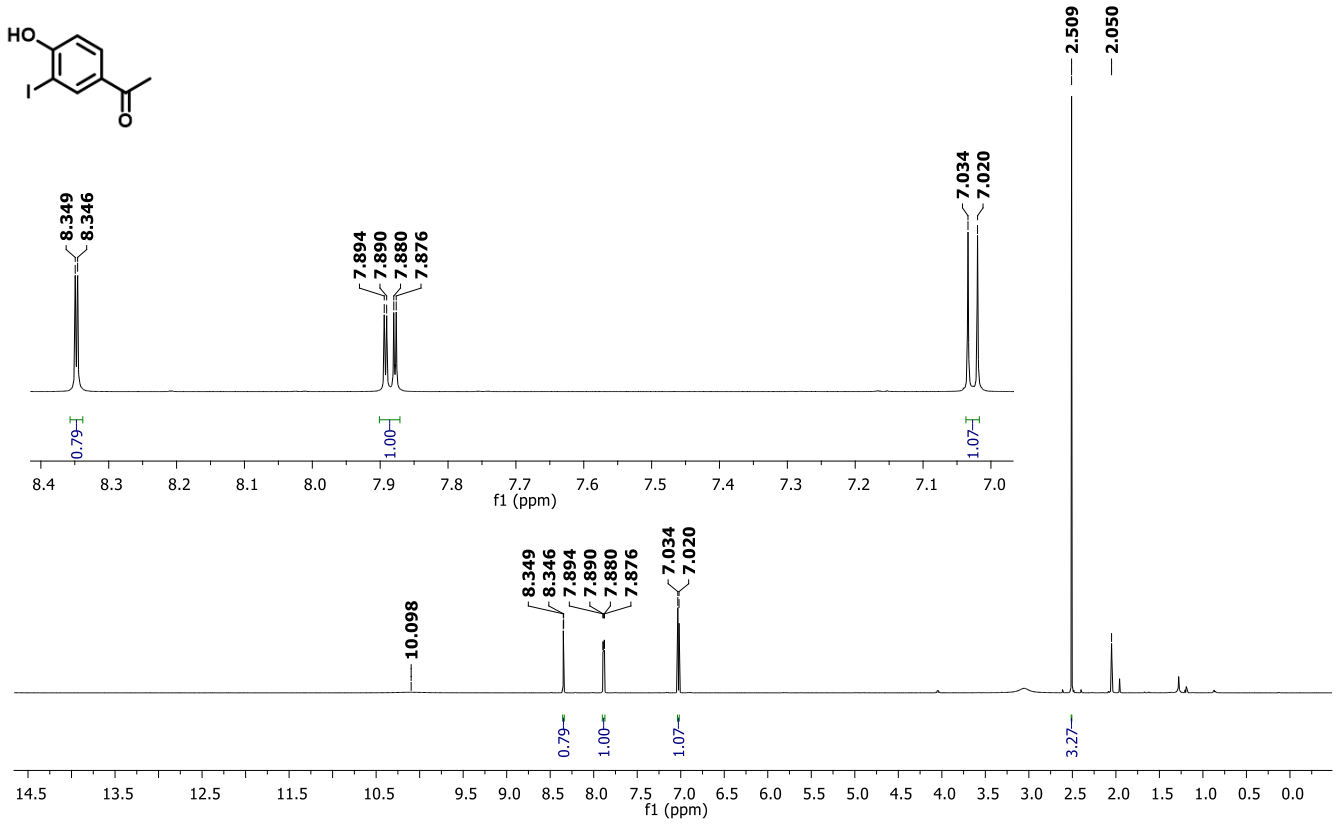

Figure S3. ^{1}H NMR spectrum of **A.5** ($CDCl_3$; 600 MHz)

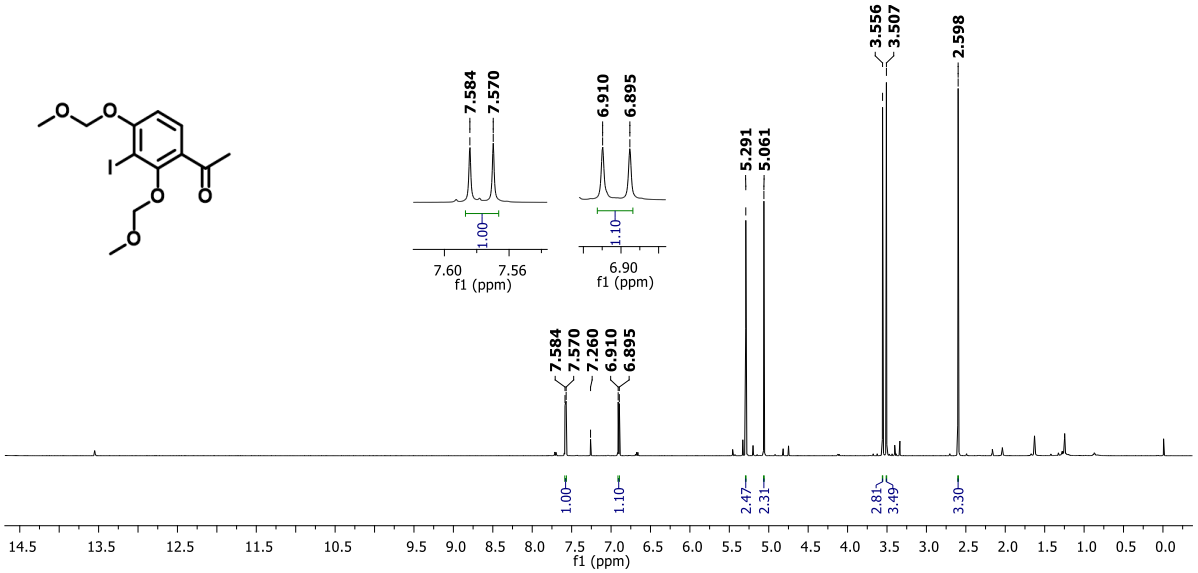

Figure S4. ^{1}H NMR spectrum of **A.6** ($CDCl_3$; 600 MHz)

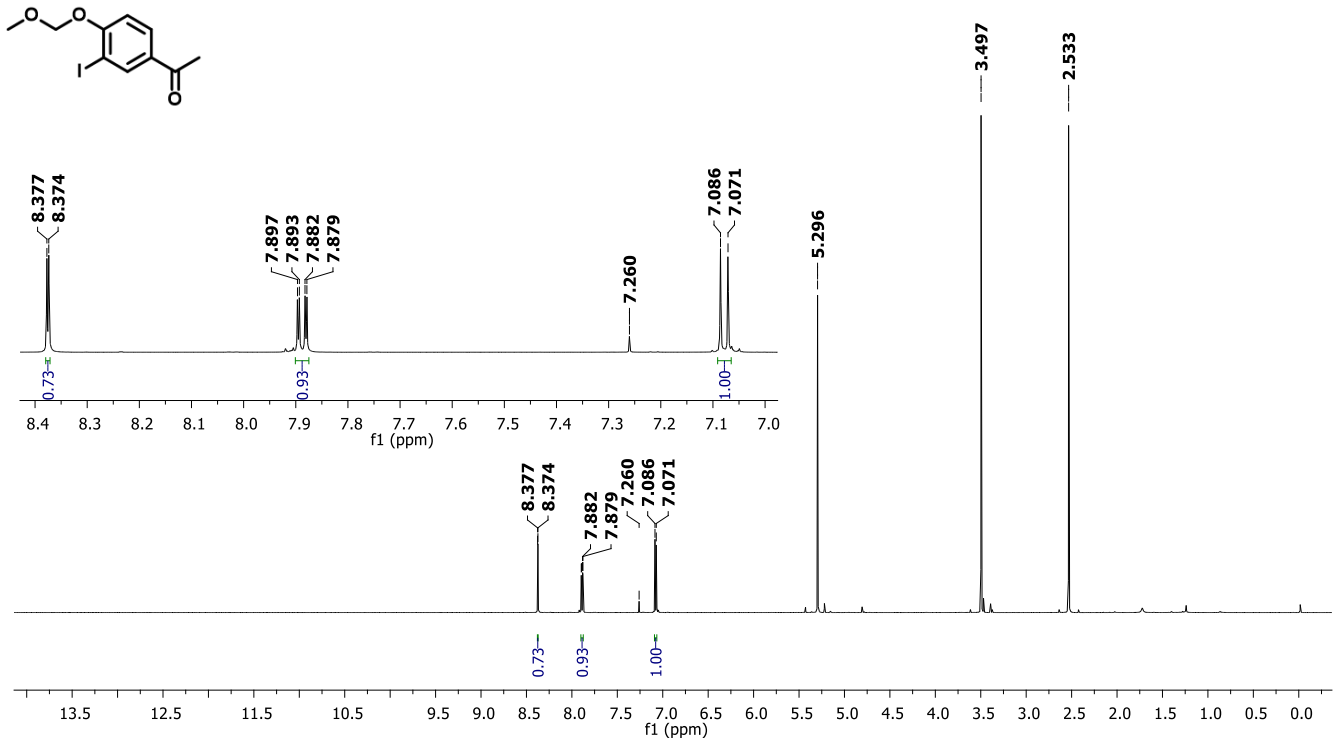

Figure S5. ^{1}H NMR spectrum of **C.1** ($CDCl_3$; 600 MHz)

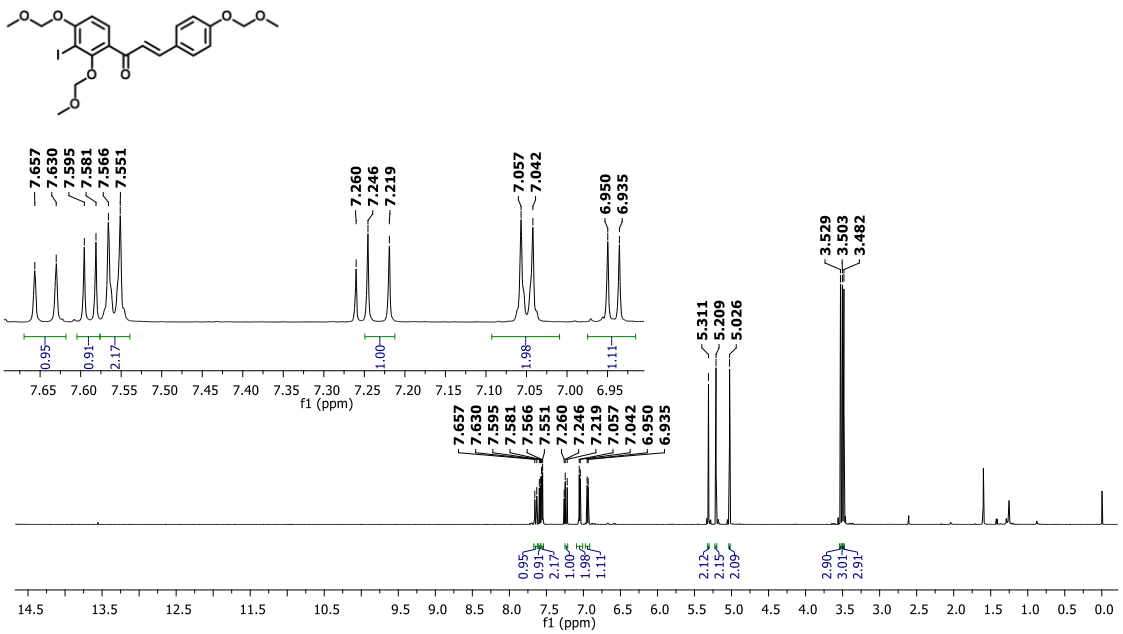

Figure S6. ^{1}H NMR spectrum of **C.2** ($CDCl_3$; 600 MHz)

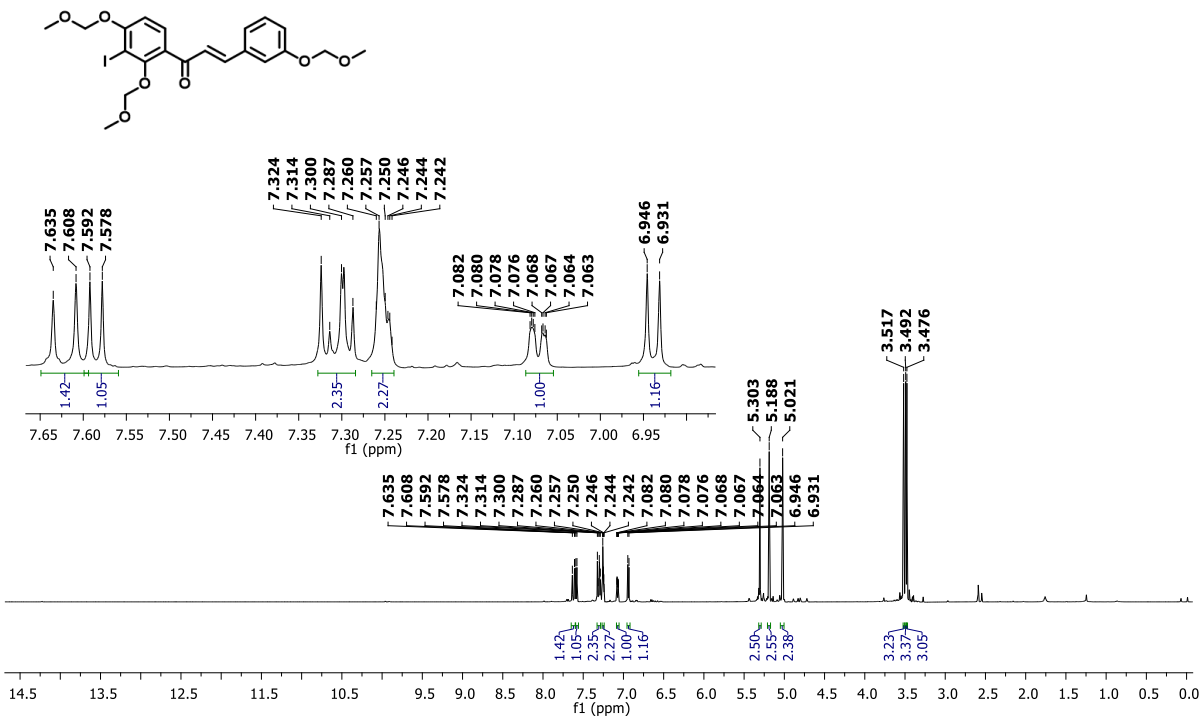

Figure S7. ^{1}H NMR spectrum of **C.3** ($CDCl_3$; 600 MHz)

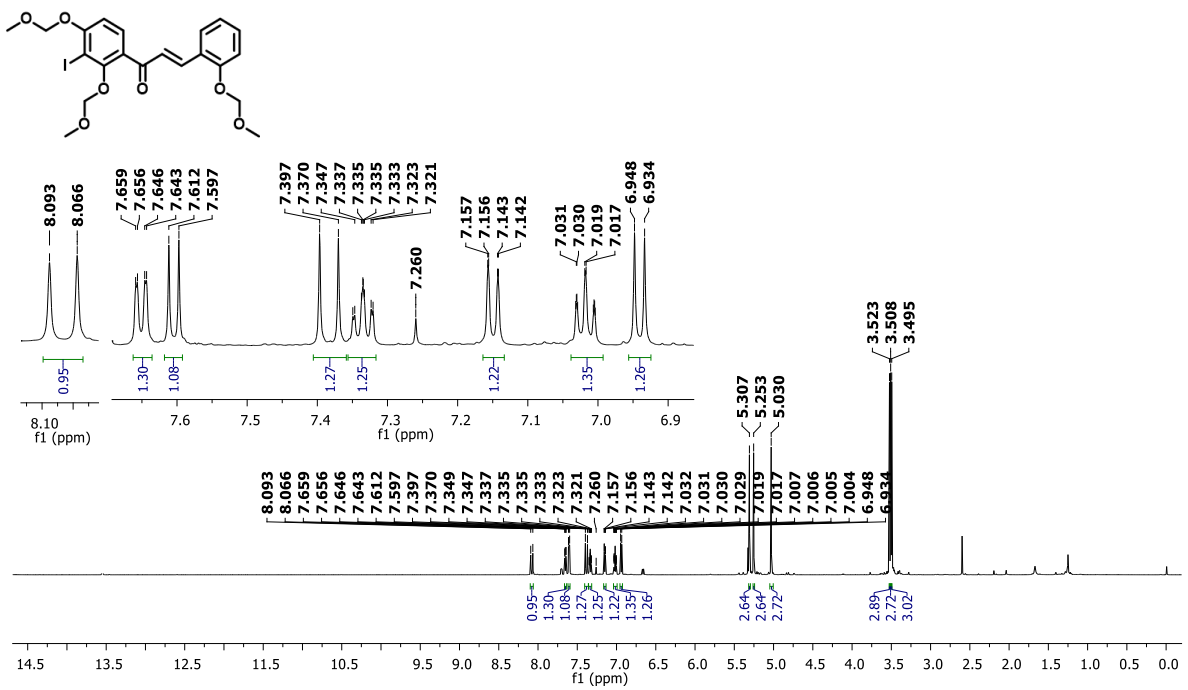

Figure S8. ^{1}H NMR spectrum of **C.4** ($CDCl_3$; 600 MHz)

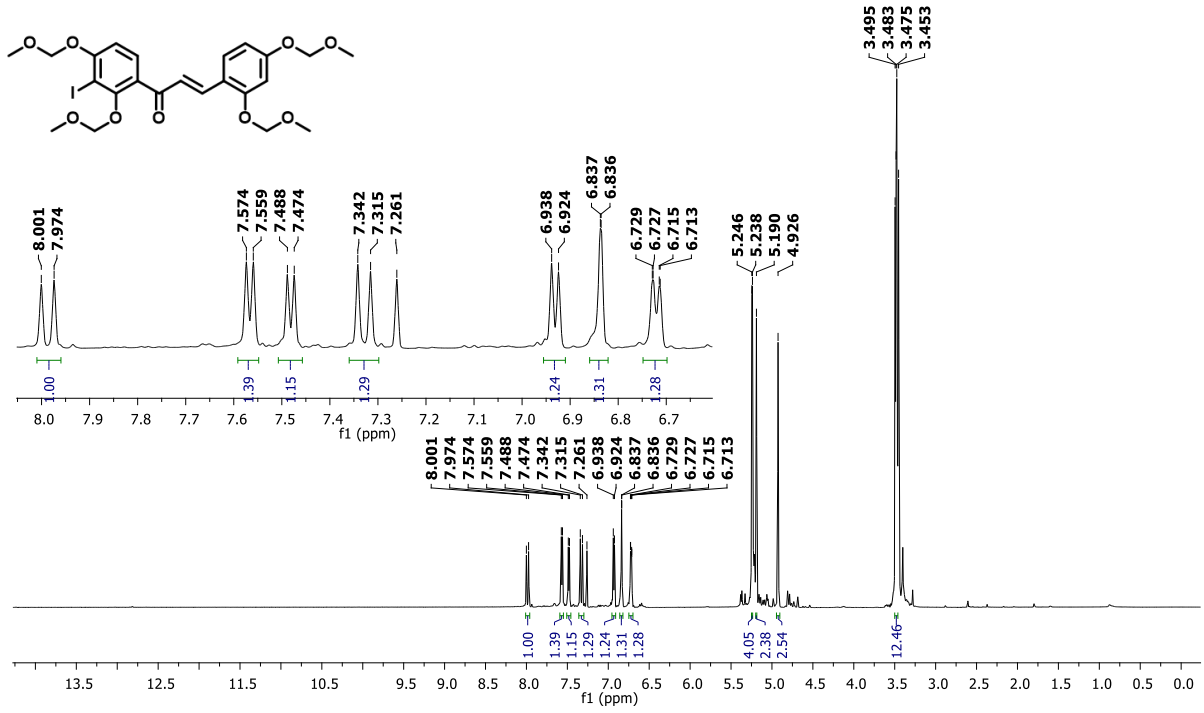

Figure S9. ^{1}H NMR spectrum of **C.5** ($CDCl_3$; 600 MHz)

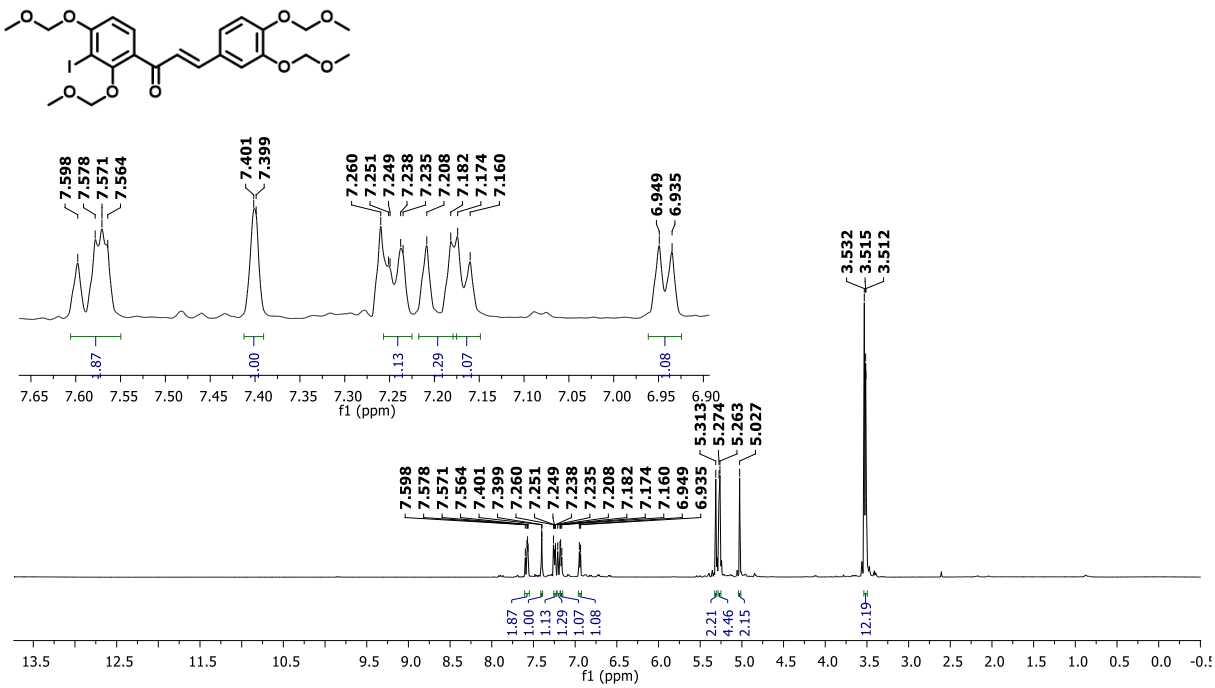

Figure S10. ^{1}H NMR spectrum of **C.6** ($CDCl_3$; 600 MHz)

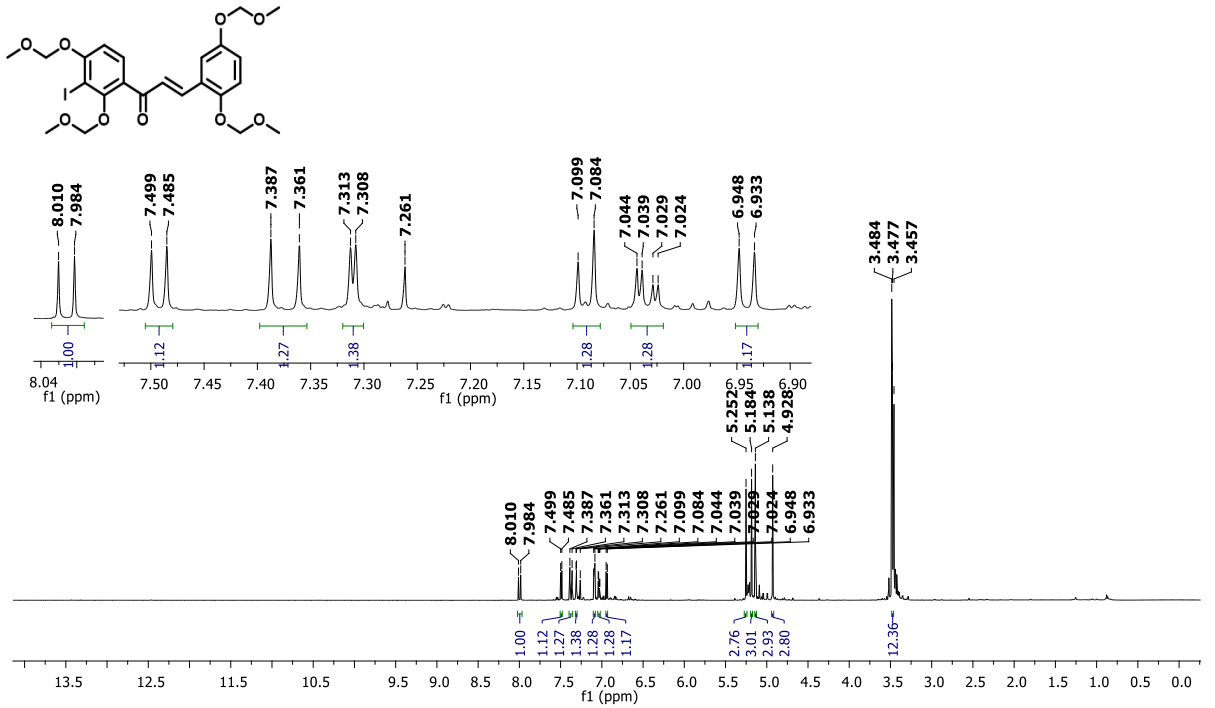

Figure S11. ^{1}H NMR spectrum of **C.7** ($CDCl_3$; 600 MHz)

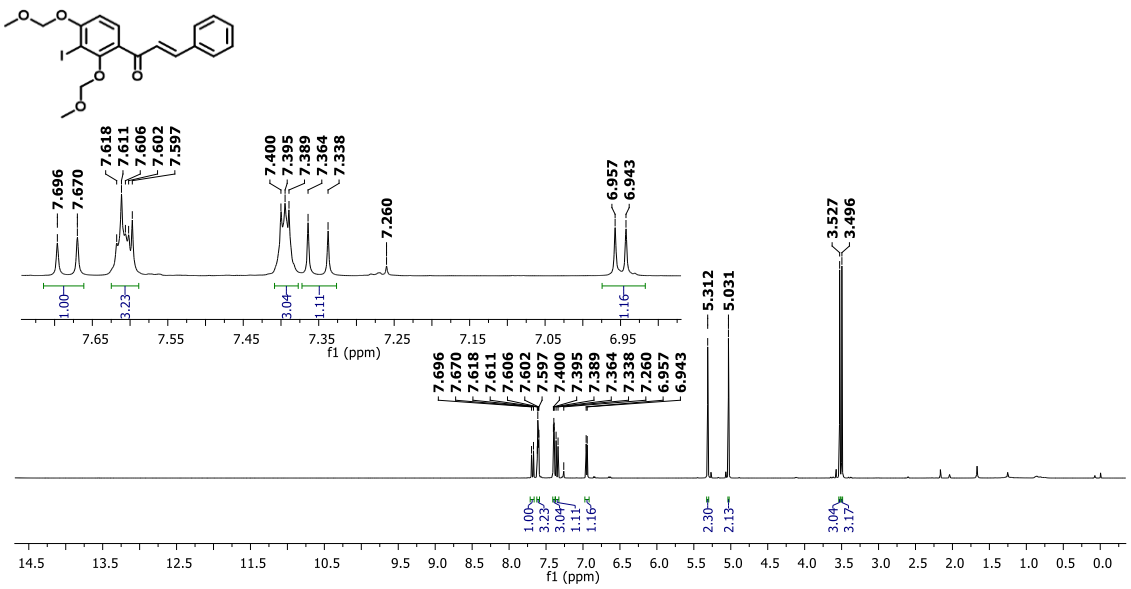

Figure S12. ^{1}H NMR spectrum of **C.8** ($CDCl_3$; 600 MHz)

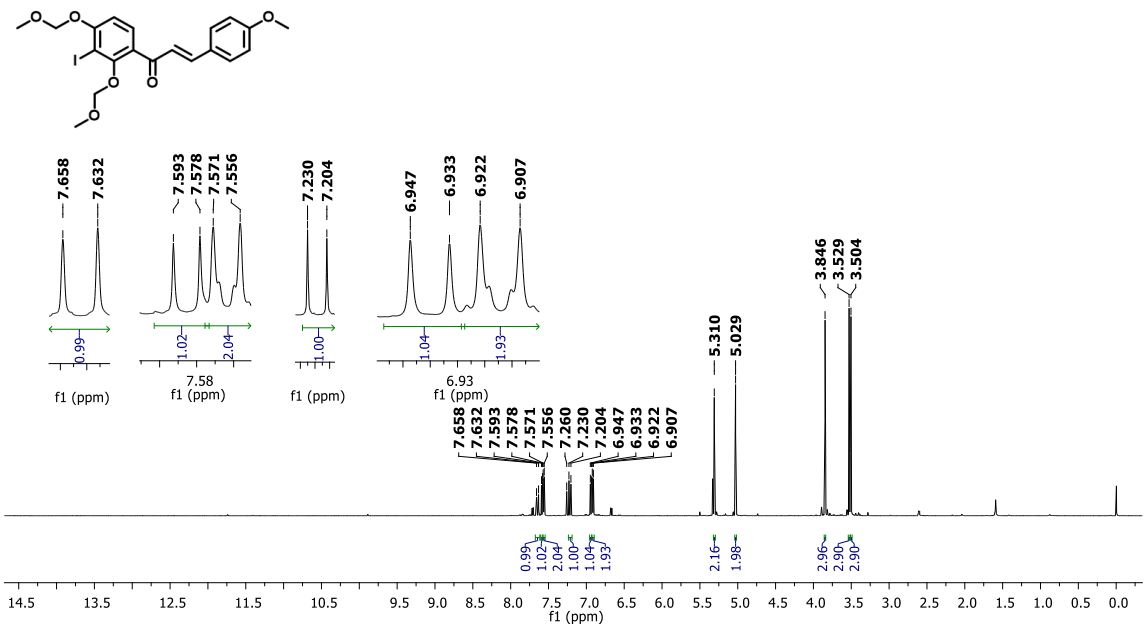

Figure S13. ^{1}H NMR spectrum of **C.9** ($CDCl_3$; 600 MHz)

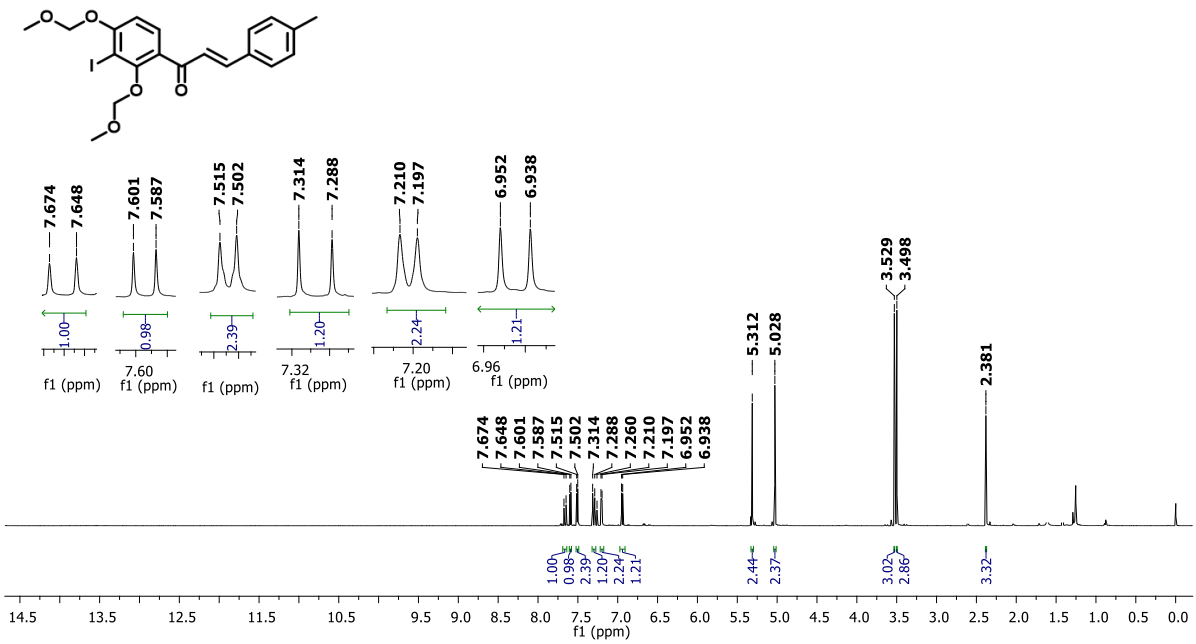

Figure S14. ^{1}H NMR spectrum of **C.10** ($CDCl_3$; 600 MHz)

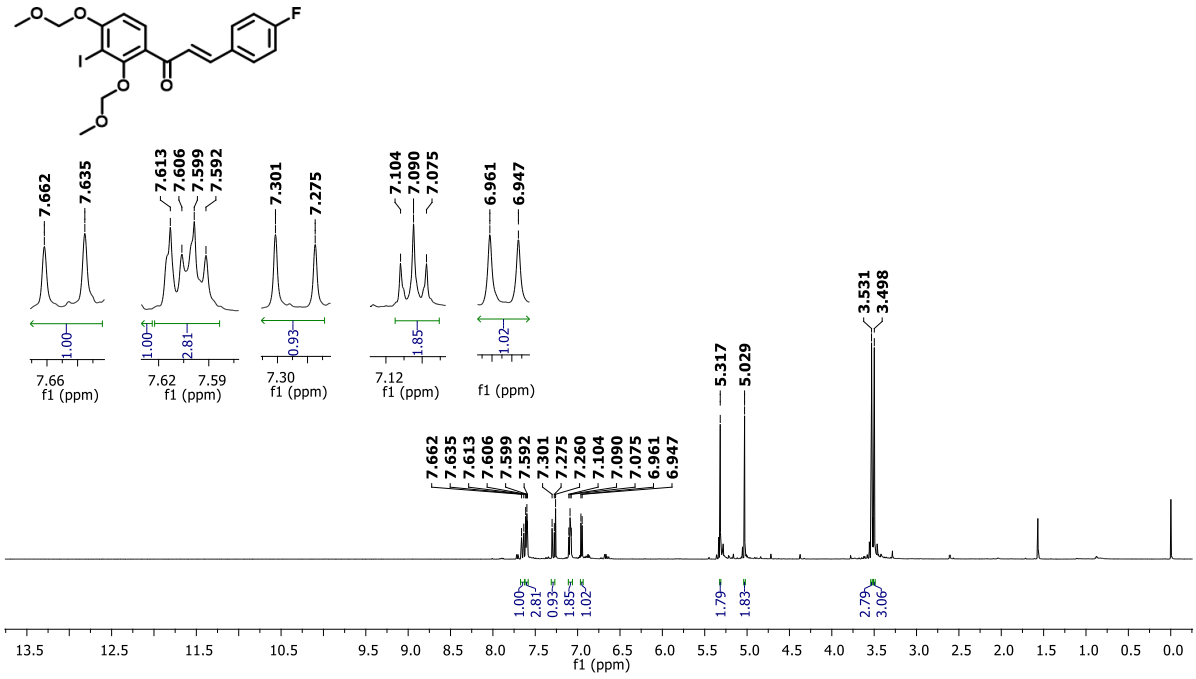

Figure S15. ^{1}H NMR spectrum of **C.11** ($CDCl_3$; 600 MHz)

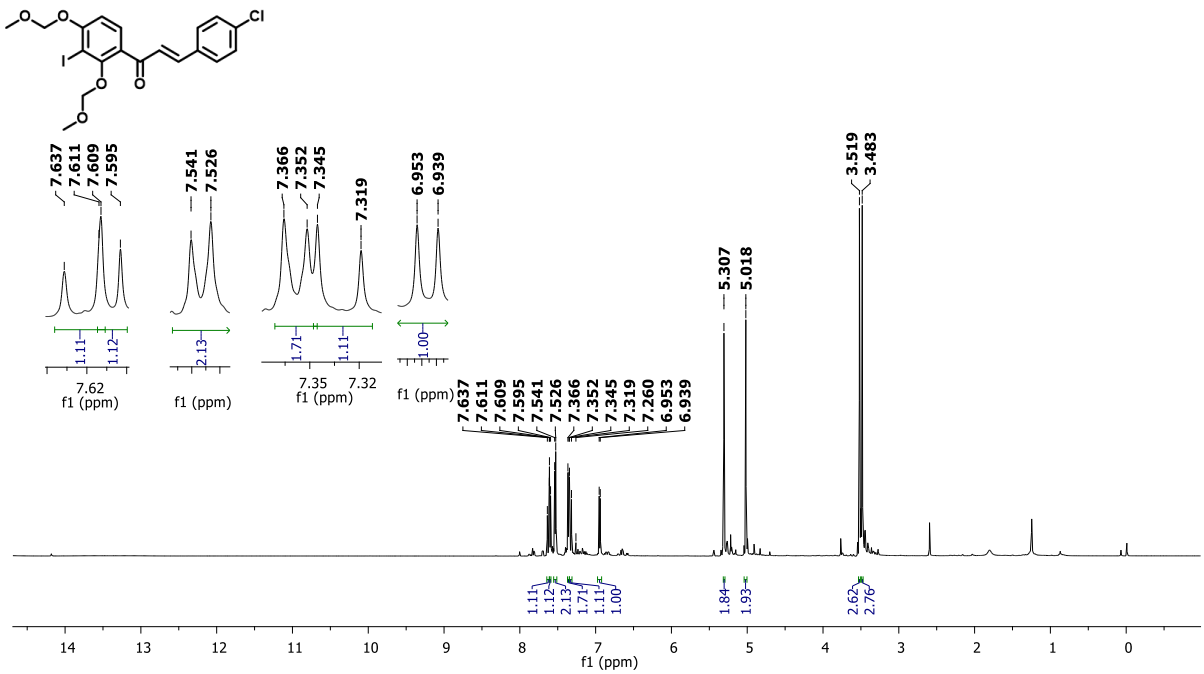

Figure S16. ^{1}H NMR spectrum of **C.12** ($CDCl_3$; 600 MHz)

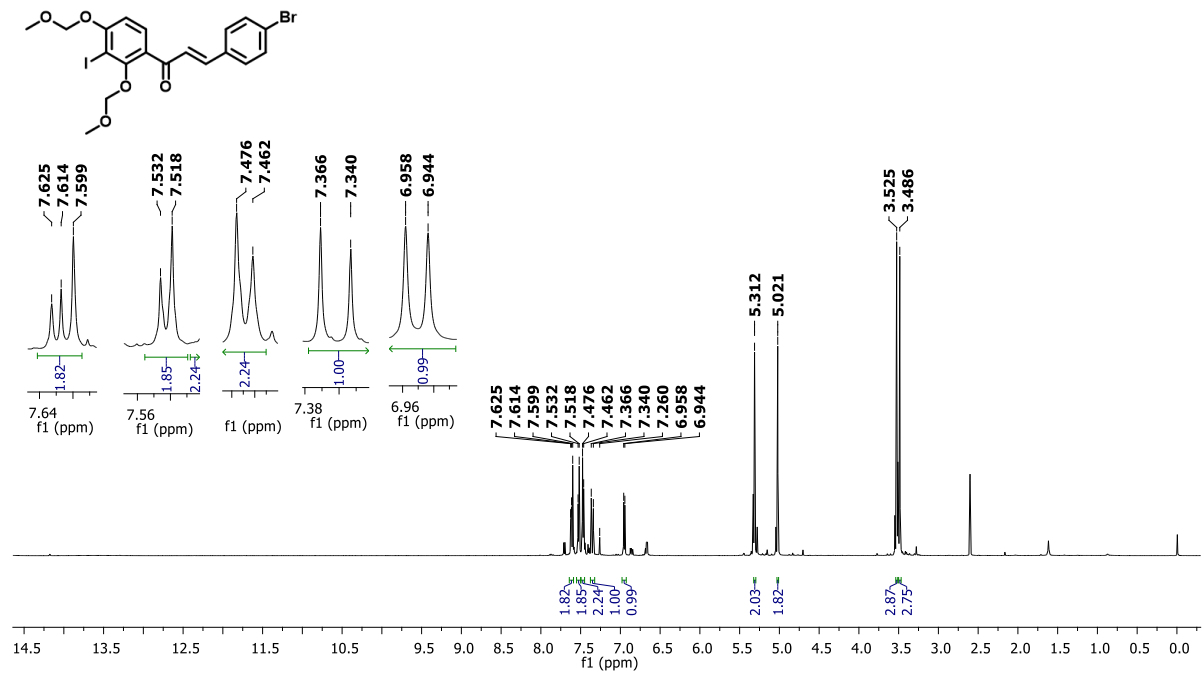

Figure S17. ^{1}H NMR spectrum of **C.13** ($CDCl_3$; 600 MHz)

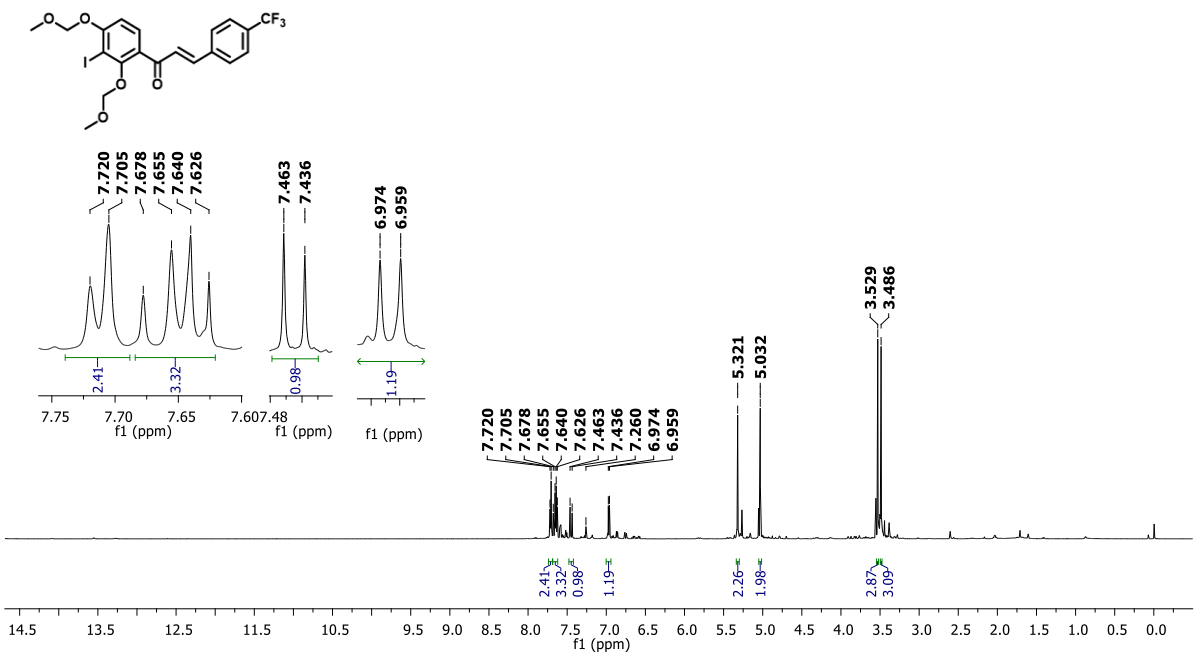

Figure S18. ^{1}H NMR spectrum of **C.14** ($CDCl_3$; 600 MHz)

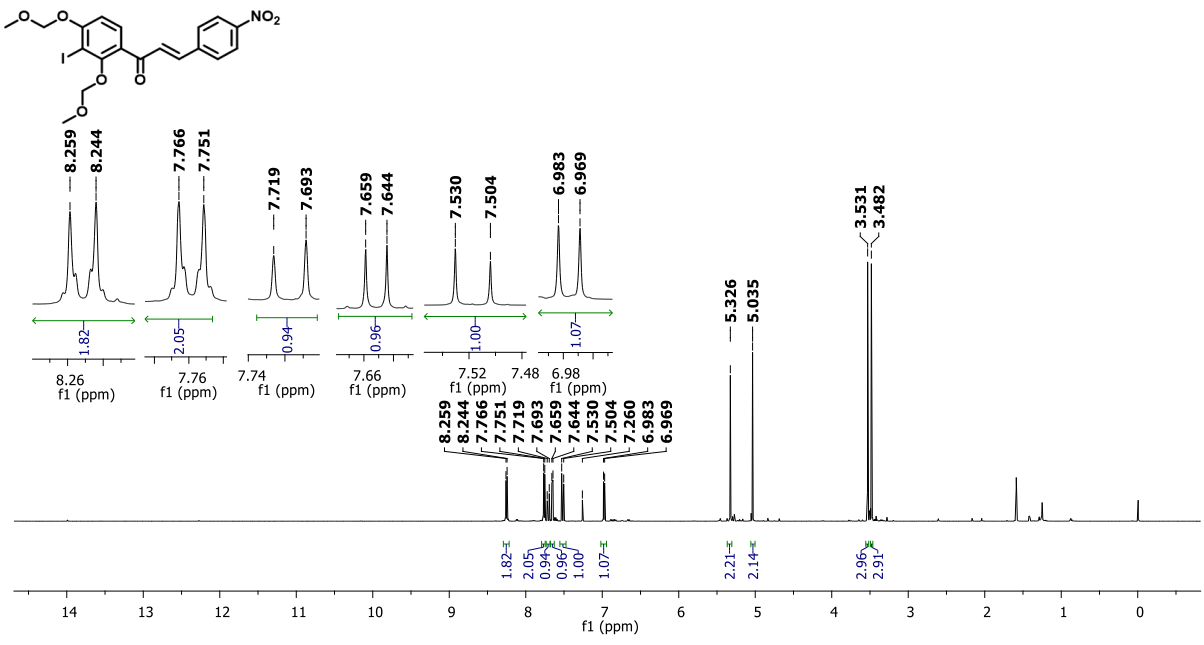

Figure S19. ^{1}H NMR spectrum of **C.15** ($CDCl_3$; 600 MHz)

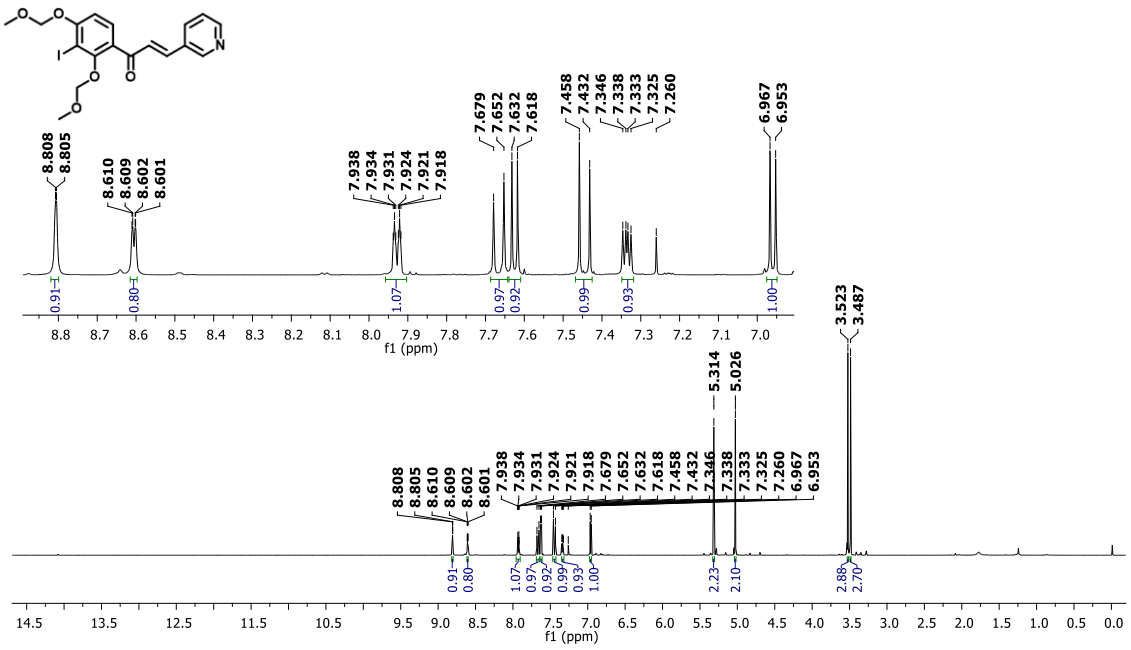

Figure S20. ^{1}H NMR spectrum of **C.16** ($CDCl_3$; 600 MHz)

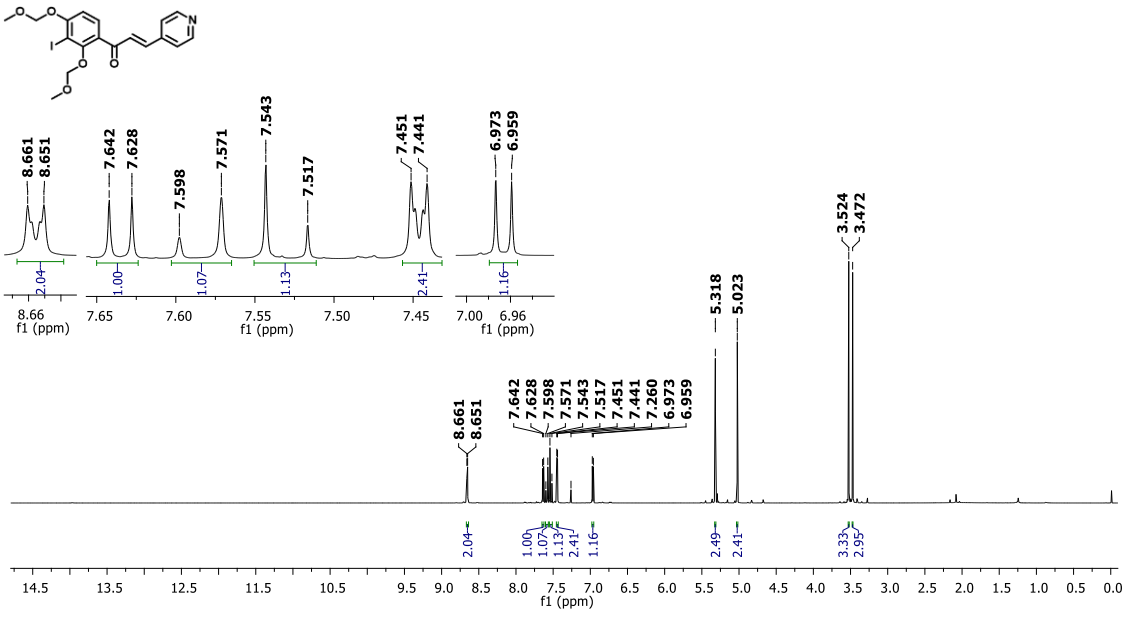

Figure S21. ^{1}H NMR spectrum of **C.17** ($CDCl_3$; 600 MHz)

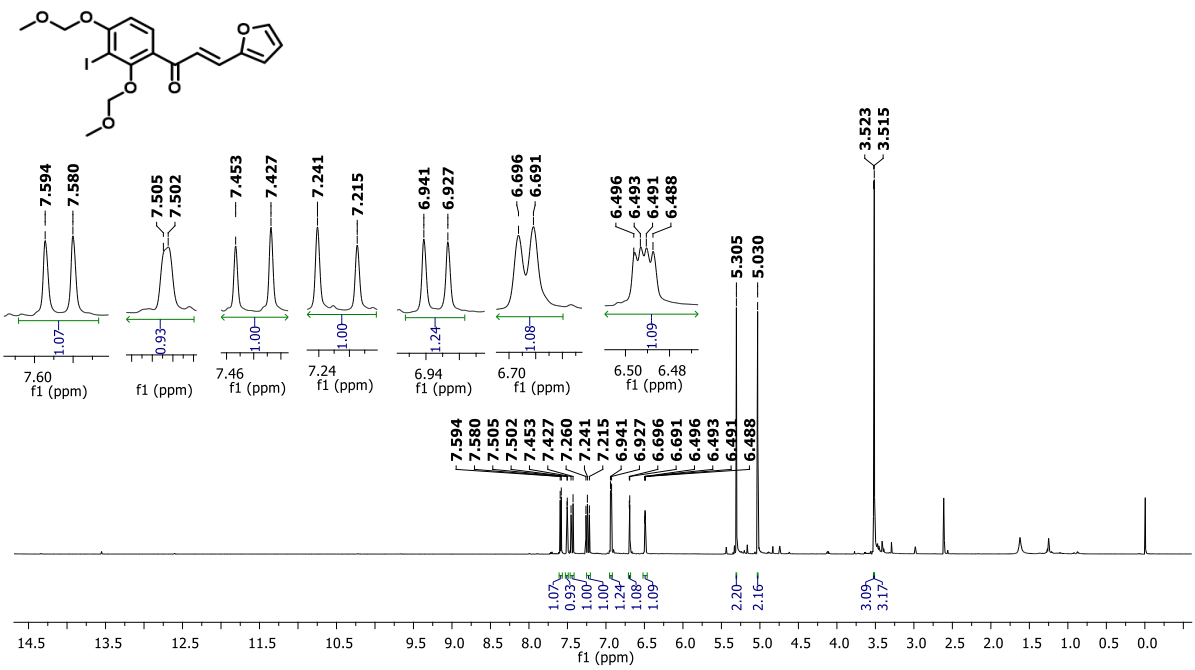

Figure S22. ^{1}H NMR spectrum of **C.18** ($CDCl_3$; 600 MHz)

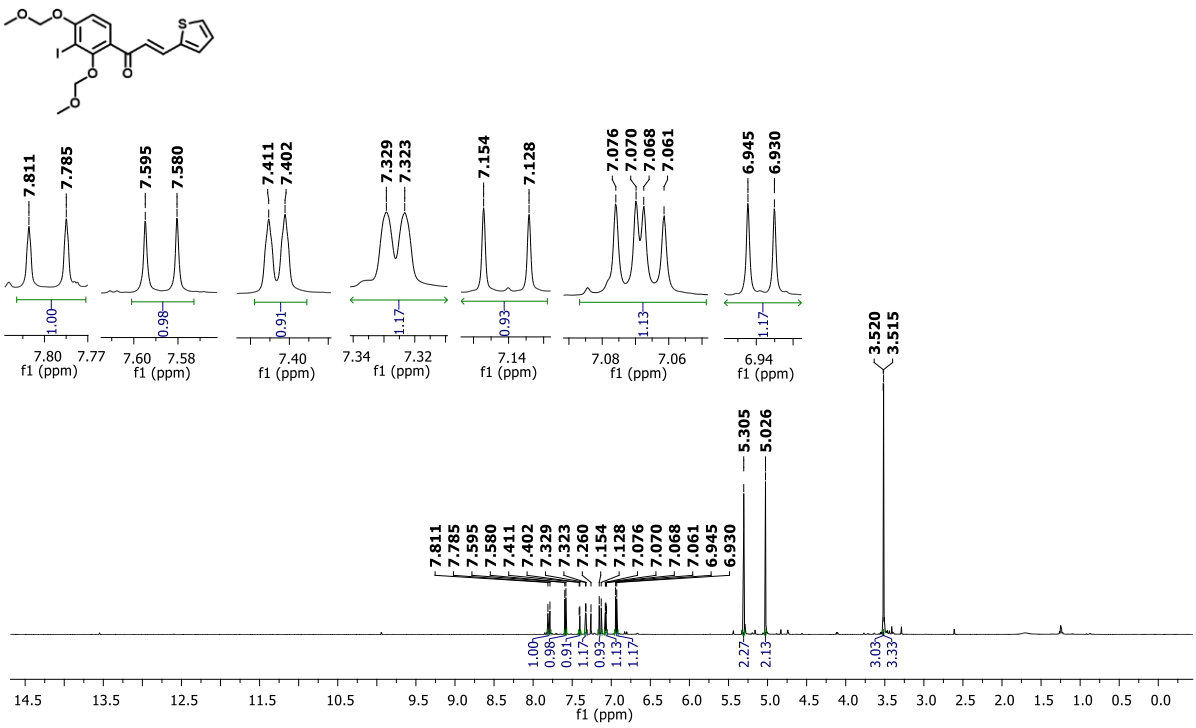

Figure S23. ^{1}H NMR spectrum of **C.19** ($CDCl_3$; 600 MHz)

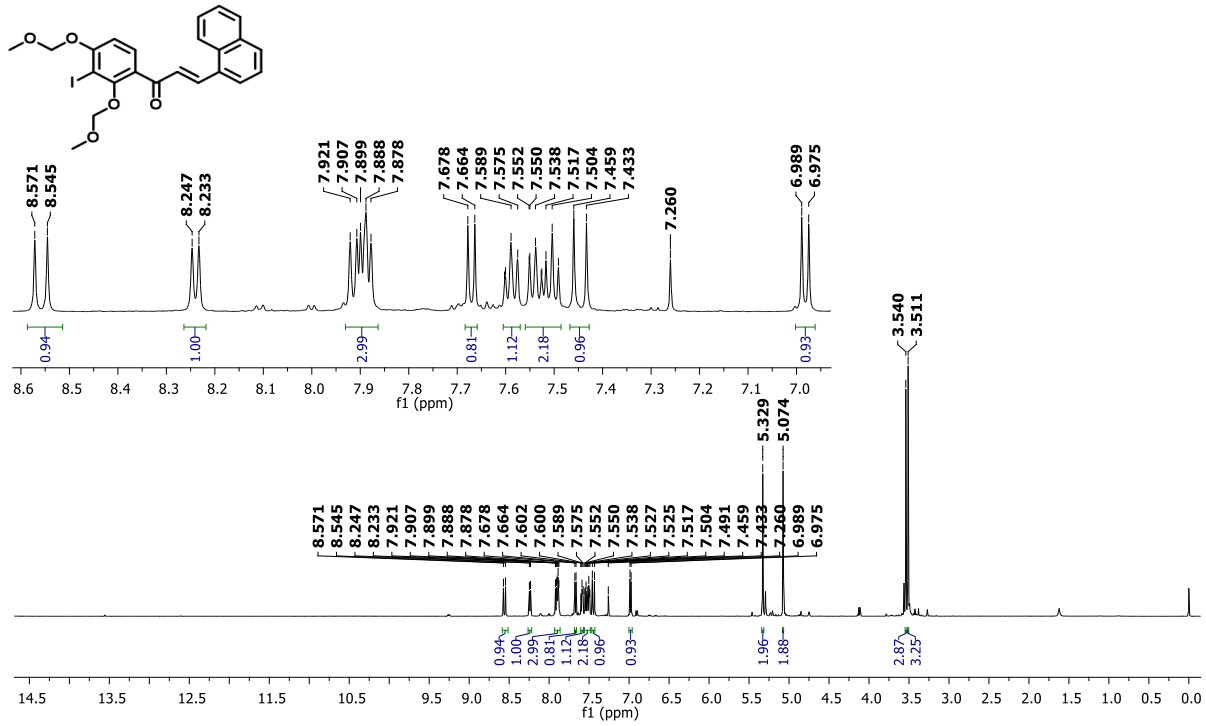

Figure S24. ^{1}H NMR spectrum of **C.20** ($CDCl_3$; 600 MHz)

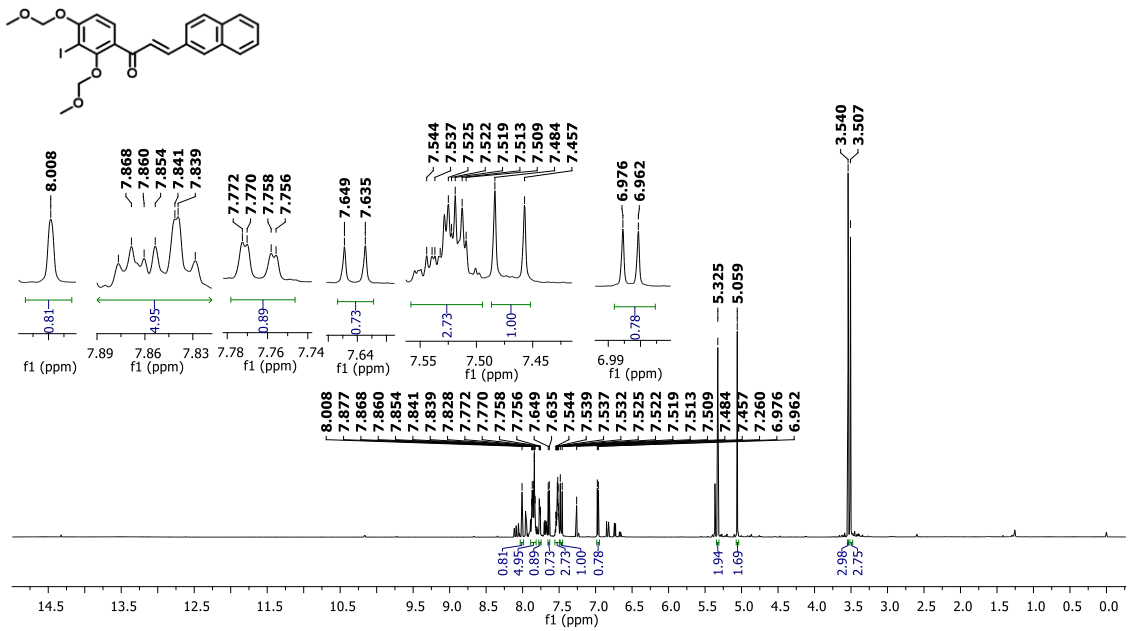

Figure S25. ^{1}H NMR spectrum of **C.21** ($CDCl_3$; 600 MHz)

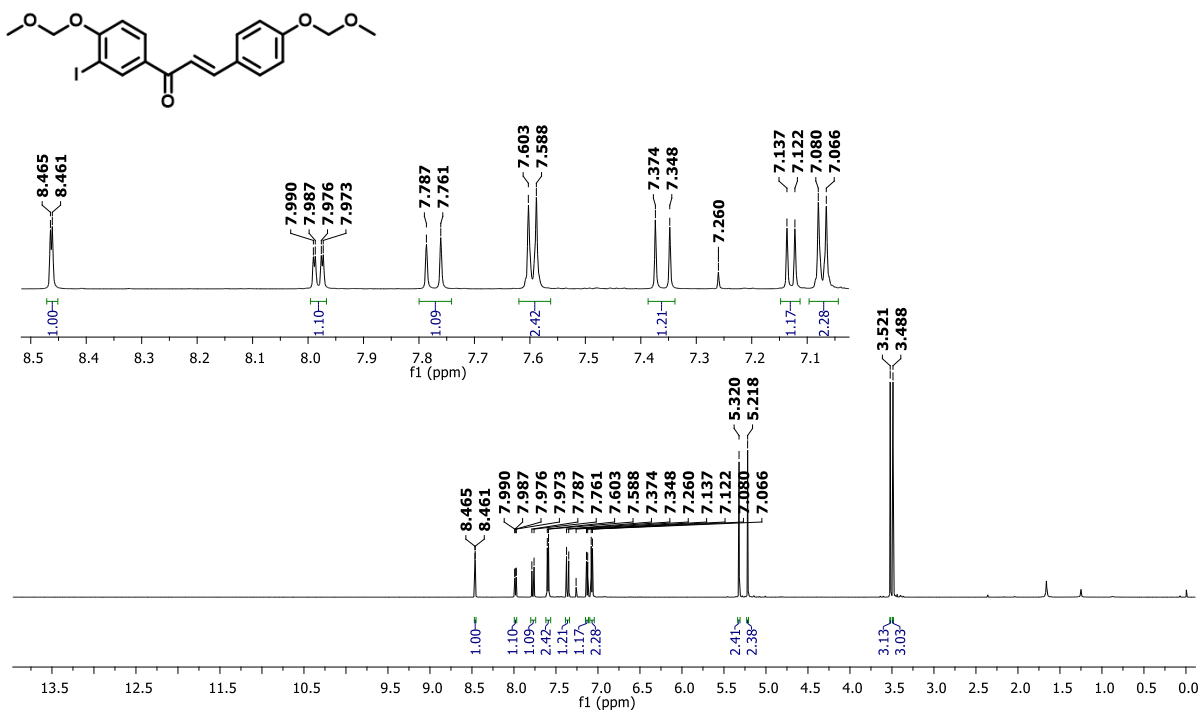

Figure S26. ^{1}H NMR spectrum of **C.22** ($CDCl_3$; 600 MHz)

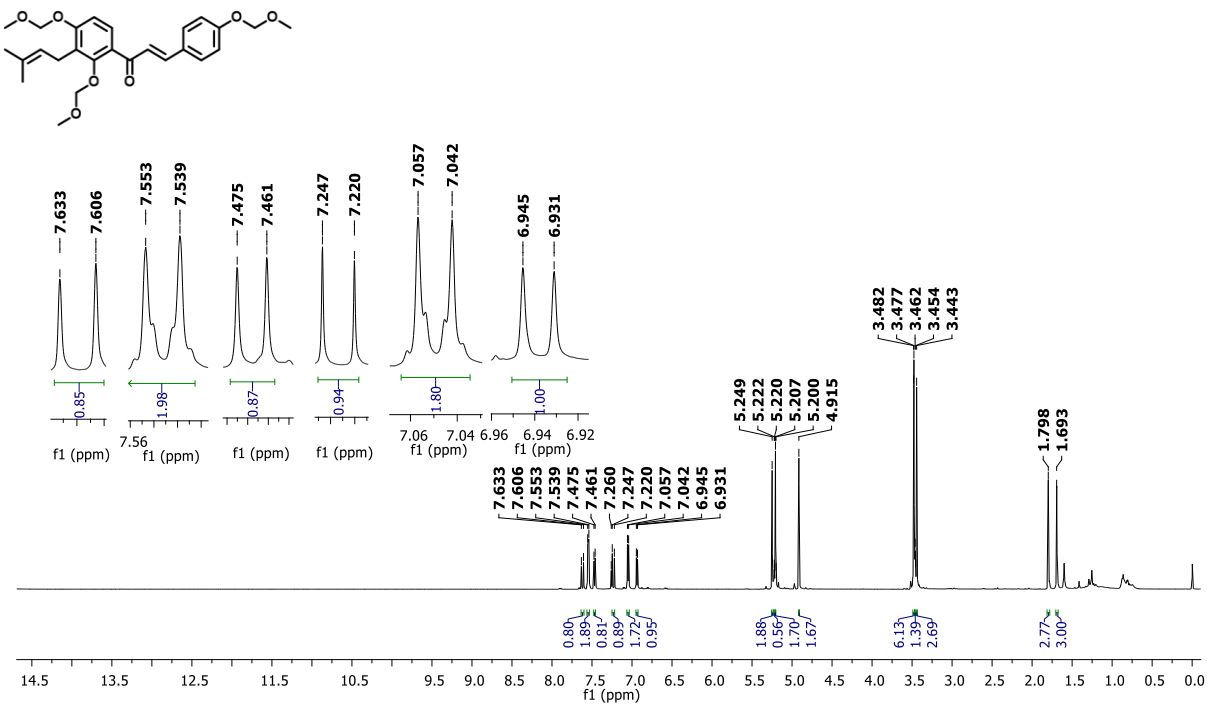

Figure S27. ^{1}H NMR spectrum of **C.23** ($CDCl_3$; 600 MHz)

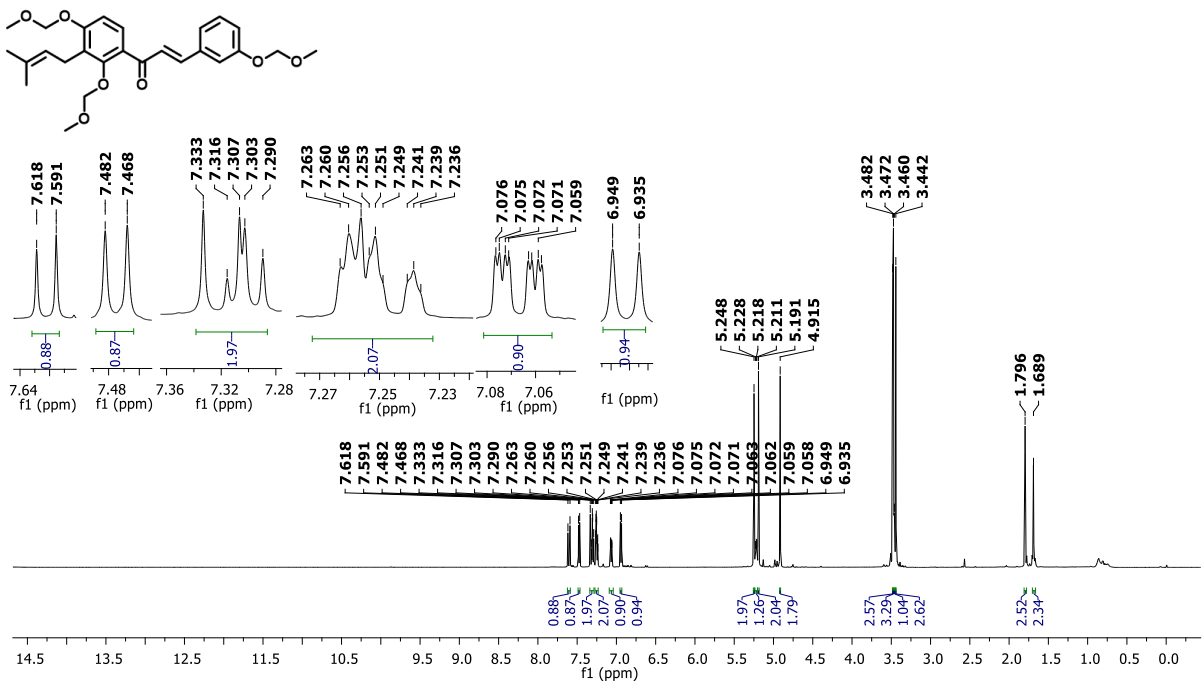

Figure S28. ^{1}H NMR spectrum of **C.24** ($CDCl_3$; 600 MHz)

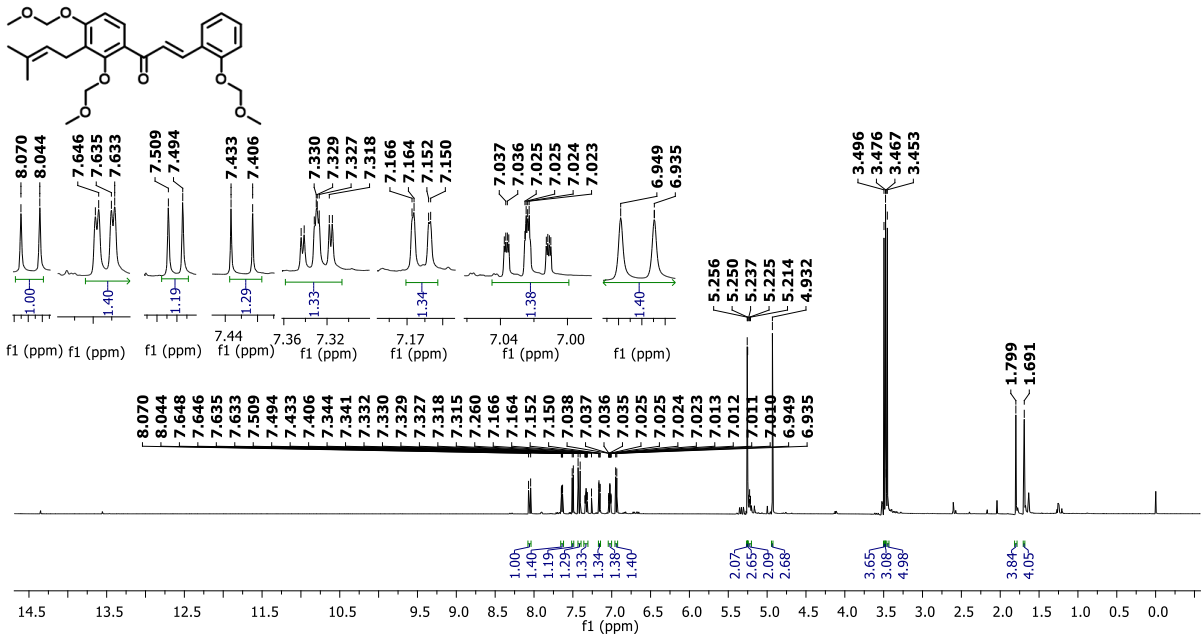

Figure S29. ^{1}H NMR spectrum of **C.25** ($CDCl_3$; 600 MHz)

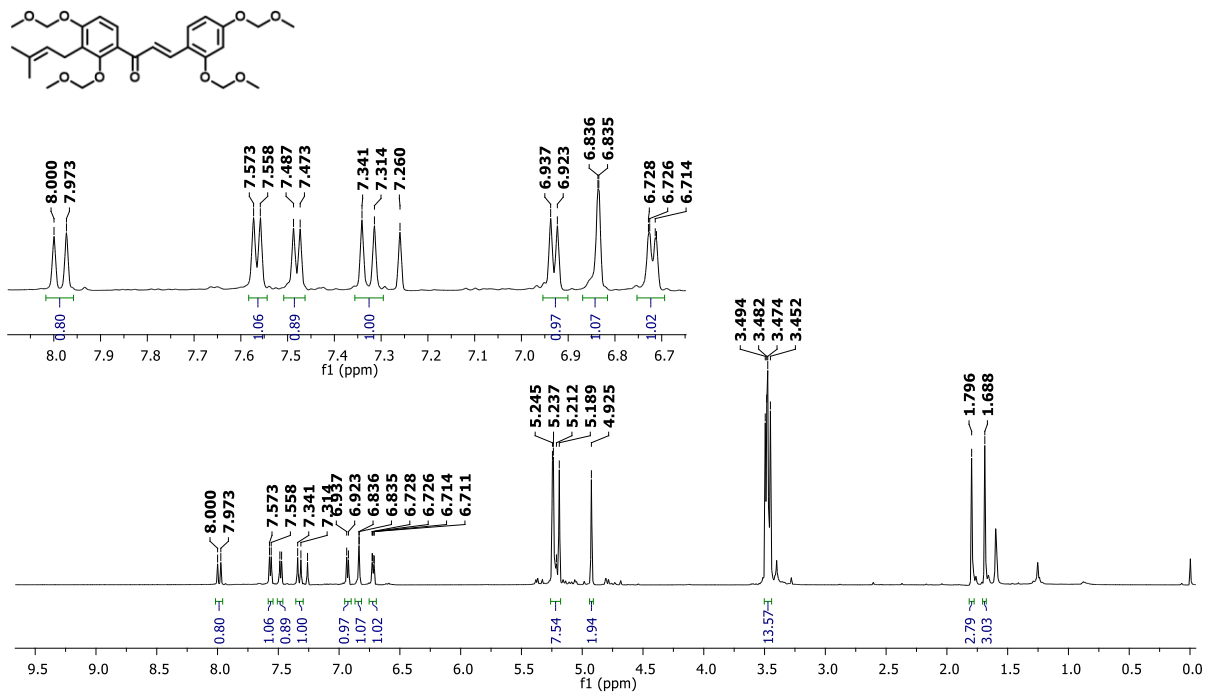

Figure S30. ^{1}H NMR spectrum of **C.26** ($CDCl_3$; 600 MHz)

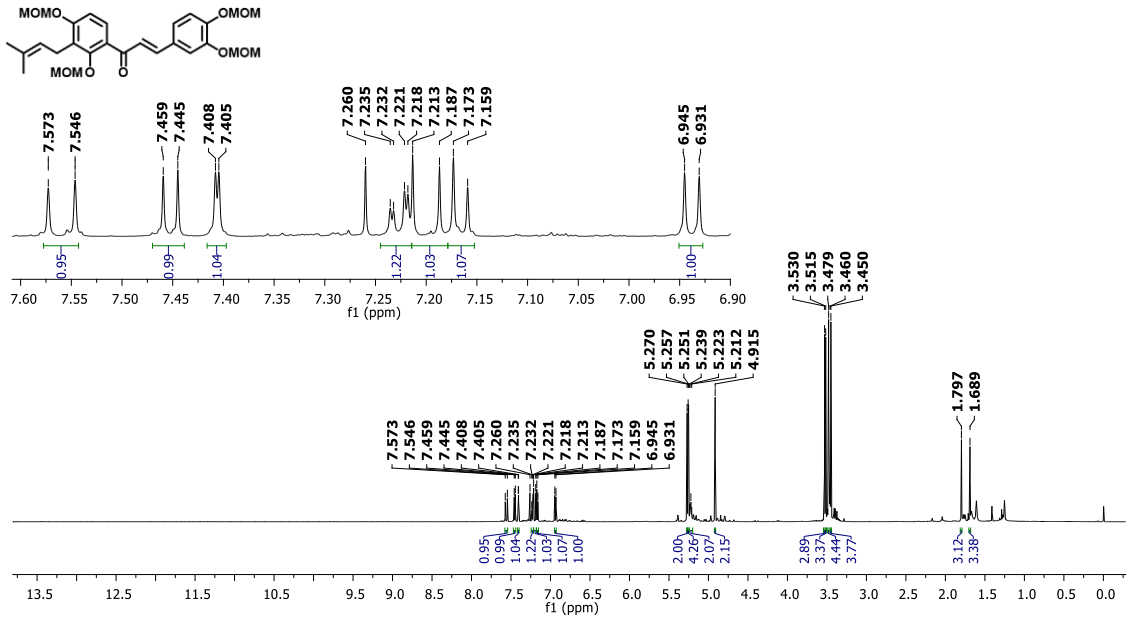

Figure S31 ^{1}H NMR spectrum of **C.27** ($CDCl_3$; 600 MHz)

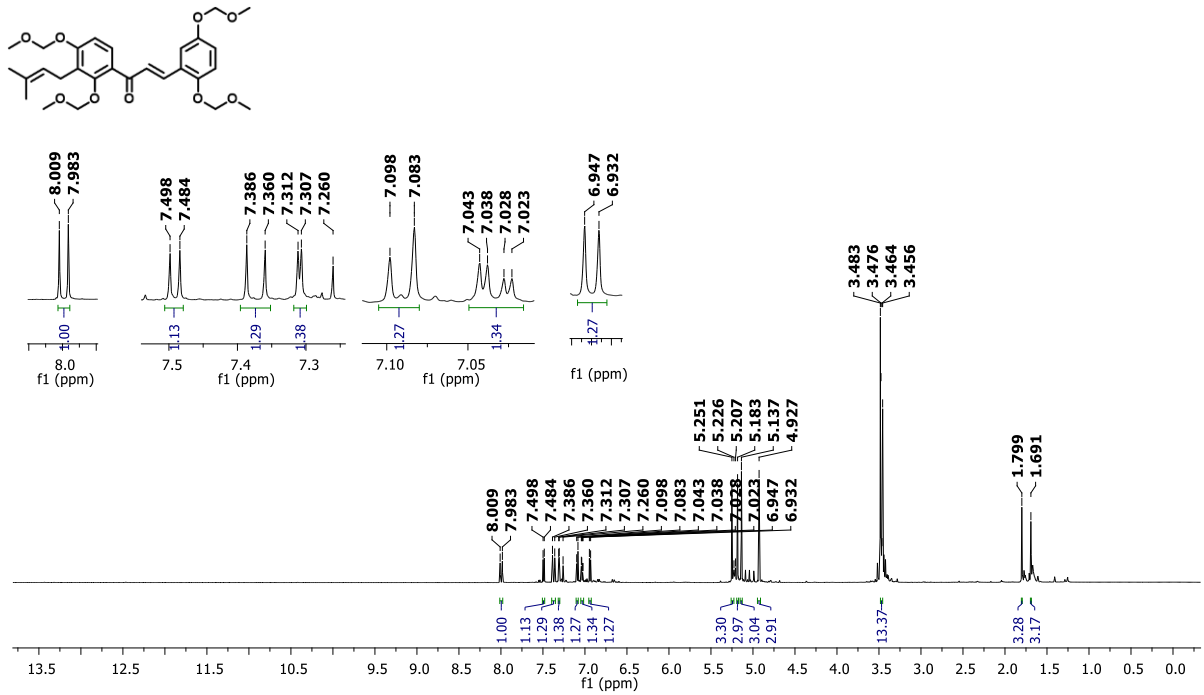

Figure S32. ^{1}H NMR spectrum of **C.28** ($CDCl_3$; 600 MHz)

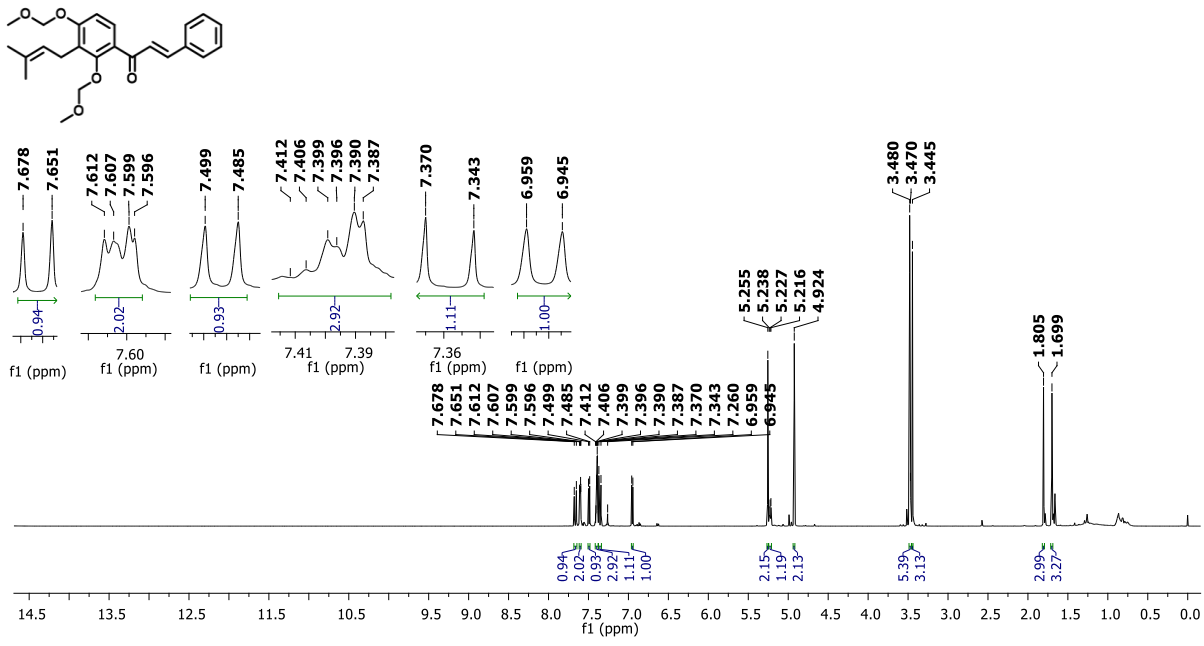

Figure S33. ^{1}H NMR spectrum of **C.29** ($CDCl_3$; 600 MHz)

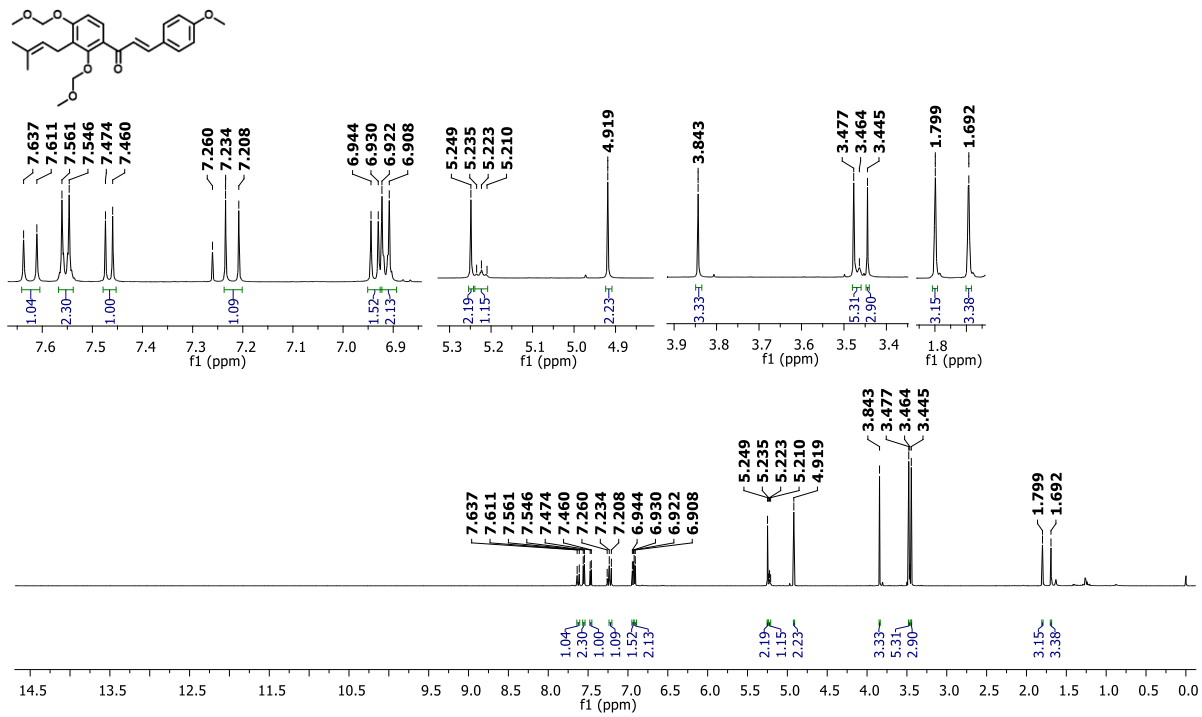

Figure S34. ^{1}H NMR spectrum of **C.30** ($CDCl_3$; 600 MHz)

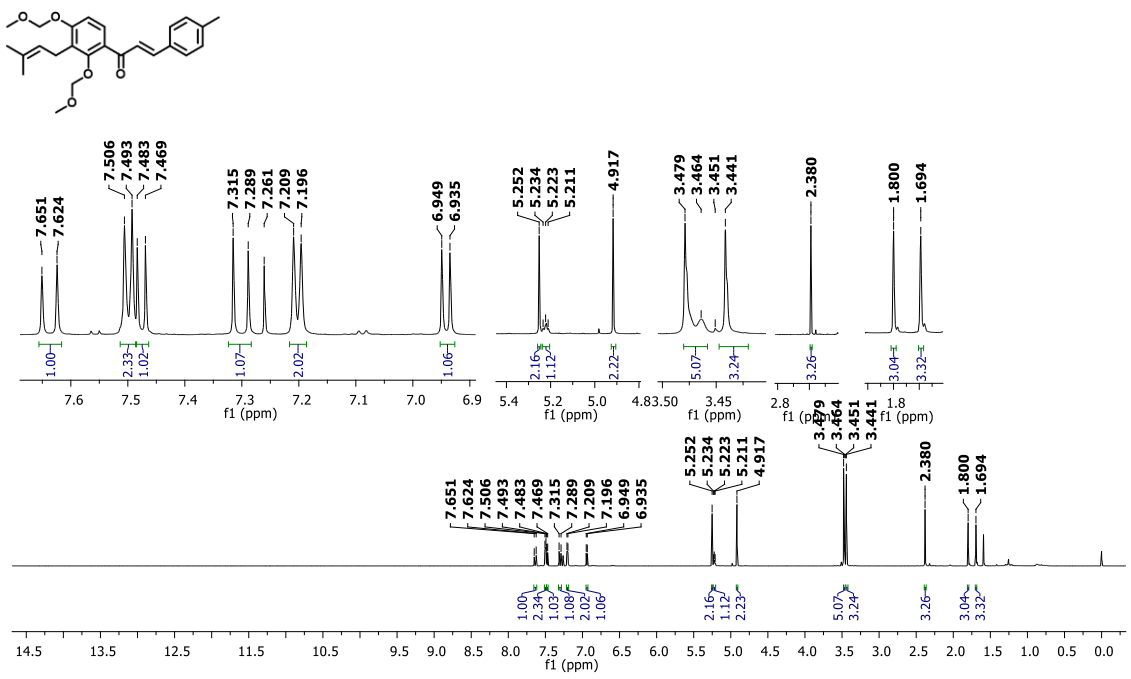

Figure S35. ^{1}H NMR spectrum of **C.31** ($CDCl_3$; 600 MHz)

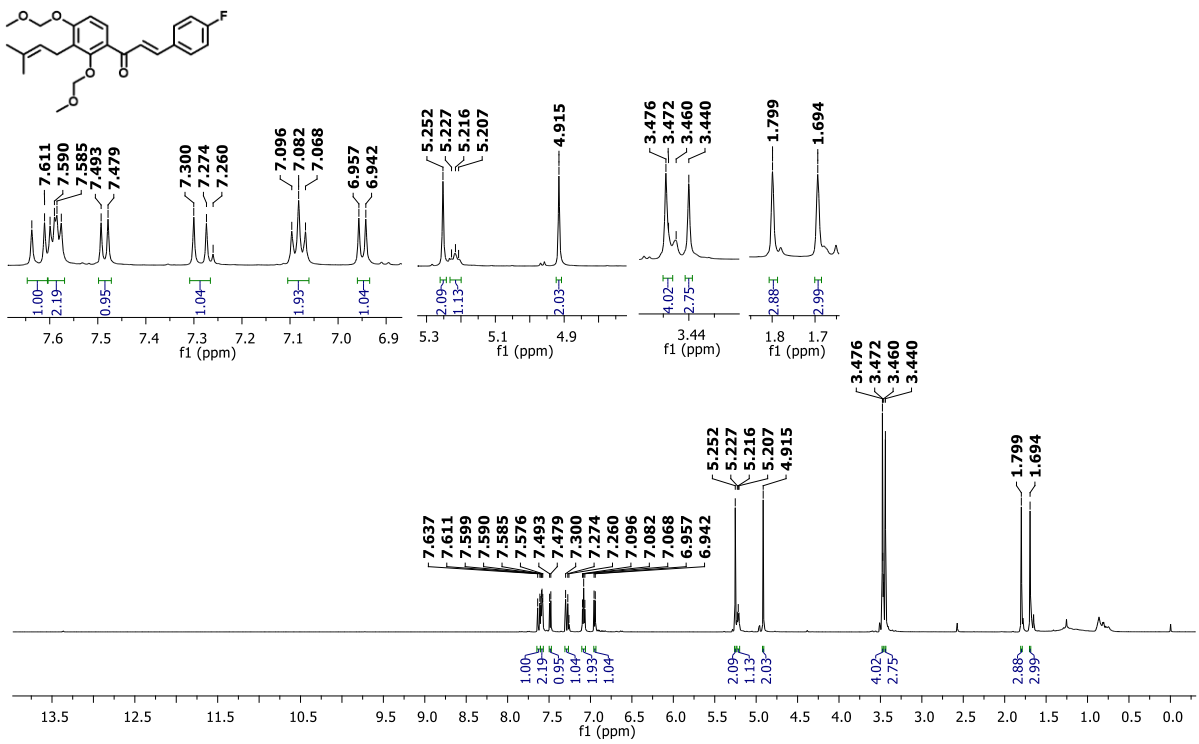

Figure S36. ^{1}H NMR spectrum of **C.32** ($CDCl_3$; 600 MHz)

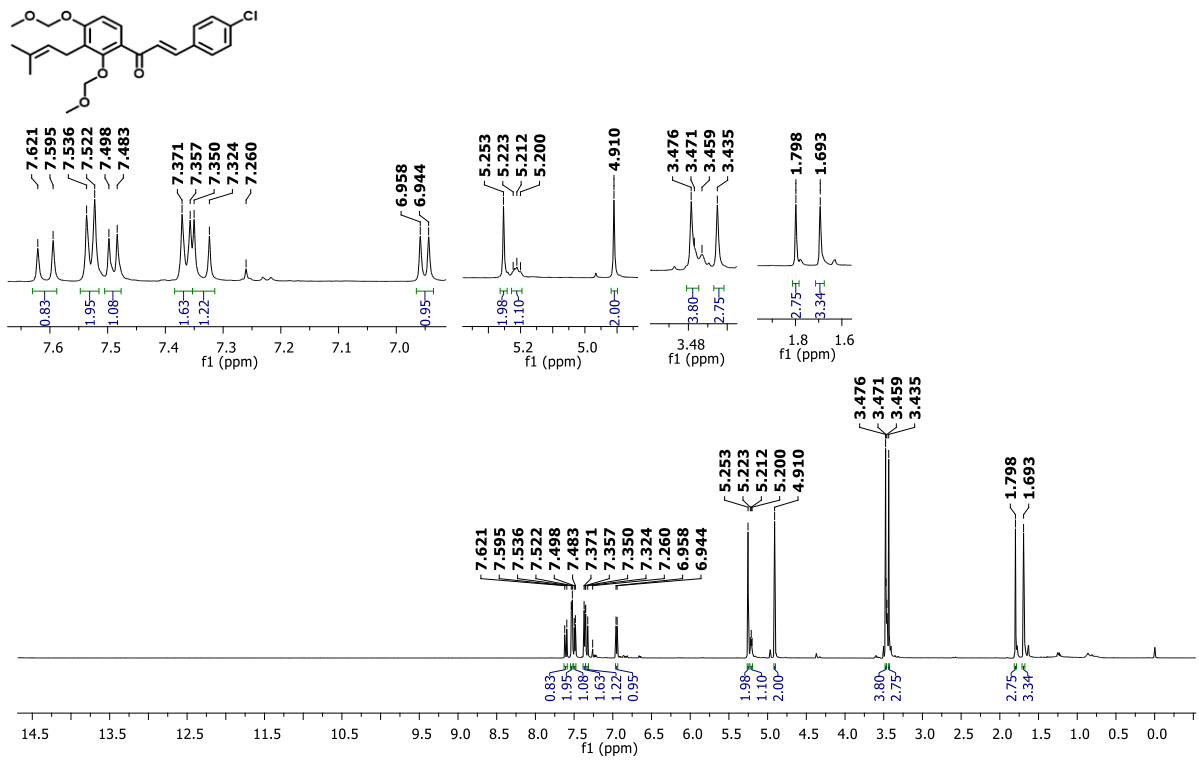

Figure S37. ^{1}H NMR spectrum of **C.33** ($CDCl_3$; 600 MHz)

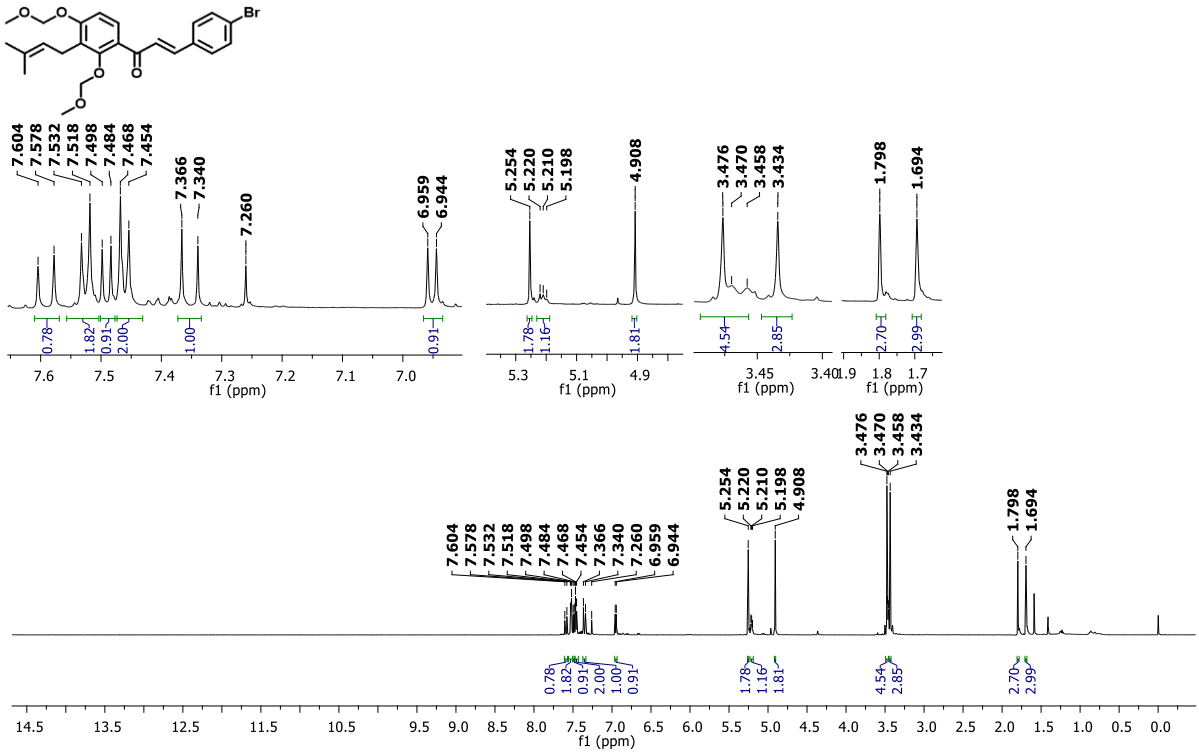

Figure S38. ^{1}H NMR spectrum of **C.34** ($CDCl_3$; 600 MHz)

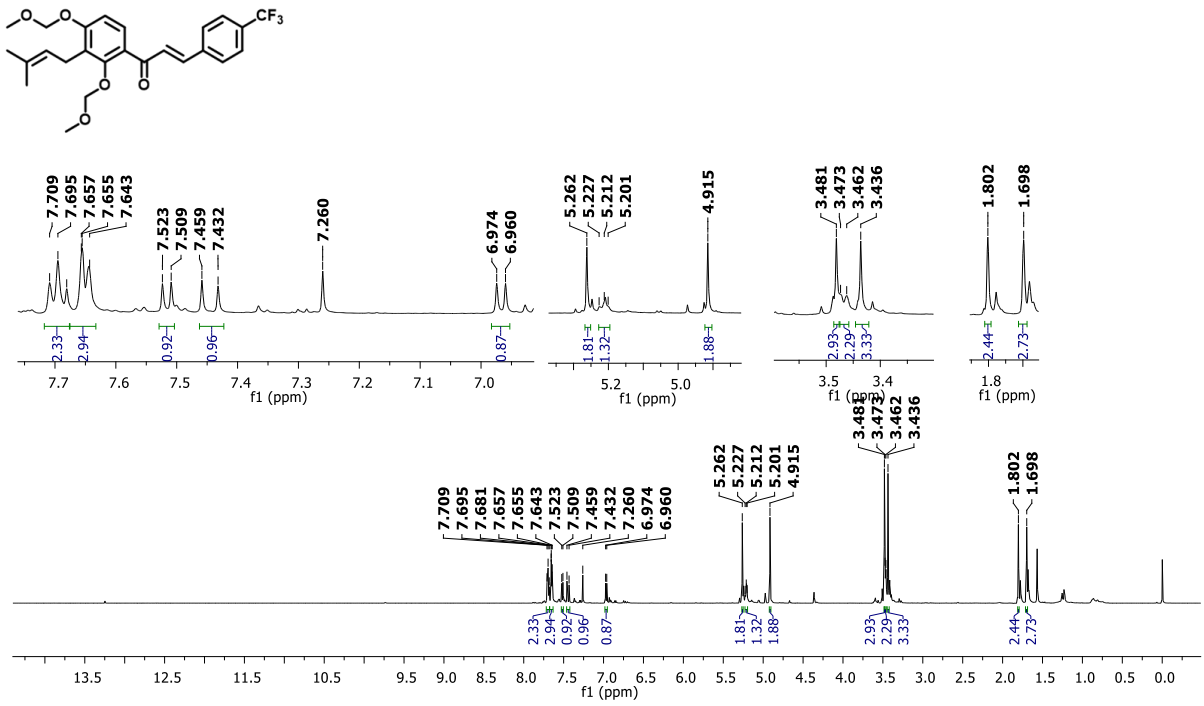

Figure S39. ^{1}H NMR spectrum of **C.35** ($CDCl_3$; 600 MHz)

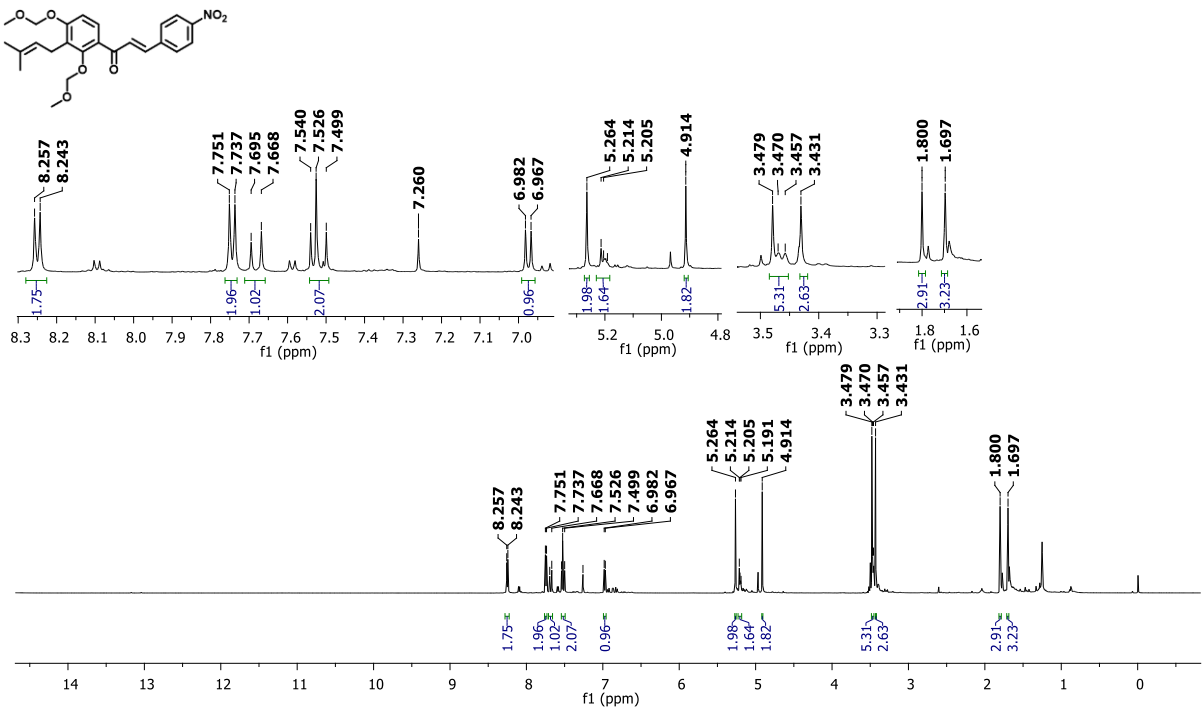

Figure S40. ^{1}H NMR spectrum of **C.36** ($CDCl_3$; 600 MHz)

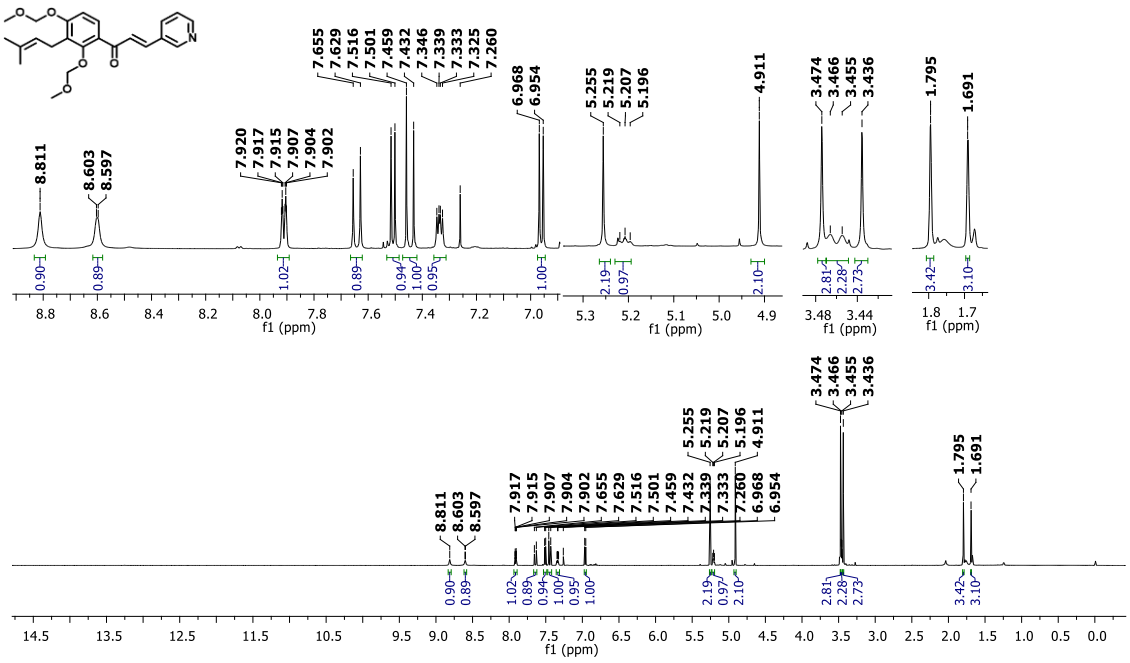

Figure S41. ^{1}H NMR spectrum of **C.37** ($CDCl_3$; 600 MHz)

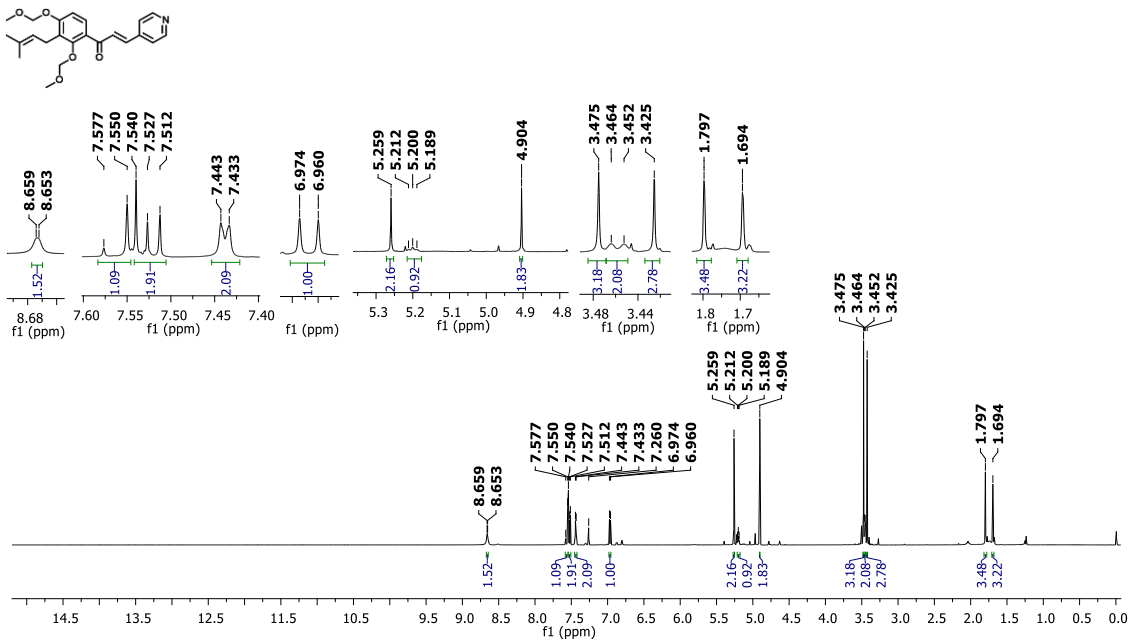

Figure S42. ^{1}H NMR spectrum of **C.38** ($CDCl_3$; 600 MHz)

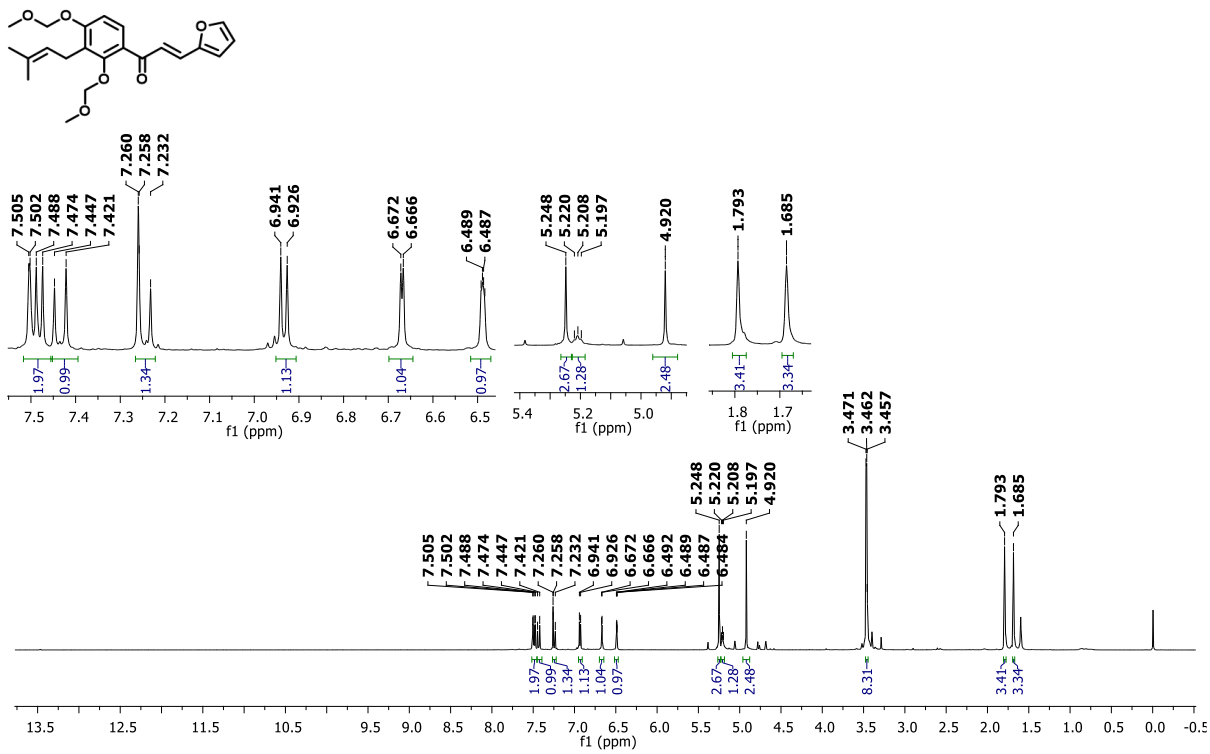

Figure S43. ^{1}H NMR spectrum of **C.39** ($CDCl_3$; 600 MHz)

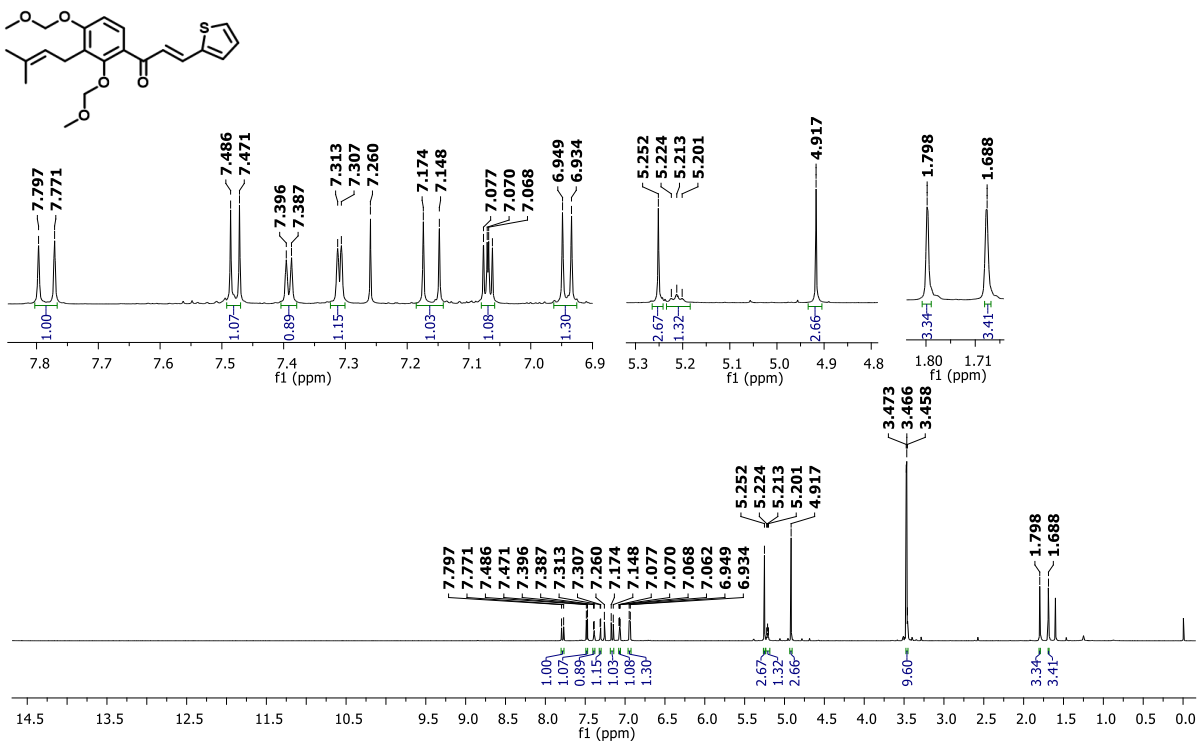

Figure S44. ^{1}H NMR spectrum of **C.40** ($CDCl_3$; 600 MHz)

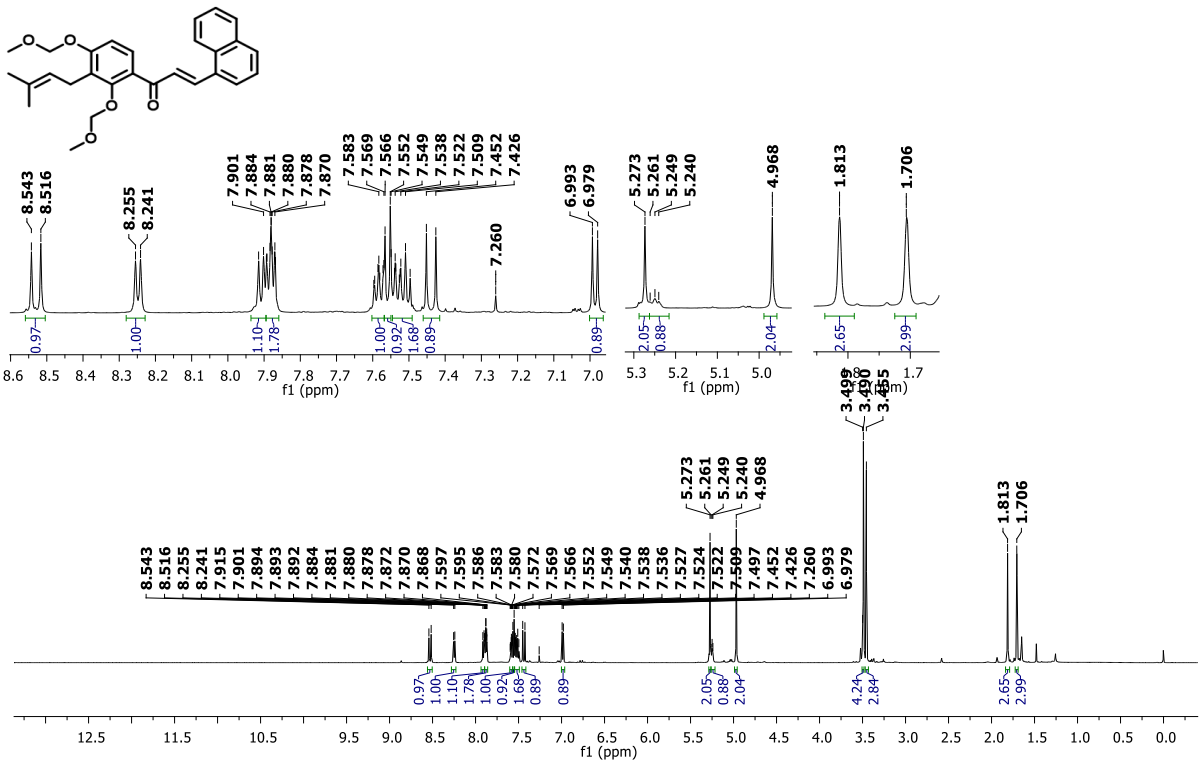

Figure S45. ^{1}H NMR spectrum of **C.41** ($CDCl_3$; 600 MHz)

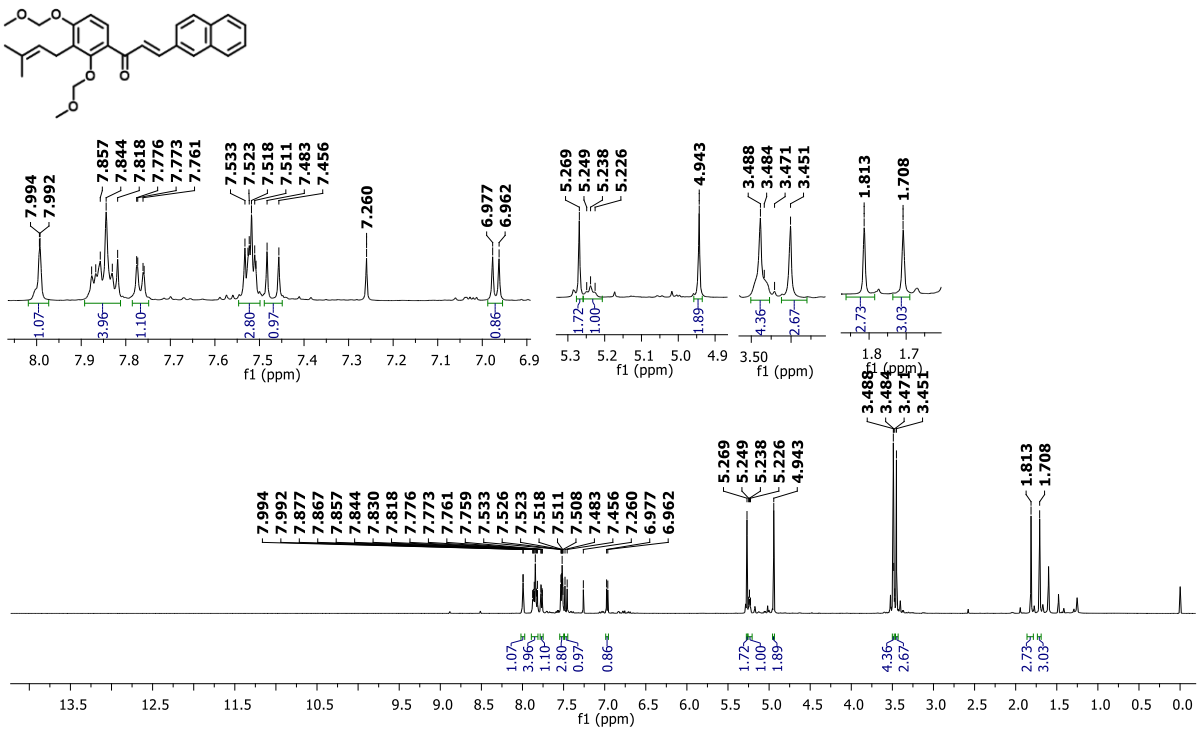

Figure S46. ^{1}H NMR spectrum of **C.42** ($CDCl_3$; 600 MHz)

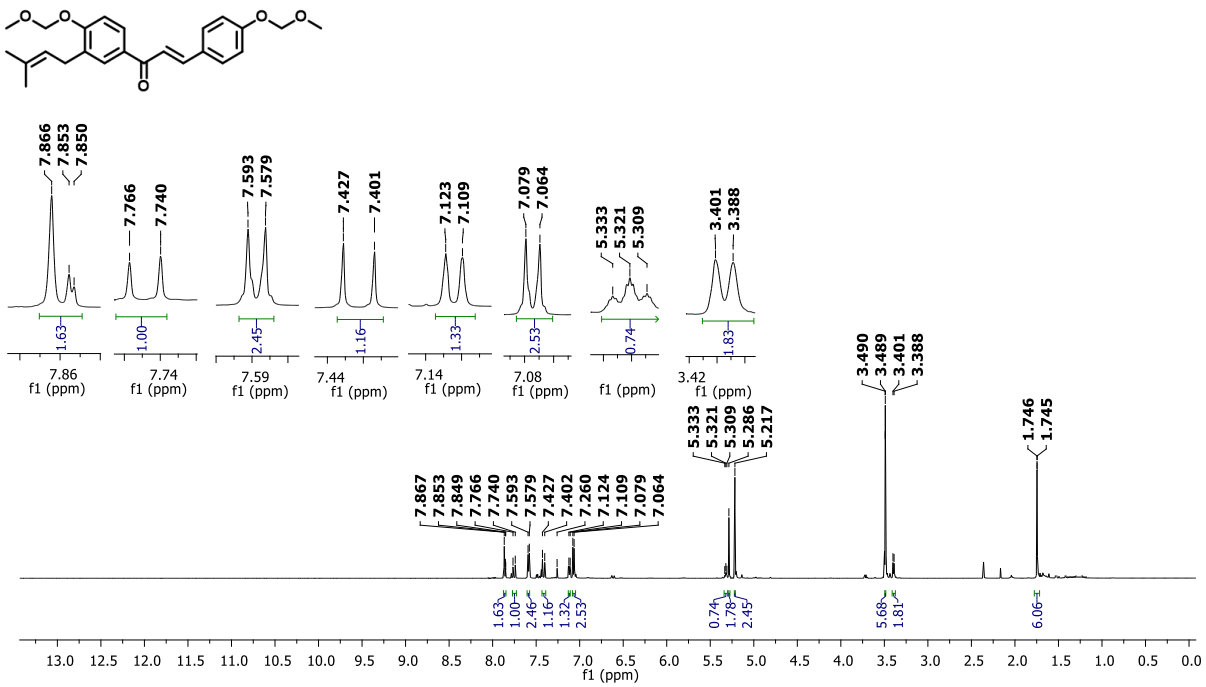

Figure S47. ^{1}H NMR spectrum of **C.44** ($CDCl_3$; 600 MHz)

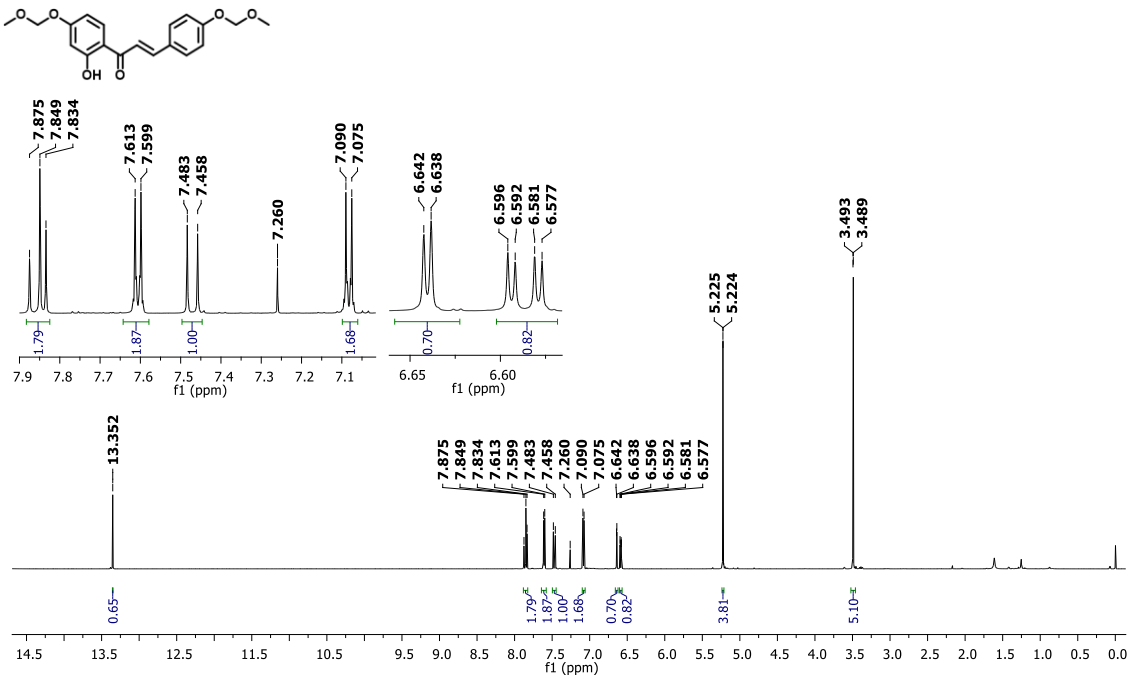

Figure S48. ^{1}H NMR spectrum of **C.45** (Acetone-d_6; 600 MHz)

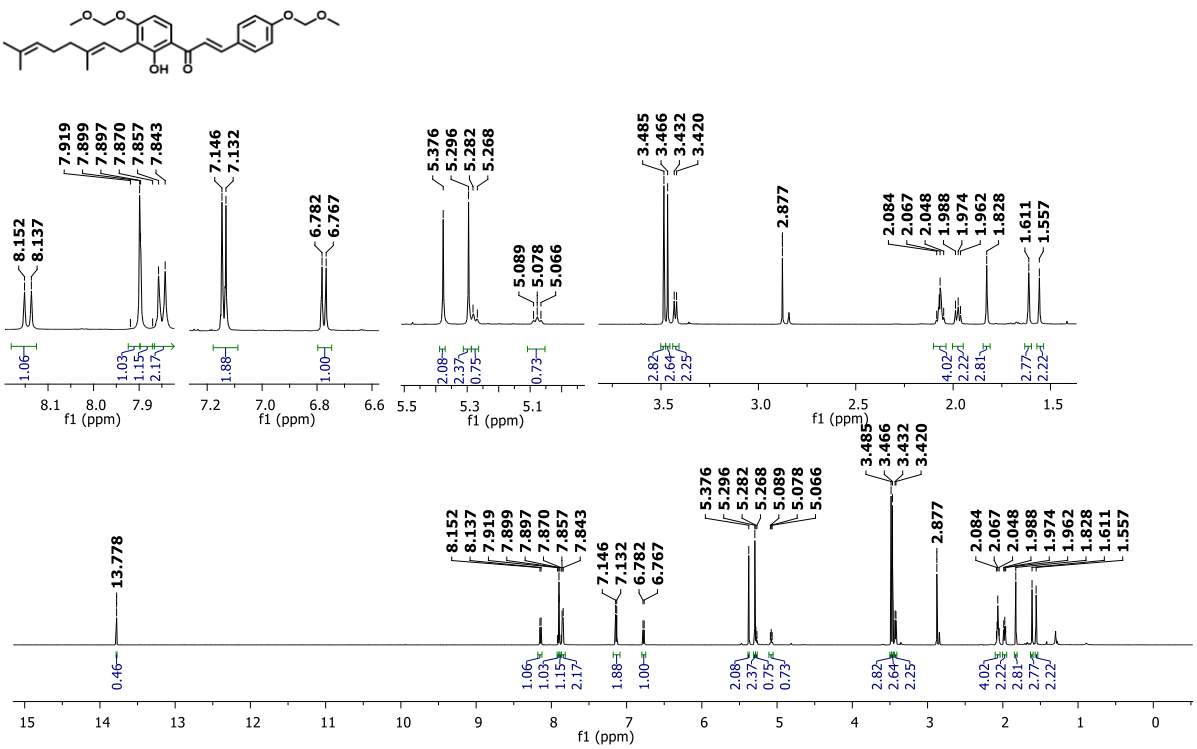

Figure S49a. ^{1}H NMR spectrum of **IBC 1** (Acetone-d_6; 600 MHz)

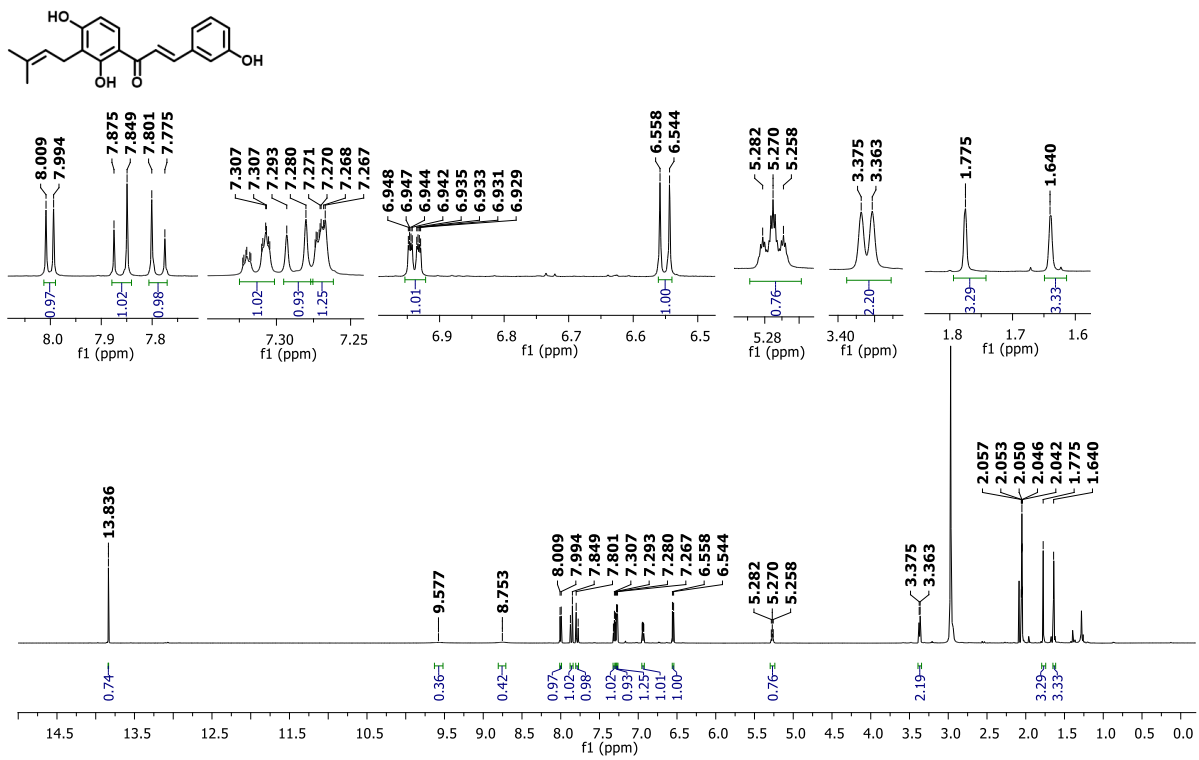

Figure S49b. ^{13}C NMR spectrum of **IBC 1** (Acetone-d_6; 150 MHz)

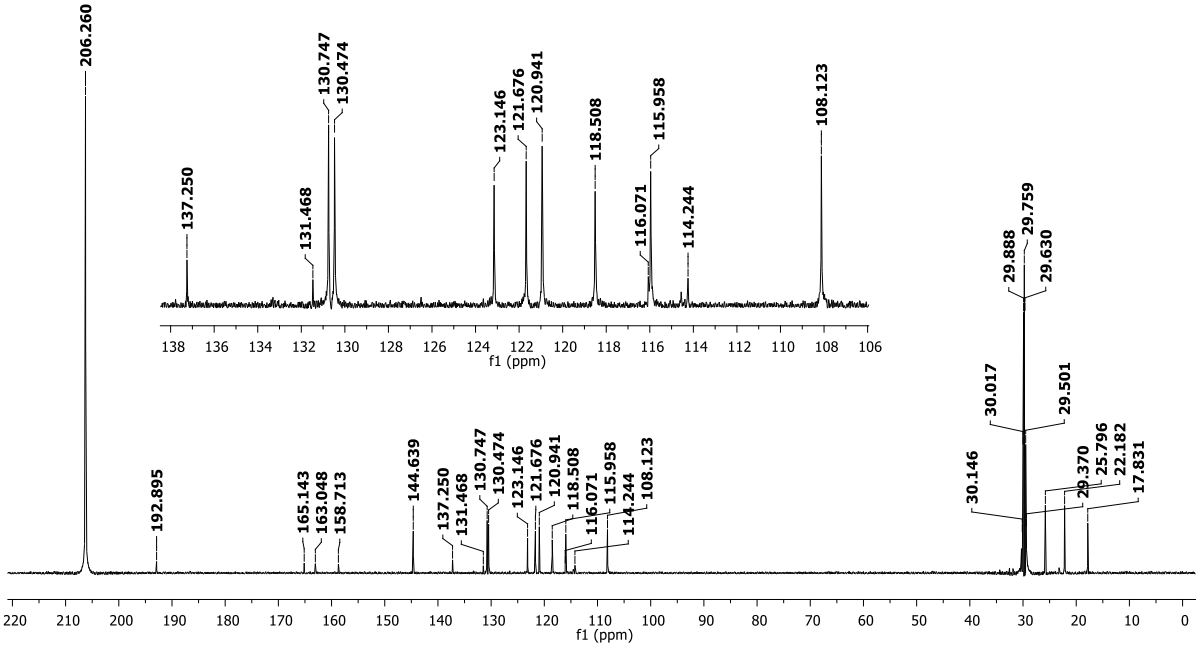

Figure S49c. HPLC chromatogram of **IBC 1**. Methanol:Water (3:1), 365 nm

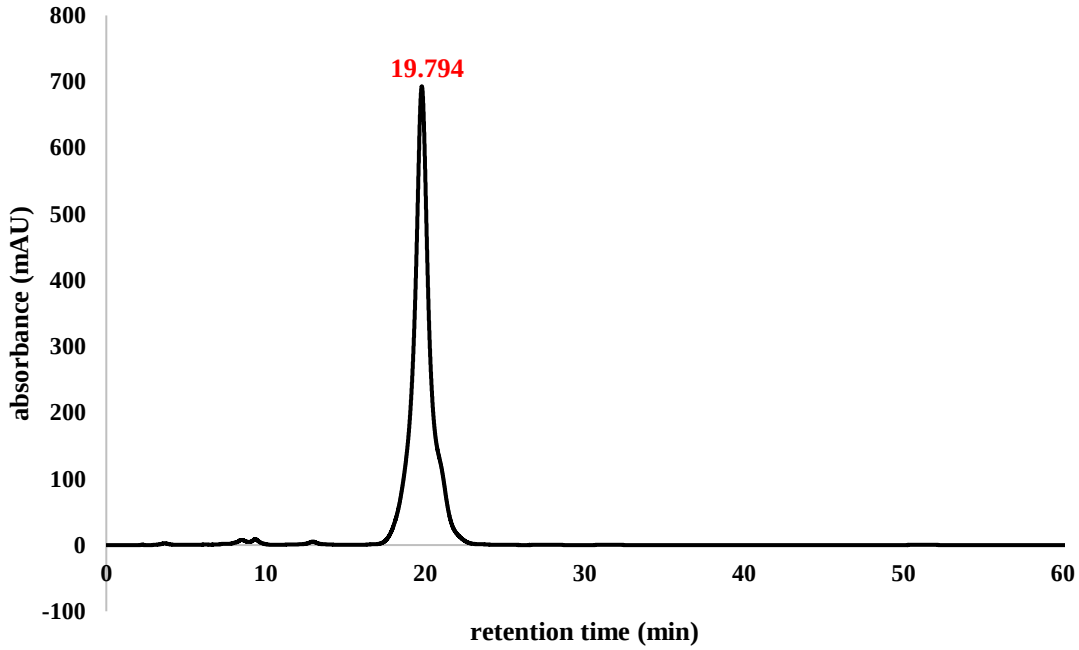

Figure S49d. UV-Vis spectrum of **IBC 1**

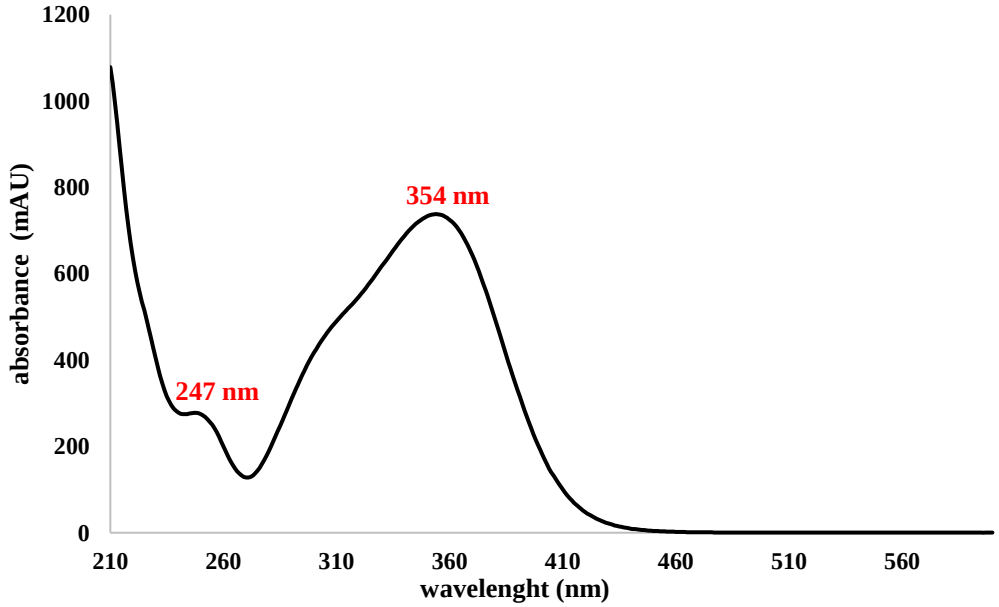

Figure S50a. ^{1}H NMR sprectrum of **IBC 2** (Acetone-d_6, 600 MHz)

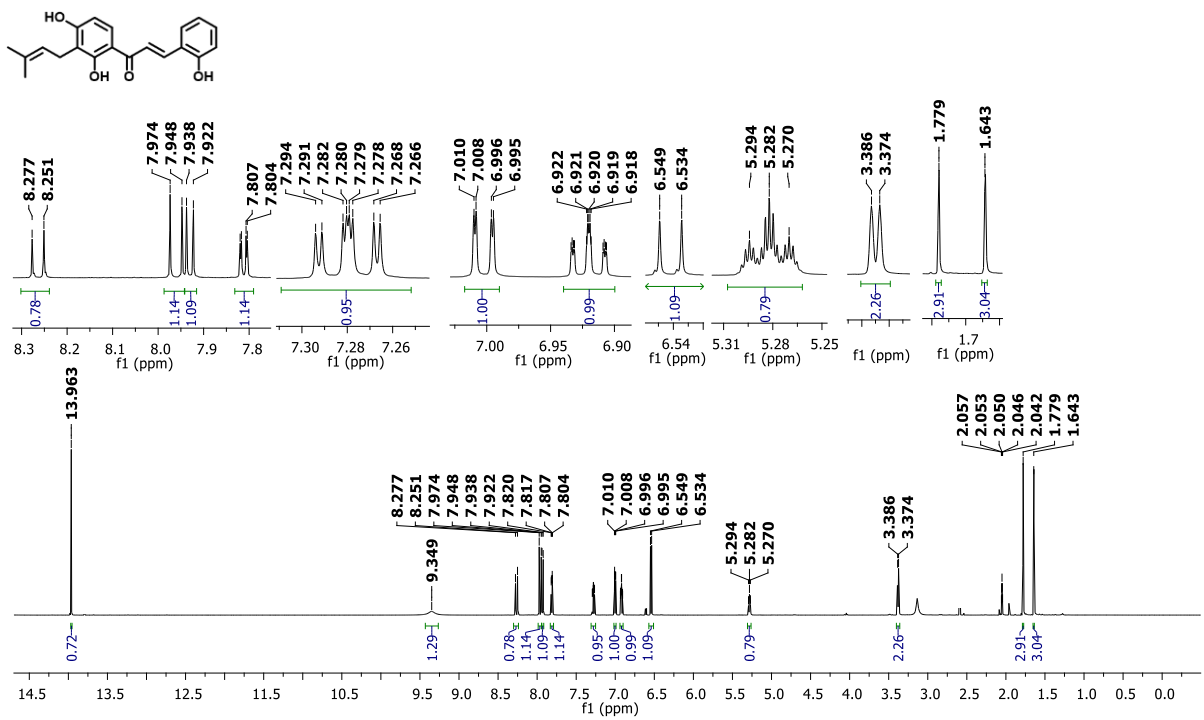

Figure S50b. ^{13}C NMR sprectrum of **IBC 2** (Acetone-d_6, 150 MHz)

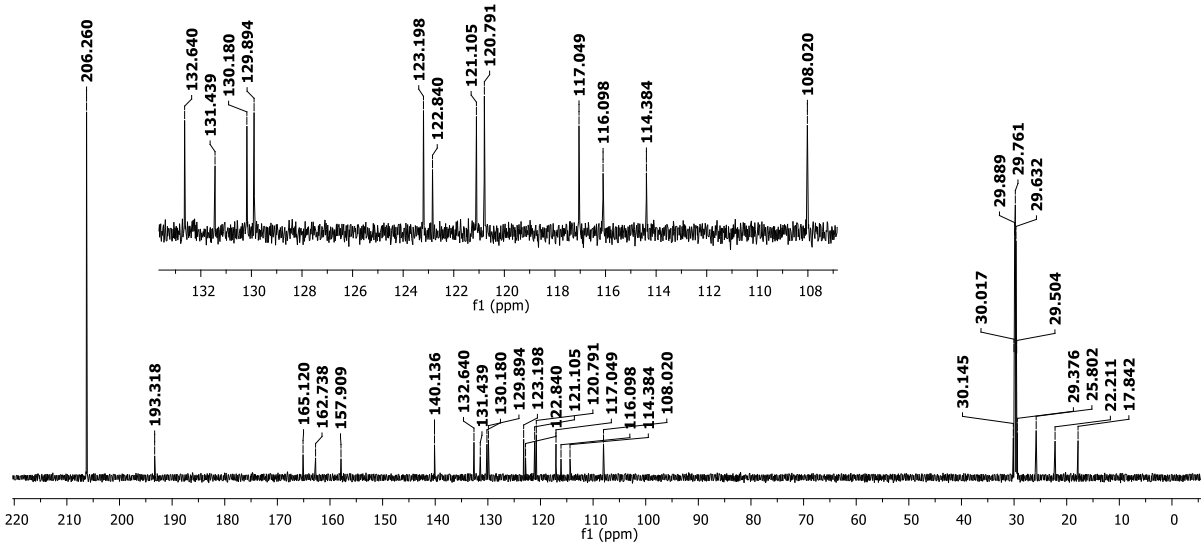

Figure S50c HPLC chromatogram of **IBC 2.** Methanol:Water (3:1), 365 nm

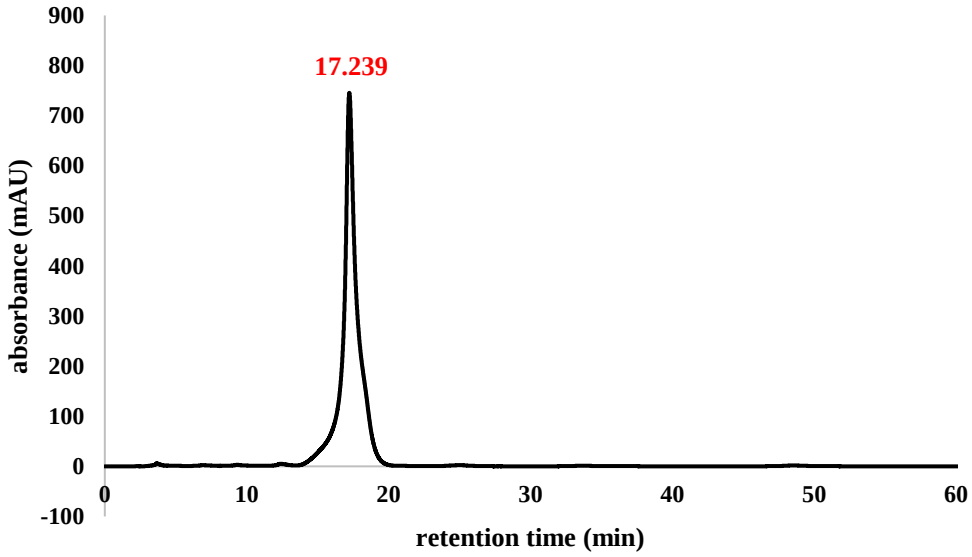

Figure S50d. UV-Vis spectra of **IBC 2**

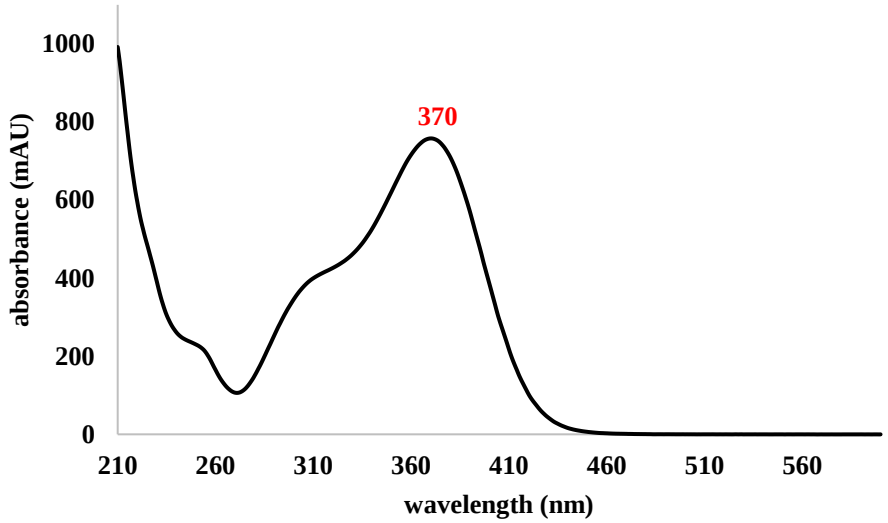

Figure S51a. ^{1}H NMR spectrum of **IBC 3** (Acetone-d_6; 600 MHz)

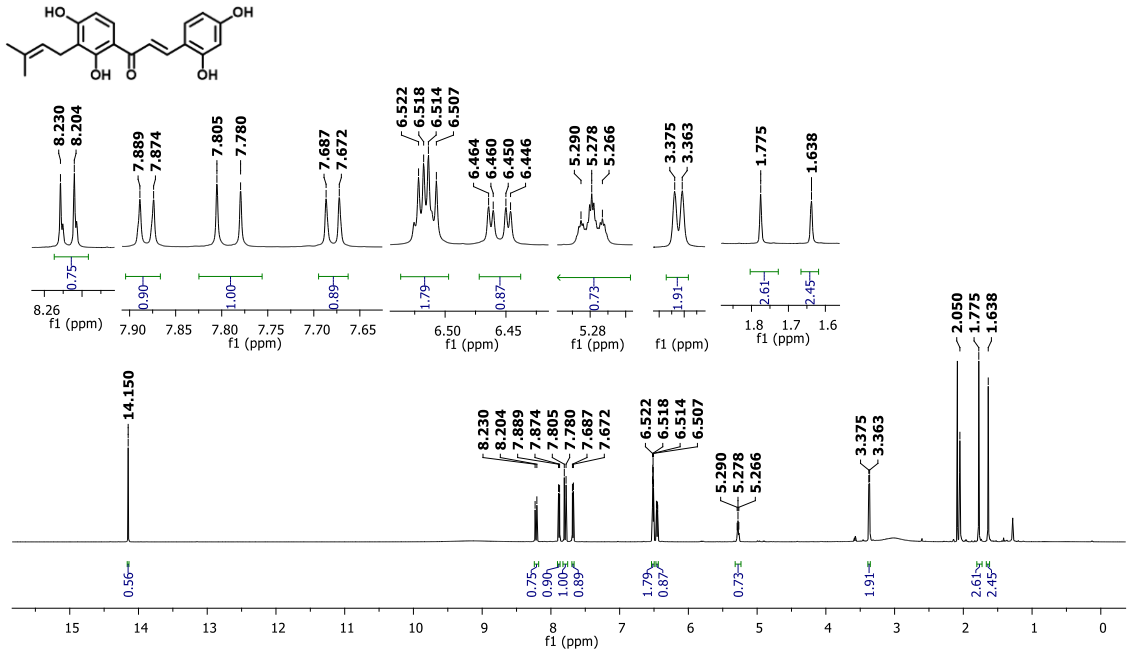

Figure S51b. ^{13}C NMR spectrum of **IBC 3** (Acetone-d_6; 150 MHz)

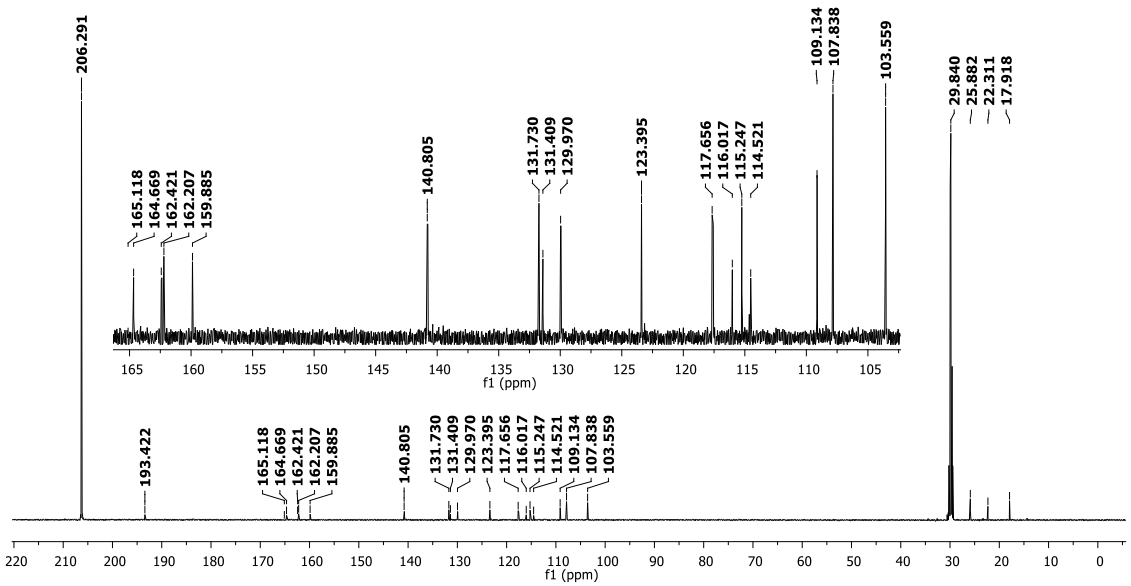

Figure S51c. HPLC chromatogram of **IBC 3**. Methanol:Water (3:1), 365 nm

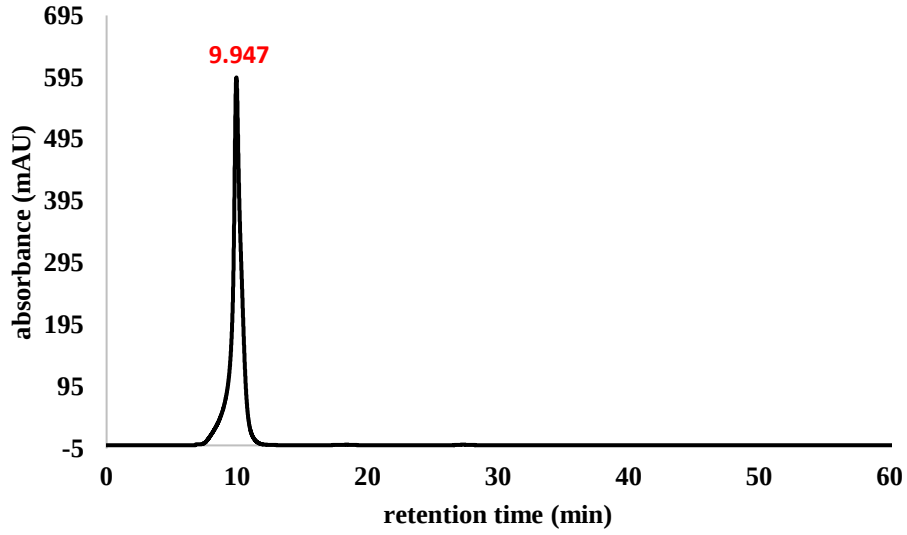

Figure S51d. UV-Vis spectrum of **IBC 3**

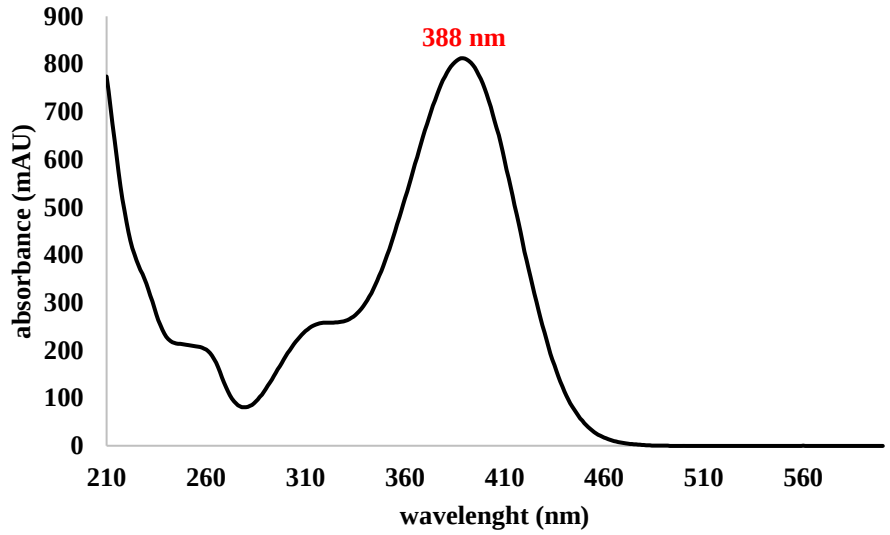

Figure S52a. ^{1}H NMR spectrum of **IBC 4** (Acetone-d_6; 600 MHz)

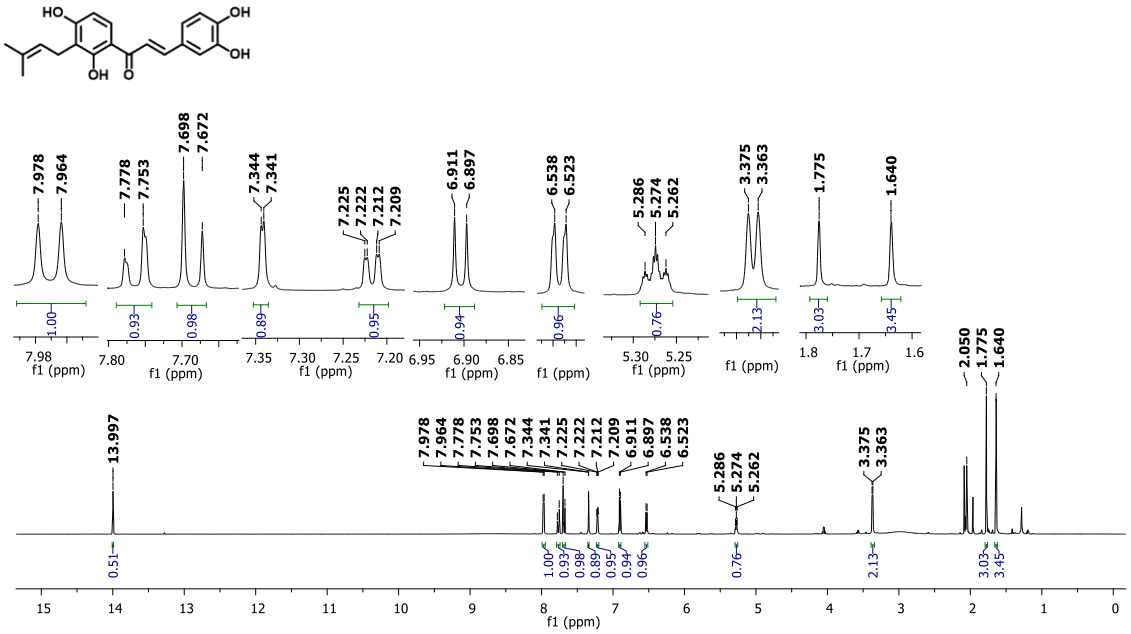

Figure S52b. ^{13}C NMR spectrum of **IBC 4** (Acetone-d_6; 150 MHz)

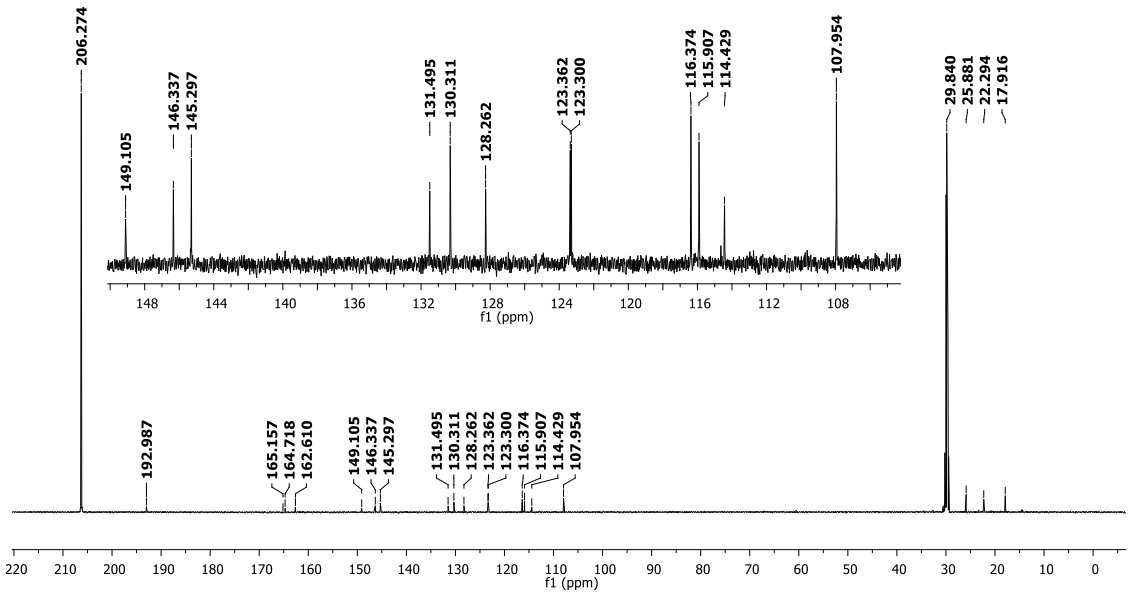

Figure S52c. HPLC chromatogram of **IBC 4**. Methanol:Water (3:1), 365 nm

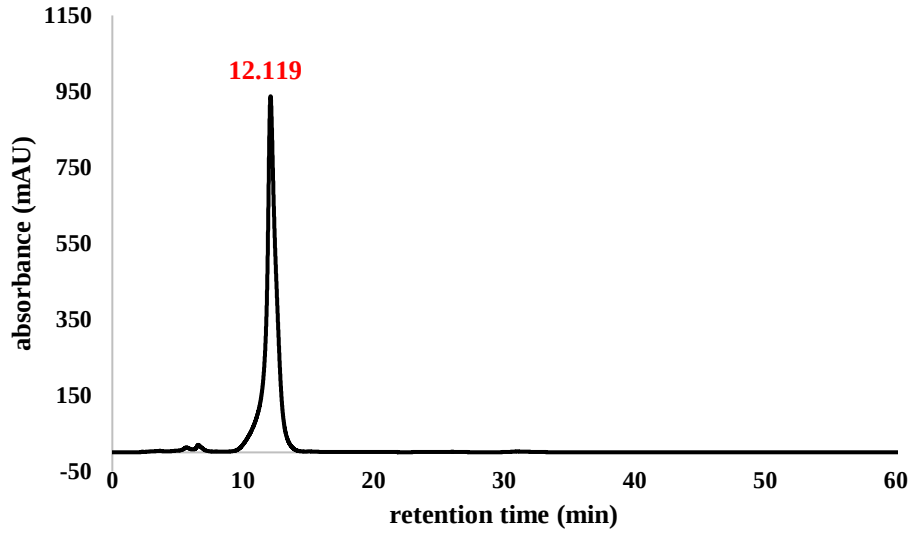

Figure S52d. UV-Vis spectrum of **IBC 4**

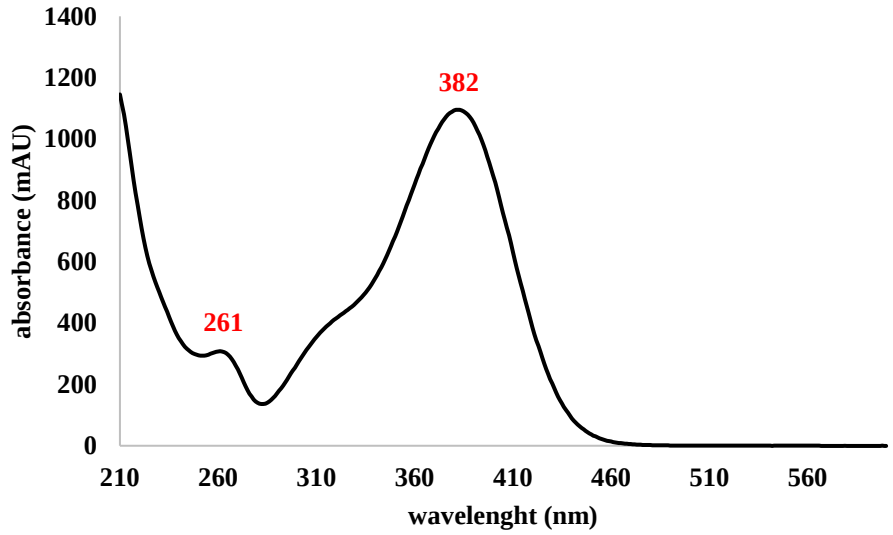

Figure S53a. ^{1}H NMR spectrum of **IBC 5** (Acetone-d_6; 600 MHz)

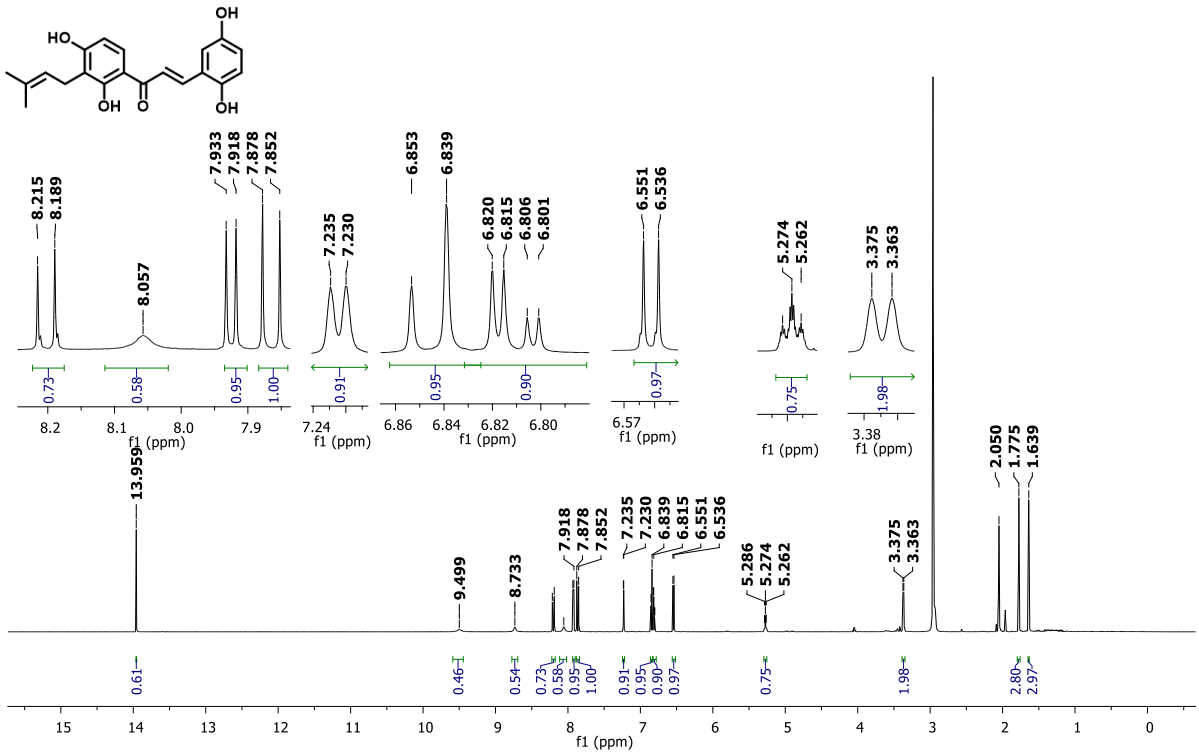

Figure S53b. ^{13}C NMR spectrum of **IBC 5** (Acetone-d_6; 150 MHz)

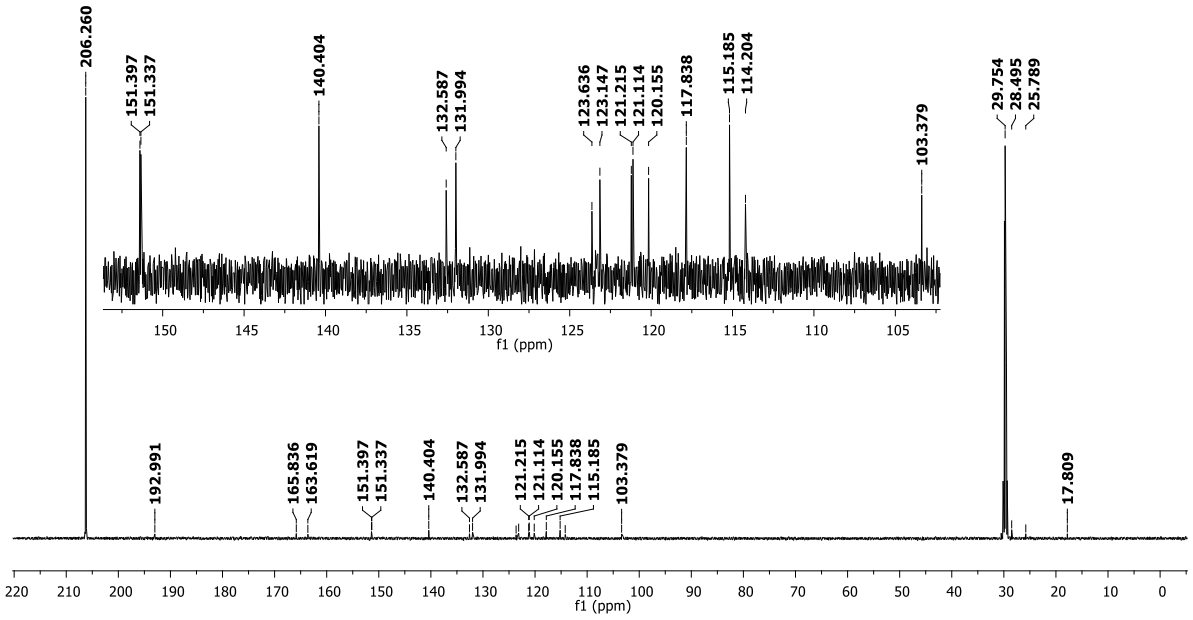

Figure S53c. HPLC chromatogram of **IBC 5**. Methanol:Water (3:1), 365 nm

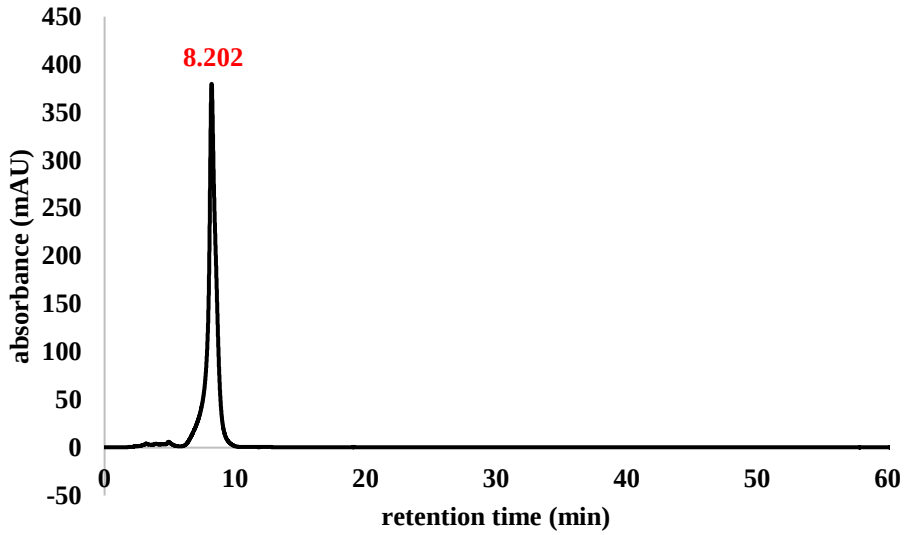

Figure S53d. UV-Vis spectrum of **IBC 5**

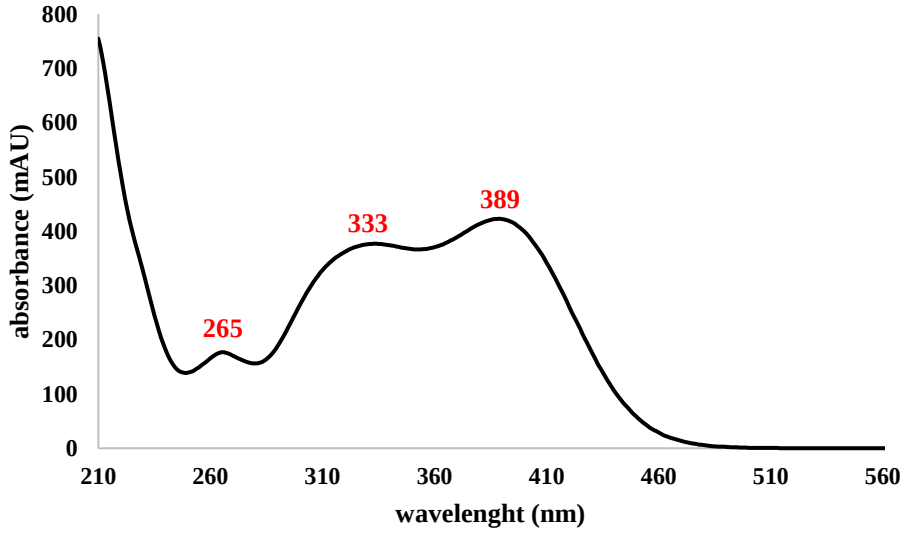

Figure S54a. ^{1}H NMR spectrum of **IBC 6** (Acetone-d_6; 600 MHz)

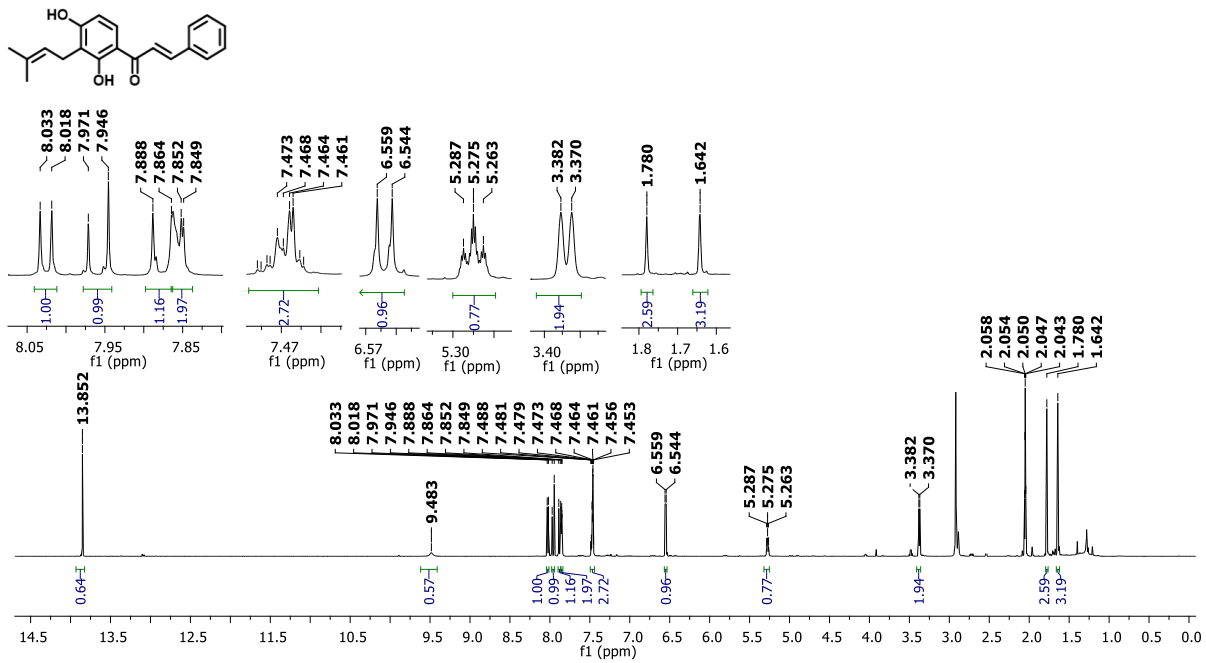

Figure S54b. ^{13}C NMR spectrum of **IBC 6** (Acetone-d_6; 150 MHz)

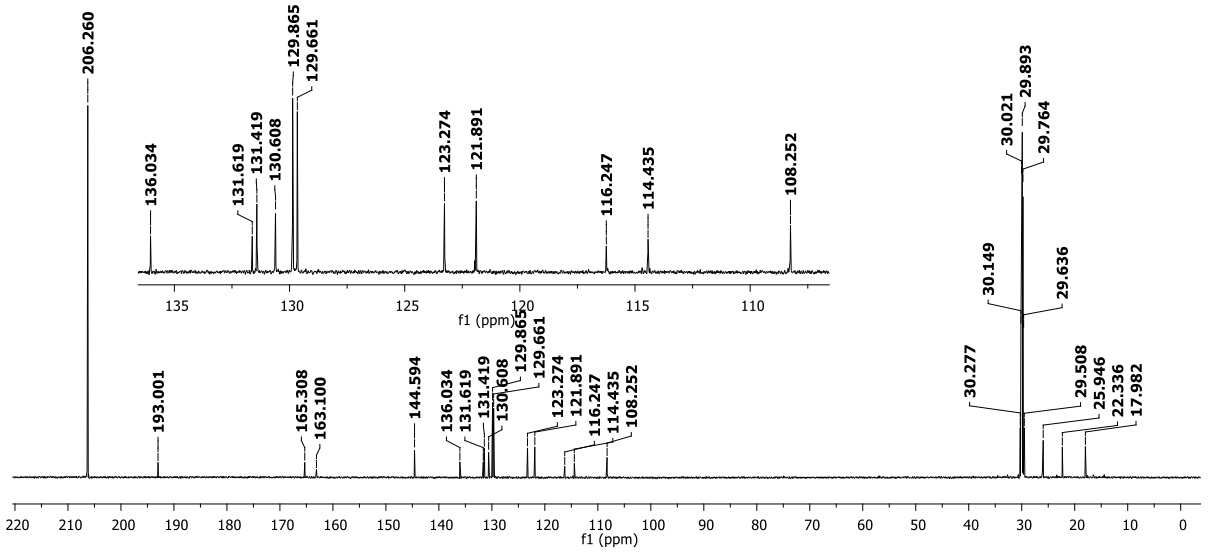

Figure S54c. HPLC chromatogram of **IBC 6**. Methanol:Water (3:1), 365 nm

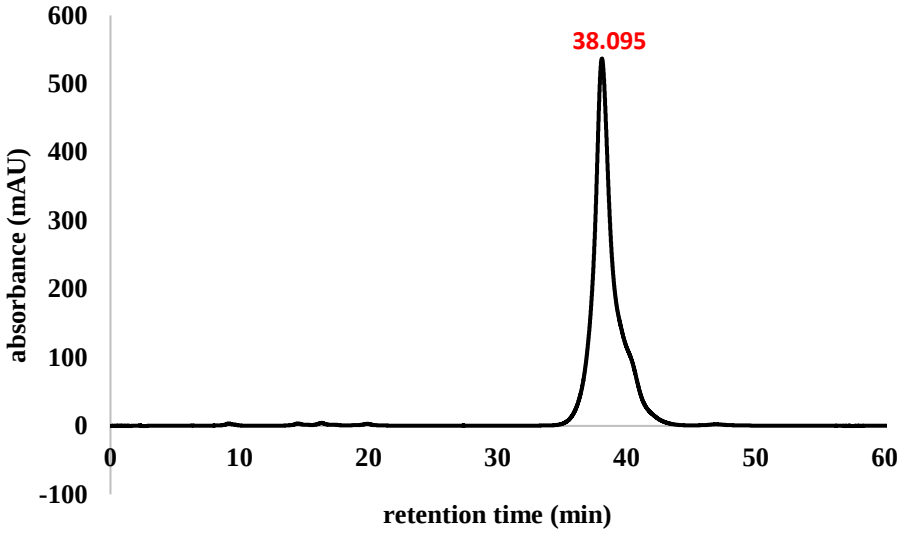

Figure S55a. ^{1}H NMR spectrum of **IBC 7** (Acetone-d_6; 600 MHz)

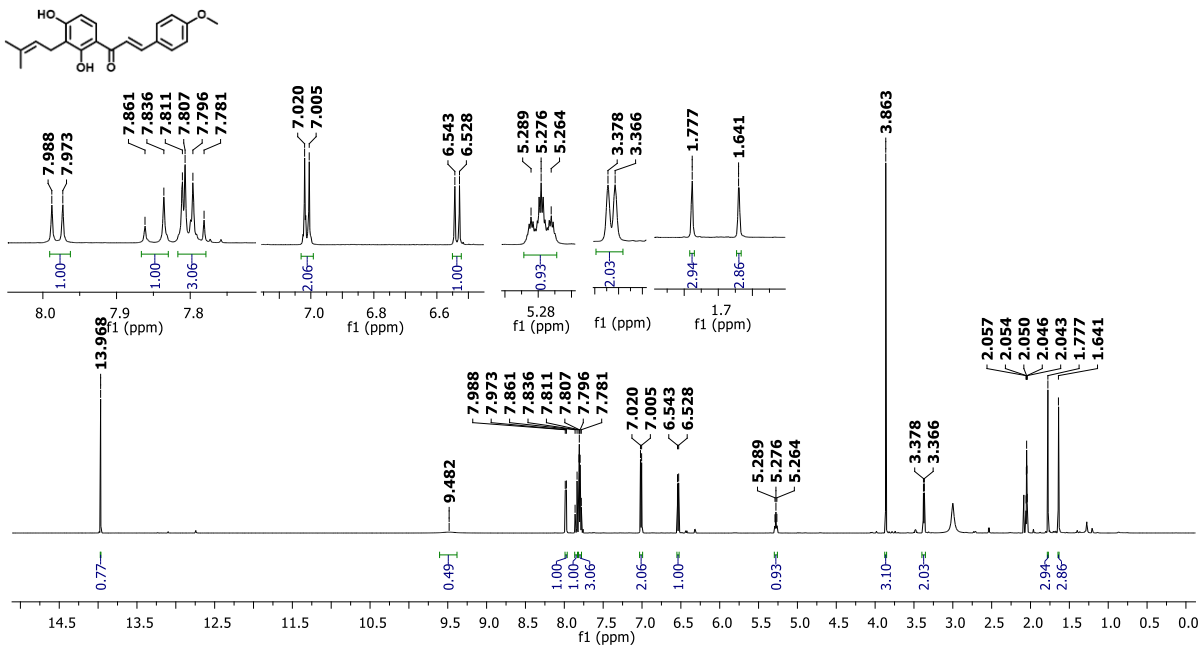

Figure S55b. ^{13}C NMR spectrum of **IBC 7** (Acetone-d_6; 150 MHz)

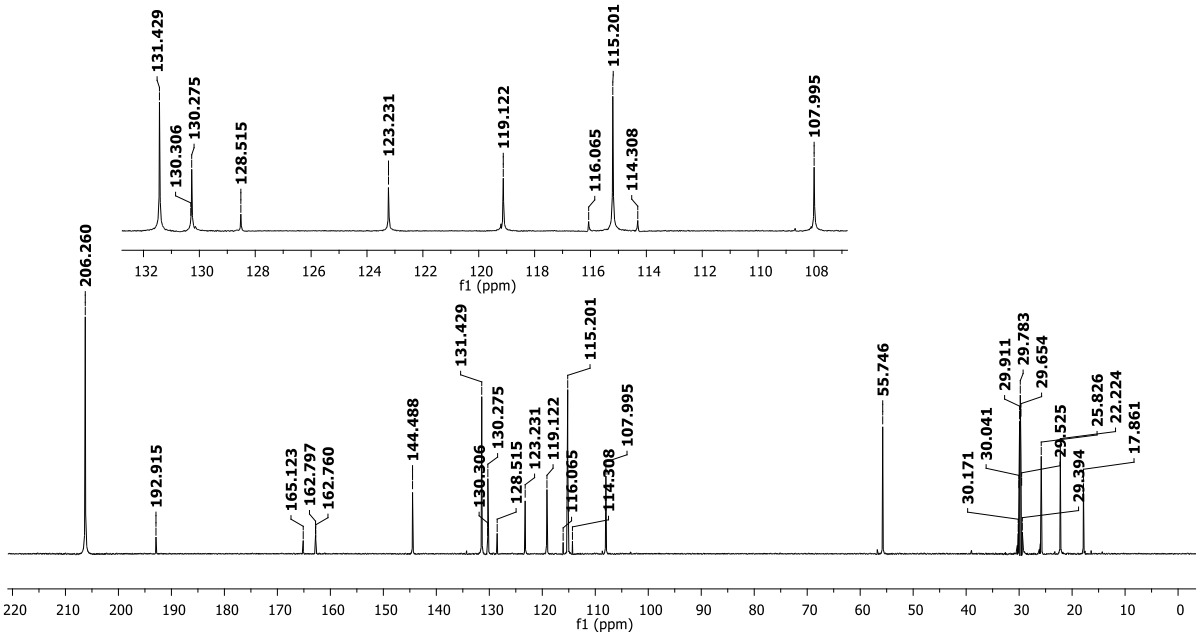

Figure S55c. HPLC chromatogram of **IBC 7**. Methanol:Water (3:1), 365 nm

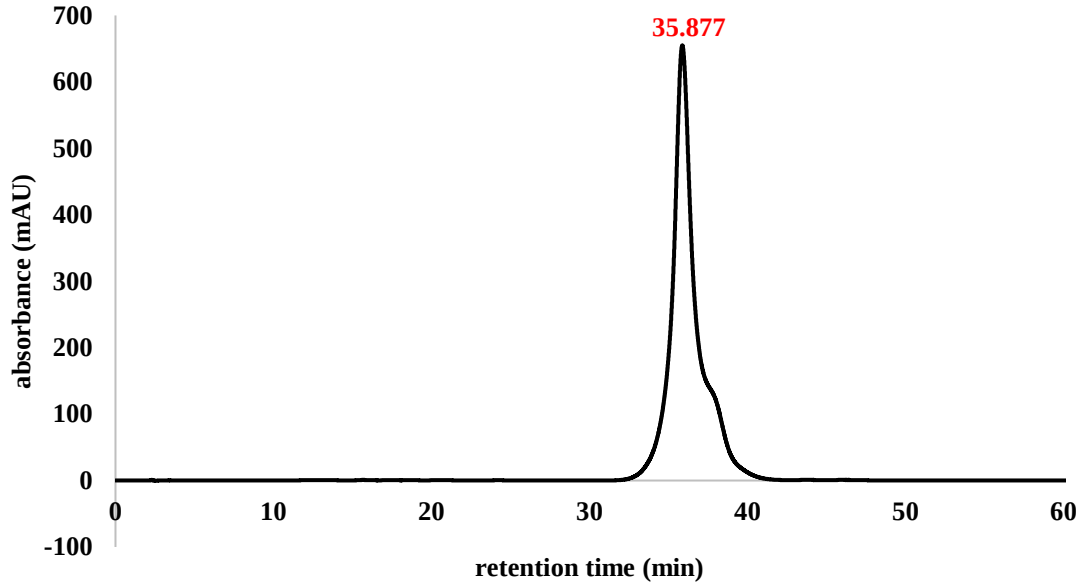

Figure S56a. ^{1}H NMR spectrum of **IBC 8** (DMSO-d_6; 600 MHz)

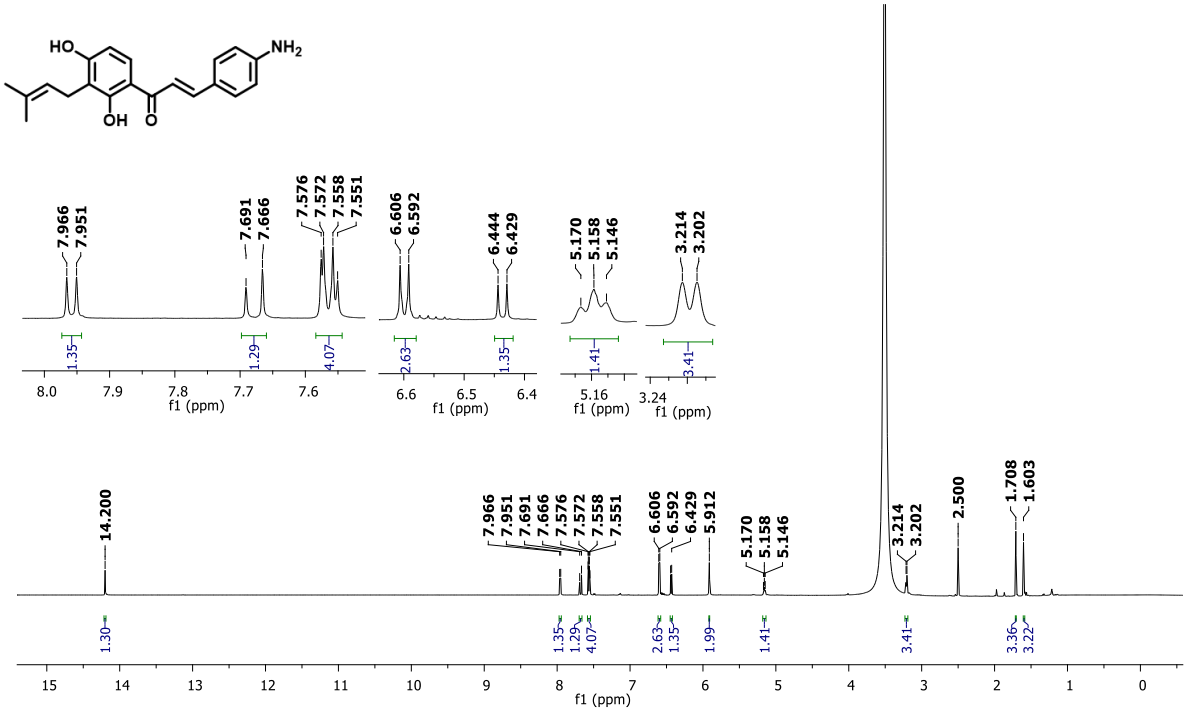

Figure S56b. ^{13}C NMR spectrum of **IBC 8** (DMSO-d_6; 150 MHz)

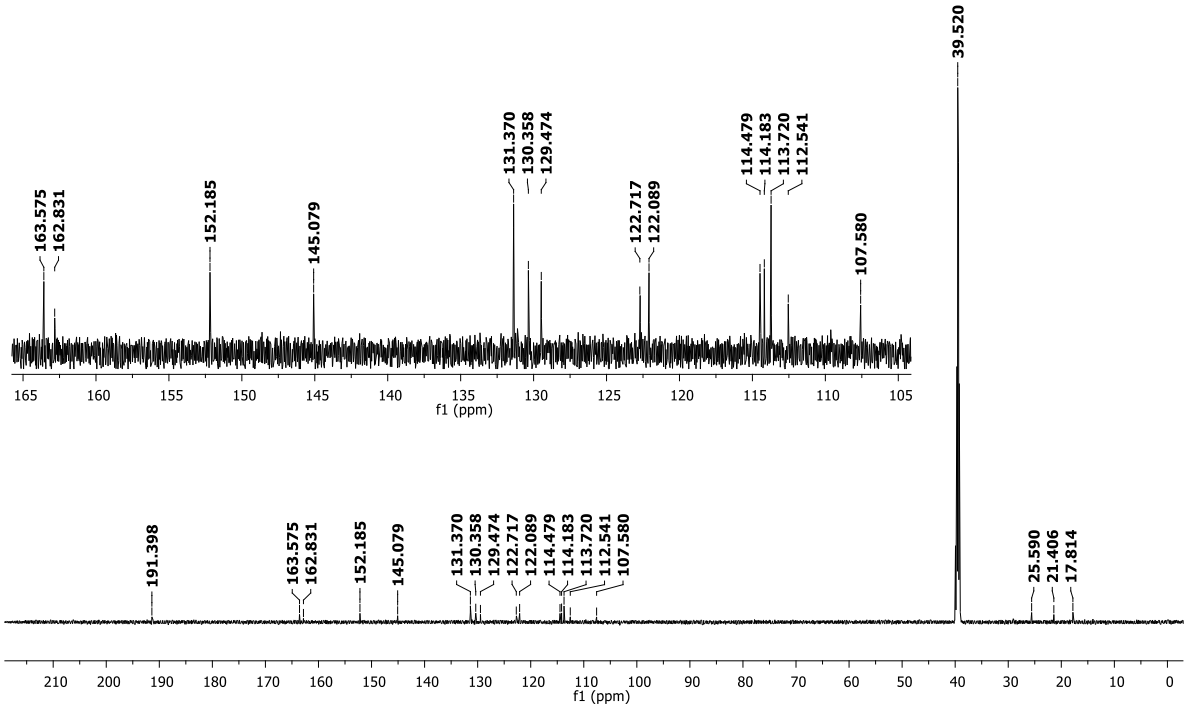

Figure S56c. HPLC chromatogram of **IBC 8**. Methanol:Water (3:1), 365 nm

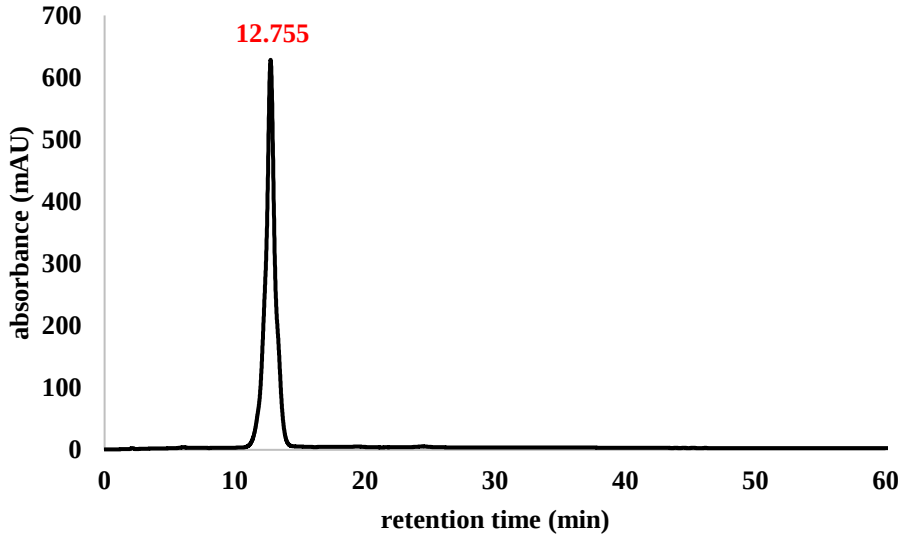

Figure S56d. UV-Vis spectrum of **IBC 8**

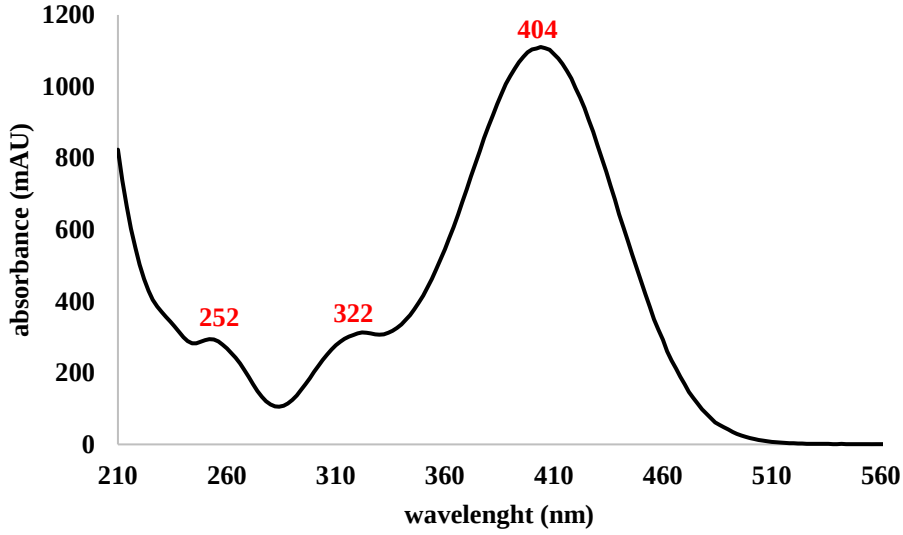

Figure S57a. ^{1}H NMR spectrum of **IBC 9** (Acetone-d_6; 600 MHz)

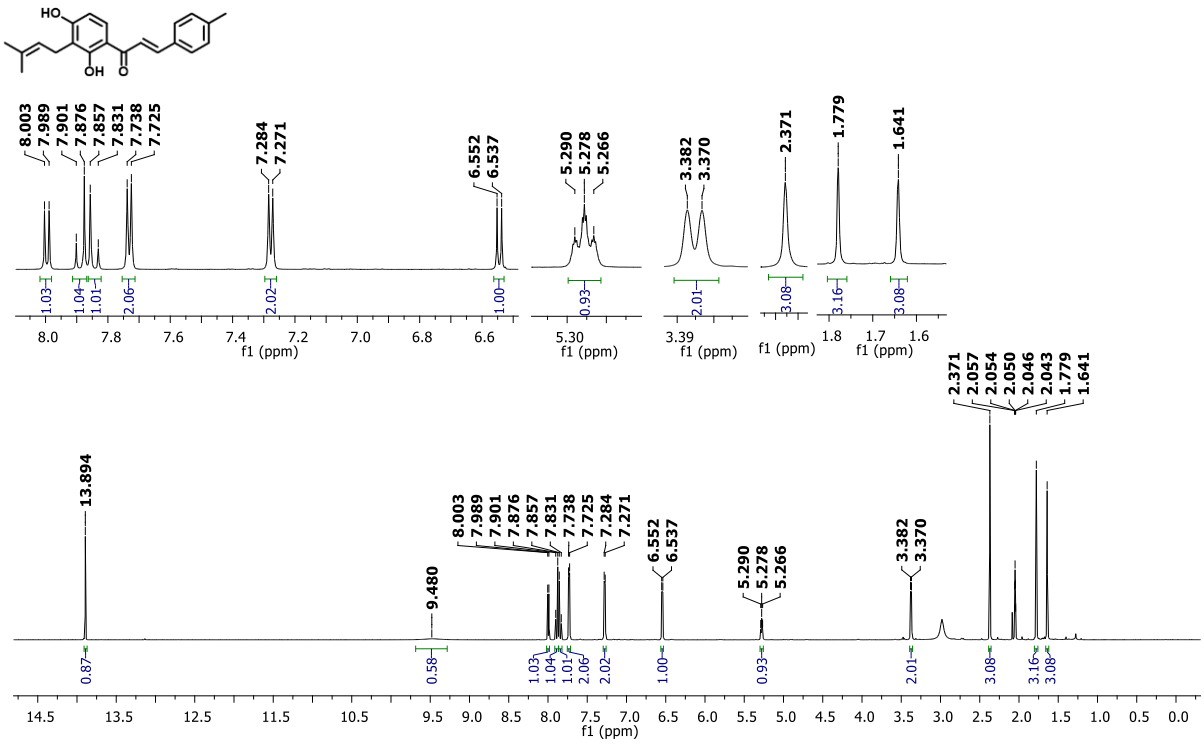

Figure S57b. ^{13}C NMR spectrum of **IBC 9** (Acetone-d_6; 150 MHz)

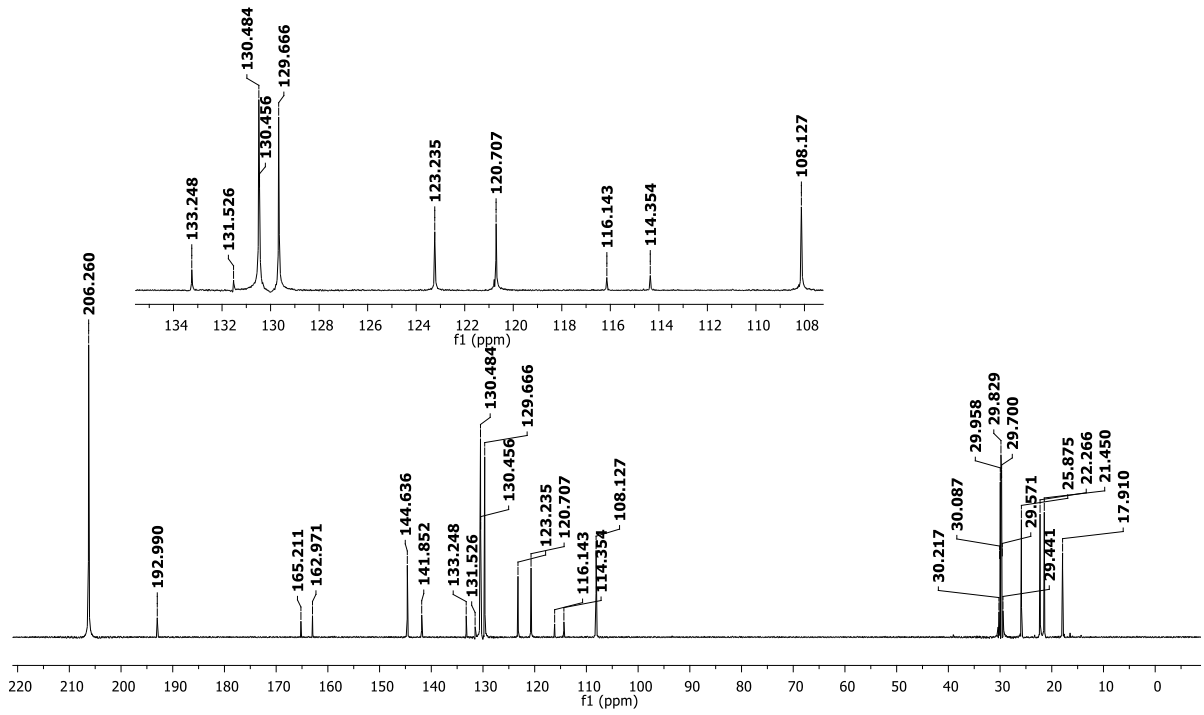

Figure S57c. HPLC chromatogram of **IBC 9**. Methanol:Water (4:1), 365 nm

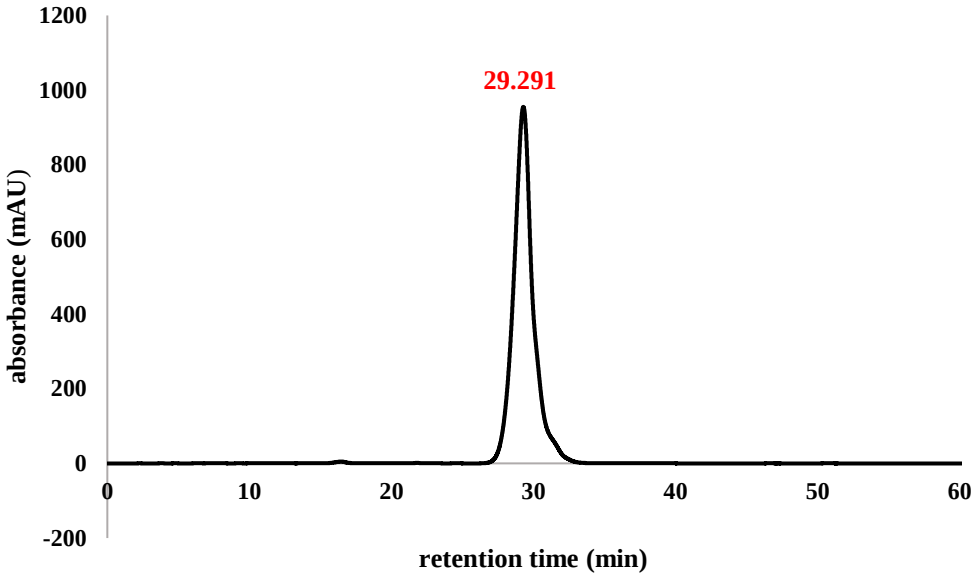

Figure S58a ^{1}H NMR spectrum of **IBC 10** (Acetone-d_6; 600 MHz)

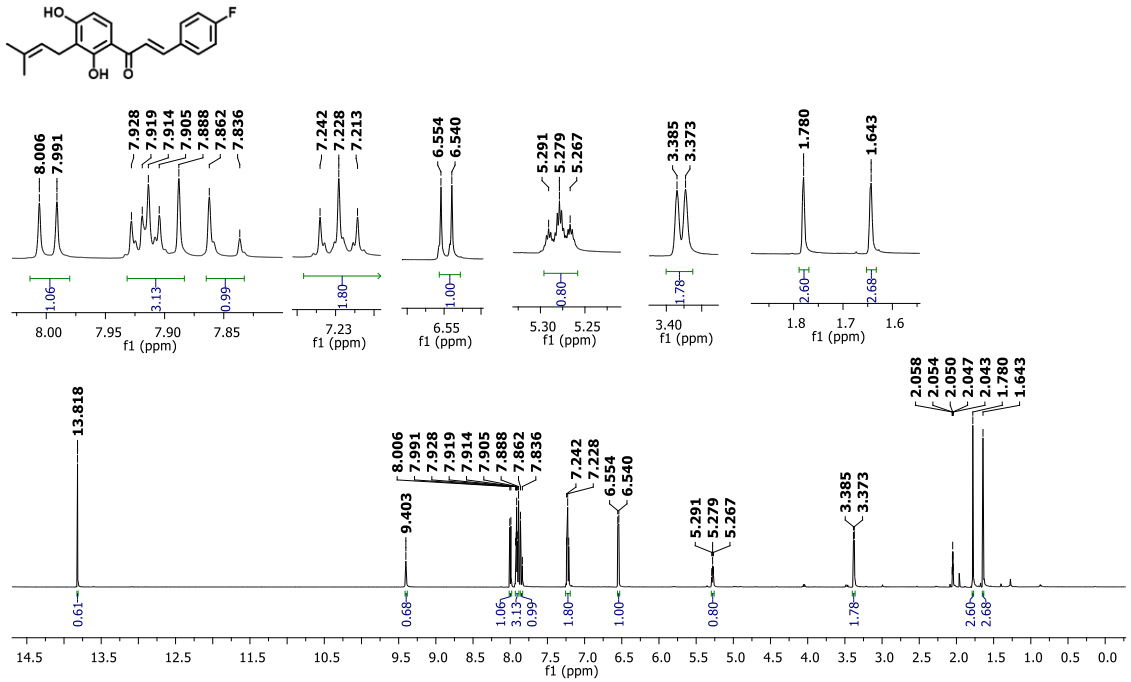

Figure S58b. ^{13}C NMR spectrum of **IBC 10** (Acetone-d_6; 150 MHz)

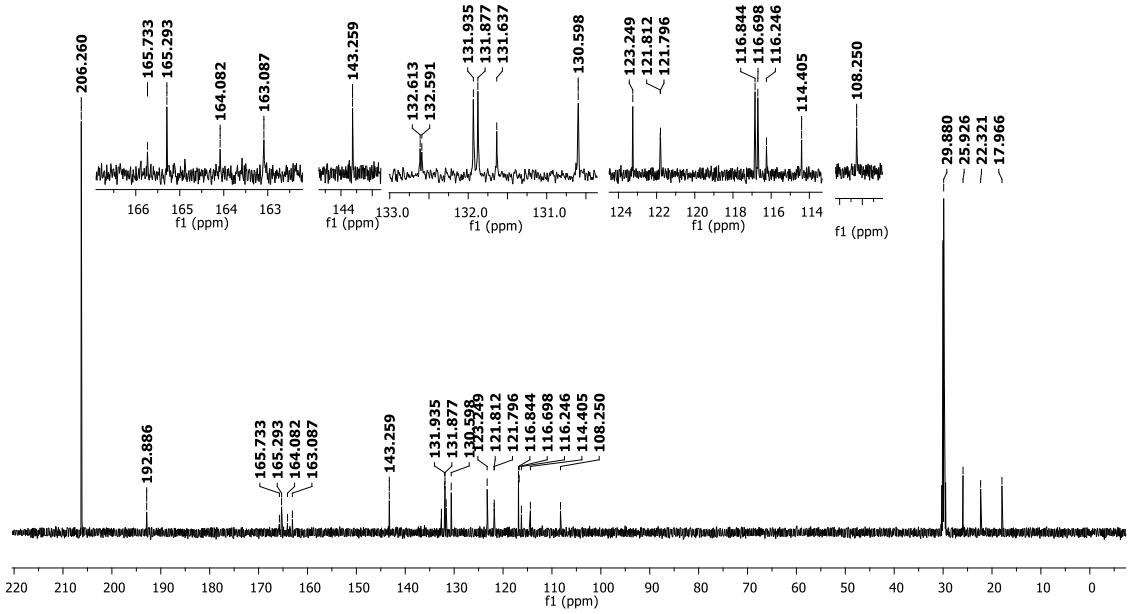

Figure S58c. HPLC chromatogram of **IBC 10**. Methanol:Water (4:1), 365 nm

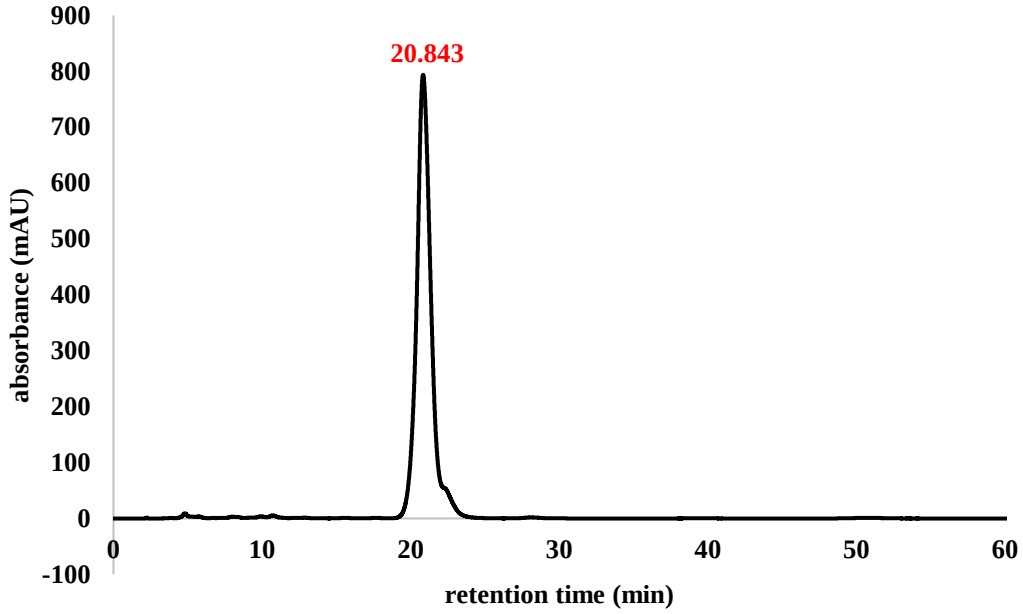

Figure S58d. UV-Vis spectrum of **IBC 10**

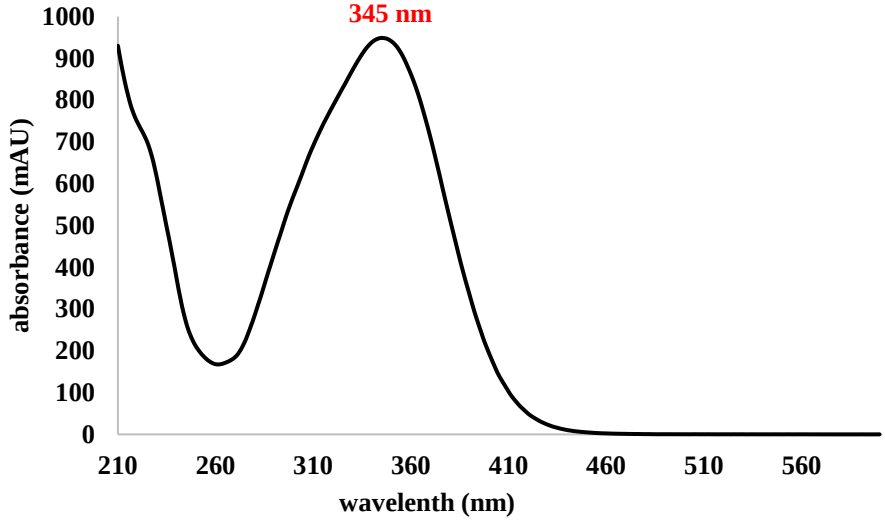

Figure S59a. ^{1}H NMR spectrum of **IBC 11** (Acetone-d_6; 600 MHz)

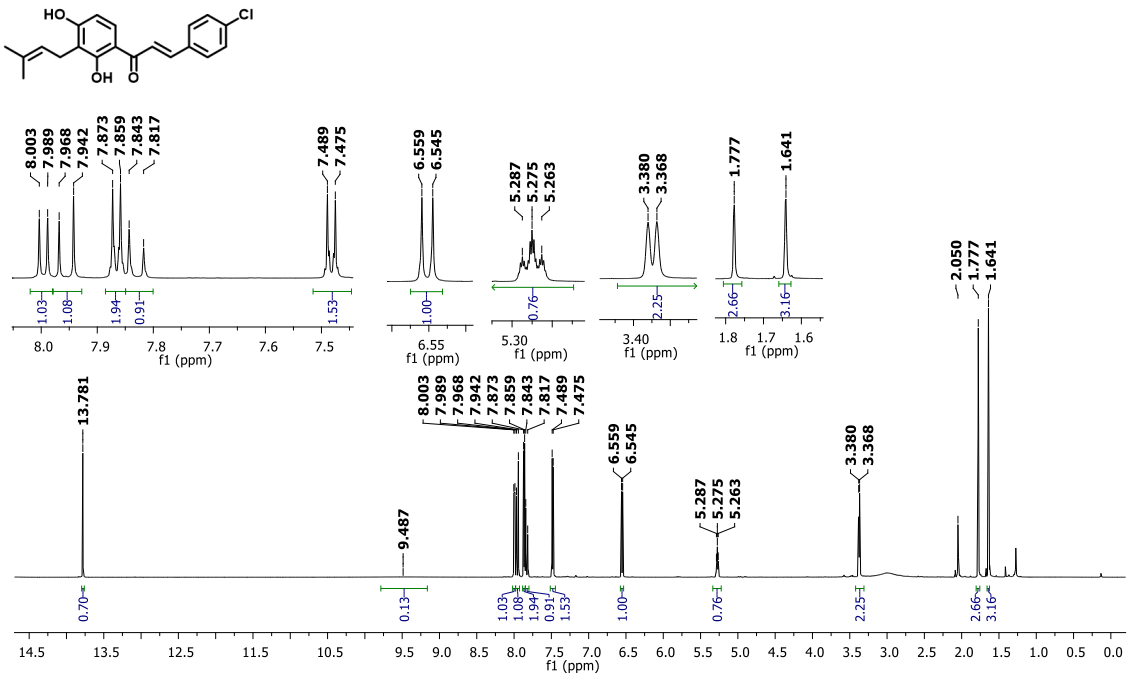

Figure S59b. ^{13}C NMR spectrum of **IBC 11** (Acetone-d_6; 150 MHz)

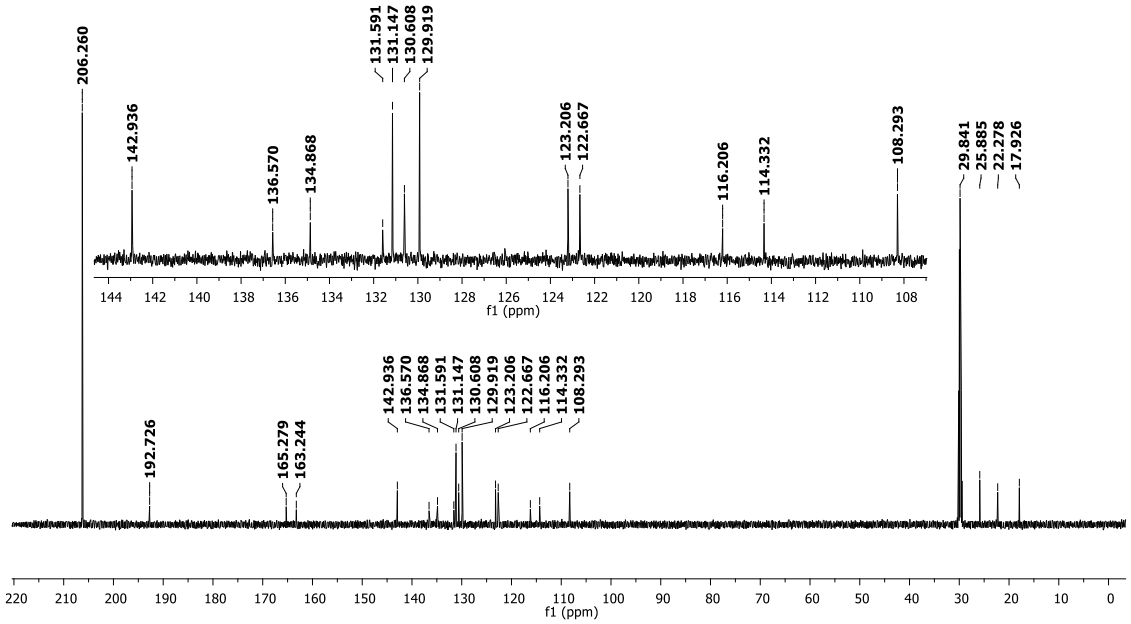

Figure S59c. HPLC chromatogram of **IBC 11**. Methanol:Water (4:1), 365 nm

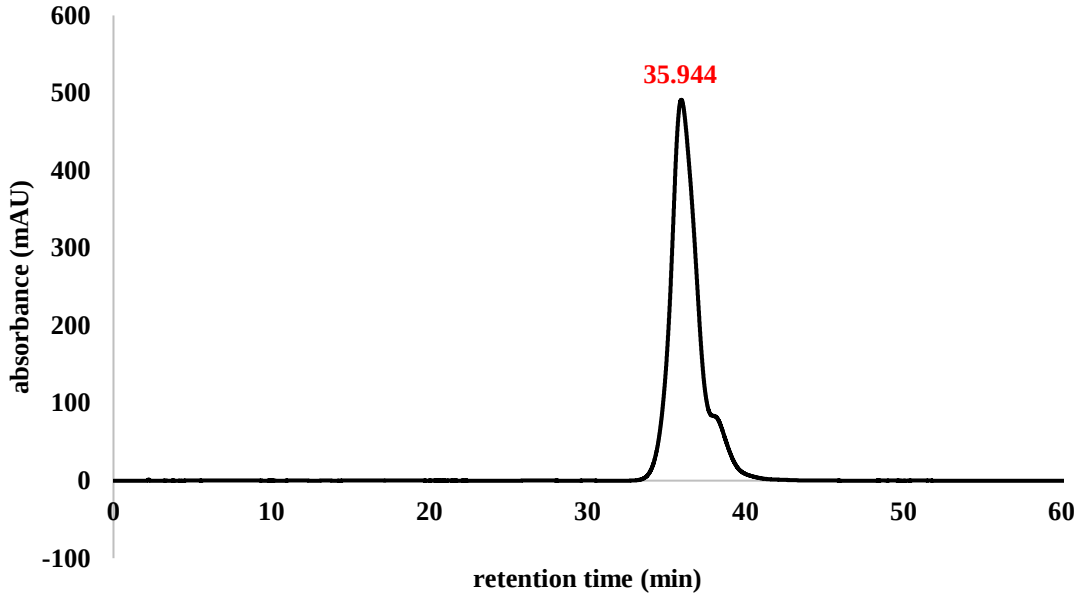

Figure S60a. ^{1}H NMR spectrum of **IBC 12** (Acetone-d_6; 600 MHz)

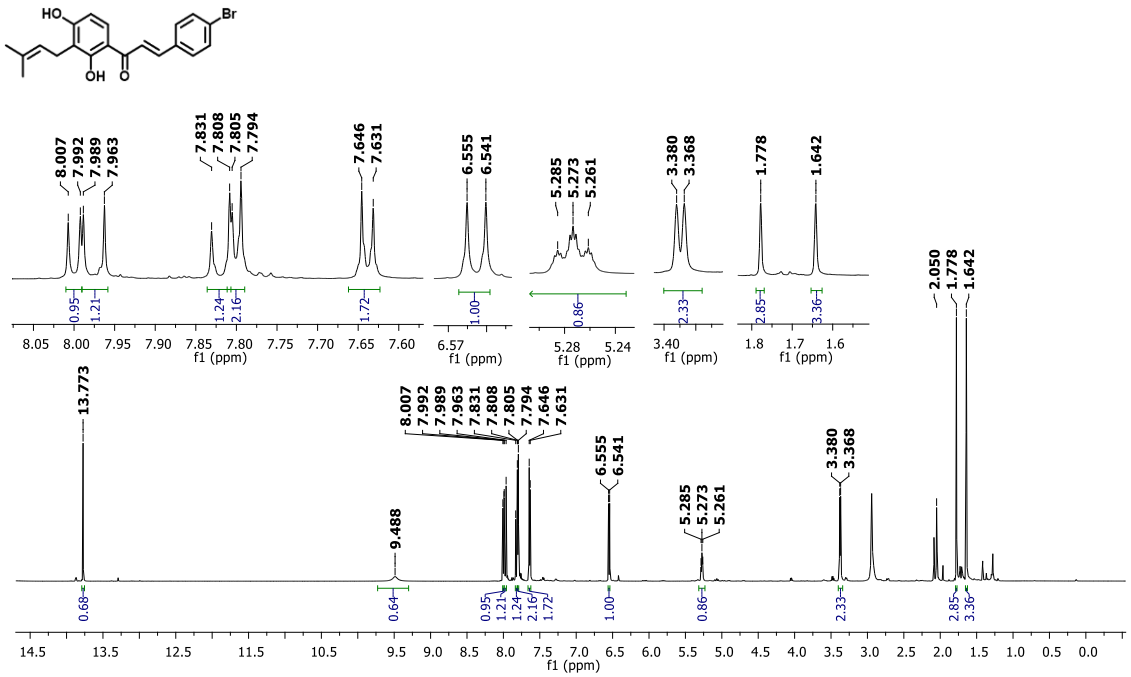

Figure S60b. ^{13}C NMR spectrum of **IBC 12** (Acetone-d_6; 150 MHz)

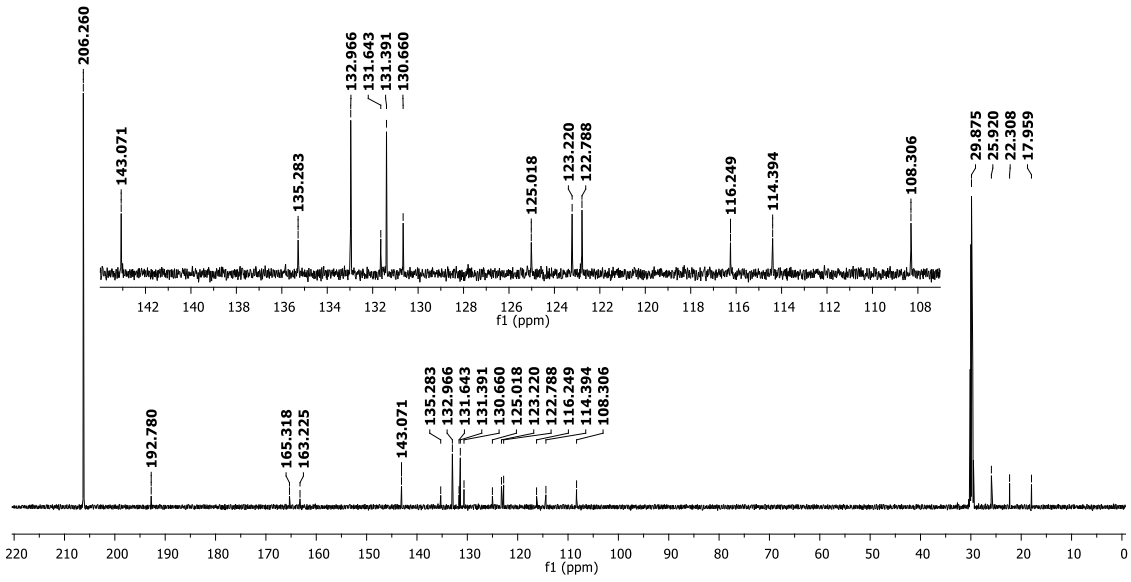

Figure S60c. HPLC chromatogram of **IBC 12**. Methanol:Water (4:1), 365 nm

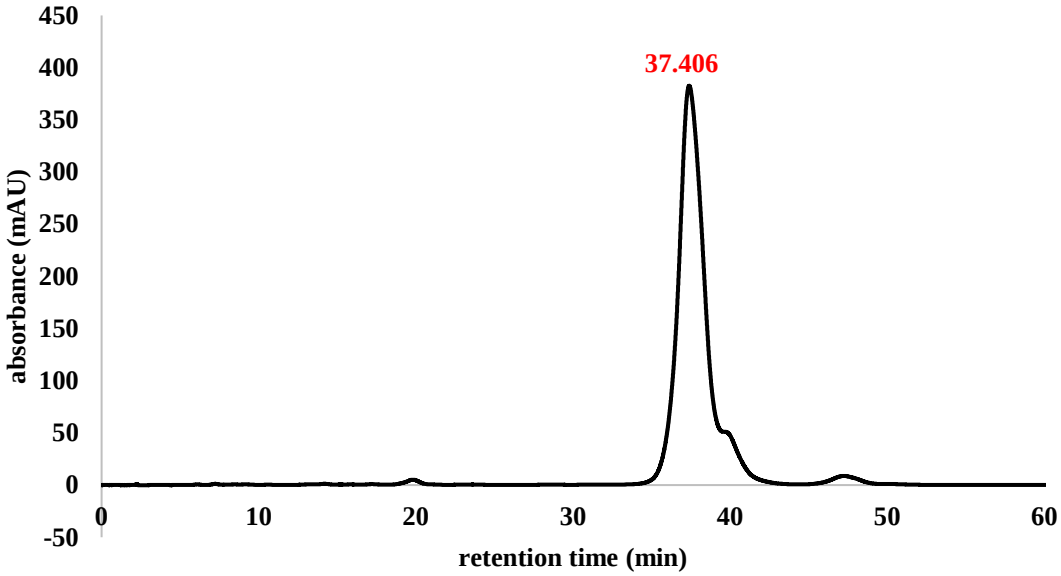

Figure S61a. ^{1}H NMR spectrum of **IBC 13** (Acetone-d_6; 600 MHz)

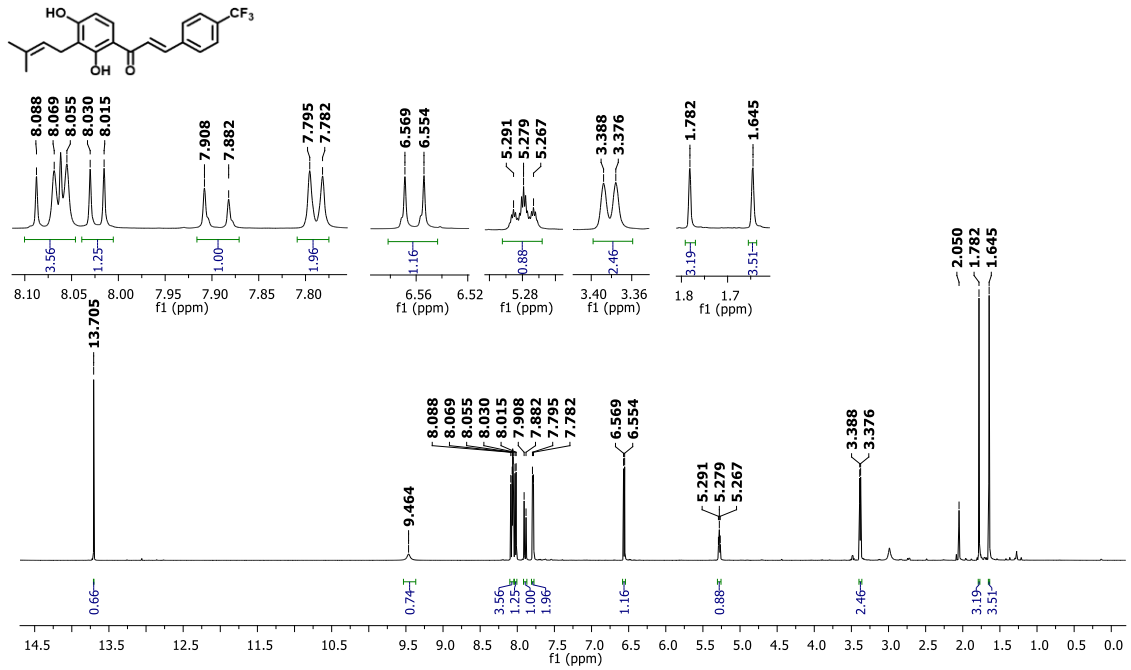

Figure S61b. ^{13}C NMR spectrum of **IBC 13** (Acetone-d_6; 150 MHz)

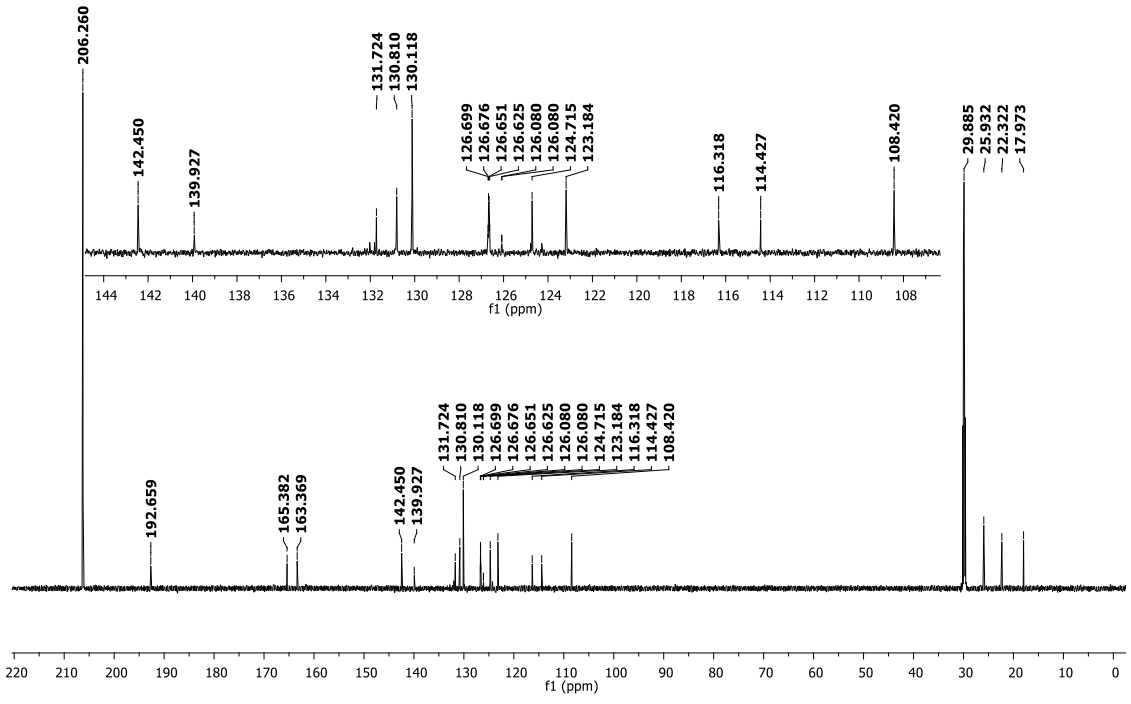

Figure S61c. HPLC chromatogram of **IBC 13**. Methanol:Water (4:1), 365 nm

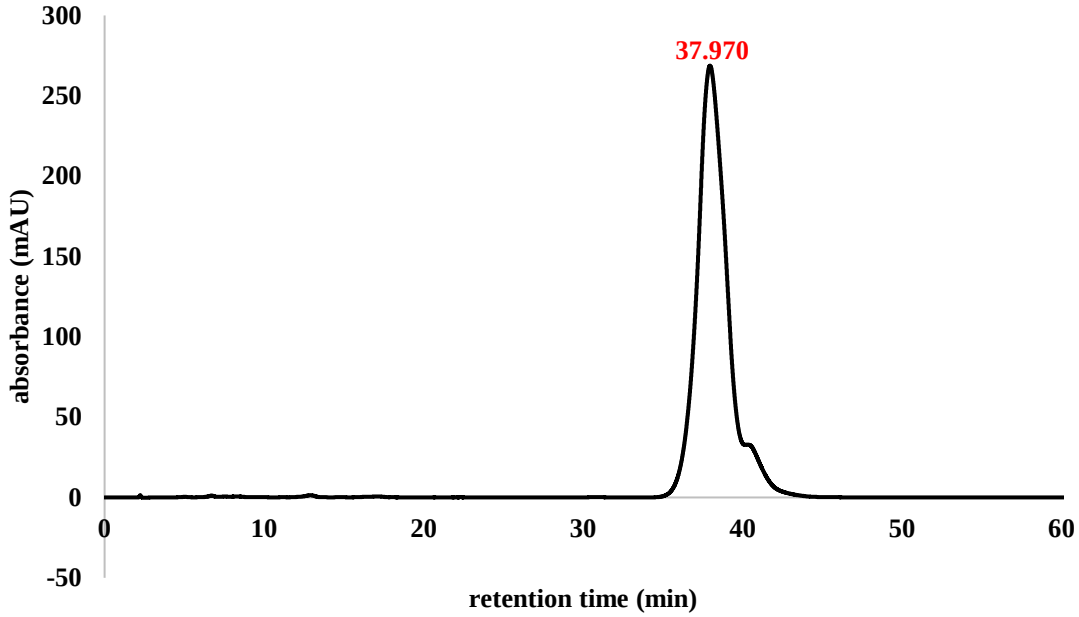

Figure S62a. ^{1}H NMR spectrum of **IBC 14** (Acetone-d_6; 600 MHz)

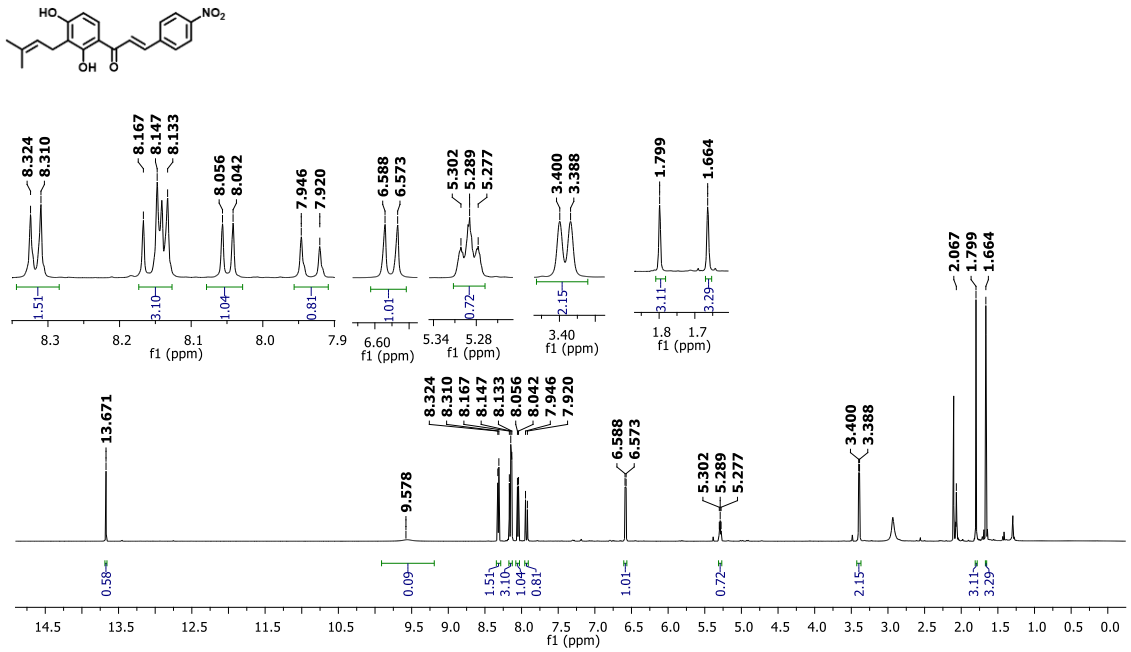

Figure S62b. ^{13}C NMR spectrum of **IBC 14** (Acetone-d_6; 150 MHz)

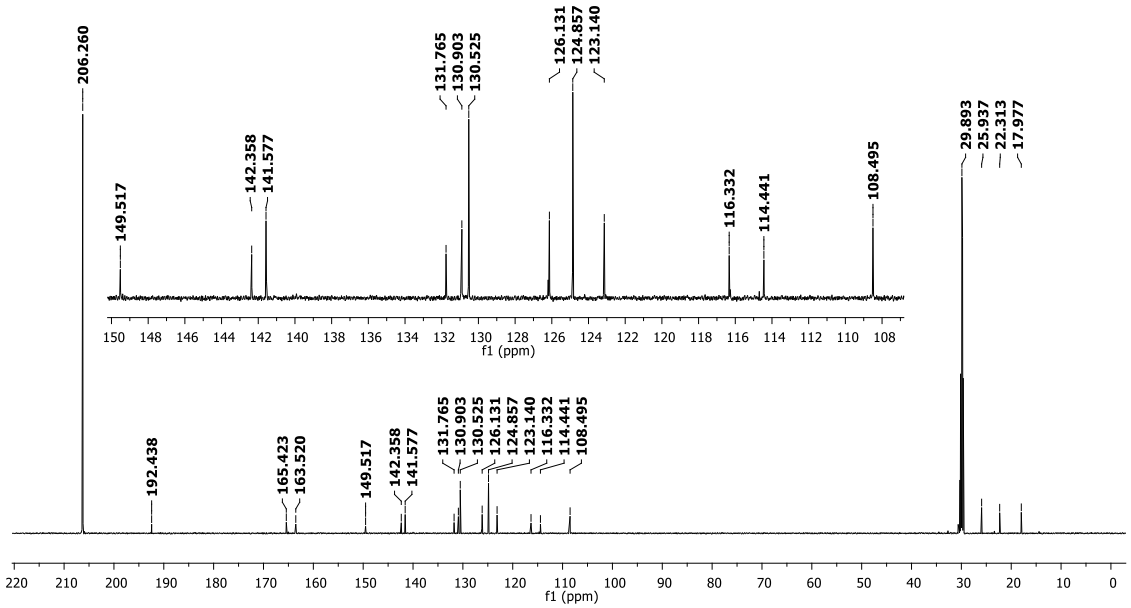

Figure S62c. HPLC chromatogram of **IBC 14**. Methanol:Water (3:1), 365 nm

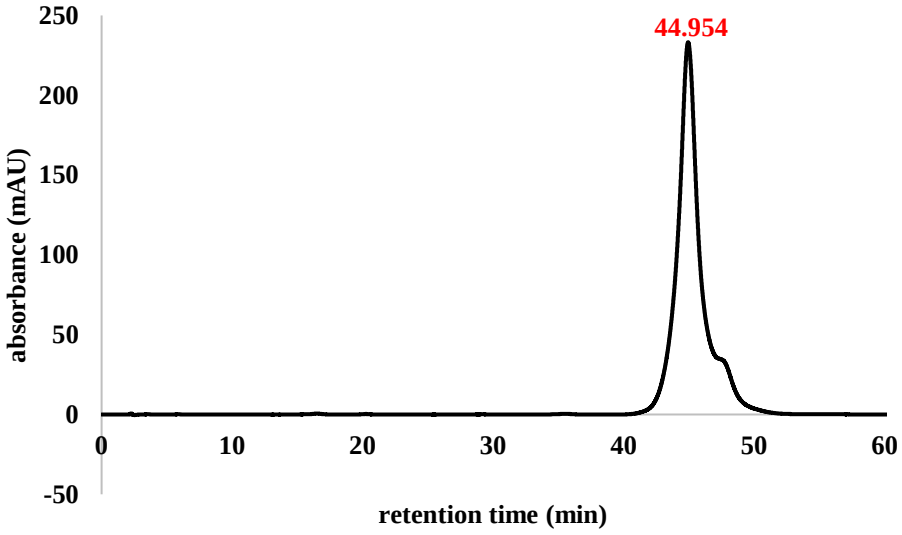

Figure S63a. ^{1}H NMR spectrum of **IBC 15** (DMSO-d_6; 600 MHz)

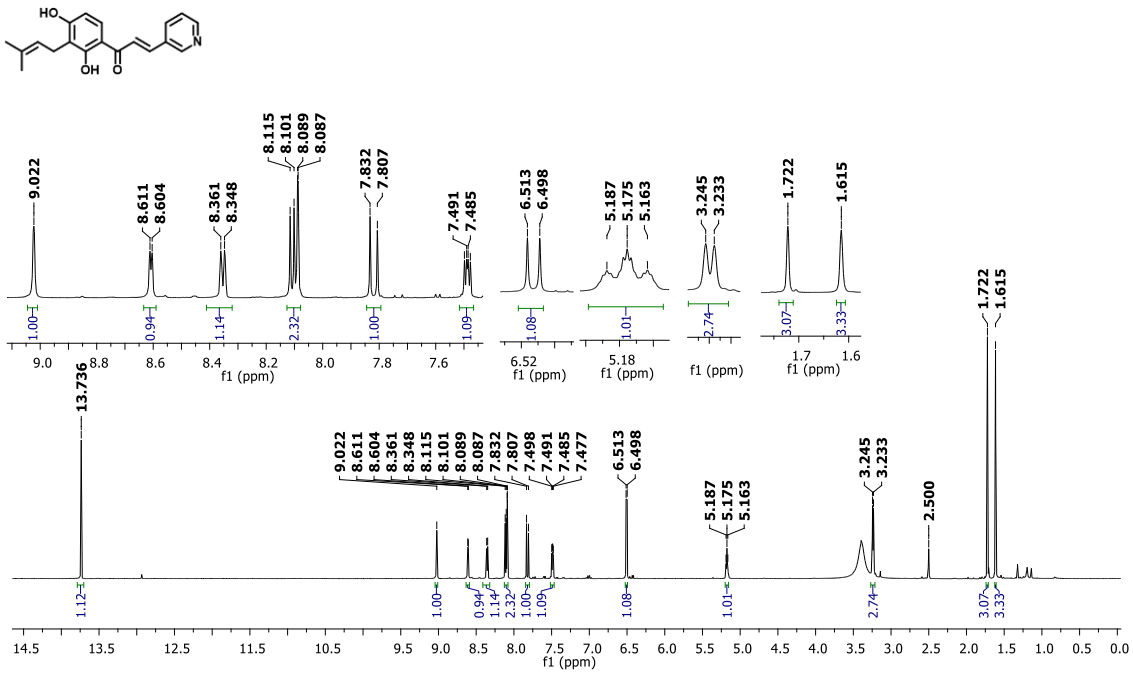

Figure S63b. ^{13}C NMR spectrum of **IBC 15** (DMSO-d_6; 150 MHz)

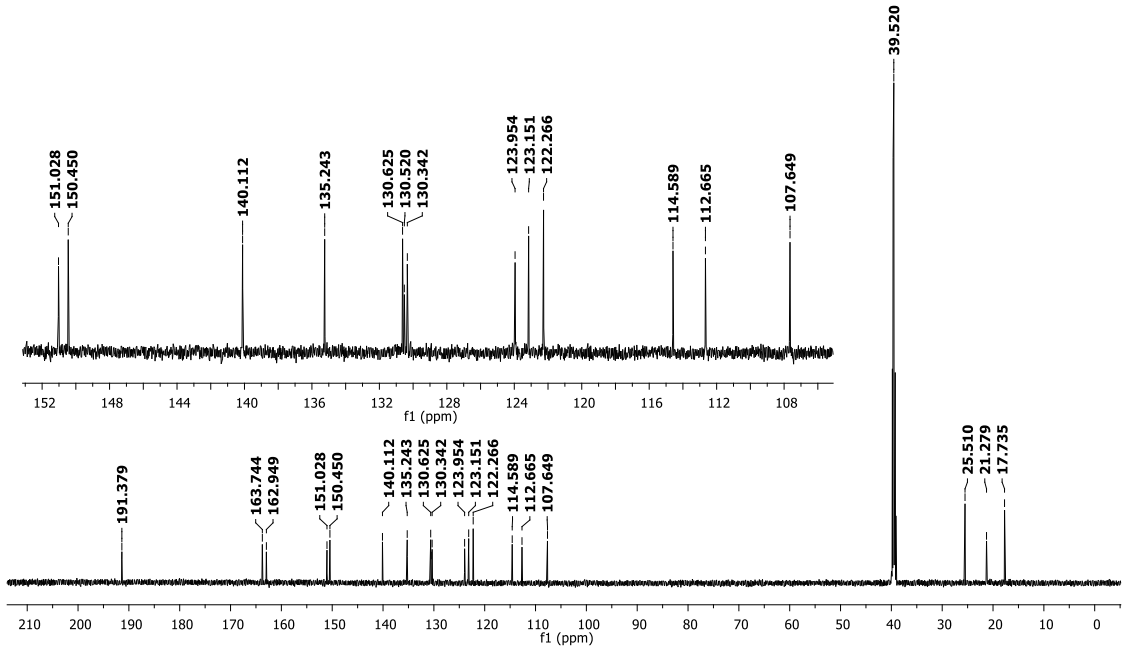

Figure S63c. HPLC chromatogram of **IBC 15**. Methanol:Water (3:1), 365 nm

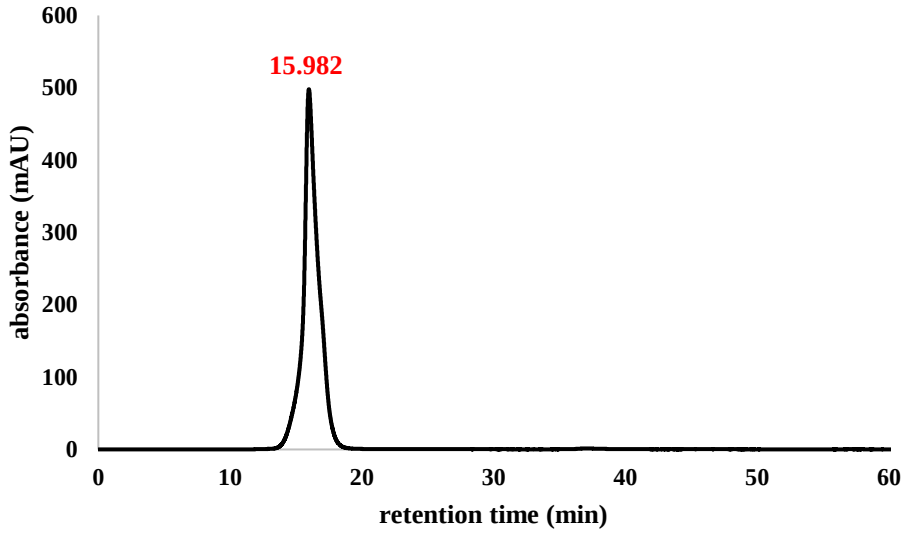

Figure S64a. ^{1}H NMR spectrum of **IBC 16** (DMSO-d_6; 600 MHz)

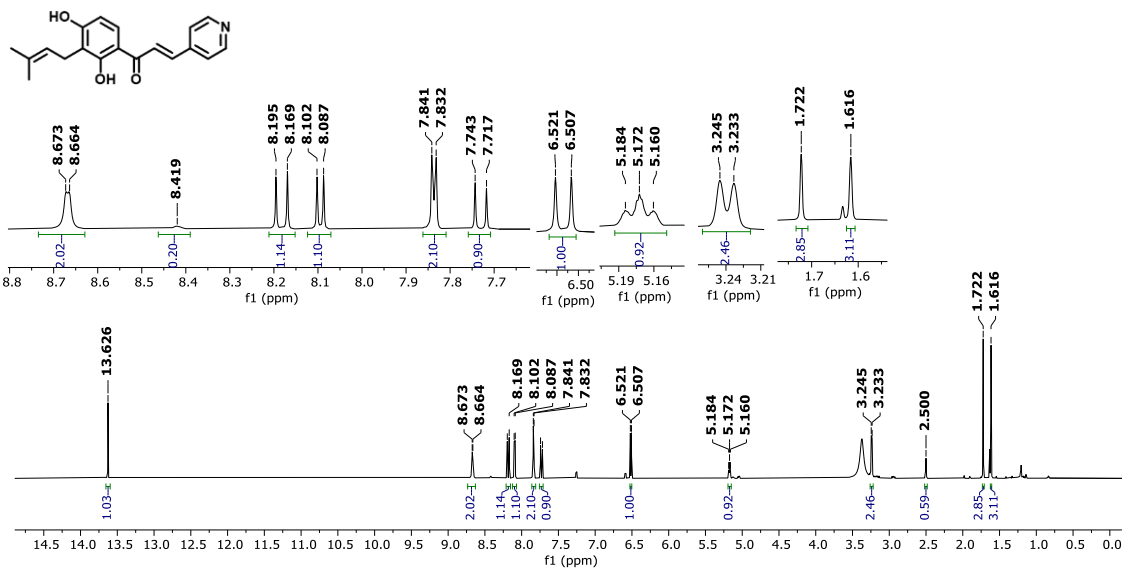

Figure S64b. ^{13}C NMR spectrum of **IBC 16** (DMSO-d_6; 150 MHz)

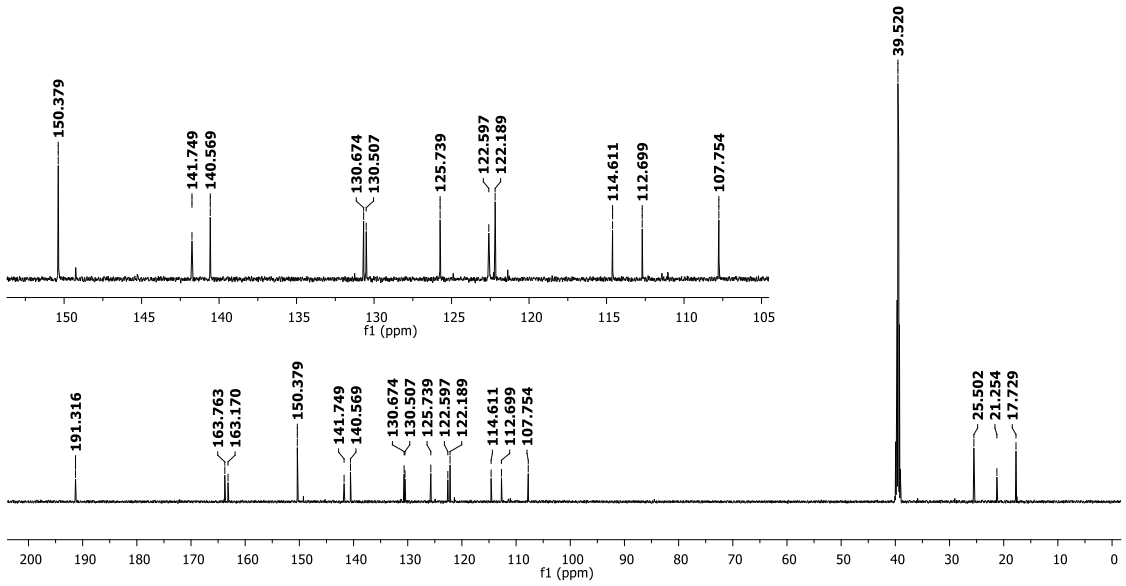

Figure S64c. HPLC chromatogram of **IBC 16**. Methanol:Water (3:1), 365 nm

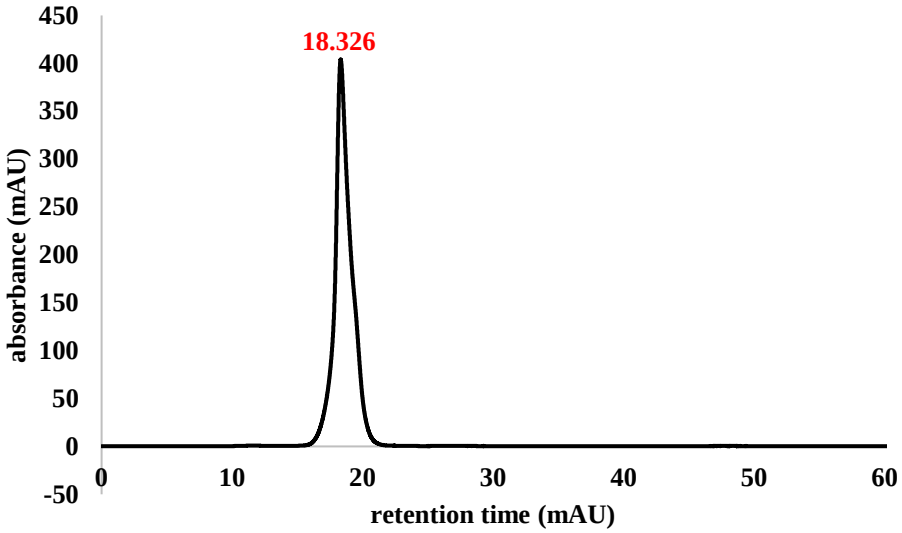

Figure S65a. ^{1}H NMR spectrum of **IBC 17** (Acetone-d_6; 600 MHz)

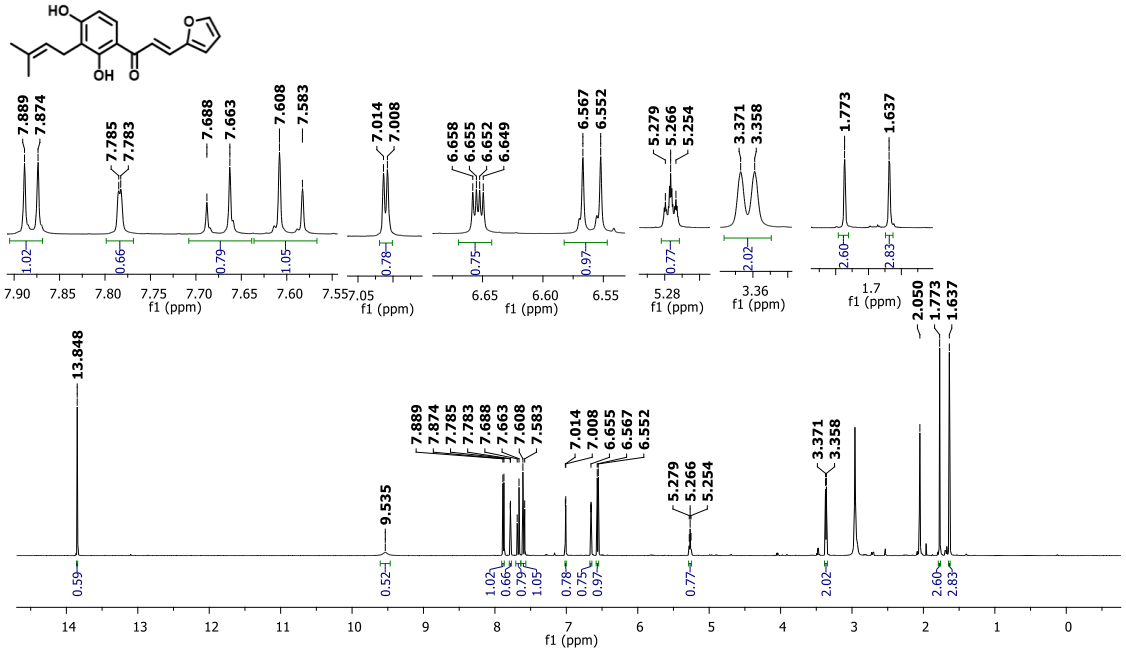

Figure S65b. ^{13}C NMR spectrum of **IBC 17** (Acetone-d_6; 150 MHz)

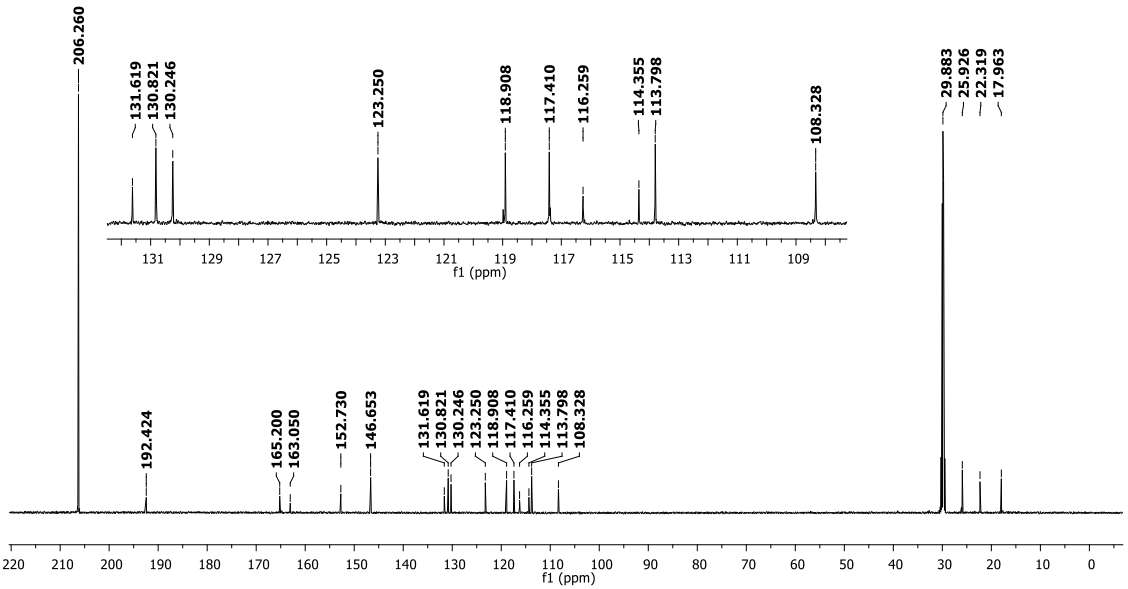

Figure S65c. HPLC chromatogram of **IBC 17**. Methanol:Water (3:1), 365 nm

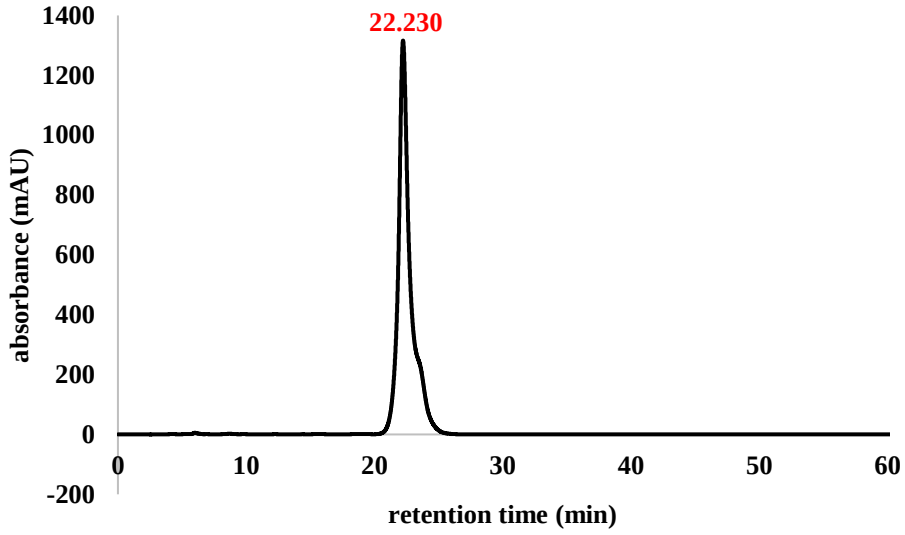

Figure S65d. UV-Vis spectrum of **IBC 17**

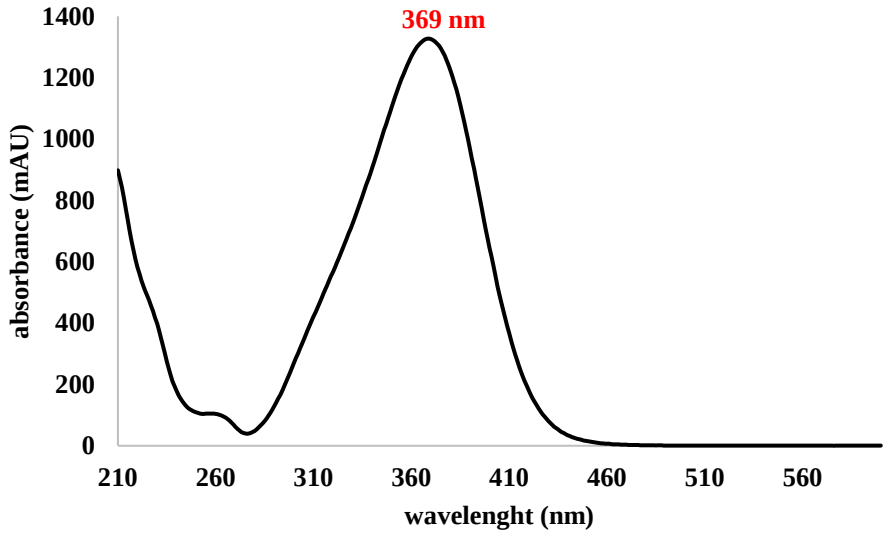

Figure S66a. ^{1}H NMR spectrum of **IBC 18** (Acetone-d_6; 600 MHz)

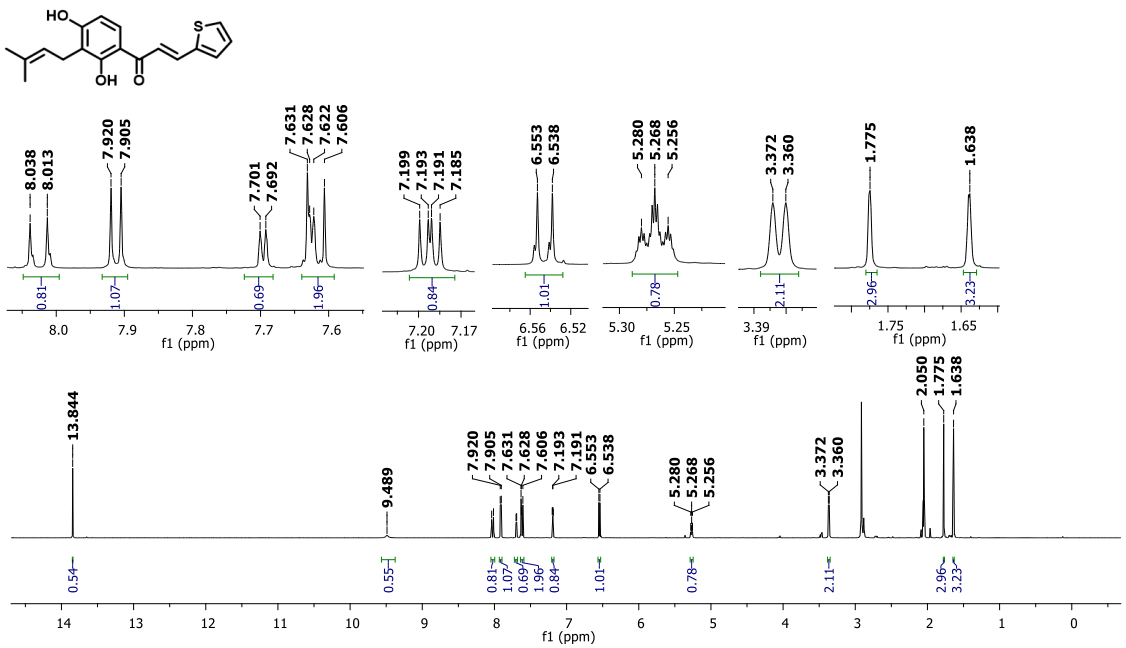

Figure S66b. ^{13}C NMR spectrum of **IBC 18** (Acetone-d_6; 150 MHz)

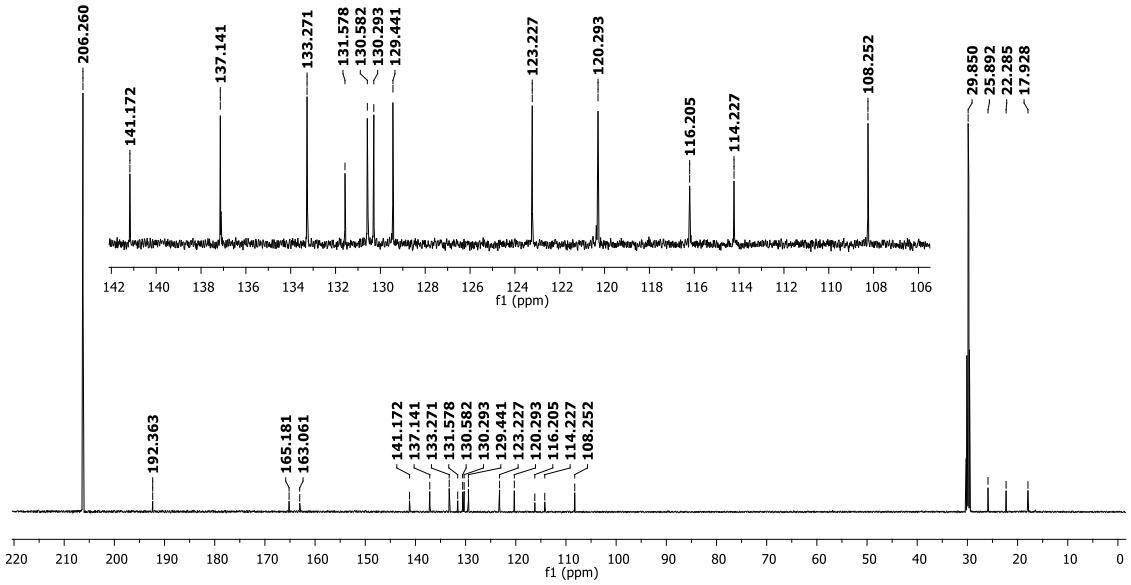

Figure S66c. HPLC chromatogram of **IBC 18**. Methanol:Water (3:1), 365 nm

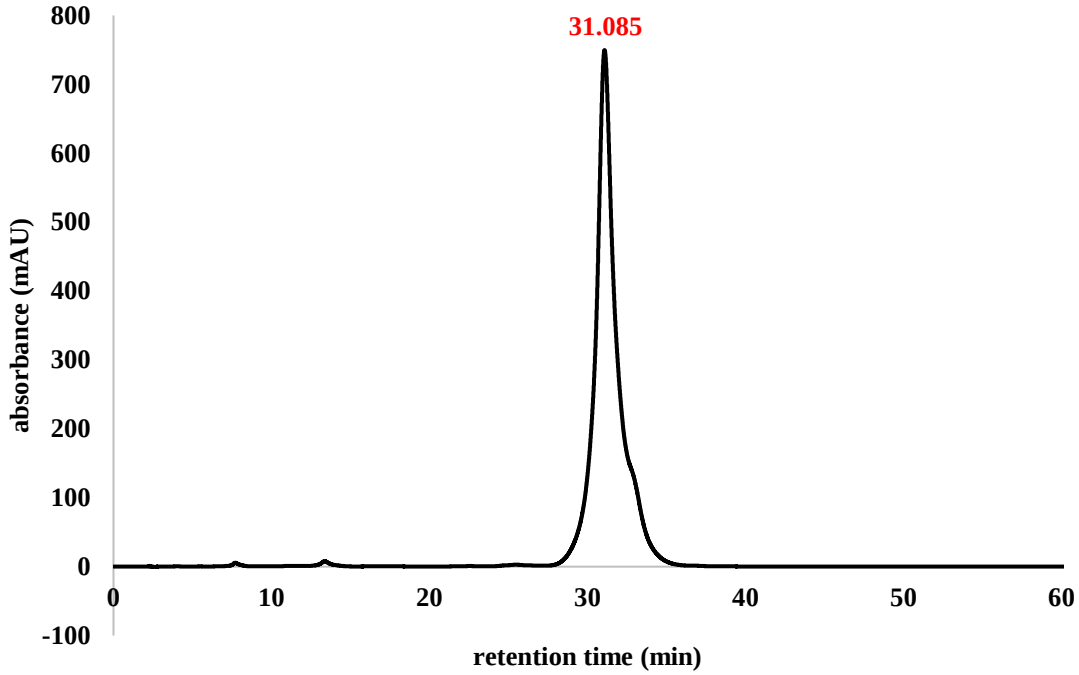

Figure S67a. ^{1}H NMR spectrum of **IBC 19** (Acetone-d_6; 600 MHz)

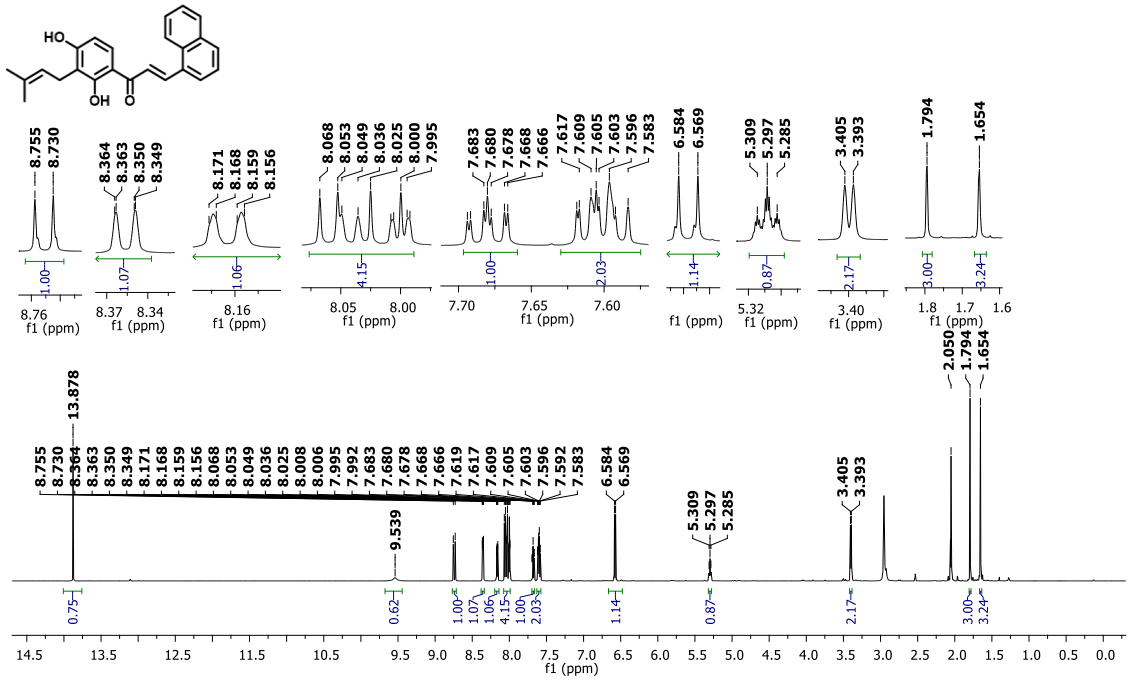

Figure S67b. ^{1}H NMR spectrum of **IBC 19** (Acetone-d_6; 150 MHz)

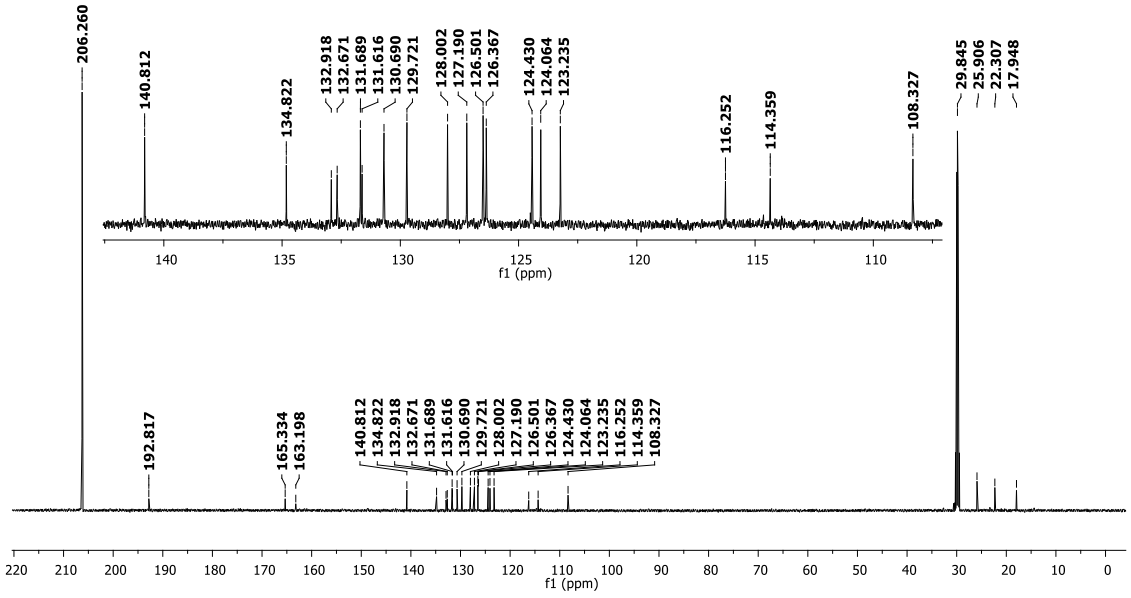

Figure S67c. HPLC chromatogram of **IBC 19**. Methanol:Water (4:1), 365 nm

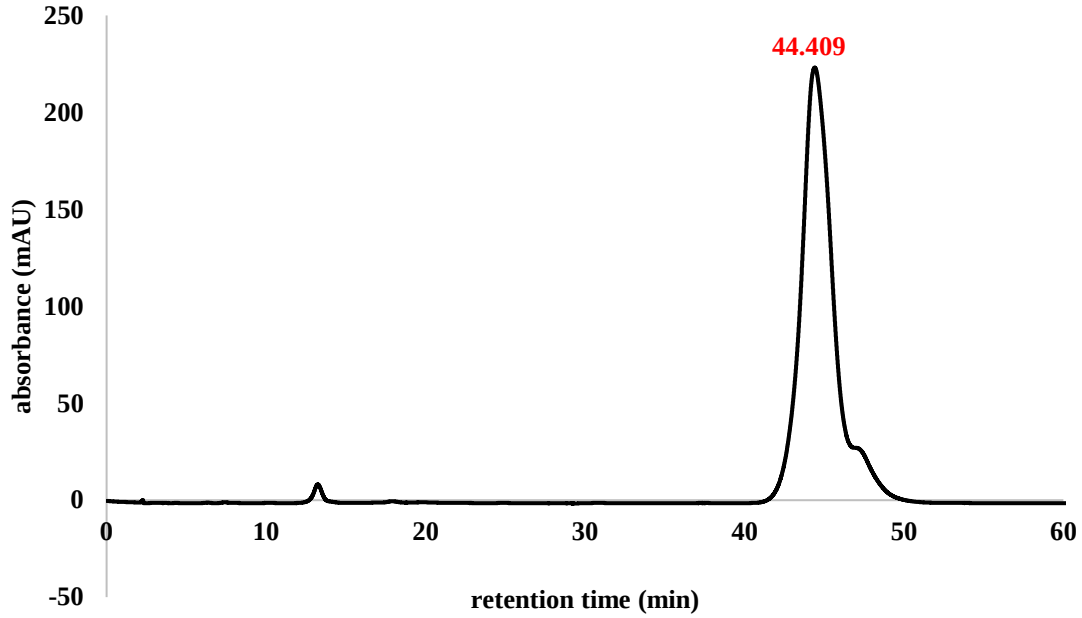

Figure S68a. ^{1}H NMR spectrum of **IBC 20** (Acetone-d_6; 600 MHz)

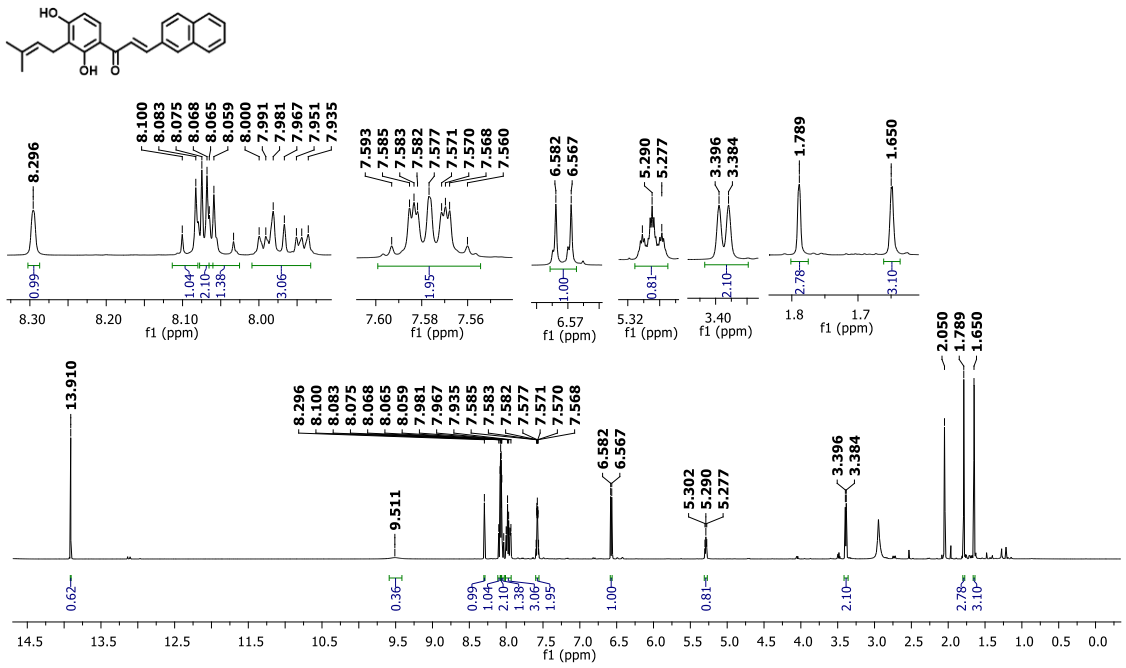

Figure S68b. ^{13}C NMR spectrum of **IBC 20** (Acetone-d_6; 150 MHz)

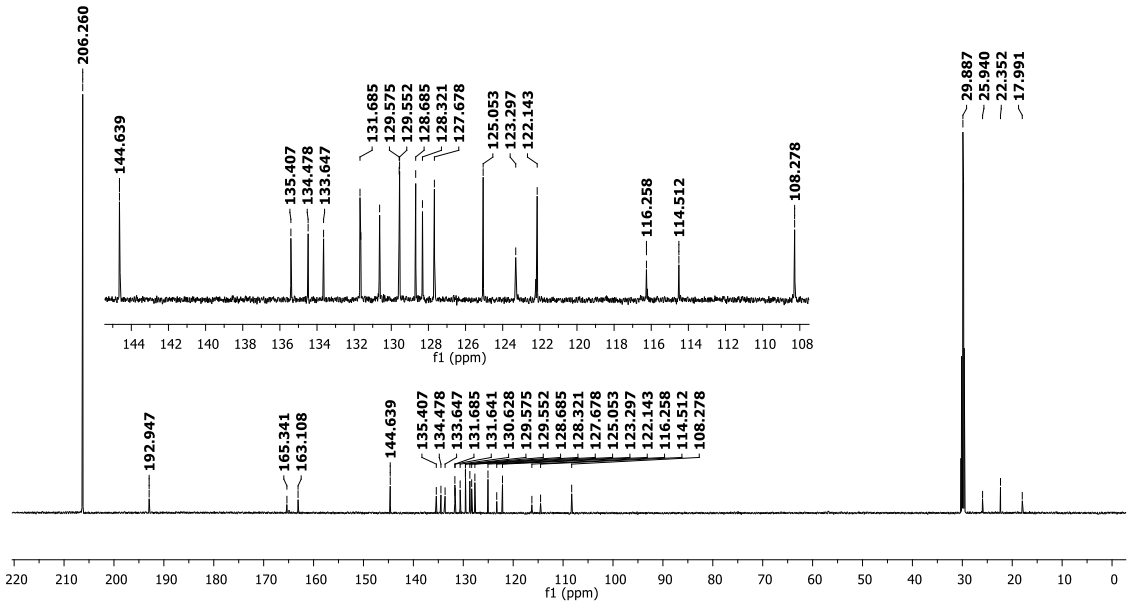

Figure S68c. HPLC chromatogram of **IBC 20**. Methanol:Water (4:1), 365 nm

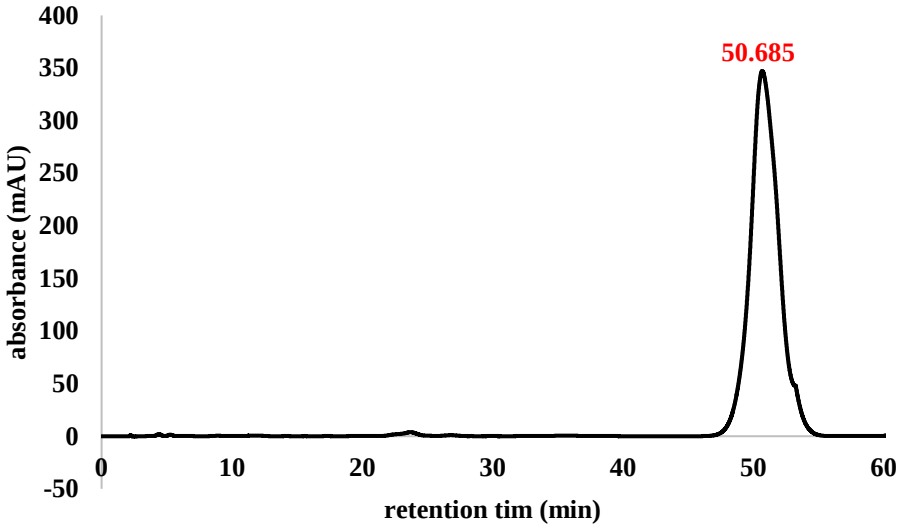

Figure S69a. ^{1}H NMR spectrum of **IBC 21** (DMSO-d_6; 600 MHz)

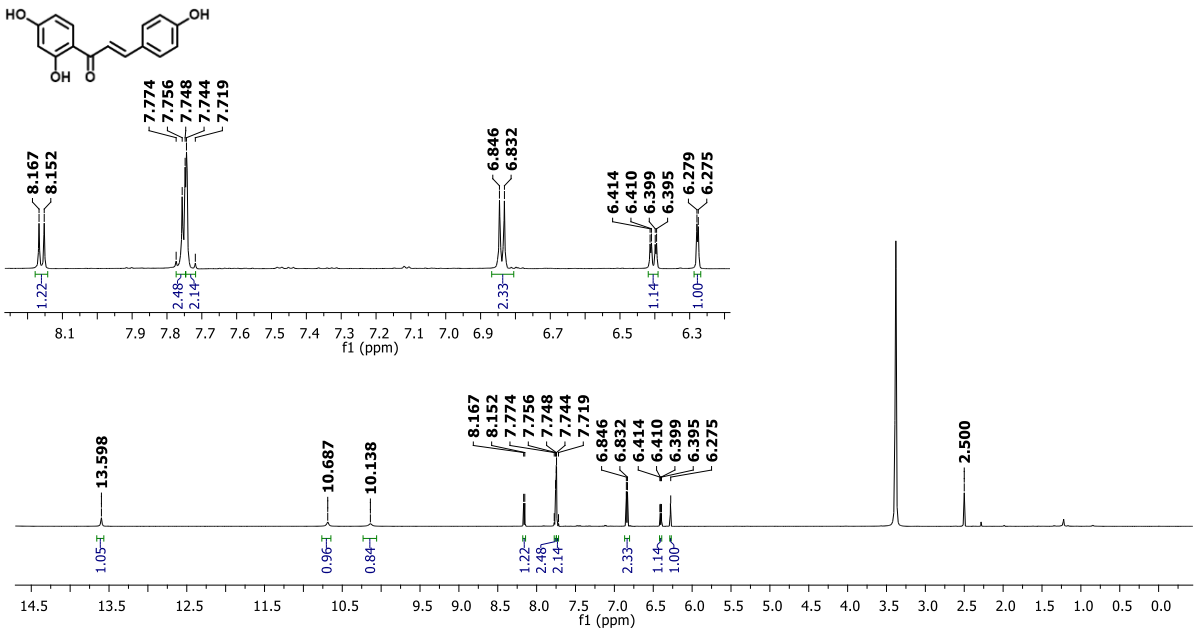

Figure S69b. ^{13}C NMR spectrum of **IBC 21** (DMSO-d_6; 150 MHz)

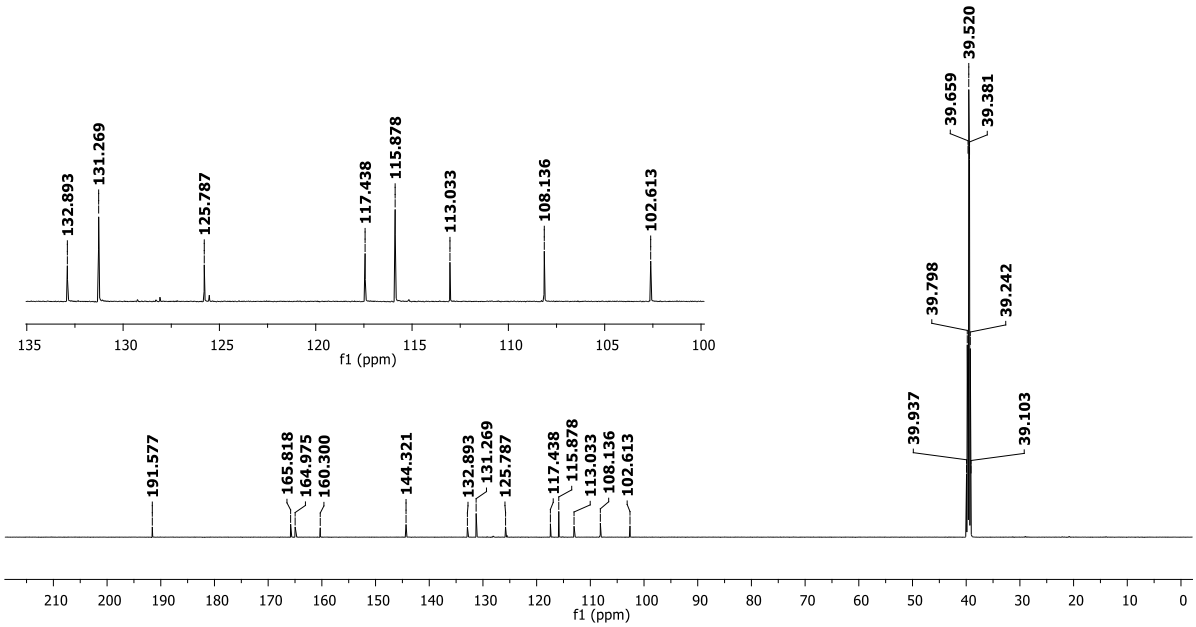

Figure S69c. HPLC chromatogram of **IBC 21**. Methanol:Water (7:3), 365 nm

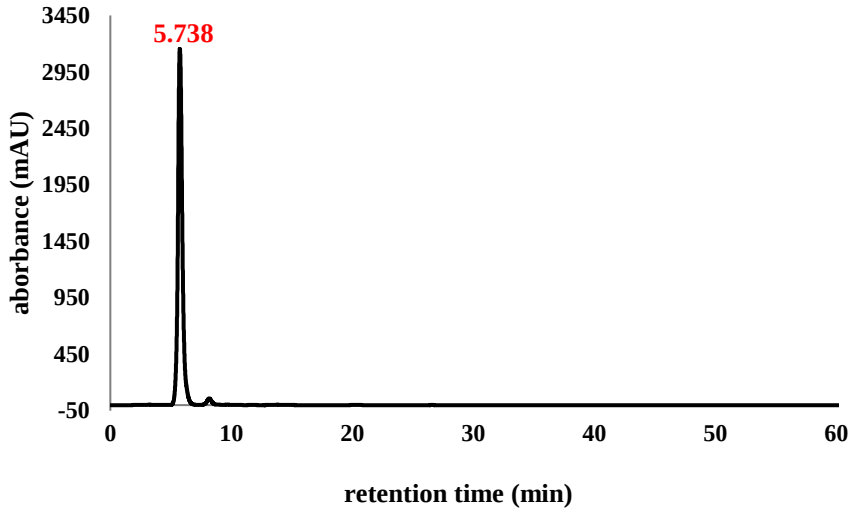

Figure S69d. UV-Vis spectrum of **IBC 21**

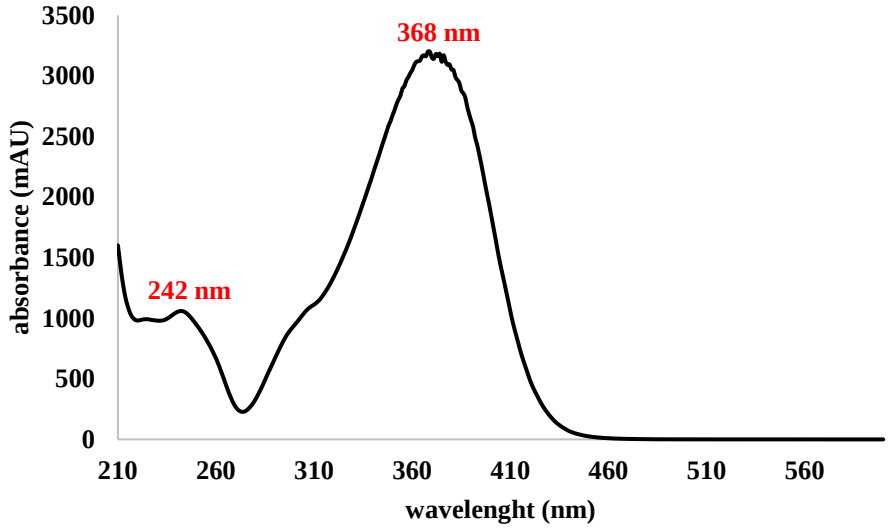

Figure S70a. ^{1}H NMR spectrum of **IBC 22** (Acetone-d_6; 600 MHz)

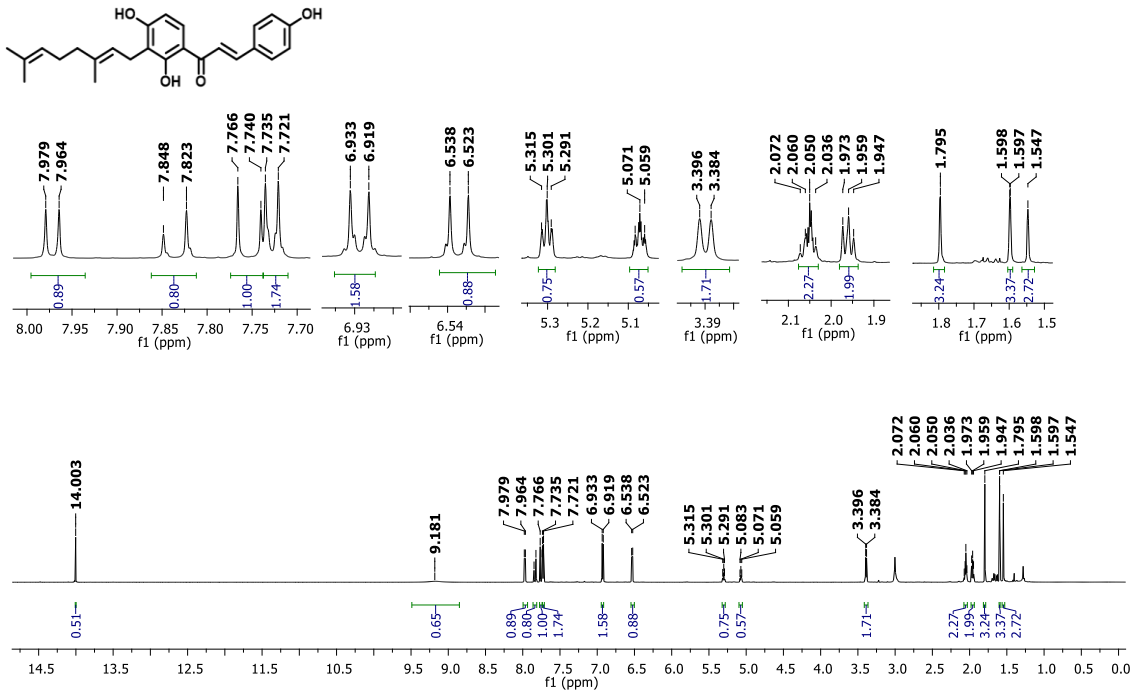

Figure S70b. ^{13}C NMR spectrum of **IBC 22** (Acetone-d_6; 150 MHz)

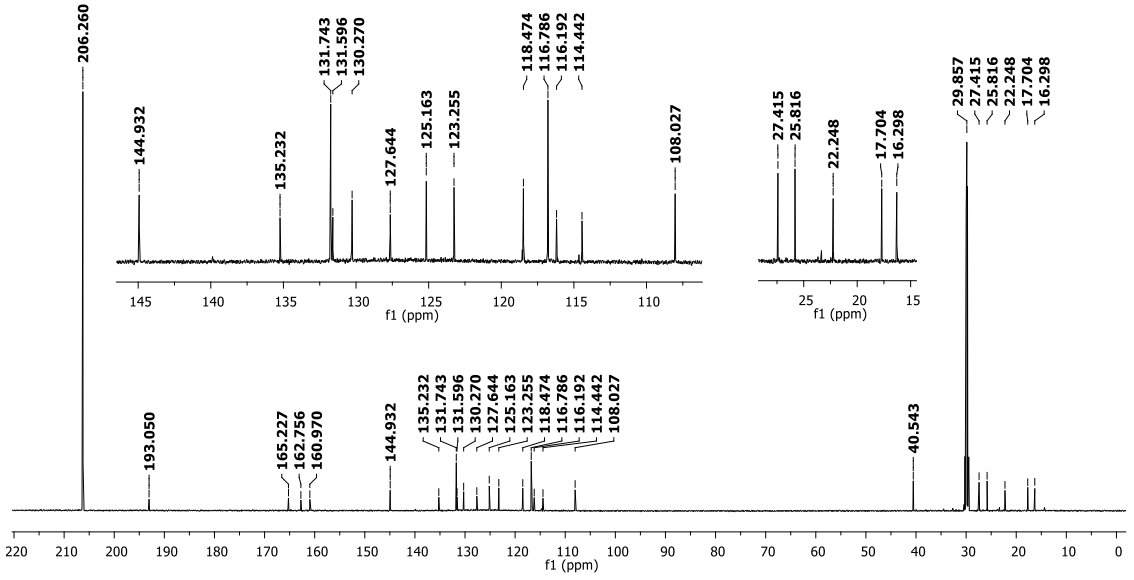

Figure S70c. HPLC chromatogram of **IBC 22**. Methanol:Water (4:1), 365 nm

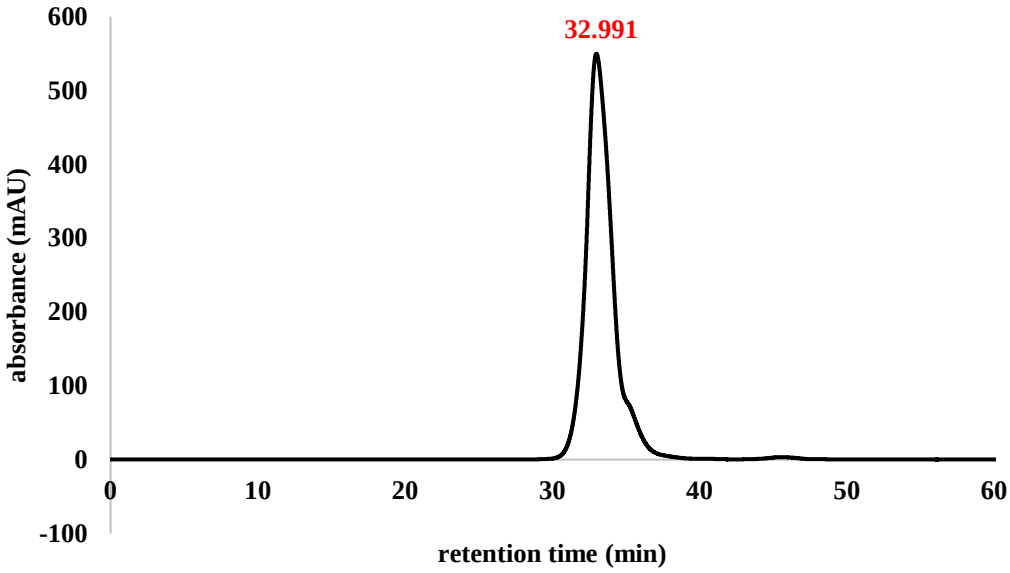

Figure S71a. ^{1}H NMR spectrum of **IBC 23** (Acetone-d_6; 600 MHz)

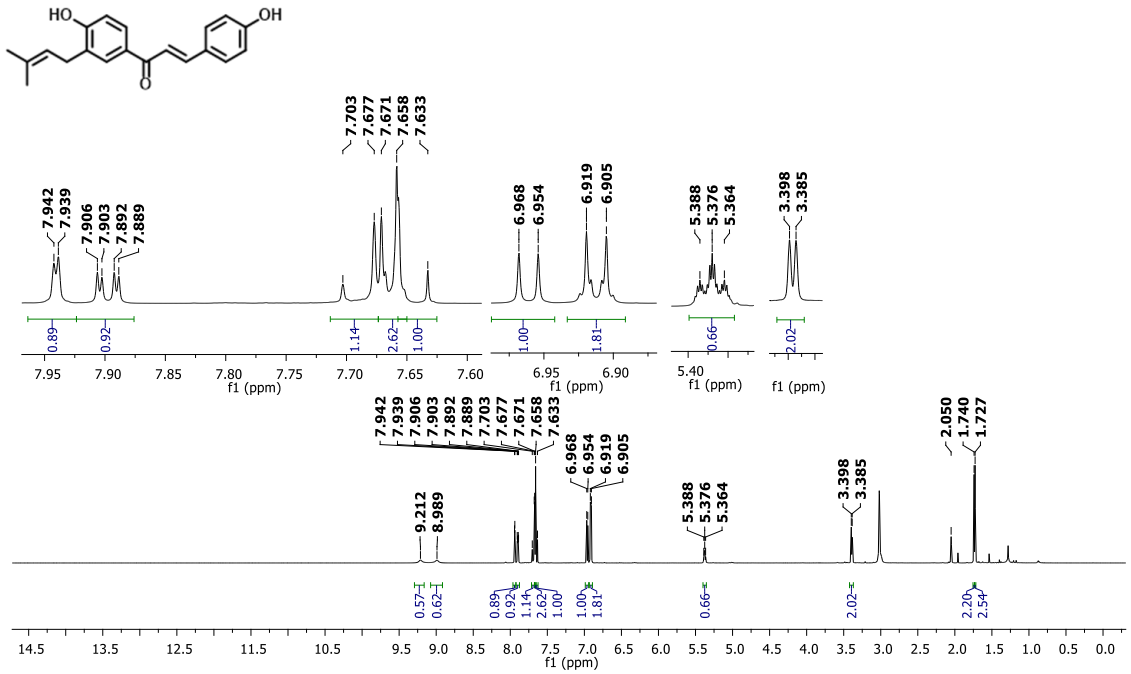

Figure S71b. ^{13}C NMR spectrum of **IBC 23** (Acetone-d_6; 150 MHz)

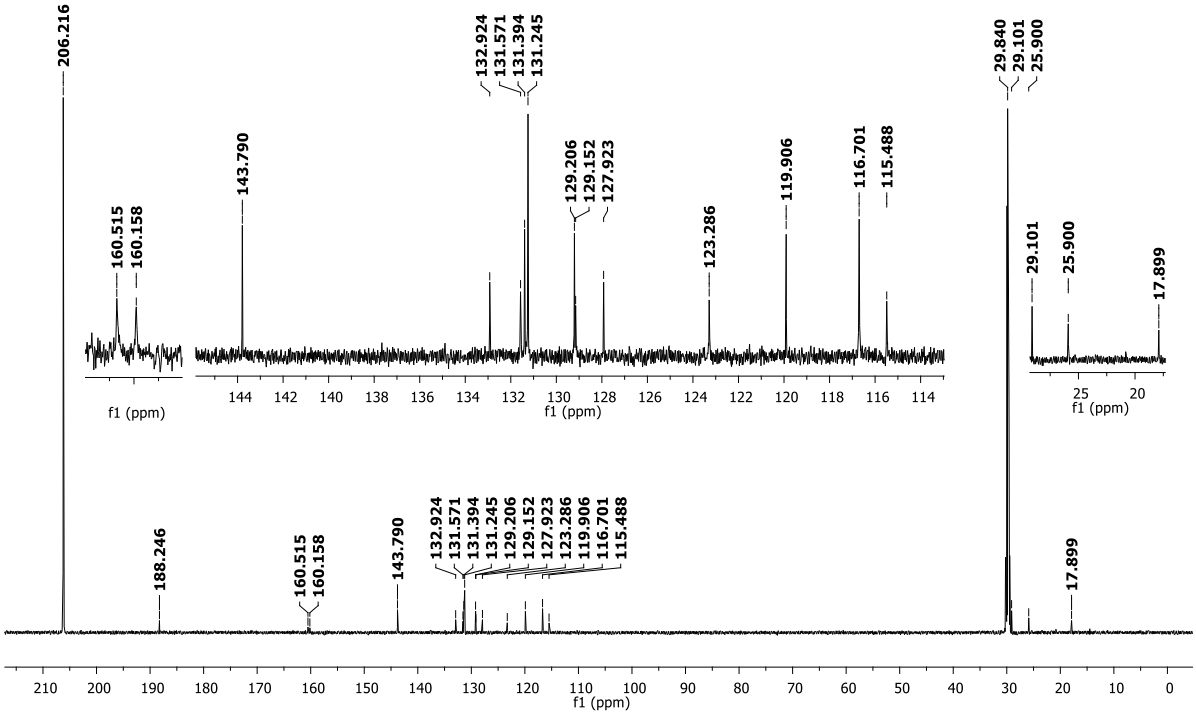

Figure S71c. HPLC chromatogram of **IBC 23**. Methanol:Water (3:1), 365 nm

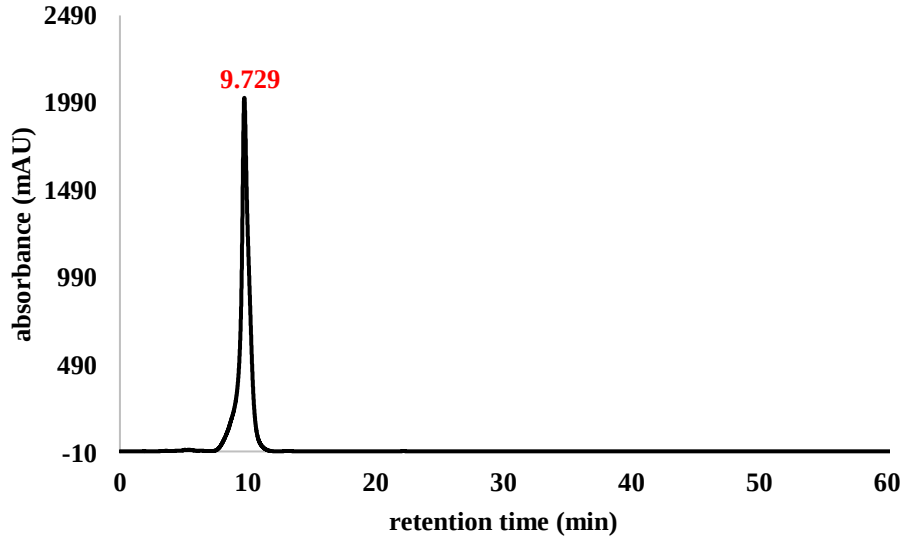

Figure S72a. ^{1}H NMR spectrum of **DHIBC** (Acetone-d_6; 600 MHz)

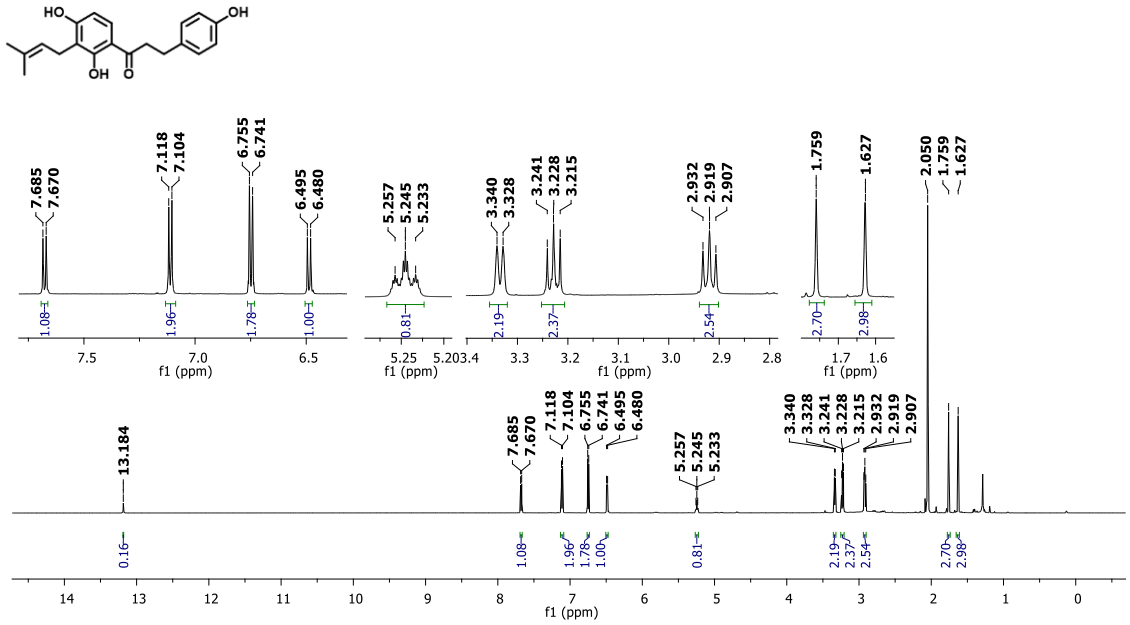

Figure S72b. ^{13}C NMR spectrum of **DHIBC** (Acetone-d_6; 150 MHz)

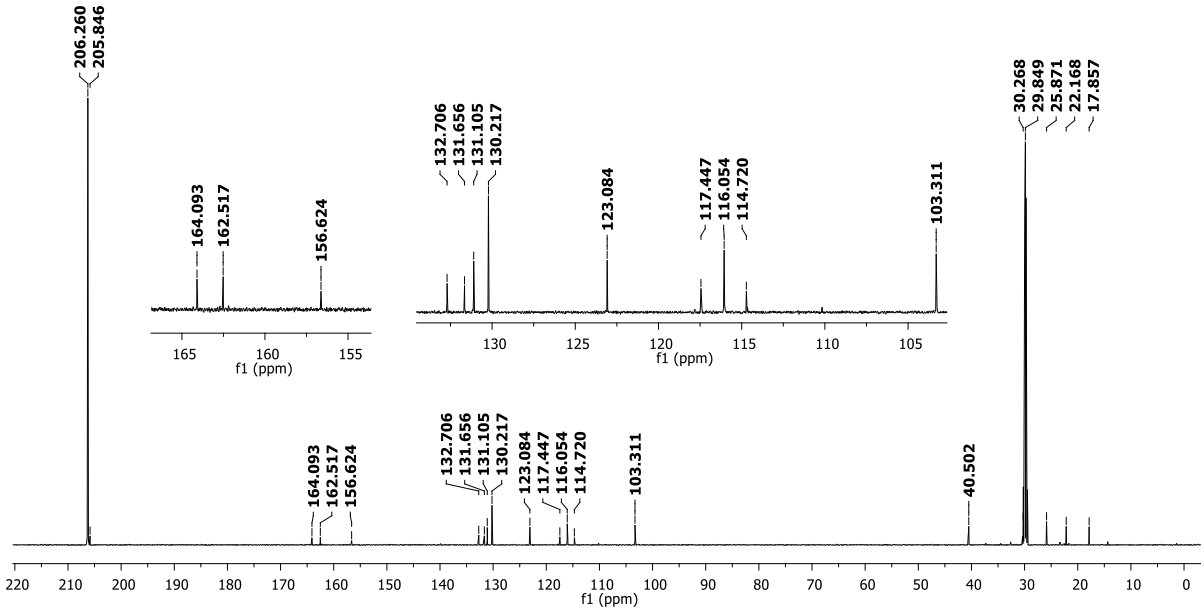

Appendix III

Supplementary material of chapter IV

2-hydroxyisocordoin inhibits MSSA and MRSA biofilm formation and targets the cell membrane of Gram-positive bacteria

Leticia Ribeiro de Assis[a], Reinaldo dos Santos Theodoro[a], Julyanna Andrade Silva Nascentes[a], Maria Beatriz Silva Costa[a], Meliza Arantes de Souza Bessa[b], Ralciane de Paula Menezes[b], Guilherme Dilarri[c], Vanessa R. dos Santos[d], Cristiane Duque[d], Henrique Ferreira[c], Carlos Henrique Gomes Martins[b], Luis Octavio Regasini[a]

[a]Institute of Biosciences, Humanities and Exact Sciences, São Paulo State University (UNESP), Department of Chemistry and Environmental Sciences, São José do Rio Preto CEP 15054-000, SP, Brazil.

[b]Institute of Biomedical Sciences, Federal University of Uberlândia (UFU), Department of Microbiology, Institute of Biomedical Sciences, Uberlândia, CEP 38405-320, MG, Brazil

[c]Institute of Biosciences, São Paulo State University (UNESP), Department of Biochemistry and Microbiology, Rio Claro, CEP 130506-900, SP, Brazil.

[d]São Paulo State University (UNESP), School of Dentistry, Department of Preventive and Restorative Dentistry, Araçatuba, CEP 16015-050, SP, Brazil

Figure S1. ^{1}H NMR sprectrum of **DH-IBC 2** (Acetone-d_6, 600 MHz)

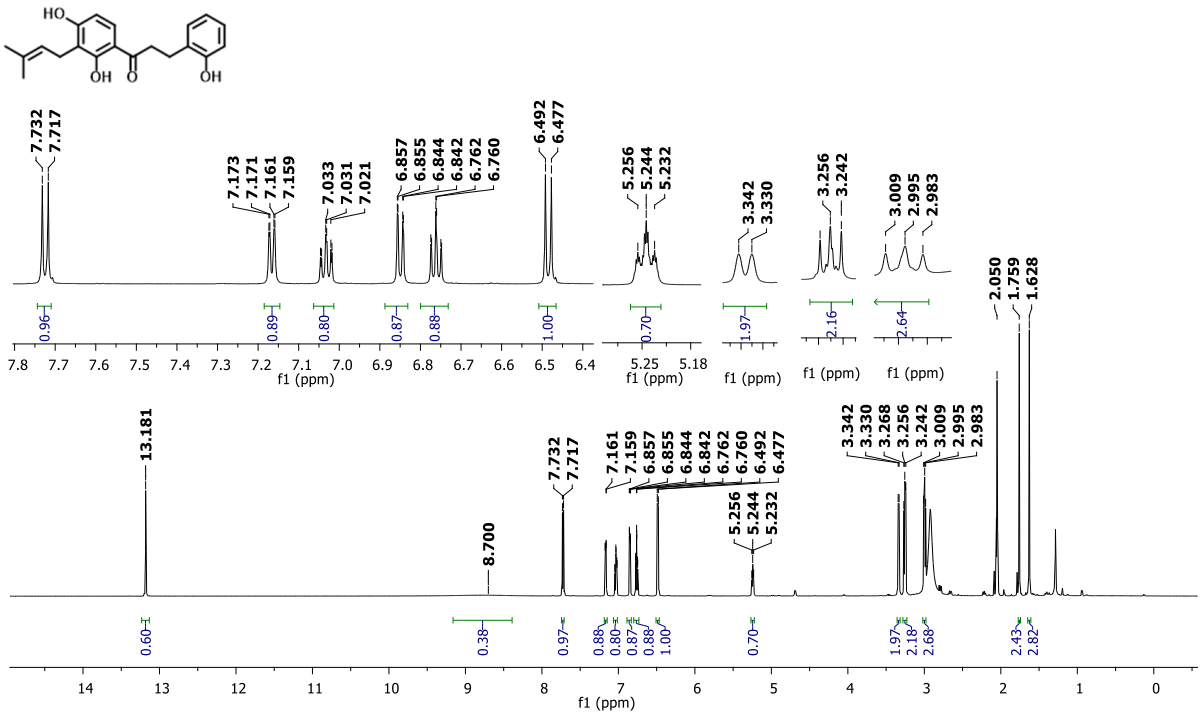

Figure S2. HPLC chromatogram of **DH-IBC 2.** Methanol:Water (3:1), 300 nm

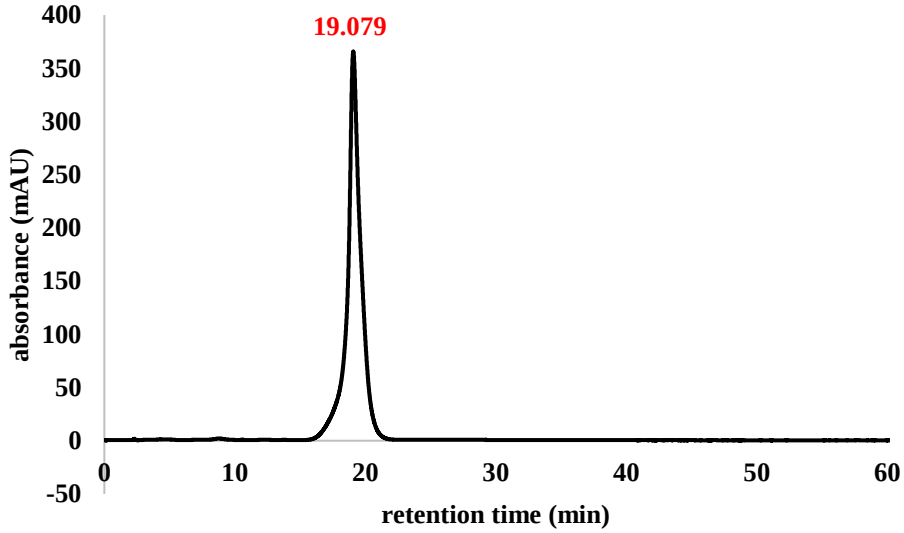

Figure S3. UV-Vis spectra of **DH-IBC 2**